Laboratory Tests of Artificial Ground Freezing of Silty Sand using Pipe Piles

by

Juan Carlos Camacho Botello

A thesis submitted in partial fulfillment of the requirements for the degree of

Master of Science

Geotechnical Engineering

Department of Civil and Environmental Engineering
University of Alberta

Abstract

In the Canadian Arctic, permafrost presents challenges to pile foundations for the existing and future infrastructure. The permafrost of Canada is vulnerable to the threats of climate change, which can lead to the long-term settlement of pile foundations in the Canadian Arctic, particularly during the summer when the permafrost is warm. Current solutions to this problem are more passive than active. One solution involves thermopiles that work in active mode during the winter but become dormant during the summer. Screw piles may be an alternative to foundation solutions for infrastructure in the Canadian Arctic. Prevention of screw pile settlement in warm permafrost is therefore critical to the performance of this pile type. To stabilize piles in warm permafrost, this research investigates an Artificial Ground Freezing (AGF) method that actively circulates glycol through screw piles. The experimental model evaluated a configuration that differs from the traditional AGF. Full-size close-ended pipe piles were installed into a soil chamber and filled with a glycol bath, and then glycol was circulated through a copper coil submerged in the glycol bath to freeze the soil around the pile. Effects of the pile installation method, water content, and initial soil temperature were evaluated. This configuration allows for reduction of the pump size, glycol reservoir and cooling energy in the system due to the small diameter of the copper coil. The initial water content and soil temperature were changed among a series of freezing tests. It is observed that soil temperatures of -13 ± 1 °C were reached within several hours. In addition, a closed-form solution (CFS) and a finite element analysis (FEA) were executed to compare the energy to be removed, the time needed for freezing and the refrigeration plant capacity versus laboratory results. The FEA

predicts the temperature vs. time curves in the transient analysis. The CFS predicts the suitable energy extracted and its rate that is comparable to lab results.

Acknowledgements

I thank God for everything.

A big Thank You to all my family: my girlfriend Maja for her unwavering support and patience, my parents Carlos and Mariela, and my brother Santiago and sister Carolina for their support. A sincere Thank You to my friend Ben Trudeau for his ideas, guidance and patience. I also extend a heartfelt Thank You to Colin Michaelchuk for his help and expertise.

Thanks also goes to the Faculty of Engineering, the Department of Civil and Environmental Engineering, and the School of Mining and Petroleum at the University of Alberta. Thank you to Dr. Lijun Deng and Dr. Nicolas Beier for their help and support.

A thank you also goes to NSERC – Engage Grants (538566-19) for their funding.

I have learned a great deal on this journey and am happy to take all the lessons forward into my future.

Table of Contents

List of Tables

List of Figures

List of Symbols

Symbol	Definition
a	characteristic soil test parameter, internal radius of the curved wall
A	cross-sectional area
a_r	factor when multiplied by R defines the distance of temperature influence from the freeze pipe location
b	characteristic soil test parameter, external radius of the curved wall
C	temperature on the centigrade or Celsius scale
c	heat capacity
c_{glycol}	specific heat of the glycol
c_m	heat capacity, specific heat capacity, mass heat capacity
c_v	volumetric heat capacity
c_{vf}	frozen volumetric heat capacity
c_{vu}	unfrozen volumetric heat capacity
c_{vw}	volumetric heat capacity of water
D_h	hydraulic diameter
e	void ratio
G_s	specific gravity of solids
h	convective heat transfer coefficient
i	thermal gradient dT/dx
K	temperature on the Kelvin or absolute scale
k_0	thermal conductivity of other minerals
k_b	thermal conductivity of the glycol
k_{dry}	thermal conductivity of dry natural soil, thermal conductivity of dry crushed rock materials
K_e	kersten number
k_f	frozen thermal conductivity
k_i	thermal conductivity of ice
k_q	thermal conductivity quartz (of the total solids content)
k_s	thermal conductivity of the soil particles
k_{sat}	thermal conductivity of saturated unfrozen soil, thermal conductivity of saturated frozen soil
k_u	thermal conductivity of unsaturated unfrozen soil, thermal conductivity of unsaturated frozen soil
k_w	thermal conductivity of the pore water
k_f^1	thermal conductivity of frozen soil with w_u
L	volumetric latent heat of the soil

L'	amount of heat when water is converted into ice with no change in temperature
L_l	equivalent latent heat for stage I
L_f	equivalent latent heat for stage II
m	mass, meters
m_{air}	mass of air
m_i	mass of ice
mm	millimeter
m_s	solids mass
m_w	mass of water
n	porosity
N_u	Nusselt number
P	rate energy extracted, wetted perimeter, cooling power
P_I	refrigeration load for stage I
P_{IIF}	refrigeration load for stage II
P_{loss}	power loss
Q	energy extracted
q	heat flux per unit area, rate of heat flow per unit area, quartz fraction
Q_{glycol}	flux of glycol
Q_I	energy extracted during stage I
Q_{IIF}	energy extracted during stage II
R	radius ice-soil column
r_0	freeze pipe radius
R_A	a_rR
R_p	the radius of the freeze pipe circle
S	freeze pipe spacing
s	second
S_r	degree of saturation
T	temperature
t	time
T_0	freezing point of water (0 °C)
T_g	ambient ground temperature
t_I	time to freeze stage I
t_{IIF}	time to freeze stage II
T_{in}	temperature of the glycol entering the system
T_{out}	temperature of the glycol leaving the system
T_s	temperature at the surface of the freeze pipe
t_{total}	t_I+t_{IIF}
V	soil volume
v_0	Ts-Tg=temperature difference
v_1	temperature at radius r_1

v_2	temperature at radius r_2
v_s	T_o-T_s=temperature difference
w	(moisture) water content (in the soil)
W	width, Watt
w_i	ice content
w_u	unfrozen water content
X	coordinate
x	distance along X-axis
Y	coordinate
y	distance along Y-axis
Z	coordinate
z	distance along Z-axis
γ	(total) unit weight of the soil (sample) void spaces contain both water and air
γ_w	unit weight of water (4 °c)
δ	0.393S
ΔT	differential of temperature
ρ	density of the soil (inclusive of all phases solids, water and air)
ρ_d	dry density
ρ_{df}	dry density of the frozen soil
ρ_f	bulk density of the frozen soil
ρ_w	density of water

1. Introduction

1.1 Background

The growing need for natural resources and expanding communities in the Arctic require the construction of new facilities and infrastructure. Construction in these regions presents several challenges like remoteness, weather, environment, and permafrost (Government of Canada, 2019).

The active layer of permafrost has some adverse effects on the performance of pile foundations. When the ground starts to freeze it also begins to expand, causing frost heave. During the summer months, the melting active layer and warming permafrost underneath the active layer may lead to permanent settlement in piles. With the existing infrastructure, once the permafrost thaws by natural or unnatural circumstances, piles sink and damage the building (National Snow and Ice Data Center, 2019).

Deep foundations built into permafrost demand a deep understanding of pile performance in soils at warm or frozen temperatures; this is the reason why qualifications and experience are so crucial for specialist engineers.

One solution to prevent the thawing ground is elevating the building a few feet above the ground; this space beneath the building creates a circulation of winter air that prevents the ground from warming up in the winter and summer (Smoltczyk, 2003).

Another method in practice is to use Thermosyphons (thermopiles) that are closed natural convection devices. Thermosyphons do not require moving parts and have zero power consumption. To create two-phase liquid/vapor convection refrigeration, these piles require large diameters and have to be installed into deep underground, which implies considerable equipment. The mechanisms of thermosyphons makes the manufacturing and installation of this pressure vessel very expensive. Convection inside thermosyphons would be active during the winter and inactive during the summer, which means that for longer summers this method is inefficient; thermopile foundations were designed to maintain the ground frozen in a steady climate which is not always true (Halubec, 2008a ; Halubec, 2008b).

These passive methods have low effectiveness against climate change and are more passive than active solutions.

Deep foundations built in permafrost in northern regions must be sufficiently deep to satisfy the design criteria for creep settlement and axial capacities. Concrete can freeze before it gains strength and can set more slowly at low temperatures creating breaks inside its matrix structure (Concrete Network, 2019). Deep foundations (more specifically steel and timber piles) are commonly used in the Arctic regions.

1.1.1 Screw Micropiles

The screw micropile, also termed "ground screw" in trade, is a new foundation system introduced to the North American market. This pile type uses reusable galvanized steel pipes designed with threads and a reinforced tip that can be installed under torque (Krinner the ground screw, 2018).

It might be easier to install a screw micropile in the frozen ground than other pile types such as helical piles or driven piles (Schmidt, 2004), thus making this pile type suitable for use in the Arctic. Therefore, as a means of freezing adjacent soils, screw micropiles were adopted in laboratory tests of the present research. However, since the research is only limited to laboratory tests where the dimensions of piles are constrained, a short segment of screw micropile shaft was used instead of the full-length pile in this research.

1.1.2 Artificial Ground Freezing (AGF)

Artificial ground freezing is a versatile method that accepts a full spectrum of soil and rock types and keeps the ground frozen by using a refrigeration plant that circulates coolant in freezing pipes, the latter being installed vertically into the ground to convert in-situ pore water to ice. The ice bonds the soil particles together increasing the soil's strength and making it impermeable (Moretrench, 2018).

The present research investigates screw micropiles and artificial ground freezing (AGF) as a joint solution to the problem of warming permafrost in the Arctic and the northern territories. It is assumed that using screw micropiles as freezing pipes in an active Artificial Ground Freezing System could improve the strength of the soil thereby significantly reducing pile settlements.

1.2 Research Objectives

The primary objective of the test program was to examine the feasibility of an active artificial ground freezing method in freezing soil that surrounds a steel pipe pile (i.e., a part of a screw micropile) segment in the warming permafrost. The outcome of the test program will provide the data needed for the design of AGF system for a full-length screw micropile intended for use in the permafrost. The study also examined the usefulness of a conceptual full-size AGF method that circulates the coolant inside a pipe pile. This new method differs from the conventional methods of AGF, making this research unique and innovative in comparison with previous research and practice.

1.3 Research Program

The present research program consisted of primarily two components: laboratory AGF tests and modeling of freezing tests (analytical closed-form solution and finite element).

For the laboratory tests, the AGF equipment composed of a soil cell, glycol-circulating copper coils, pipe pile segments, soil, and two temperature baths were collected or fabricated and eventually assembled for subsequent test programs. The procedures of preparing soil-pile model in the soil test cell and the AGF testing were developed, which can simulate the AGF in the soil field with warm permafrost. Three batches of AGF tests were conducted using the developed equipment and the Cold Regions lab at the University of Alberta. The initial water content of soils, initial soil temperature, pile segment shape, and the temperature boundary conditions were changed among the batches.

In Batch (1) tests, a soil sample with 35% water content (w) and three trials with homogeneous initial soil temperatures of 5, 0, and -2.5 °C; the soil was frozen using a thread screw pile segment (140 mm diameter) when the circumferential soil boundary was controlled at a constant temperature (when both temperature baths were working at the same time after the homogenization stage). During the homogenization stage, both temperature baths always worked together to reach the desired temperature.

In Batch (2) tests, a soil sample with 35% water content and five trials with homogeneous initial soil temperatures of 5, 0, and -2.5 °C; the soil was frozen using a straight screw pile segment (140 mm diameter). Three trials were conducted when the circumferential soil boundary was

controlled at a constant temperature same as the previous initial soil temperatures. Two trials were conducted with homogenization temperatures of -2.5 and 0 °C for a straight screw pile segment when just the pile temperature bath was working after the homogenization stage.

Batch (3) was similar to Batch (2) in configuration but with a soil sample with 20% water content.

The second part of the present research was the validation of laboratory tests using closed-form solution and the finite element modeling. The objective was to estimate and compare the energy to be removed, the time needed for freezing and the refrigeration plant size versus laboratory outcomes.

The best test results when compared with the theoretical methods (Finite-element and Closed-form solution) were observed in the trials where just the pile temperature bath was working after the homogenization stage.

1.4 Scope of Thesis

Chapter 2 presents a literature review regarding permafrost challenges, screw piles, AGF, a closed-form solution to the artificial freezing, and the finite element method for artificial ground freezing with one single pile in the middle of a field without seepage.

Chapter 3 describes the laboratory AGF test program. It includes sample preparation, description of apparatus, a detailed test procedure (test matrix), and a location of thermocouples in all testing batches.

Chapter 4 presents and discusses the laboratory AGF test results. This chapter is divided into three main parts: grain size distribution, consolidation, and freezing of the soil sample. Some example results are presented and all results are highlighted in Appendix A.

Chapter 5 presents and examines the theoretical thermal analyses. It includes the initial physical soil sample properties and thermal parameters, the closed-form solution, the finite element analysis, power and energy demand, and a comparison of the solutions. All the analyses of the research are presented in Appendix A.

Chapter 6 summarizes the conclusions extracted from the present research. The outcomes of this experimentation are examined related to the design of AGF in permafrost. Recommendations are also presented for better performance of the model AGF proposed and for further research required to improve design guidelines.

Appendix A presents all the test results and analytical results of the tests.

Appendix B presents photographs of the consolidation loading frame, load plates and adapters, test cell, the screw micropile, test pile segments, temperature baths, instrumentation, data logger, cold room, copper coil, soil sample preparation, consolidation of the soil sample, ethylene glycol, copper coil inside of the pile, test cell´s fiberglass insulation, hose insulation, laboratory setup, density measuring ring and power loss test.

Appendix C presents a flow diagram of the test procedure and analysis.

2. Literature Review

2.1 Introduction

2.1.1 The Permafrost Challenges

Any construction project to be developed in the Arctic involves a series of challenges; not only is the cold weather a factor of consideration but also the soil condition plays a huge role. When the active soil layer freezes, frost heave will take place; when the active layer melts, everything on the surface sinks and subsequently, potential damage could be generated as indicated by National Snow and Ice Data Center (2019). The permafrost underlying the active layer is currently under the threats of climate change, which in turn can lead to the long-term settlement of pile foundations in the Arctic. Fig. 2.1 presents the permafrost distribution in Canada and Fig. 2.2 shows the air and ground temperature changes in Inuvik.

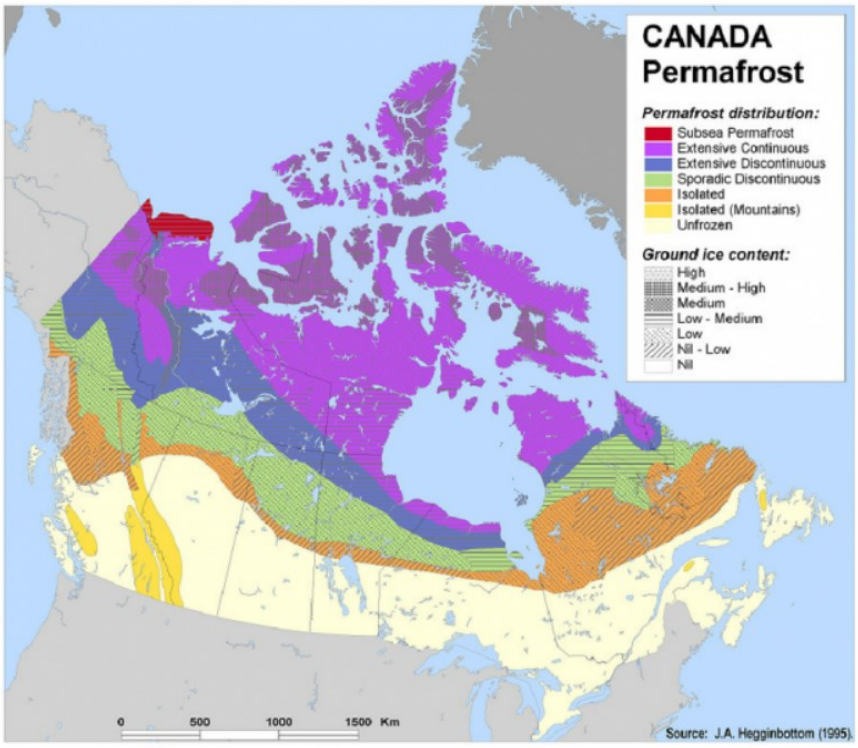

FIGURE 2.1 Permafrost distribution in Canada (Government of the Northwest Territories, 2015).

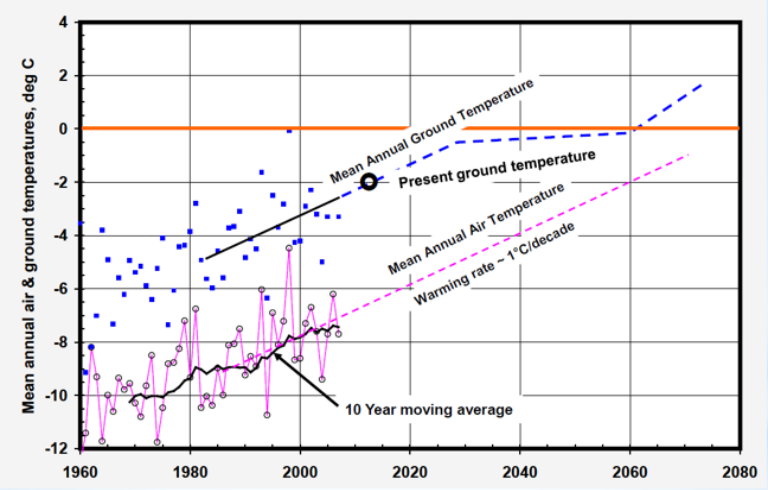

FIGURE 2.2 Air and ground temperature changes in Inuvik (Halubec, 2008b).

Foundations in the Artic are more expensive than in other places due to the permafrost and the obvious logistical challenges including the necessity to dig deeper to avoid the active layer.

The current solutions to this problem are not actively responding to the circumstances and characteristics of this phenomenon and are more partial solutions. One such example is building on top of a steel frame while lifting the structure a few centimeters above to avoid warming the soil (National Snow and Ice Data Center, 2019). The thermopile (such as thermosyphon) solution works in active mode during winter transferring heat by convection without moving parts (no pump) and no power (McFadden, 2000) but during the summer it is totally dormant (Geoslope, 2018b). The construction of thermopiles is complicated and expensive due to the big diameter and thickness.

Due to the factors mentioned above, the vulnerability of these cooling methods is very high, and their adaptive capacity to climate change, especially during summertime, is deficient as reported by Halubec (2008a). It is evident that it is necessary to find an active solution that is viable and sustainable. This research focuses on filling this evident gap.

Field monitoring program was carried out by Aurora Research Institute about pile foundations in permafrost regions; it compared traditional piling with convective piling at depths ranging from 0.5 to 14 meters, showing that the convective piling method might be not reliable. In actuality, the rate of freeze-back only increased by 16 days in comparison with the traditional piles and at the top 2 meters of the soil the seasonal variability is high (Aurora Research Institute, 2016).

Aurora Research Institute conducted the study in the western arctic research centre building where underground temperatures were collected beneath the middle of the structure for an extended period over approximately four years (Fig. 2.3).

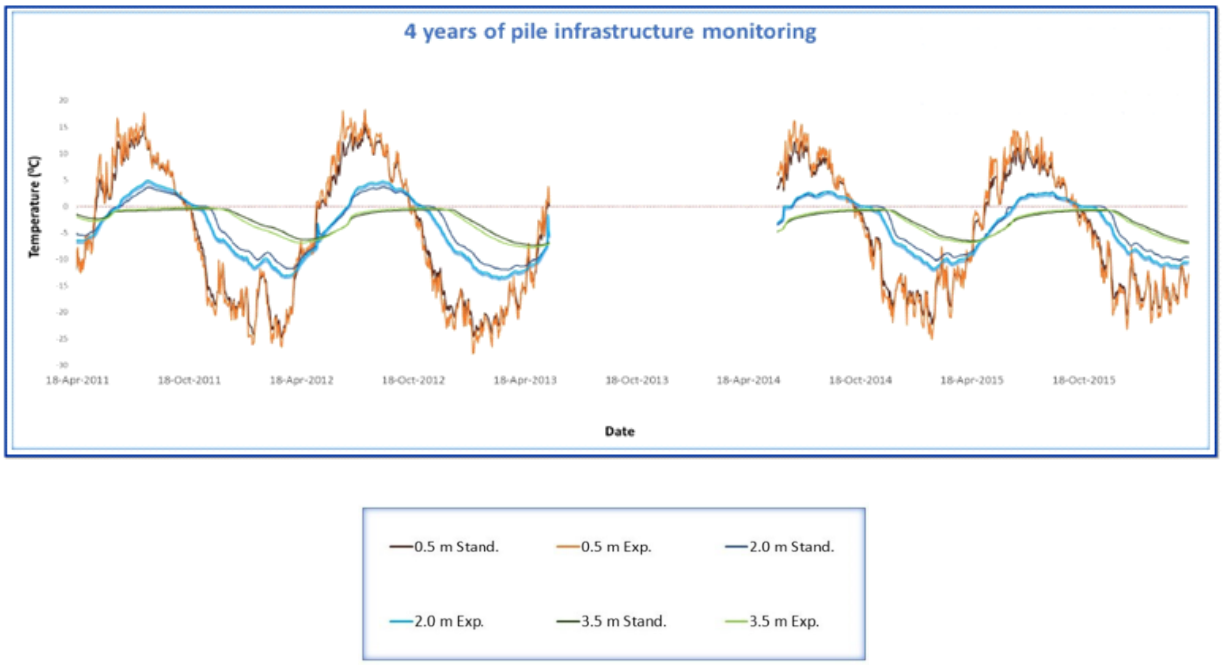

FIGURE 2.3 Western Artic Research Center underground temperatures (Aurora Research Institute, 2016).

The field temperature shown in Figure 2.3 was used when deciding the initial soil temperatures for the present laboratory freezing tests. The soil temperatures considered in the present research were 5, 0 and -2.5 °C during the summer between the middle of April and the middle of October, as representative of the ground temperature at 2 meters and 3.5 meters deep which is shown in Fig. 2.3 during 2011.

It should be remarked that starting to artificially freeze the ground just before the end of winter, when the temperatures are still low, is more efficient due to the high thermal conductivity from the ice already present; moreover, the system can operate only for the summer as the rest of the year it is not necessary, which could improve the whole freezing process significantly. Evaluating these factors is also one of the objectives of the present research.

2.1.2 Screw Micropiles

The screw micropile, also termed “ground screw” in trade, is a new foundation system introduced to the North American market. This pile type uses reusable galvanized steel pipes designed with threads and a reinforced tip that can be installed under torque (Krinner the ground screw, 2018).

It might be easier to install a screw micropile in the frozen ground than other pile types such as helical piles or cast-in place (Schmidt, 2004), thus making this pile type suitable for use in the Arctic. Therefore, as a means of freezing adjacent soils, screw micropiles were adopted in laboratory tests of the present research. However, since the research is only limited to laboratory tests where the dimensions of piles are constrained, a short segment of screw micropile shaft was used instead of the full-length pile in this research.

2.1.3 Artificial Ground Freezing (AGF)

In 1883, the German scientist F. Hermann Poetsch patented his "Method of and Apparatus for Sinking Shafts through Quicksand." Nowadays, groundwater control and excavation support for shaft sinking is the main application (Moretrench, 2018).

The principle of AGF consists of converting pore water trapped in the soil structure to ice by removing heat. Freezing connects the soil particles and thereby increases the strength, stiffness, and permeability of the material as noted by Harris (1995).

Frozen soil structures are created by installing freezing pipes vertically underground in which the cooling liquid (coolant) flows down in an inner pipe and returns via an annular space between the freezing pipes themselves, as illustrated in Fig. 2.4. The coolant is provided by a refrigeration plant located on the construction site, as demonstrated in Fig. 2.5 (Andersland & Ladanyi, 2004).

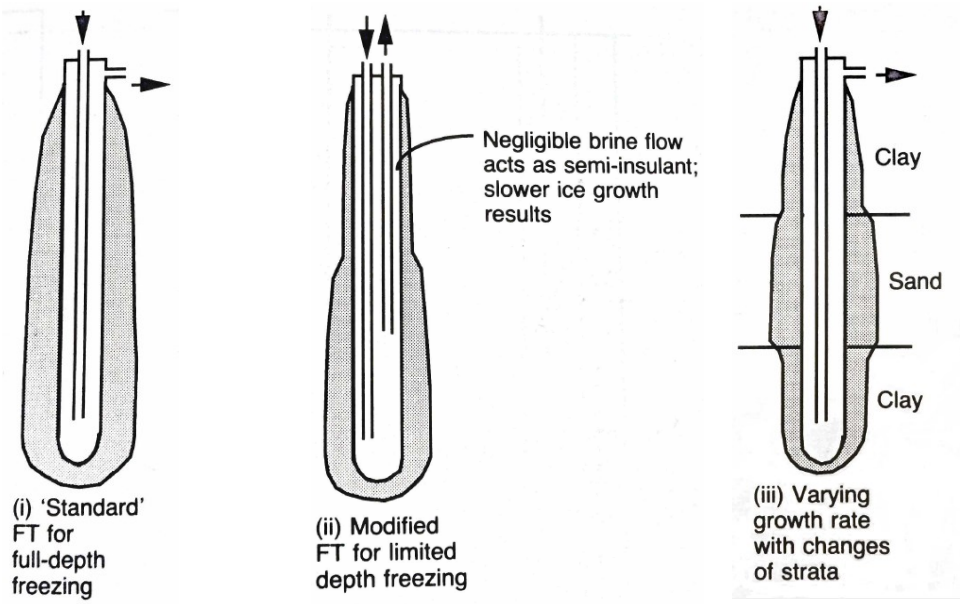

FIGURE 2.4 Conventional freeze tube assemblies and ice-wall profiles (Harris, 1995).

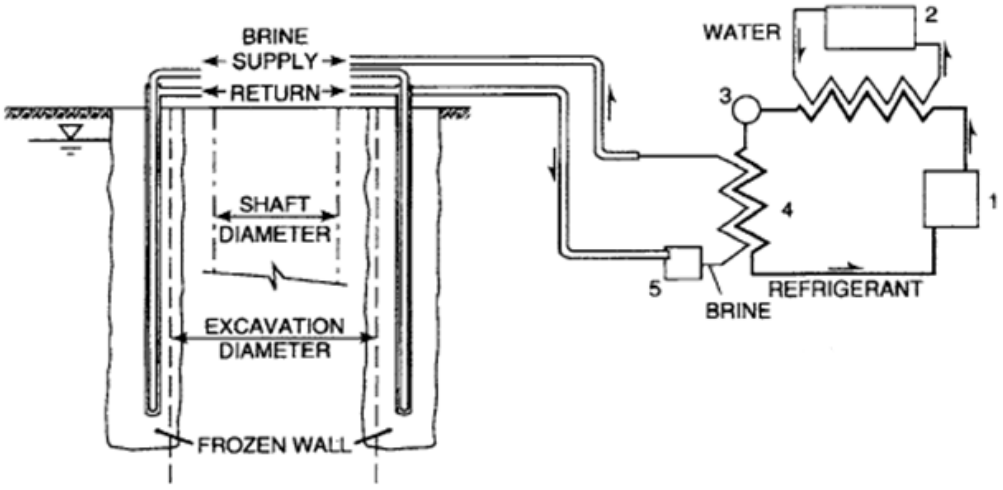

FIGURE 2.5 Typical frozen ground support system (Andersland & Ladanyi, 2004).

In the beginning, a frozen soil column forms around each freeze pipe. As the heat continues to be extracted, the frozen soil columns grow in diameter until they start to unite and create a frozen wall (Andersland & Ladanyi, 2004).

Ground freezing can be performed in all soils and in porous or fissured rock (Harris, 1995). Fig. 2.6 presents the applicability of geotechnical processes according to soil type.

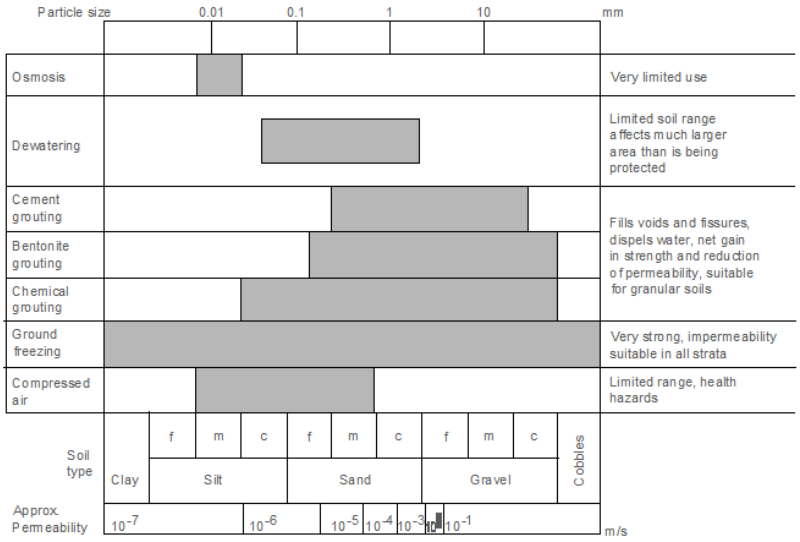

FIGURE 2.6 Applicability of geotechnical processes according to soil type (Harris, 1995).

The AGF can be classified into the Active and Passive methods (see Figs. 2.7 and 2.8). The Active method requires pumps, circulating coolant and direct energy input. The Passive method does not need direct energy input because it utilizes convective flow of the coolants that encounter the phase changes of coolants (Arctic Foundations of Canada, 2019).

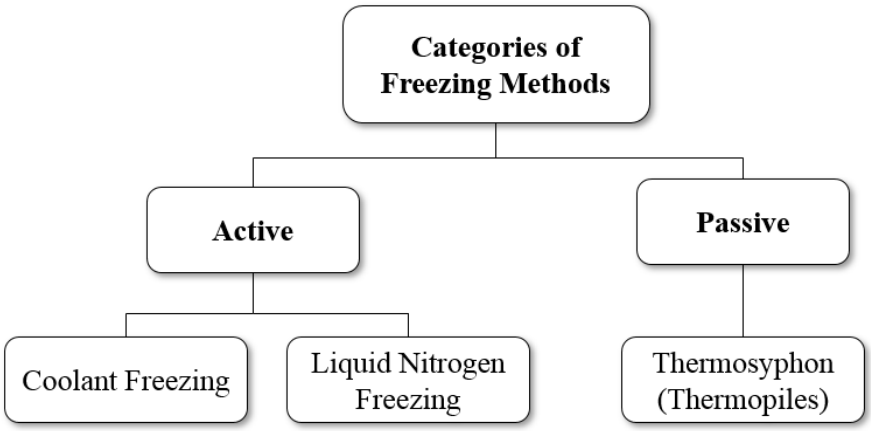

FIGURE 2.7 Categories of freezing methods (Arctic Foundations of Canada, 2019).

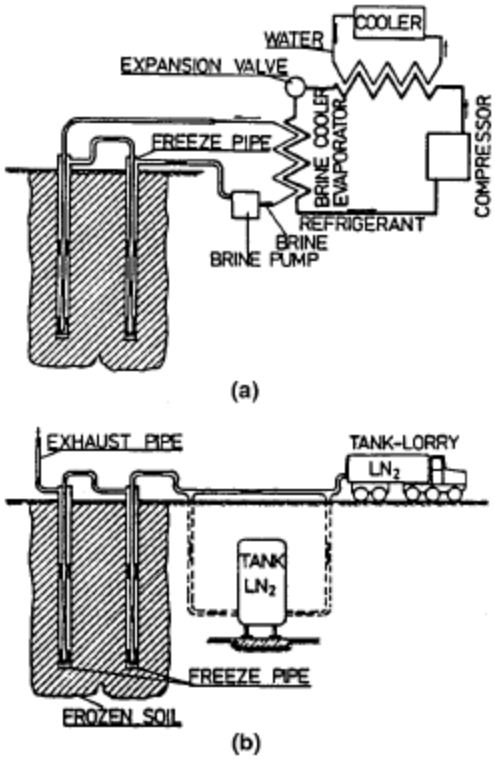

FIGURE 2.8 Refrigeration methods a) primary plant and pumped loop secondary coolant; b) expandable liquid refrigerant (Jessberger, 1980).

For large, long term projects brine freezing is generally used (see Fig. 2.8).

The most traditional coolant is calcium chloride brine. Commonly, it is iced to temperatures between -15 °C and -25 °C and pumped down to the depths of the freeze pipe, and subsequently flows up through the annular space. Frequently, the freeze pipes are connected in series-parallel. The brine is routed back to the refrigeration plant, where it is chilled and recirculated.

Liquid nitrogen functions faster than brine, making it highly efficient in situations when time is of the essence and when the ground condition is disturbed. The costs of utilizing nitrogen are greater than brine, but the quick-freezing time makes this method more competitive (Harris, 1995) (see Fig. 2.8).

Pimentel (2012) reported that the published database of physical model studies of AGF is not sufficient for detailed assessments of computational models. The present research aims to help fill this gap.

2.2 Thermal Analysis of the Soil Sample

The numerical modeling of conductive heat transfer in soil needs multiple input parameters related to geometry, thermal boundary conditions, and soil properties (Smoltczyk, 2003).

2.2.1 Physical Properties of Materials

The first input properties required for this thermal analysis are water content (w), Specific Gravity of Solids (G_s), and total unit weight (γ) for the soil sample (solids, water and air).

The water requirements are the unit weight at 4 °C (γ_w) = 9.807 kN/m^3 and the density (ρ_w) = 1000 kg/m^3.

With these properties from the soil sample and water and with the use of soil weight/mass and volume relationships it is possible to have the complete picture of the components of the sample necessary for the analysis and the first steps. Following properties are considered:

Void ratio,

$$e = \frac{(1+w)G_S\,\gamma_w}{\gamma} - 1 \tag{2.1}$$

Porosity,

$$n = \frac{e}{1+e} \tag{2.2}$$

Saturation,

$$S_r = \frac{G_s w}{e} \tag{2.3}$$

Soil density (inclusive of all phases solids, water and air),

$$\rho = \gamma / g \tag{2.4}$$

Dry density,

$$\rho_d = \frac{\rho}{1+w} \tag{2.5}$$

Apart from the physical soil properties it is necessary to define other crucial thermal soil properties such as heat capacity, thermal conductivity, and latent heat.

Heat capacity (c_m), is defined "as the quantity of heat required to raise the temperature of a unit mass of a substance by a unit change in temperature" (Smoltczyk, 2003).

Thermal conductivity (k), is defined "as the quantity of heat that flows through a unit area in a unit time under a unit temperature gradient" (Smoltczyk, 2003).

Latent heat of fusion (L), is defined as "the amount of heat energy absorbed when a unit mass of ice is converted into a liquid at the melting point" (Andersland & Ladanyi, 2004).

2.2.2 Thermal Parameters

Previous to estimate the soil sample thermal properties is necessary to define these parameters. The thermal conductivity of the soil particles (k_s), as can be seen in the Table 2.1, is a function of the quartz content (q) and the grain size.

TABLE 2.1 Thermal Conductivity of Solids k_s as a Function of the Quartz Content (Smoltczyk, 2003)

Quartz content	Grain size < 0.02 mm	Density kg/m^3	
		2700	2900
Unknown	< 20%	4.5	3.5
	> 60%	2.5	
Known=q	< 20%	$2^{1-q} \times 10^q$	$3^{1-q} \times 10^q$
	> 60%	$2^{1-q} \times 10^q$	

Sands and gravels normally are high in quartz, with silts and clays composed of other minerals. The thermal conductivity of the pore water (k_w), is a constant with a value of 0.57 W/m · K (Andersland & Ladanyi, 2004). Unfrozen water content (w_u) was founded on test outcomes from Johansen & Frivik (1980). Subsequently Makowski (1986) presented the unfrozen water content (w_u) correlated to the temperature (T) for some natural soils by a power-law curve of the following form (Smoltczyk, 2003):

$$w_u(T) = a \cdot T^b \tag{2.6}$$

where:

w_u= Unfrozen water content (%)

T= Temperature (°C)

a, b = Characteristic soil test parameters

Empirical data for parameters a and b for diverse soil types are presented in Table 2.2

TABLE 2.2 Parameters a and b to Determine Unfrozen Water Content w_u (Smoltczyk, 2003)

Soil type	a	b
Sand, gravel	0.8	-0.727
Silty sand	1.5	-0.699
Silt	3.0	-0.574
Silty clay	6.0	-0.602
Clay	12.0	-0.536
Clay of high plasticity	20.0	-0.456

The thermal conductivity of ice (k_i) is a constant with a value of 2.2 W/m · K (Andersland & Ladanyi, 2004).

Kersten (1949) conducted test on natural soils and crushed rock from which empirical equations were developed. Kersten Number (K_e) is a constant function of the degree of saturation (S_r). Johansen (1975) expresses thermal conductivity of saturated unfrozen and frozen soil as a function of dry and saturated thermal conductivities using the Kersten Number (K_e) as a basis.

Kersten Number (K_e), for unfrozen coarse-grained soil for clay content < 2% is (Smoltczyk, 2003):

$$K_e = 0.7 \log S_r + 1.0 \tag{2.7}$$

Kersten Number (K_e), for unfrozen fine-grained soil for clay content > 2% is:

$$K_e = \log S_r + 1.0 \tag{2.8}$$

Kersten number for frozen soil is:

$$K_e = S_r \tag{2.9}$$

The volumetric heat capacity of water (c_{vw}) is a constant with a value of 4.187 MJ/m^3 · °C (Andersland & Ladanyi, 2004).

2.2.3 Thermal Properties

Having considered the above it is now possible to calculate the heat capacities, thermal conductivities, and latent heat.

2.2.3.1 Heat Capacity

The heat capacity ((J/g)/ °C) of a soil sample is the amount of heat required to raise its temperature 1 degree.

The volumetric heat capacity (c_v) is estimated by multiplying the specific heat capacity by the soil density (ρ) (Smoltczyk, 2003):

$$c_V = c_m \rho \tag{2.10}$$

where:

c_v= volumetric heat capacity (J/m^3 K)

c_m= specific heat capacity (J/kg K)

ρ= soil density (kg/m^3)

According to (Williams, 1973), the heat capacity of a multi-phase soil system is determined as the weighted arithmetic mean of all soil components.

Let m_s, m_w, m_i, and m_{air} to symbolize the mass fractions and c_s, c_w, c_i and c_{air} the heat capacities of solids, water, ice, and air, respectively in a soil volume V with total mass m. The heat capacity of the soil is:

$$c(kJ/kg \cdot \ ^\circ C) = \frac{1}{m}(c_s m_s + c_w m_w + c_i m_i + c_{air} m_{air}) \tag{2.11}$$

Dividing by V and neglecting the minimum air term obtains the volumetric heat capacity of the soil:

$$c_v(MJ/m^3 \cdot °C) = c_m\rho_f = \rho_{df}(c_s + c_w w_u + c_i w_i) \quad (2.12)$$

where ρ_f and ρ_{df} are the bulk and dry densities of the frozen soil, respectively, and w_u and w_i are the unfrozen and frozen water contents, respectively.

Utilizing the specific heat of a material described as the ratio of its heat capacity to that of water in degrees Celsius, volumetric heat capacities for mineral unfrozen and frozen soils can be estimated as:

$$c_{vu} = \left(\frac{\rho_d}{\rho_w}\right)\left(0.17 + 1.0\frac{w}{100}\right)c_{vw} \quad (2.13)$$

$$c_{vf} = \left(\frac{\rho_d}{\rho_w}\right)\left[\left(0.17 + \frac{1.0w_u}{100}\right) + 0.5\left(\frac{w - w_u}{100}\right)\right]c_{vw} \quad (2.14)$$

where c_{vw}=4.187 MJ/m^3 · °C and ρ_d and ρ_w are the unit mass of the dry soil and water, respectively. The specific heats 0.17, 1.0, and 0.5 correspond to mineral soil, water, and ice, respectively (Andersland & Ladanyi, 2004). For organic soils (peat), replace the specific heat for mineral soils (0.17) with that for organic soils (0.4).

2.2.3.2 Thermal Conductivity

Heat conduction in soils involves a transfer of kinetic energy from molecules in a warm part of the mass to those in a cooler part. Considering a prismatic element of soil with a cross-section area A, the rate at which heat is transferred by conduction is given in the form

$$Q = -k_u A \frac{dT}{dx} \quad (2.15)$$

and

$$q = \frac{Q}{A} - k_u \frac{dT}{dx} = k_u i \quad (2.16)$$

Where Q/A = q is the rate of heat flow per unit area (J/m^2 · s), k_u is the unfrozen thermal conductivity (J/s · m · K or W/m · K), $dT/dx = i$ is the thermal gradient (°C/m), and A is the area (m^2). The minus sign indicates heat flow from high to low temperature. The quantities in Eq.

(2.15) are illustrated in Fig. 2.9. The soil element must be large enough by comparison to represent a homogeneous soil.

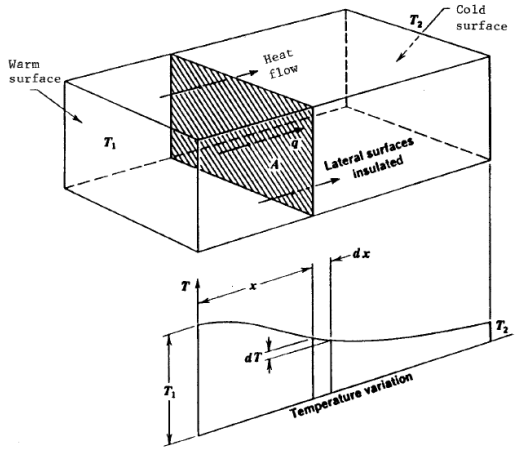

FIGURE 2.9 Heat flow through a soil element.

The method produced by Johansen (1975) and compiled in Table 3 applies to unfrozen and frozen mineral soils (Andersland & Ladanyi, 2004). This method is a interpolation between dry and saturated values.

TABLE 2.3 Method for Calculating the Thermal Conductivity of Mineral Soils (Andersland & Ladanyi, 2004)

$k = (k_{sat} - k_{dry})\ K_e + k_{dry}$			(a)	Main equation
	Natural	$(0.137\gamma_d + 64.7)/(2700 - 0.947\gamma_d)$	(b)	Dry conductivity
	Crushed	$0.039n^{-2.2}$	(c)	
Unfrozen	Coarse	$0.7 \log S_r + 1.0$	(d)	
	Fine	$\log S_r + 1.0$	(e)	Kersten number
Frozen		S_r	(f)	
Unfrozen		$0.57^n k_s^{1-n}$	(g)	Saturated conductivity
Frozen		$2.2^n k_s^{1-n} \cdot 0.269^{w_u}$	(h)	
		$7.7^q \cdot 2.0^{1-q}$	(i)	Particle conductivity
	$q < 0.20$ Coarse	$7.7^q \cdot 3.0^{1-q}$	(j)	

The principal equation for calculating thermal conductivity of soil k is:

$$k = (k_{sat} - k_{dry})K_e + k_{dry} \tag{2.17}$$

where k_{sat} and k_{dry} are the saturated and dry thermal conductivities, respectively. The kersten number K_e was defined previously. For dry natural soils, the following is the semi-empirical equation for k_{dry} (Johansen, 1975).

$$k_{dry}\left(\frac{W}{m \cdot K}\right) = \frac{0.137\rho_d + 64.7}{2700 - 0.947\rho_d} \pm 20\% \tag{2.18}$$

where ρ_d is the dry density (kg/m^3) and the solids density is 2700 kg/m^3. Johansen (1975) noted that crushed rock materials provided higher thermal conductivity amounts:

$$k_{dry}\left(\frac{W}{m \cdot K}\right) = 0.039n^{-2.2} \pm 25\% \tag{2.19}$$

where n is the soil porosity. For saturated soils, Johansen (1975) recognized that changes in microstructure had a little effect on thermal conductivity. He suggested the use of a geometric mean equation founded on thermal conductivities of the soil components and their corresponding volume fractions. For saturated unfrozen soils, this provides

$$k_{sat} = k_s^{1-n} k_w^n \tag{2.20}$$

and for saturated frozen soils including some unfrozen water w_u,

$$k_{sat} = k_s^{1-n} k_i^{n-w_u} k_w^{w_u} \tag{2.21}$$

Applying the thermal conductivity of ice, k_i= 2.2 W/m · K and k_w=0.57 W/m · K Eq. (2.21) reduces to

$$k_{sat} = k_s^{1-n}(2.2)^n(0.269)^{w_u} \tag{2.22}$$

Johansen (1975) proposed the use of a geometric mean equation to calculate k_s:

$$k_s = k_q^q k_0^{1-q} \tag{2.23}$$

where k_q and k_0 are the thermal conductivities of quartz and other minerals, respectively, and q is the quartz fraction of the total solids content. Johansen (1975) applied k_q = 7.7 W/m · K and k_0 = 2.0 W/m · K. For coarse grained soils with a quartz content of less than 20%, Johansen (1975) adopted k_0 = 3.0 W/m · K to account for the presumable mineral makeup of such soils (Andersland & Ladanyi, 2004).

Johansen (1980) suggested the use of Eq. (2.24) for the determination of the thermal conductivity k_f of frozen soil if the unfrozen water content w_u has to be taken into account:

$$k_f^1 = k_f + \left(k_u - k_f\right) \cdot \frac{w_u}{w} \tag{2.24}$$

Where k_u and k_f are the thermal conductivities unfrozen and frozen, respectively, and w is the water content.

2.2.3.3 Latent Heat of Fusion

The quantity of heat energy consumed when a unit mass of ice is transformed into a liquid at the melting point is established as its latent heat of fusion. The same amount of heat (333.7 kJ/kg) is released when the water is turned into ice with no difference in temperature (Andersland & Ladanyi, 2004). The volumetric latent heat of fusion of soil, L (kJ/m^3), is defined as:

$$L = \rho_d L' \frac{w - w_u}{100} \tag{2.25}$$

Where, L´= 333.7 kJ/kg is the mass latent heat for water, ρ_d (kg/m^3) is the dry soil density, w is the total water content, and w_u is the unfrozen water content (percentage dry mass basis) of the frozen soil. For those soils (sands and gravels) with little or no unfrozen water, the w_u term will be very small. For many practical problems, the assumption that w_u is zero will give acceptable L values for estimation purposes (Andersland & Ladanyi, 2004).

Frozen soils are far from being a uniform material. They are better described as a multi-phase system; their thermal properties are a direct function of the particles themselves and their composition. For example, the water ice phase configuration depends on the particle mineral structure, specific surface area of the particle, presence of solutes, and the temperature. In addition to the above soil pores with free and bound water freezes at various negative temperatures (Smoltczyk, 2003).

2.2.4 Closed-Form Solution

As the ground freezes phase conversion of water to ice starts and therefore shifts in thermal conductivity and heat capacity occur as well; this complicates the numerical resolution of this heat conduction problem. So, in order to overcome these difficulties, assumptions allow design computations for the amount of energy to be removed for freezing, the time expected for freezing, and the refrigeration plant capacity or size (Andersland & Ladanyi, 2004).

These assumptions include the next:

1. Isotherms move so slowly that they resemble those for steady-state conditions. This assumption is not strictly correct, but the practice has shown that this postulate is satisfactory for engineering design (Sanger & Sayles, 1979).

2. The radius of unfrozen soil influenced by freeze pipe superficial temperature can be expressed as a multiple of the frozen soil radius predominating at that time.

3. The total latent and sensible heat can be expressed as a specific energy which, when multiplied by the frozen soil volume, gives the same total as the two quantities calculated independently (Sanger & Sayles, 1979) .

Sanger & Sayles (1979) suggested three stages for the estimates concerning vertical pipes: (I) the ice soil columns are increasing around separate refrigeration pipes; (II) separate frozen soil columns have fused to form a continuous wall with cross-section thickening conditioned with time; and, (III) walls formed by two or more rows of frozen soil columns have joined into a single wall that is increasing in thickness with time (Andersland & Ladanyi, 2004).

2.2.4.1 Single Freeze Pipe (Andersland & Ladanyi, 2004)

Considering the Fourier Equation (Jaeger & Carslaw, 1959) of steady state radial heat flow to the refrigeration pipe in two dimensions:

$$\frac{d^2v}{dr^2} + \frac{1}{r}\frac{dv}{dr} = 0 \tag{2.26}$$

where v is the temperature at radius r. Integration of Eq. (2.26) and substitution of the boundary conditions ($v = v_s$ at $r = r_0$, $v = 0$ at $r = R$, and $v = v_0$ at $r = R_A$) provides

$$v_1 = \frac{v_s}{\ln\left(\frac{R}{r_0}\right)} ln\frac{R}{r_1} \quad for\ r_0 < r_1 < R \tag{2.27}$$

$$v_2 = \frac{v_0}{\ln\left(\frac{R_A}{R}\right)} ln\frac{r_2}{R} \quad for\ R < r_2 < a_r R \tag{2.28}$$

where v_1 is the temperature at radius r_1 in the frozen cylinder, v_2 the temperature at radius r_2 in the unfrozen region, R the radius to the frozen-unfrozen soil interface, r_0 the radius of the freeze pipe, and a_rR is defined in Fig. 2.10a.

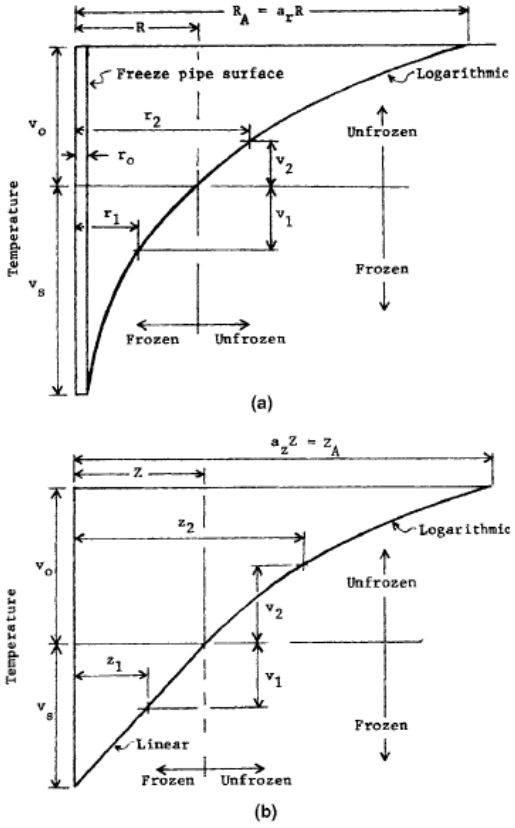

FIGURE 2.10 Temperature distribution curves (a) single freeze pipe (b) flat wall (Sanger & Sayles, 1979).

The temperature $v_s = (T_s\text{-}T_0)$ is the difference between the freeze pipe surface temperature (T_s) and the freezing point of water (T_0). The temperature $v_0 = (T_g\text{-}T_0)$ is the difference between the ambient ground temperature (T_g) and the freezing point of water. For practicality, use absolute

values of v_0 and v_s. A possible temperature distribution through stage I is represented in Fig. 2.10a.

The ratio $a_r = R_A/R$ denotes the radius of temperature impact of the refrigeration pipe in the unfrozen soil.

The total energy obtained from the ground to freeze a soil column of radius R (Fig. 2.11) involves: (1) sensible heat associated in cooling the soil column from ambient ground temperature to the freezing point of water (normally, 0 °C); (2) latent heat of the frozen soil; (3) sensible heat in cooling the frozen soil from 0 °C to its temperature at radius r_1; and finally, (4) sensible heat for freezing the unfrozen soil outside the frozen column.

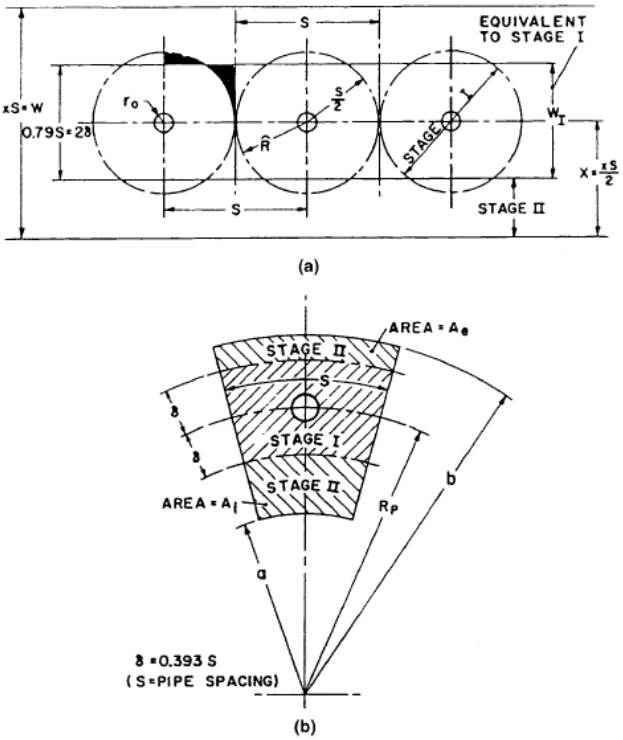

FIGURE 2.11 Two stages assumed for thermal computations: (a) straight wall (b) curved wall (Sanger & Sayles, 1979).

This energy (Q1) for stage I at a time in agreement with a frozen radius R is

$$Q_I = \pi(R^2 - r_0^2)L + \pi(R^2 - r_0^2)c_{vu}v_0 + \frac{2\pi c_{vf}v_s}{\ln\left(\frac{R}{r_0}\right)}\int_{r_0}^{R} r_1 \, ln\frac{R}{r_1} dr_1 + 2\pi c_{vu}v_0 \int_{R}^{R_A}\left[1 - \frac{ln\left(\frac{r_2}{R}\right)}{ln\left(\frac{R_A}{R}\right)}\right] r_2 \, dr_2 \quad (2.29)$$

Integration, combining terms, and neglecting r_0^2, in comparison with R_2 provides

$$Q_I = \pi R^2\left[L + \frac{a_r^2 - 1}{2lna_r}c_{vu}v_0 + \frac{c_{vf}v_s}{2ln\left(\frac{R}{r_0}\right)}\right] \quad (2.30)$$

where L is the volumetric latent heat of soil, c_{vf} and c_{vu} the volumetric heat capacity for the frozen and unfrozen soil, respectively. A value of $a_r = R_A/R = 3$ is frequently employed in computations.

Sanger & Sayles (1979) recorded that the sensible heat obtained from unfrozen soil outside the frozen soil column is approximately 30% of the total and should be incorporated in every thermal calculation. The time (t_1) needed to freeze a soil column of radius R (Sanger and Sayles 1979) utilizes the case that the rate of heat flow through the freeze pipe wall must be enough to support growth of the cylinder.

Implementing the heat conduction law to the frozen soil column provides

$$t_I = \frac{R^2 L_1}{4k_f v_s}\left(2ln\frac{R}{r_0} - 1 + \frac{c_{vf}v_s}{L_1}\right) \quad (2.31)$$

where

$$L_I = L + \frac{a_r^2 - 1}{2lna_r}c_{vu}v_0 \quad (2.32)$$

and k_f is the thermal conductivity of the frozen soil.

The needed refrigeration plant capacity (size) for a design is defined by the soil volume to be frozen, the soil thermal parameter, time available for freezing, size and arrangement of the

freezing pipes, the ambient ground temperature, coolant temperature, and groundwater seepage velocity.

Assuming the nonexistence of groundwater flow and using the derivative of the energy Q_I for stage I (transient case) with respect to time it is possible to obtain the power (load) expected for each unit length of freeze pipe when the freezing soil columns are growing:

$$P_I = \frac{dQ_I}{d_t} = \frac{2\pi k_f v_s}{ln\left(\frac{R}{r_0}\right)} \text{ (W/m)} \tag{2.33}$$

The rate of energy extraction (P_I) could be displayed in tons of refrigeration per unit length of freeze pipe, where 1 ton of refrigeration equals 200 Btu/min or 3.5169 kJ/s.

Standard curves of time, freezing radius, energy per unit length, and power needed per unit length of freeze pipe are presented in Fig. 2.12.

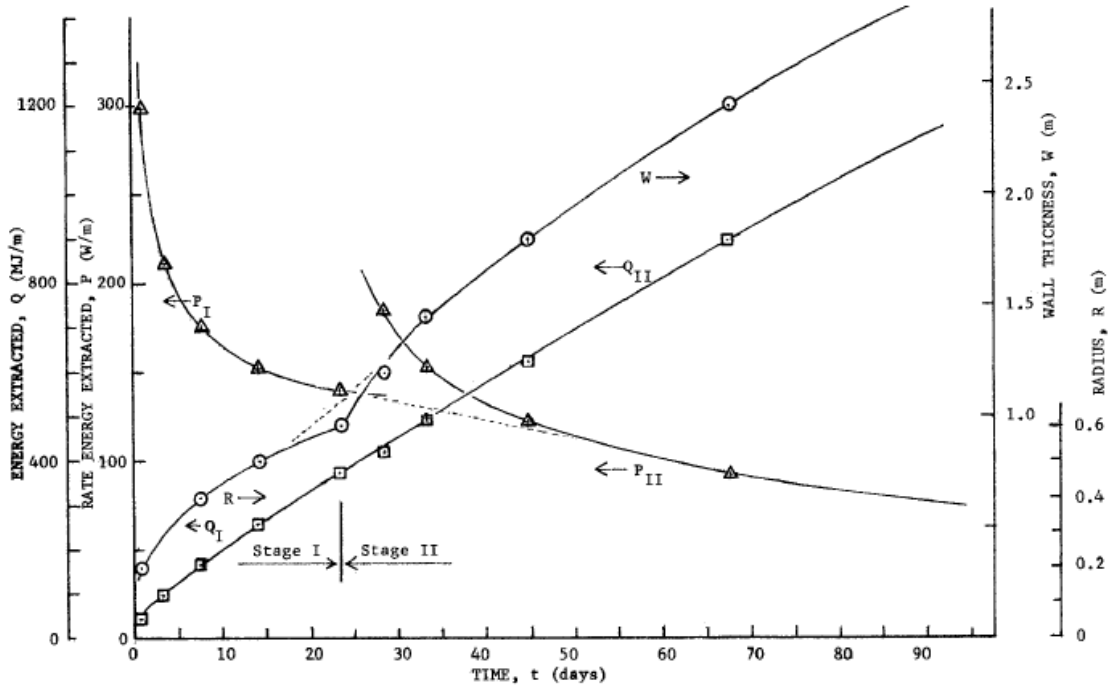

FIGURE 2.12 Straight wall: time versus radius R, wall thickness W, energy extracted Q, and rate energy extracted P (Sanger & Sayles, 1979).

2.2.4.2 Wall Formation

Once the frozen soil columns start to merge (Fig. 2.10a) with an equivalent wall thickness of $W_I = 0.79S = 2\delta$ (Fig. 2.11a) the stage I ends.

The wall thickness increases while more heat is removed. Depending on the geometry (distribution) of the freezing pipes required by the project, computations vary for straight and curved walls.

Examine first the energy Q_{IIF} removed per unit wall area in thickening one side of a straight wall. The latent and sensible heat extracted from the soil is portrayed here:

$$Q_{IIF} = ZL + \frac{1}{2}c_{vf}v_sZ + Zc_{vu}v_0 + c_{vu}\int_Z^{a_zZ}(v_0 - v_2)dz_2 \tag{2.34}$$

where Z is the distance from the stage I wall face to the freezing plane and z_2 is the distance from the freeze pipes to a point in the unfrozen soil. The temperature distribution curve for the straight wall with a supposed linear disparity in the frozen soil and a logarithmic curve in the unfrozen zone are shown in Fig. 2.10b.

Andersland & Ladanyi (2004) reported that theoretically, these curves are wrong functions. Sanger & Sayles (1979) declared that field measurements reveal that the assumed curves (Fig. 2.10b) are satisfactory for design. Substituting the relationship

$$v_2 = \frac{v_0}{lna_z}ln\frac{z_2}{Z} \tag{2.35}$$

Into Eq. (2.34) and integrating provides

$$Q_{IIF} = Z\left(L + \frac{1}{2}c_{vf}v_s + c_{vu}v_0\frac{a_z - 1}{lna_z}\right) = ZL_F \tag{2.36}$$

where $a_z = Z_A/Z$ in Fig. 2.10b, L_F is the equivalent latent heat of fusion for flat walls, and the other terms are as specified earlier.

Khakimov (1957) observed in the field that a_z ranges from 4.5 to 5.0, with a suggested value of 5. For both surfaces of the wall, apply $Q_{IIF} = 2ZL_F$.

By assuming once again steady-state heat conduction at any given moment it is possible to calculate the time t_{IIF} expected to increase Z. The rate of heat flow to both planes of the wall per unit area is

$$P_{IIF} = \frac{dQ_{IIF}}{dt} = 2k_f \frac{\Delta v}{\Delta z} = 2k_f \frac{v_s}{Z} \tag{2.37}$$

And the rate of heat removal per increase in total wall thickness is

$$\frac{dQ_{IIF}}{dz} = 2\left(L + \frac{1}{2}c_{vf}v_s + c_{vu}v_0 \frac{a_z - 1}{lna_z}\right) = 2L_F \tag{2.38}$$

Joining Eqs. (2.37) and (2.38) provides

$$\frac{dt}{dz} = \frac{ZL_F}{K_f v_s} \tag{2.39}$$

During stage II, the frozen wall surface goes from, Z = ½ W_I to Z = ½ W (Fig. 2.11a), producing

$$t_{IIF} = \int_{\frac{W_I}{2}}^{\frac{W}{2}} \left(\frac{L_F}{k_f} v_s\right) Z dZ = \frac{L_F}{2k_f v_s}\left(\frac{w^2}{4} - \frac{w_I^2}{4}\right) = \frac{L_F S^2}{8k_f v_s}(x^2 - 0.62) \tag{2.40}$$

where x = W/S and W_I = 0.79 S.

For curved walls and stage I, the same equations are used in design. For stage II (Fig. 2.10b), similar equations can be developed for energy requirements and the time for increase in wall thickness (Andersland & Ladanyi, 2004).

2.2.5 Finite Element (Temp/w)

Temp/w is a commercial software made in Canada that helps generate models of thermal variations due to climate alterations or due to the construction of any infrastructure that interacts with the soil. It can be used for systems exposed to freezing and thawing temperature variations (Geo-slope International Ltd, 2014).

Natural soil is very heterogeneous and anisotropic. Consequently, a numerical solution when modeling the flow of heat in the ground can be quite complicated. Boundary conditions frequently vary with time and occasionally the correct boundary condition can be part of the solution, as is the case with artificial ground freezing. Moreover, sometimes the boundary condition cannot be precisely established at the origin of a study.

Temp/w can be used in conjunction with Seep/w, another software by the same manufacturer to model the influence of seepage on heat transfer. Generally speaking, it is possible to model heat transfer through porous or solid material with moisture or a lack thereof. It is useful to estimate an appropriate number of freezing pipes, pipes' location, energy flux demands, freezing time demands, and the size of frozen zones in artificial ground freezing projects. Nevertheless, the effect of seepage was not considered in the present study.

The amount of heat extracted depends on the ground temperature, coolant temperature, coolant flow type (rate), and freezing pipe geometry.

In this research, the analysis was approached using a convective heat transfer boundary condition applied to a single node in end view to simulate the circumstances present when a single freezing pipe is in a vast area. The advantage of this strategy is that it is not necessary to assume the freeze pipe wall temperature.

Every finite element analysis has three principal parts. The first is discretization which is when the domain is divided into a small areas called elements. The second part is defining and selecting material properties. The third is defining and implementing boundary conditions.

2.2.5.1 Geometry and Meshing

The concept behind the finite element numeral method is to subdivide a given continuum into small pieces, describing the performance of every single piece and next reconnecting all the pieces to reproduce the performance of the continuum as a total.

Meshing (discretization) is one of the critical conditions of finite element modeling, as mentioned before. It includes establishing geometry, distance, area, and volume dealing with the physical dimensions of the domain.

2.2.5.2 Material Models and Properties

To describe the soil material performance we can use the properties alike in situ volumetric water content, frozen and unfrozen thermal conductivity and frozen and unfrozen volumetric heat capacities. Temp/w has three main material models that you can choose, they are: the thermal model, the convective thermal model, and an interface model. In this research a convective thermal model was used.

2.2.5.3 Boundary Conditions (Artificial Ground Freezing Application)

In finite element analysis designating conditions on the boundaries is defined as "boundary valued" problems; being able to manage the conditions on the boundaries is an influential feature of this type of analysis.

The solution to this kind of problem is strictly related to the boundary conditions; without these conditions, there is no solution.

All finite element equations at the last stage preceding the solution of the unknowns are reduced to:

$$[\mathrm{k}]\{x\} = \{A\} \tag{2.41}$$

where:

[k]= a matrix of coefficients related to geometry and material properties

$\{x\}$= a vector of unknows which are often called the field variables, and

$\{A\}$= a vector of actions at the nodes.

For a thermal analysis the equation is:

$$[\mathrm{k}]\{T\} = \{Q\} \tag{2.42}$$

where:

$\{T\}$= a vector of the temperature at the nodes, and

$\{Q\}$= a vector of the heat flow quantities at the node.

Solving for the temperatures at each node is fundamental because it represents the main unknowns. To obtain a solution for the finite element equation, the unknowns are estimated relative to the T or Q values defined at the nodes. It is only possible to define either the T or Q at a node. T or Q values represent the boundary conditions without defining T or Q; a solution is not achievable.

2.2.5.4 Analysis Type

There are two fundamental types of finite element thermal analyses: steady-state and transient. In the steady-state analyses, the time element of the problem is removed and this simplifies the equation to solve; moreover, the term "state" refers to the temperature and heat flow rates in thermal analysis. When these two parameters reach a steady value throughout the whole geometry, it means that they will be in that state permanently.

On the other hand, a transient analysis is transforming because it reflects how long the soil needs to react to the user boundary conditions. Transient analysis was used in this research.

3. Artificial Ground Freezing Test Program

3.1 Scope

The primary objective of the program was to examine the feasibility of an active artificial ground freezing method in freezing soil surrounding a steel pipe pile segment. The outcome of this test program may improve the stability of the foundation system in the warming permafrost during climatic cycles that occur as a result of natural seasons, more specifically during the transition of winter to summer and summer to winter.

The study also examined the usefulness of a full-size test and procedure to estimate design considerations for the amount of energy to be removed, the time needed for freezing and the cooling plant size.

3.2 Sample Preparation

The particle size distribution was intended to be characteristic of soils found in the northern territories which at the same time represents a genuine standard of reference of a well identified material. The chosen soil was silty sand which at the University of Alberta has been called Devon Silt and has been widely referenced in various research Sego, Shultz, & Banasch (1982), Hutchinson (1989), Hivon (1993), Biggar (1993); this soil is available in the City of Devon, about 40 km from the City of Edmonton.

The soil sample was prepared with a proportion by weight, i.e. 2:1 mixture of Devon Silt and Silica Sand (Biggar, 1993).

3.3 Description of Apparatus

3.3.1 The Consolidation Loading Frame

The load frame was used in the consolidation stage and is a constant load test apparatus that operates by a compressed air system (Fig. 3.1). The air transmits the pressure to a diaphragm inside a cylinder made of an engineered metal called the bellofram or jack (here on in referred to as the jack). Physically it is a structural metal frame form with 150 mm wide channels located at the highest and at the lowest points, attached by four 33 mm thread rods that serve as pillars and at the same time adjust the height of the load to be used. To adjust the height of the test, nuts are

used. The jack was connected to the upper channel and used to apply the desired load to the load plate being established by a pressure regulator. One of the advantages of this constant load system is the capability to maintain the selected load with not observable variability in the pressure desired. A 24.6 mm steel sphere bearing was positioned between the jack ram and the load plate to guarantee the correct axial load application on the load plate. This device is similar to the equipment used by Biggar (1993) (see photo in Appendix B).

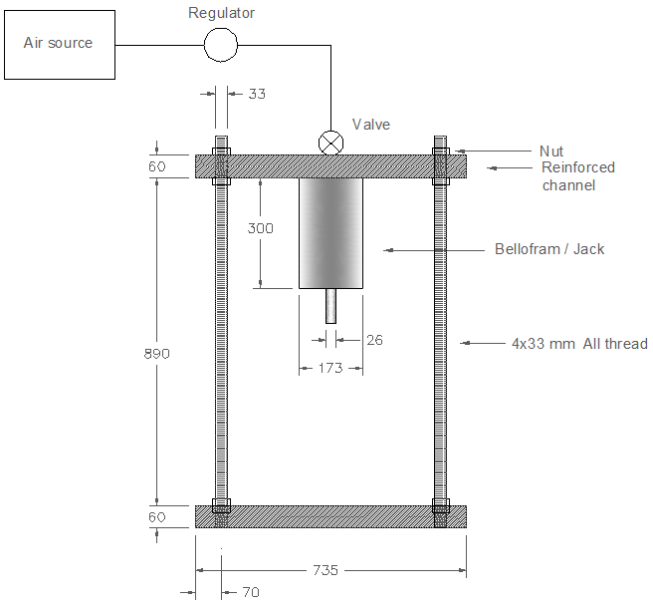

FIGURE 3.1 Loading frame for consolidation. Unit: mm.

3.3.2 Load Plates (Caps) and Adapter

To ensure an even density and saturation from consolidation tests, load plates were needed at the top of the sample (Hutchinson, 1989). The load plates and adapter were manufactured in aluminum and steel to guarantee that they can withstand the applied loads and are suitable for the inner space of the test cell. Geotextile was placed between the area of the load caps and the soil sample, allowing possible drainage in a small gap between the cell walls and the plates.

Two types of load plates were created, as can be clearly seen in Fig. 3.2 and Fig. 3.3, each for a different segment of the pile, emulating the installation process (see photos in Appendix B).

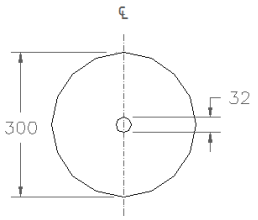

Plan view

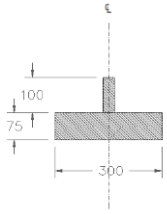

Section view

FIGURE 3.2 Load plate 1. Unit: mm.

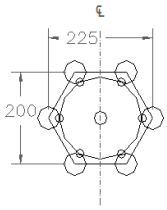

Plan view adapter

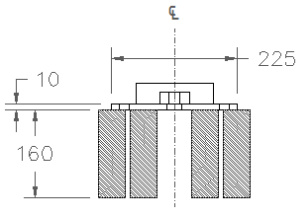

Section view adapter

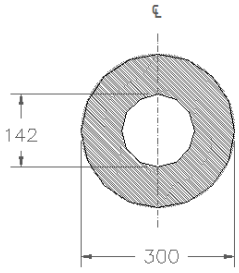

Plan view plate (thickness 5 mm)

FIGURE 3.3 Load plate 2 and adapter. Unit: mm.

3.3.3 Test Cell

The test cell is an engineered metal container with a double wall (Fig. 3.4). This double wall creates two coaxial holes, each one having a different diameter. The center space was filled with the soil sample. The circular external area was filled with a mixture of water and ethylene glycol approximately reaching the top; also, a copper coil was situated in this gap where water and ethylene glycol were circulated from temperature bath (TB2) equipment (within ±0.5 °C) at a constant flow rate in order to transfer this constant temperature to the soil sample (Biggar, 1993) (see photo in Appendix B).

During the consolidation and freezing stage, a PVC baseplate was used at the bottom of the test cell.

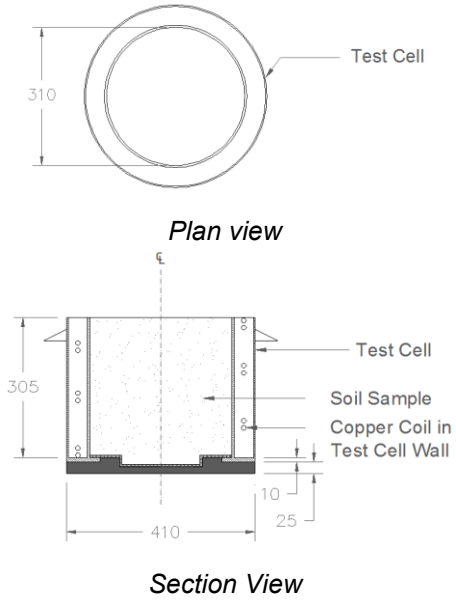

FIGURE 3.4 Test cell. Unit: mm.

3.3.4 Test Pile Segment

A schematic diagram of the pile is shown in Fig. 3.5. The pile selected consisted of a hot-dip galvanized steel screw micropile with a welded helix at the lower section, produced by Krinner Canada. The serial number was KSF M 140 x2100-M24 with a nominal length of 2100 mm, a tube diameter of 140 mm, weight of 26 kg and a thickness of approximately 4 mm (Krinner the ground screw, 2018) (see photos in Appendix B).

For the research, 2 types of pile segments were used, one with the straight part and the other with the threaded portion of approximately 40 cm in length and 14 cm in diameter. Each was welded at the bottom to create a sealed container. A layer of silicon glue was added to the interior bottom part of each pile to guarantee an even better seal.

It must be mentioned that for each pile segment, there is a different procedure of installation inside of the test cell.

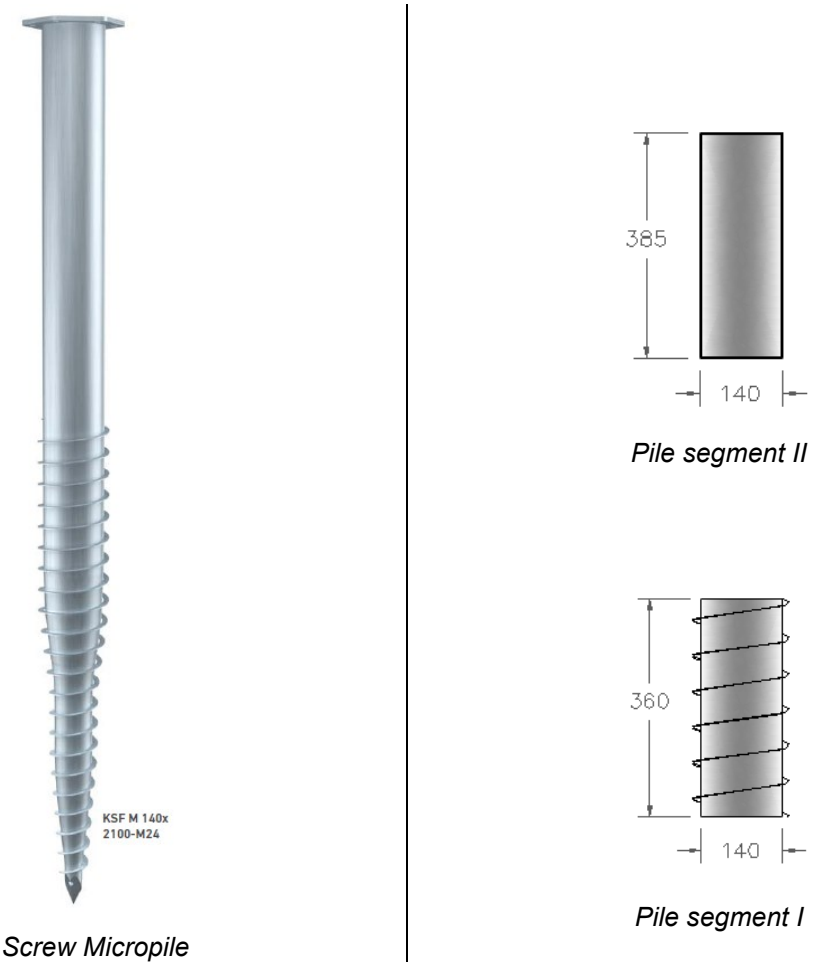

Screw Micropile

Pile segment II

Pile segment I

FIGURE 3.5 A model of screw micropiles and test pile segments. Unit: mm. Both segments are sealed at the base.

3.3.5 Temperature Bath

The temperature bath consisted of a refrigerated and heating bath circulator unit in a stainless-steel box that provides control over the temperature requirements for the experiment, with a

temperature range from -25 to 100 °C and stability of ±0.01 °C. The unit used was an Isotemp from Fisher Scientific that comes with a heating and refrigerated bath combination; the model used was 1028 with 28 liters capacity in the reservoir for a mixture of water and ethylene glycol used as antifreeze coolant. This unit circulates the coolant fluid at a constant flow velocity of 15 L/min (Fisher Scientific, 2005). A scheme is shown in Fig. 3.6 (see photos in Appendix B).

Two temperature baths were used in this research, TB1 was connected to the copper coil inside of the pile segment and TB2 to the test cell, to reach the desired temperature during the homogenization stage and to achieve freezing conditions during the trials. The baths were verified for each temperature considered.

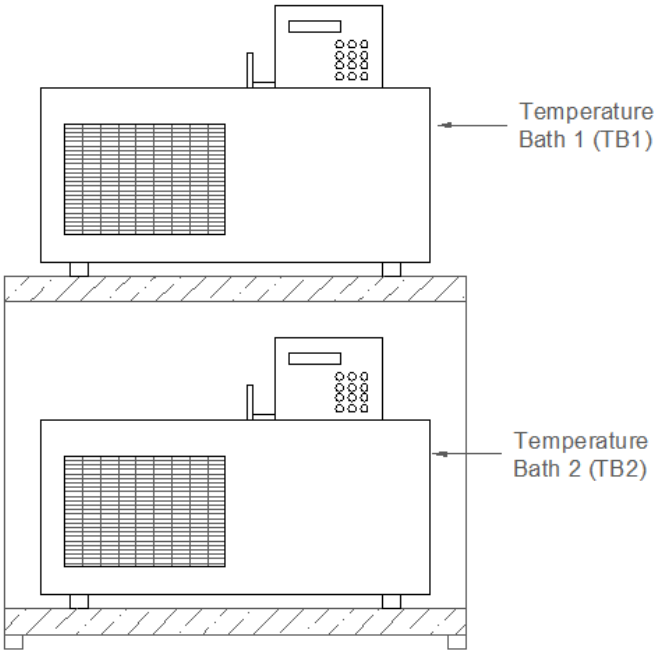

FIGURE 3.6 Temperature baths 1 and 2.

3.3.6 Instrumentation

Linear displacement sensors SLS 130 and SLS 190 manufactured by Penny & Giles were used to measure the ground deformation during consolidation tests. These sensors provide a stroke length of 200 mm and 350 mm respectively, with typical independent linearity of ±% 0.07-0.15. The sensor's body was connected in a bracket attached to a laboratory metal base supported on the floor during the consolidation stage. Therefore, the movement of the jack ram was registered, as shown in Fig. 3.7 (Penny Giles , 2012a) and Fig. 3.8 (Penny Giles , 2012b).

FIGURE 3.7 SLS130 Linear displacement sensor (Penny Giles , 2012a).

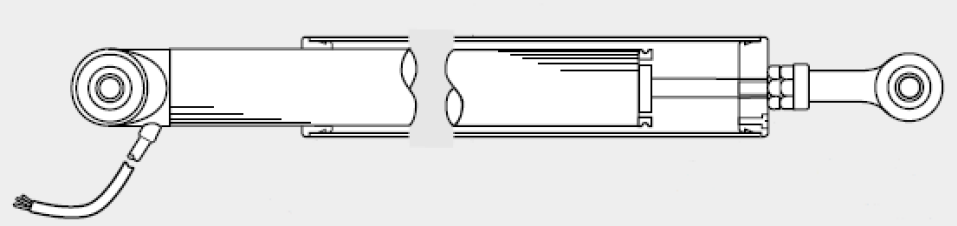

FIGURE 3.8 SLS190 Linear displacement sensor (Penny Giles , 2012b).

The Instrument Society of America (ISA) identifies the thermocouple type by letter designations, which are associated with their capabilities, recommended temperature ranges, and limitations.

Thermocouples sensor type T (Copper (+) versus nickel -45% copper (-)) were used to measure temperatures in different locations during the entire set up of the experiments. This type of sensor is designed to be resistant to corrosion in a moist atmosphere and is deemed appropriate for sub-zero temperature measurements with a temperature range of -200 to 370 °C (Park & Hoersch, 1993), with a standard limit of error (Above 0 °C) in the order of ± 1 °C or 0.75%. (Optimum Instruments Inc, 2019). (see photos in Appendix B).

3.3.7 Data Logger

The outputs of all sensor thermocouples and linear displacements were recorded using a Campbell Scientific datalogger CR3000 that stored electrical signals. According to specifications, this data logger is suitable for use between -25 °C to 50 °C in a non-condensing environment (Campbell Scientific Inc, 2015). During all the tests, the device was located in a constant and controlled room temperature of 21 °C ± 1 °C. Recalibrations are recommended

every two years. Given that this unit was recently acquired by the University of Alberta, recalibration was not necessary (shown in Fig. 3.9) (see photo in Appendix B).

The data logger was connected to a laptop to record all of the outcomes. The manufacturing company provides the acquisition system with software that permitted both the setting of the recording time interval (every 5 seconds) and how the data will be arranged for the following analyses.

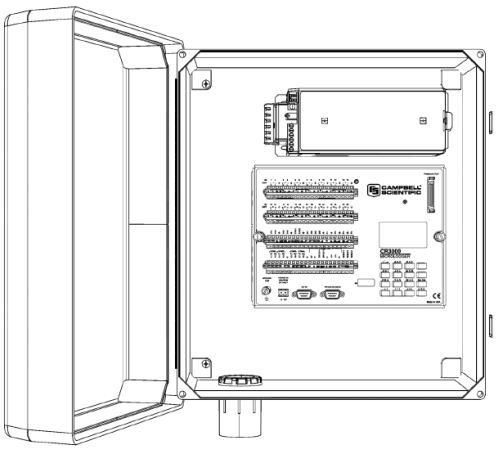

FIGURE 3.9 Data logger model CR3000 (Campbell Scientific Inc, 2015).

3.3.8 Cold Room

The cold room was a cooler 2.35 m wide, 4.8 m deep, and 2.5 m high. The temperature of the cold room was calibrated to 0 °C, but because it was a cooler, it was subjected to four fan cycles, every day. During the research, the idea of the cold room was to maintain the temperature no higher than 30 °C to keep the water content; in essence, a combination of high humidity and low temperatures helped to decrease moisture losses as reported by Clayton (1995) (see photo in Appendix B).

3.3.9 Copper Coil

A 9.9-m long copper coil of 0.375 inch (9.525 mm) in diameter was used to fabricate a suitable heat transfer by convection from the ethylene glycol that the temperature bath (TB1) circulated and the ethylene glycol (bought in Canadian Tire store) inside of the pile, with dimensions as shown in Fig. 3.10. The copper coil was made from a straight piece of pipe with closed fittings at

the ends, and later it was filled with refined sea salt making sure there was no gap inside, thereby creating the desired form and size of the coil. At the end sea salt was removed (see photo in Appendix B).

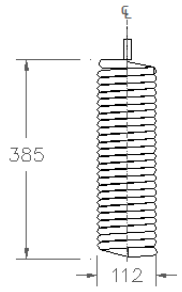

FIGURE 3.10 Copper coil. Unit: mm.

3.4 Test Procedure

Fig. 3.11 shows a schematic of the apparatus setup used in the freezing stage of the research.

TB1 was connected to the copper coil inside of the pile segment and TB2 to the test cell, to reach the desired temperature during the homogenization stage and to achieve freezing conditions during the trials. As mentioned above, the soil mixture was chosen to be comparable to the soil in the northern territories as cited by Hutchinson (1989).

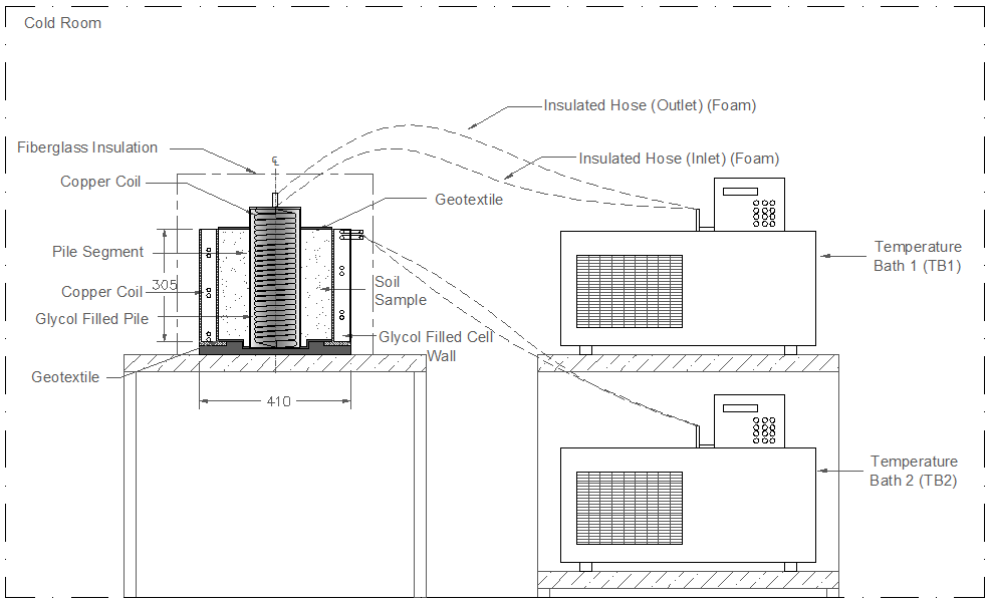

FIGURE 3.11 Complete schematic of the apparatus setup used in the freezing stage. Unit: mm

3.4.1 Dry Soil Preparation

The silty sand from Devon was dried in an oven for 24 hours at a constant temperature of 110 °C to remove any natural water content. Then the material was ground in a rock crusher miller machine and shacked through a No. 10 sieve to break up the soil pieces. Subsequently, it was combined in a 2:1 proportion by weight, 2 being the Devon silt and 1 the silica sand.

3.4.2 Cell Preparation

It is highly recommended to clean the test cell before each use since any dirt or imperfections can negatively affect the data collection. Once the cell was clean, geotextile was placed at the bottom to allow better drainage, if this was to occur. Next, the walls of the cell were marked to indicate the correct location for the thermocouples either using the sticks (35% w) or without them (20% w), depending on the water content of the soil sample.

3.4.3 Wet Soil Preparation

In order to create a homogenous soil sample, the dry Devon silt and the silica sand were placed in a heavy-duty soil mixer, with a weight of 2:1 respectively; after, tap water was added to the dry soil mixture in approximate quantities to make up a water content of 35% or 20%, depending on what is being evaluated. Records were kept of every proportion of weight during the mixing preparation to calculate the density of the soil sample before the consolidation stage.

Next, the wet soil mixture was placed in the test cell keeping the surface of the soil approximately flat by filling evenly using a rod to remove air pockets. If the preparation was done with soil with a water content of 20%, the thermocouples were each located at the middle of each layer with the layer corresponding to about1/3 of the cell's height; if the preparation was done with soil with a water content of 35% the placement of the thermocouples was done after the consolidation step, using sticks for an accurate location of the sensors. Following this, the geotextile was placed between the load cap and the soil sample for the consolidation stage. Finally, the test cell was left in the cold room to preserve moisture content.

3.4.4 Soil Consolidation (at Room Temperature)

First, the consolidation load cap was centered on top of the test cell. In the loading frame, the test cell was placed under the consolidation jack with a 24.6 mm diameter bearing to guarantee the correct axial load. Subsequently, the linear displacement sensors were secured in a bracket attached to a laboratory metal base supported on the floor. Next, the data logger was connected with the purpose of recording and monitoring the time, load, and deformation.

Afterward, a load of 80 kPa was applied. It should be noted that when the soil sample requires 35% water content, it is highly recommended to apply the pressure in stages doubling the load each time; if this is not done the deformation will be so fast that the soil could spill over the edges. Ultimately, the load and deformation were monitored until 95% consolidation refer to (Fig. 3.12 and Fig. 3.13). Two types of consolidation setup were adopted to evaluate pile installation, setup I was for the pile threaded segment (pre-drill installation) and the setup II was for the pile straight segment (correct installation).

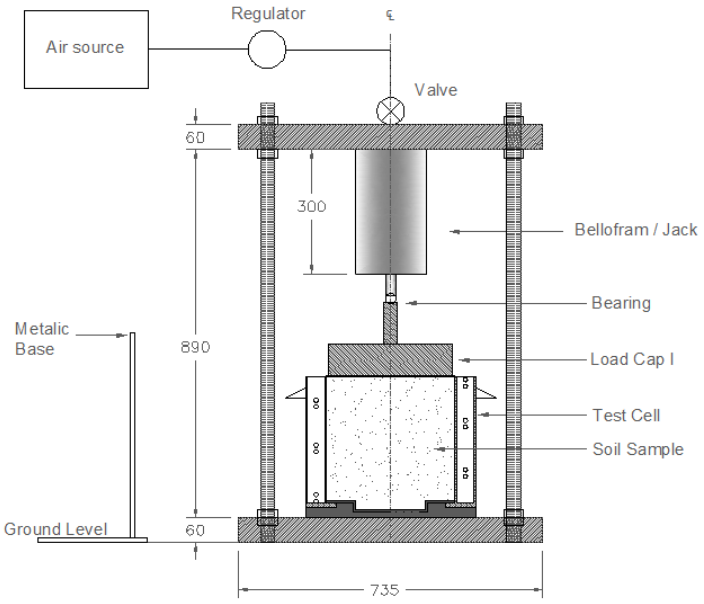

FIGURE 3.12 Consolidation setup I. Unit: mm.

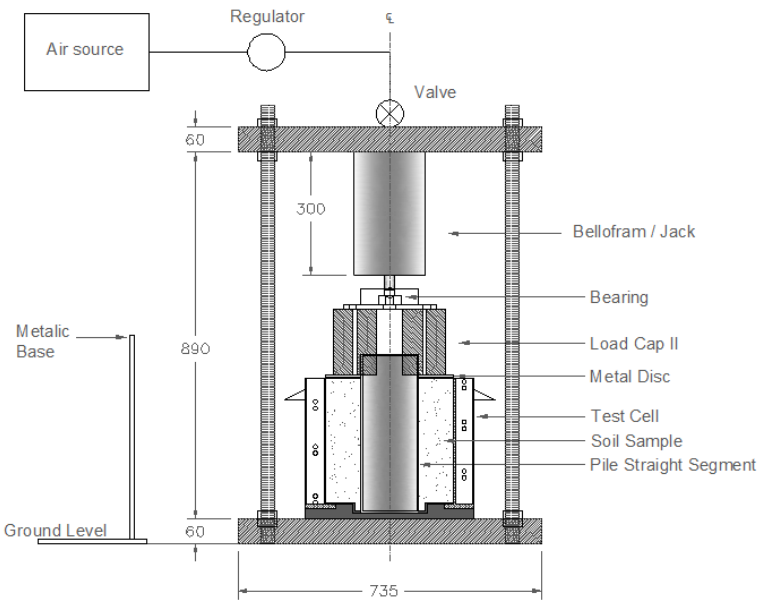

FIGURE 3.13 Consolidation setup II. Unit: mm.

3.4.5 Freezing

First, the data logging for the previous step was stopped. The consolidation pressure was adjusted in the load frame regulator to 0 kPa and the displacement sensors removed. Later on, the consolidation load cap was removed.

Next, the pile segment was installed; it should be remarked that two installation procedures were followed, one for the threaded part and another for the straight section of the pile. For the threaded segment, a piece of steel pipe (140 mm) was previously driven into the soil sample, with the plan of simulating a pre-drill process and it was then removed; afterwards, the threaded part of interest was driven under torque. For the straight portion, the soil placement and the consolidation were made with the pile segment located in the center of the test cell, with the ultimate goal being to reproduce a scenario with correct installation of the pile, perfect compaction, and a consolidation of the soil surrounding the pile.

The test cell was situated later inside the cold room; the thermocouples were placed in the designated spots inside of the soil sample (for 35% water content) and at other locations on the test set up. After this, the copper coil was connected to the temperature bath number 1 (TB1) and located inside of the hollow pile. Next, the inside of the pile was filled very carefully with

concentrated ethylene glycol (100%) trying not to contaminate the soil sample; within the test cell double walls a mixture of water and ethylene glycol approximately (60-70%) was filled with the aid of a siphon pump, a funnel, and a protective plastic layer with the purpose of protecting the soil sample. After that, the temperature bath number 2 (TB2) was connected to the test cell, carefully preventing any leakage in the fittings. Next the test cell was wrapped with fiberglass insulation material. The outlet and inlet hoses of the temperature baths were insulated with foam. Subsequently, the data logging system was connected and it started to monitor the time and temperature; regular checks were done to ensure that everything was running properly.

Before starting the experiment, the ethylene glycol levels were checked in the temperature baths (TB1 and TB2) to protect the internal pumps of each device from damage.

Then the required temperature was configured on the display of both machines and the time was recorded when both started to run. Next, the cold room was carefully closed with the whole set up running, the test cell and the temperature baths remaining inside. It should be noted that during the homogenization stage (day 1) both temperature baths were always working at the same time. Later during the trials this changed depending on the case to evaluate.

3.4.6 Removal of the Frozen Soil and Recycling

Once the freezing step was over, all the output and data records were saved and copied; next, the data logger was stopped and disconnected. Subsequently, the test cell´s fiberglass insulation (from the previous step) was removed. Next the copper coil was removed from inside of the pile and the ethylene glycol was removed from inside of the pile and from inside of the test cell's walls, while being careful not to spill it on the soil sample. This was facilitated through the use of the siphon pump and the funnel.

Then the test cell was disconnected from the temperature bath number 2 (TB2) and removed outside of the cold room into room temperature of approximately 21 °C after which it was left to defrost for approximately 6-12 hours. If the test procedure is for a sample with water content of 35%, the sensor can be removed as soon the soil is thawed just by removing the sticks.

Later, 12 samples (4 per layer) of soil were taken from the soil sample tested to measure the density and the water content in upper, mid and lower layers inside of the test cell approximately

where the thermocouples were located; this was done with the use of a metal ring of 6.65 cm in diameter and 3.7 cm in height (164.4 gr). Next, the soil was removed. If the soil sample water content was 20% one had to be careful not to damage the thermocouple sensors inside. After this, the soil was dried again and the method that was indicated in the previous step (dry soil preparation) followed; then the whole procedure was carried out all over again for another batch of data.

3.5 Location of Thermocouples

Sixteen thermocouples were located at different locations during the setups of the experiments. Every sensor was positioned based on the coordinate axes to ensure its correct placement. Different measure lines (ML1, ML2, ML3, ML4) were created to facilitate the location of the sensors in the setups of the experiments. Figs. 3.14 to 3.19 show the sensors' locations (rhombus) and layers of study inside of the soil sample in plan and section view for ML1 to ML4.

3.5.1 Locations of Thermocouples (Sensors) and Layers of Study inside Soil Sample

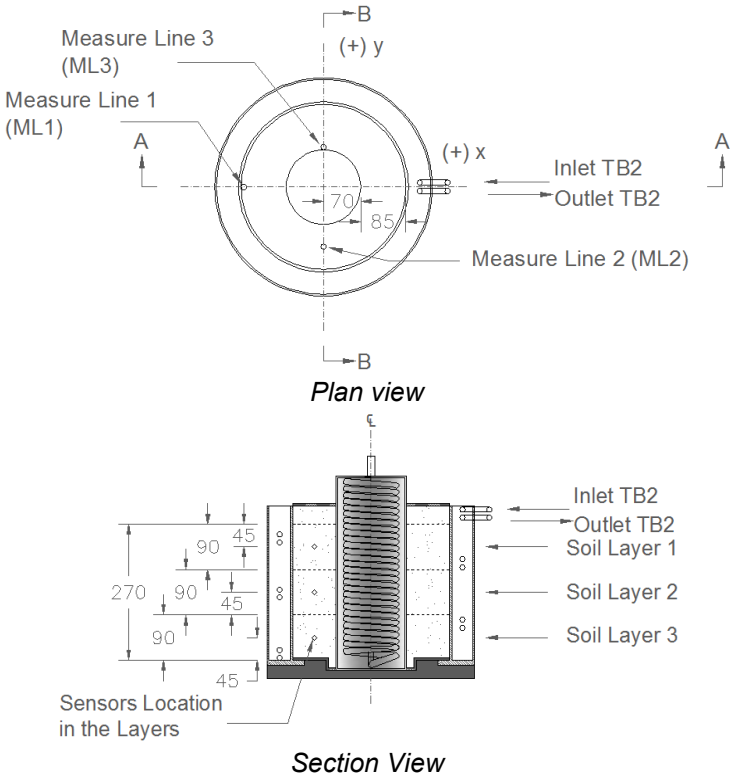

FIGURE 3.14 Sensors location and layers of study inside of the soil sample. Unit: mm.

3.5.2 Thermocouples (Sensors) inside Soil Sample (ML1, ML2, ML3) (S1 to S9)

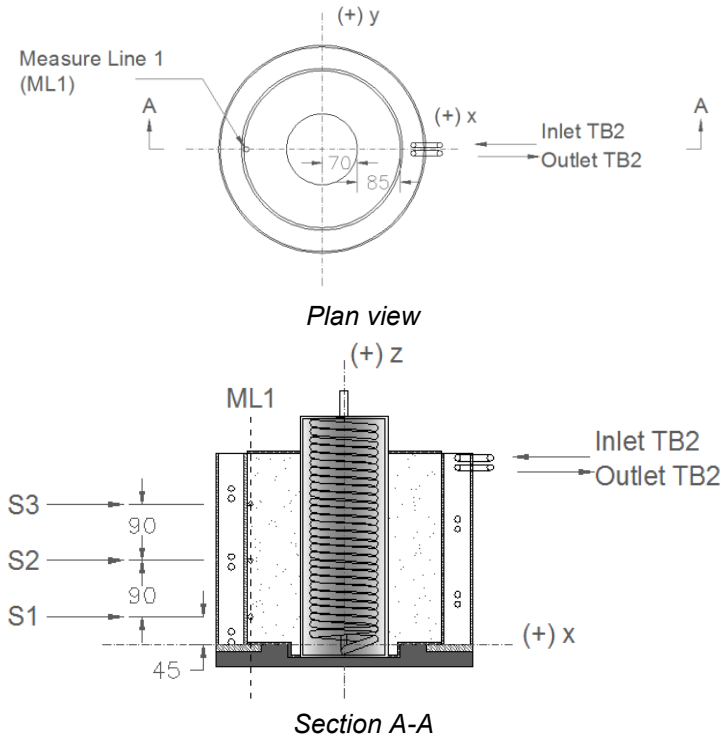

FIGURE 3.15 Measure line 1 (ML1) (S1, S2, S3). Unit: mm.

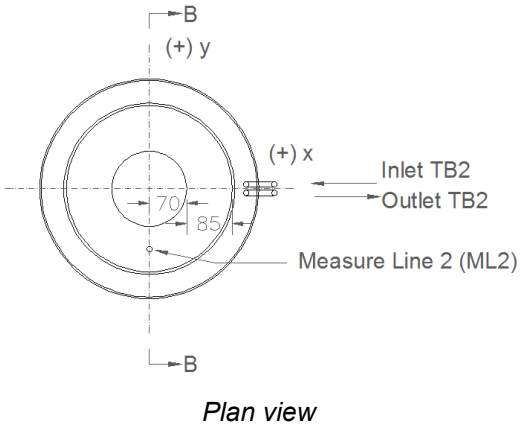

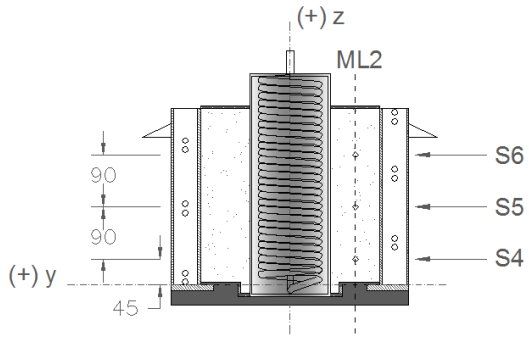

Section B-B

FIGURE 3.16 Measure line 2 (ML2) (S4, S5, S6). Unit: mm.

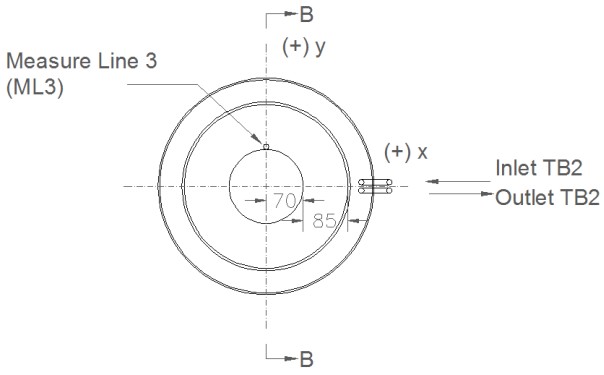

Plan view

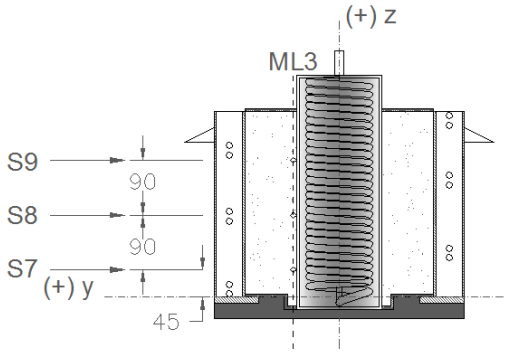

Section B-B

FIGURE 3.17 Measure line 3 (ML3) (S7, S8, S9). Unit: mm.

3.5.3 Thermocouples (Sensors) on the Copper Coil (S10 and S11)

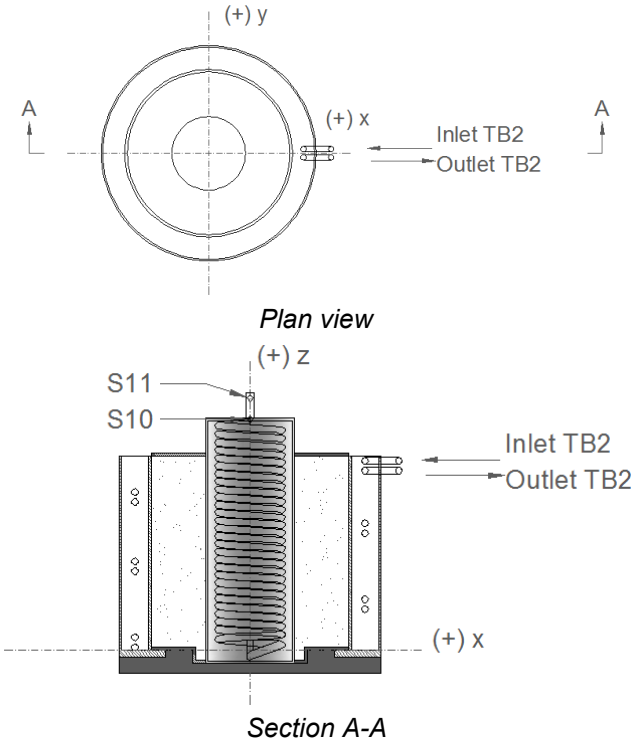

FIGURE 3.18 Thermocouples (Sensors) S10 and S11. Unit: mm.

3.5.4 Thermocouples (Sensors) inside of the Glycol within the Pile (ML4) (S13 to S15) and inside of the Test Cell Wall (S16)

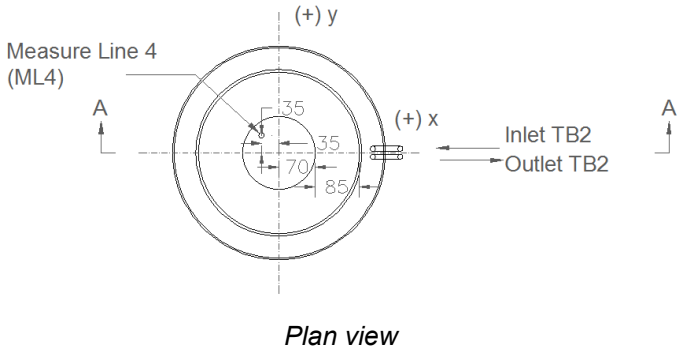

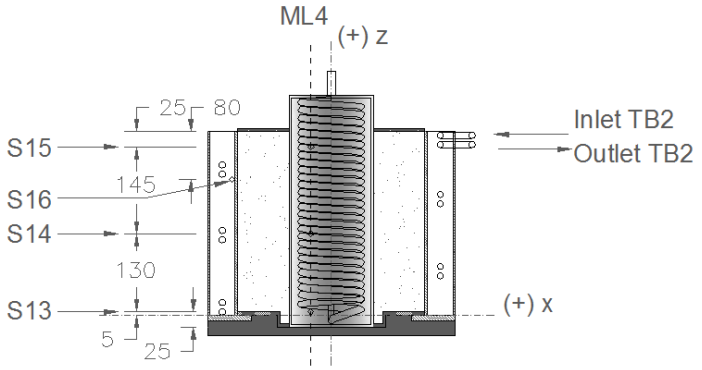

FIGURE 3.19 Measure line 4 (ML4) (S13, S14, S15) and sensor S16. Unit: mm.

Table 3.1 displays the following: the coordinates with respect to the axes previously pointed out in the figures and the locations of the thermocouples (sensors) during all the tests in the entire laboratory set-up.

TABLE 3.1 Coordinates and Locations of Temperature Sensors

Sensor	x (mm)	y (mm)	z (mm)	Location
S1	-155	0	45	ML1
S2	-155	0	135	ML1
S3	-155	0	225	ML1
S4	0	-112.5	45	ML2
S5	0	-112.5	135	ML2
S6	0	-112.5	225	ML2
S7	0	70	45	ML3
S8	0	70	135	ML3
S9	0	70	225	ML3
S10				Inlet copper coil
S11				Outlet copper coil
S12				Cold room
S13	-35	35	5	ML4
S14	-35	35	135	ML4
S15	-35	35	280	ML4
S16	-160	0	225	Test cell wall

3.6 Power Loss Procedure

Once the tests were performed, the power loss, P_{loss}, was estimated by insulating (with fiberglass insulation) and isolating the copper coil from the soil model (soil, pile and test cell) and operating the temperature bath with the identical conditions as those that were implemented throughout the trials, registering the temperature of the ethylene glycol entering and leaving the copper coil. Thereby this applies to the case where no cooling power leaves the system (P=0) (Pimentel, Sres, & Anagnostou, 2012). Later these temperatures were analysed to find P_{loss} in the system.

Power loss during the experiments can be caused by inadequate insulation of the hoses coming from the temperature bath, long distance and considerable difference of head pressure between the refrigeration unit and the soil sample, and drastic variations in temperature in the cold room.

3.7 Test Matrix

Table 3.2 presents all the experiments executed. It includes names, stages, locations of the thermocouples, type of pile segment, and duration for every batch of data collected.

TABLE 3.2 Test Matrix

Batch (#)	w (%)	Trial (Name)	Homogenization temp (°C)	TB1 (Status and temp)	TB2 (Status and temp)	Thermocouples (Sensors)					Density and water content	Pile segment (Name)	Duration (day)
						Inside soil sample (ML1, ML2 and ML3) (S1 to S9)	On the copper coil (S10 and S11)	In the cold room (S12)	Inside glycol in pile (ML4) (S13 to S15)	Inside test cell wall (S16)			
Consolidation													3
1	35	1	5	on (-20 °C)	on (5 °C)	✓	✓	×	×	×		Threaded	3
		2	0	on (-20 °C)	on (0 °C)	✓	✓	×	×	×			3
		3	-2.5	on (-20 °C)	on (-2.5 °C)	✓	✓	×	×	×			3
Consolidation													3
2	35	1	5	on (-20 °C)	on (5 °C)	✓	✓	✓	×	×	✓	Straight	3
		2	0	on (-20 °C)	on (0 °C)	✓	✓	✓	×	×			3
		3	-2.5	on (-20 °C)	on (-2.5 °C)	✓	✓	✓	×	×			3
		TB2_Off1	-2.5	on (-20 °C)	off	✓	✓	✓	×	×			3
		TB2_Off2	0	on (-20 °C)	off	✓	✓	✓	×	×			3
Consolidation													3
3	20	1	5	on (-20 °C)	on (5 °C)	✓	✓	✓	✓	✓	✓	Straight	3
		2	0	on (-20 °C)	on (0 °C)	✓	✓	✓	✓	✓			3
		3	-2.5	on (-20 °C)	on (-2.5 °C)	✓	✓	✓	✓	✓			3
		TB2_Off1	-2.5	on (-20 °C)	off	✓	✓	✓	✓	✓			3
		TB2_Off2	0	on (-20 °C)	off	✓	✓	✓	✓	✓			3
Power loss													3

Note 1: w = Water Content (i.e., w (35%)), TB = Temperature Bath, ML = Measure Line, S = Sensor.

Note 2: The density and water content column indicates that these parameters were measured for Batch (2) and (3); these measures were done at the end of the batches.

Note 3: All temperature vs. time figures were created using the values at every minute for better interpretation.

The test program configuration consisted of three batches of freezing tests.

Batch (1) represents a soil sample with 35% water content and three trials with homogenization temperatures of 5, 0, and -2.5 °C; this was done for a thread screw pile segment when both temperature baths were working at the same time after the homogenization stage, TB1 controls the temperature of glycol circulated through the copper coil inside the pile, and TB2 controls the temperature of the test cell wall (i.e. soil´s boundary temperatures).

Batch (2) represents a soil sample with 35% water content and five trials. Three trials were conducted with homogenization temperatures of 5, 0, and -2.5 °C for a straight screw pile segment when both temperature baths were working at the same time after the homogenization stage. Two trials were conducted with homogenization temperatures of -2.5 and 0 °C for a straight screw pile segment when just the pile temperature bath (TB1) was working after the homogenization stage.

Batch (3) was similar to Batch (2) in configuration but with a soil sample with 20% water content.

4. Results of Laboratory Freezing Tests

This chapter presents and further discusses meaningful and typical trial's results from the research (the results of all batches and trials are displayed in appendix A). It discusses the results of the laboratory artificial freezing test of soils using a steel pipe segment that is taken from screw micropiles. Three batches of freezing tests were conducted and the parameters that were changed from each test batches are: the initial soil water content, initial soil temperature (homogenization temp), temperature bath status and its temperature and pipe pile segment. This chapter will show the results of consolidation tests in the soil preparation stage and then will present and discuss the results of laboratory freezing tests in detail.

Table 4.1 shows the batches and trials presented in this chapter. These trials were selected because they reveal typical temperature tendencies during the research test program and allow for comparison between them.

TABLE 4.1 Configuration of Three Batches of Tests (Presented in this chapter)

Batch (#)	w (%)	Trial (Name)	Homogenization temp (°C)	TB1 (Status and temp)	TB2 (Status and temp)	Thermocouples (Sensors)					Density and water content	Pile segment (Name)
						Inside soil sample (ML1, ML2 and ML3)	On the copper coil (S10 and S11)	In the cold room (S12)	Inside of glycols pile (ML4)	Inside test cell (S16)		
1	35	2	0	on (-20°C)	on (0°C)	✓	✓	×	×	×		Threaded
2	35	2	0	on (-20°C)	on (0°C)	✓	✓	✓	×	×	✓	Straight
		TB2_Off2	0	on (-20°C)	off	✓	✓	✓	×	×		Straight
3	20	2	0	on (-20°C)	on (0°C)	✓	✓	✓	✓	✓	✓	Straight
		TB2_Off1	-2.5	on (-20°C)	off	✓	✓	✓	✓	✓		Straight

Note 1: w = Water Content (i.e., w (35%)), TB = Temperature Bath, ML = Measure Line, S = Sensor.

Note 2: The density and water content column indicates that these parameters were measured for Batch (2) and (3); these measures were done at the end of the batches.

Note 3: All temperature vs. time figures were created using the values at every minute for better interpretation.

4.1 Presentation and Discussion of Test Results

4.1.1 Grain Size Distribution

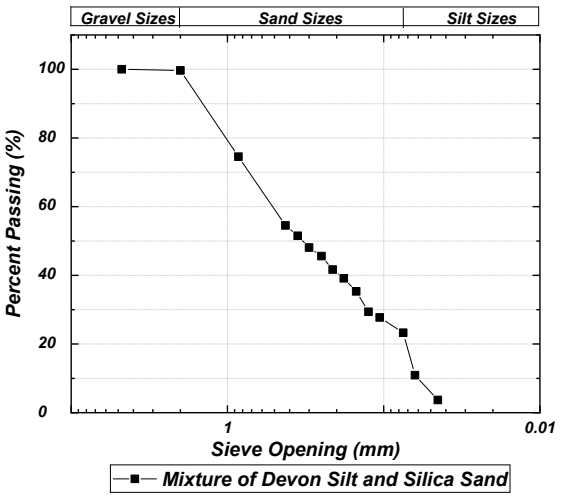

FIGURE 4.1 Grain size distribution of mixture of Devon Silt and Silica Sand.

The soil sample used in these tests was chosen specifically to simulate the soil located in Inuvik, NWT. The soil was collected from Devon close to the City of Edmonton.

Fig. 4.1 presents the grain size distribution of the mixture of Devon Silt and Silica Sand at a weight proportion of 2:1, respectively. One hundred % is passing the #4 sieve, about 20% is passing the #200 sieve, and 0 to 10% are in the course silt sizes.

4.1.2 Consolidation

Figs. 4.2, 4.3 and 4.4 show the results in terms of soil height vs sqrt(time) for the load constant tests for Batch 1, 2 and 3, respectively. The displacement was measured at an interval of 5 seconds, but the charts were created using the values at every minute for better interpretation. For Figs. 4.1 and 4.2 the soil sample contains a water content of 35%; due to this water content, consolidation pressure was applied in stages, doubling the load each time starting from 10 kPa up to 80 kPa. If this was not done sequentially the material would have spilled onto the border of the test cell and the load cap. The 310 mm in Fig. 4.2 and 4.3 represents the height of the soil sample inside the test cell. The following can be observed on the charts: at 20 kPa both samples reached a deformation of 15 mm of a total of about 295 mm in cell height; for 40 kPa both samples had reached an accumulative deformation of approximately 20 mm; and by the end of the experiment

at 80 kPa the height of the consolidated samples was around 285±5 mm at approximately 95% consolidation after three days.

In Fig. 4.4, the sample had water content of 20% and hence the loading stages were very fast i.e. in minutes it went from 10 kPa to 80 kPa. The 300 mm represents the height of the soil inside the test cell. It is easy to see that later the deformation process in these samples was very slow and less when compared to the samples with higher water content; it was approximately 7.5 mm on average. At 95% consolidation, the consolidated sample height was around 290±5 mm approximately.

In general, the consolidation of samples was fast, as expected for a material like silty sand. During the consolidation tests, an insignificant amount of water was squeezed out from the soil samples in both water content scenarios (35% and 20%). This allows considering constant values for the water content after the consolidation experiments.

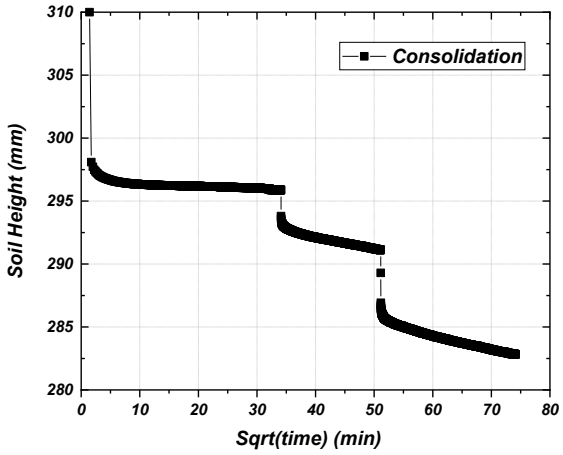

FIGURE 4.2 Consolidation curves of soil for Batch (1) tests (w = 35%).

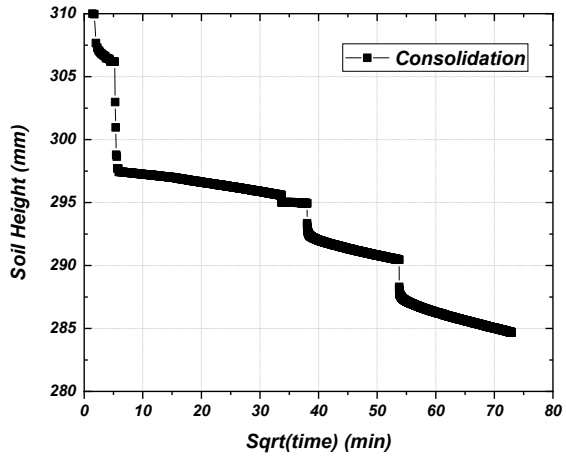

FIGURE 4.3 Consolidation curves of soil for Batch (2) tests (w = 35%).

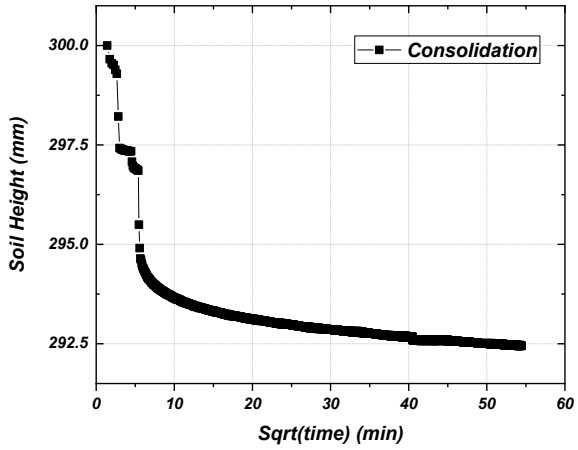

FIGURE 4.4 Consolidation curves of soil for Batch (3) tests (w = 20%).

4.1.3 Freezing

4.1.3.1 Batch 1

4.1.3.1.1 Trial 2

This batch of data represents the soil with the water content of 35%. It should be noted that for this batch the pile segment with threads was used, which was installed with a pre-drilling hole of 140 mm diameter. Because of this condition, a disturbance in the sample was created. Cracks appeared which created air gaps inside the soil which might negatively affect the thermal conductivity of soil surrounding the pile; this occurred because air is a good insulator and works like a thermal barrier.

Thermocouples inside Soil Sample

The following figures are presented directly below: figures for trial number 2 showing the temperature vs. time when Temperature Bath (TB1) was set up at -20 °C; and Temperature Bath (TB2) at 0 °C for thermocouples (sensors) located at different Measurement Lines (ML1), (ML2), and (ML3).

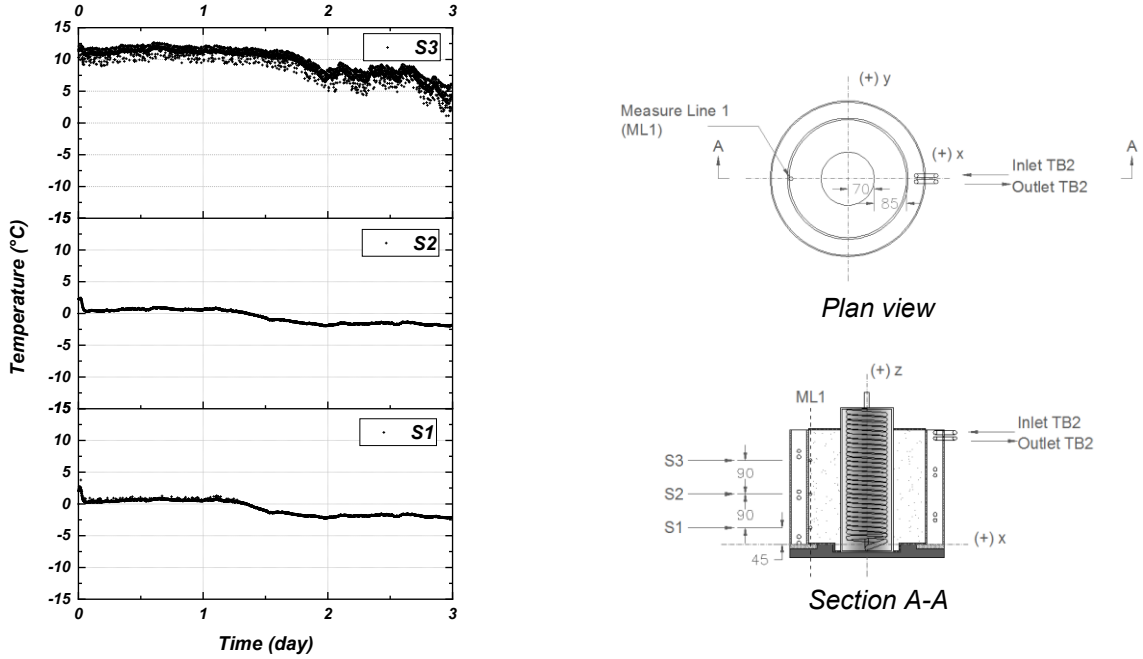

FIGURE 4.5 Temp. vs. time Batch (1), w (35%), Trial (2), starting (0 °C), TB1on (-20 °C) - TB2on (0 °C) for ML1. Unit: mm.

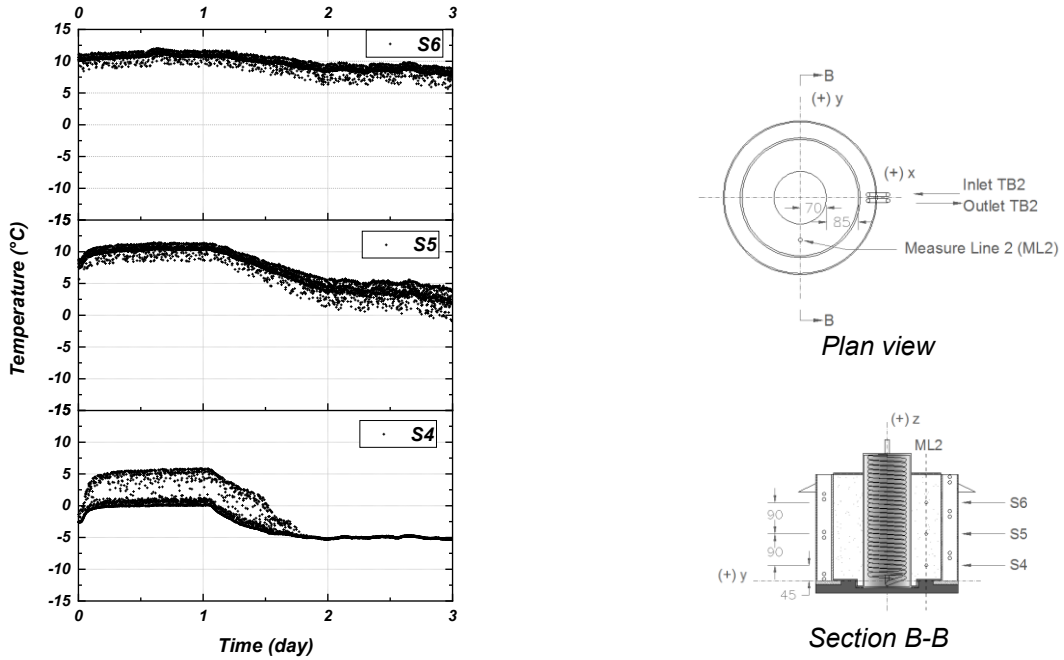

FIGURE 4.6 Temp. vs. time Batch (1), w (35%), Trial (2), starting (0 °C), TB1on (-20 °C) - TB2on (0 °C) for ML2. Unit: mm.

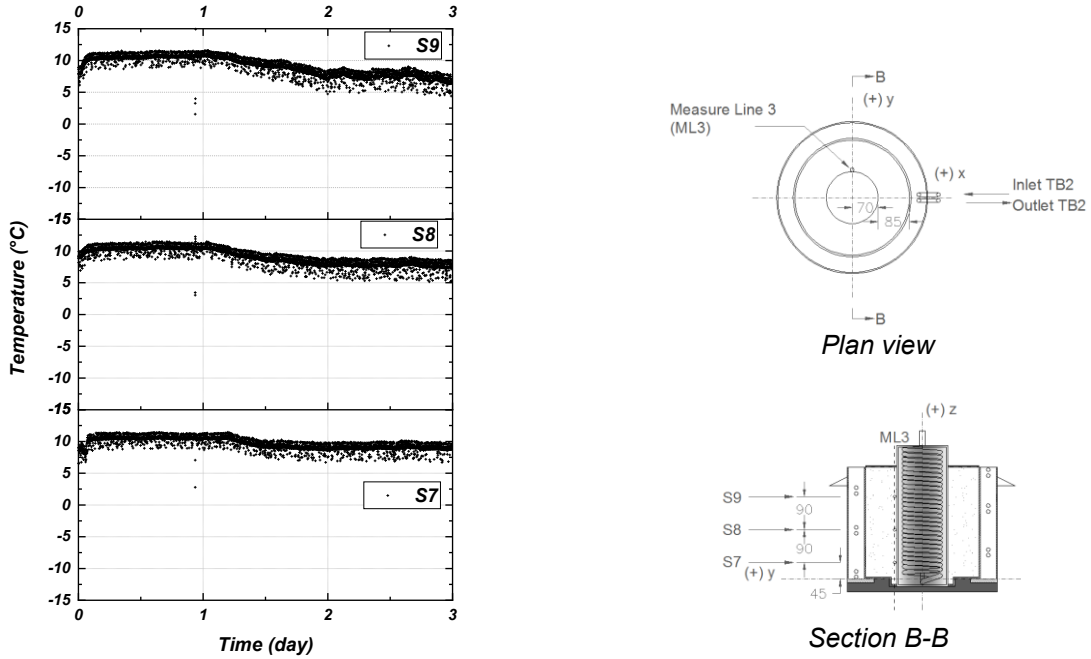

FIGURE 4.7 Temp. vs. time Batch (1), w (35%), Trial (2), starting (0 °C), TB1on (-20 °C) - TB2on (0 °C) for ML3. Unit: mm.

The temperature was recorded at 1 min intervals. Fig. 4.5 shows the temperature in °C vs. time in days. This chart shows the sensors that are located in ML1 near the test cell wall; sensors 1 and 2 show a pretty smooth tendency while sensor 3 shows more variability in the reading. This response could be due to the location of the sensors, as sensors number 1 and 2 are in the bottom and middle respectively and this is where they were well insulated. The sensor at the top shows the higher temperatures and the sensors at the bottom the lower ones; these types of results were expected due to the cell test configuration. There is a difference in temperature of approximately 10 °C at the beginning of the trial between sensor 3 at the surface layer and sensors 2 and 1 located in the middle and bottom, respectively. At the homogenization stage, between zero and one day in duration, sensors 1 and 2 reached approximately the desired temperature of 0 °C; on the other hand, sensor 3 showed a high temperature of about 11 °C. This figure of the bottom sensors shows temperatures below 0 °C, at an approximate value of -2 °C at the end of day three.

Fig. 4.6 shows temperature in °C vs. time in days. This chart shows that the sensors located in ML2 are in the middle of the soil sample in plan view. All sensors show variability in the readings and that is because both temp baths were working at the same time in both stages of homogenization and the trial. Sensor 6 at the top shows the higher temperatures. Sensor 4 shows the cooler temperatures of ML2 and the trial, and is about -5 °C by the end of day three. In the homogenization stage, the only sensor that reached a tendency with the desired temperature of 0 °C was sensor number 4, which makes sense as it was located at the bottom layer and was well protected. This figure in comparison with Fig. 4.5, shows the same tendency in terms of the location of the sensors, i.e. the sensors at the top were the warm ones, and the sensors at the bottom the cold ones.

Fig. 4.7 shows the temperature in °C vs. time in days of ML3 sensors. This chart shows the sensors located beside the pile segment. The behavior of these sensors is different than with the previous measure lines; at the end of the test, the top sensor indicates the lowest temperatures and the sensor at the bottom the highest temperatures. This response could be associated with the design of the copper coil inside of the pile. The ethylene glycol enters the copper coil from the temperature bath (TB1) from the upper part, and when it reached the bottom heat transfer had occurred, that is probably why these sensors are showing these tendencies. These sensors show the warmest temperatures.

In general, with all the measured lines, the sensors show a trend that was anticipated due to the configuration of the model, but they do not converge at the same temperature.

Thermocouples on the Copper Coil

Fig. 4.8 shows the sensors located at the inlet (beginning) and outlet (end) of the actual copper coil inside of the pile where the ethylene glycol is circulating.

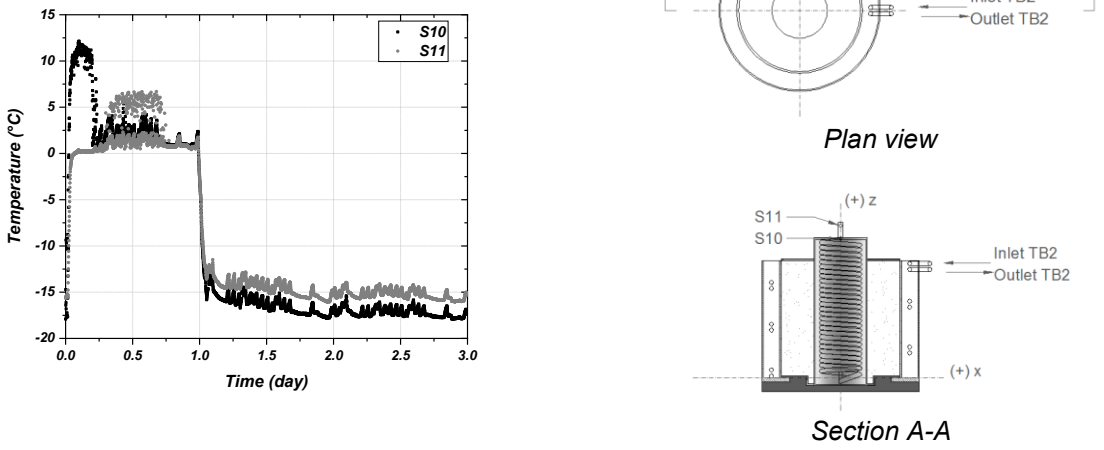

FIGURE 4.8 Temp. vs. time Batch (1), w (35%), Trial (2), starting (0 °C), TB1on (-20 °C) - TB2on (0 °C) for on copper coil.

This graph shows the temperature of the glycol coming from the temperature bath 1 (TB1) and also shows the temperature going out of the copper coil inside the pile when the soil model test is set up. The sensors were located touching the external face of the copper coil. The idea with these sensors was to capture the differential of temperature (ΔT) delivered by the glycol for later analysis of freezing power. The chart is consistent in its readings, showing a difference in temperature of about 1 °C to 2 °C. The temperature of -20 °C of the copper coil inside the pile was reached by TB1 within 2 hours after it was set up at the end of the homogenization stage (around day one).

4.1.3.2 Batch 2

4.1.3.2.1 Trial 2

This batch of data represents the soil with a water content of 35%. It should be noted that for this batch of data the pile segment with the straight part was used; the procedure for this pile segment is different from the one for the threaded one. The idea was to simulate a perfect scenario where the pile is exceptionally well installed, where there is no soil disturbance and the soil is well compacted.

Thermocouples inside of the Soil Sample

The following figures are presented below: figures for trial number 2 showing the temperature vs. time when Temperature Bath (TB1) was set up at -20 °C and Temperature Bath (TB2) at 0 °C for thermocouples (sensors) located at different Measurement Lines (ML1), (ML2), and (ML3).

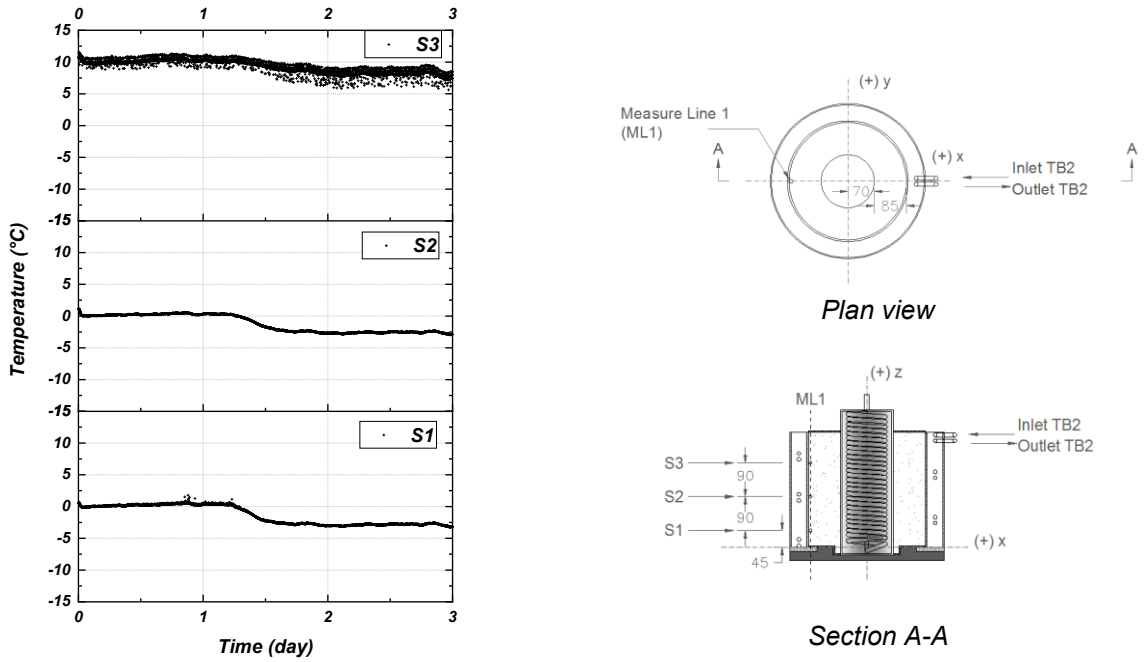

FIGURE 4.9 Temp. vs. time Batch (2), w (35%), Trial (2), starting (0 °C), TB1on (-20 °C) - TB2on (0 °C) for ML1. Unit: mm.

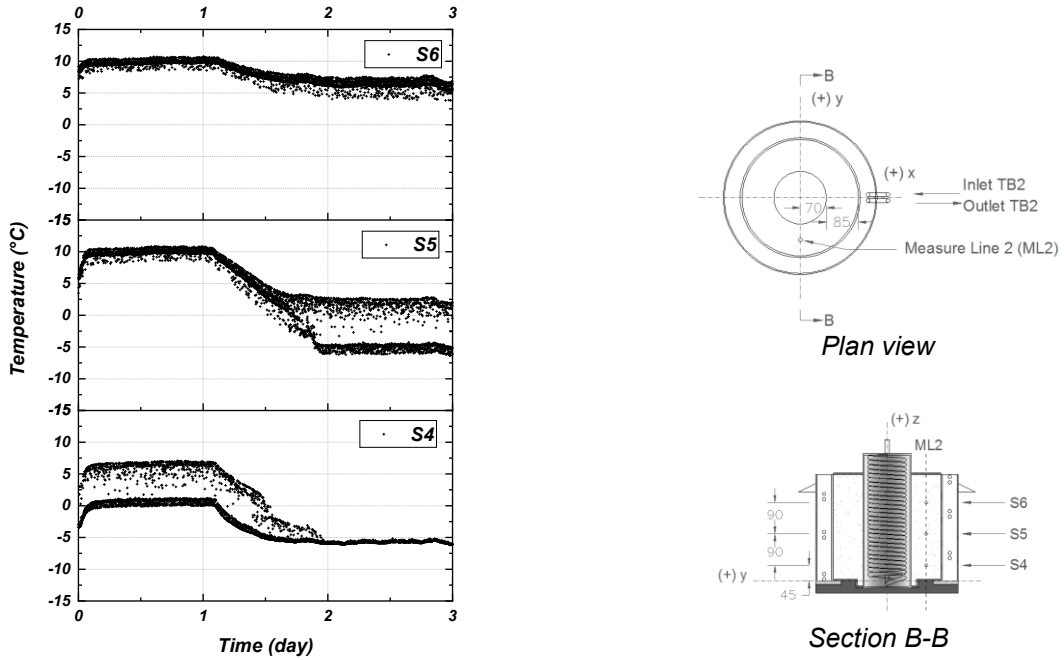

FIGURE 4.10 Temp. vs. time Batch (2), w (35%), Trial (2), starting (0 °C), TB1on (-20 °C) -TB2on (0 °C) for ML2. Unit: mm.

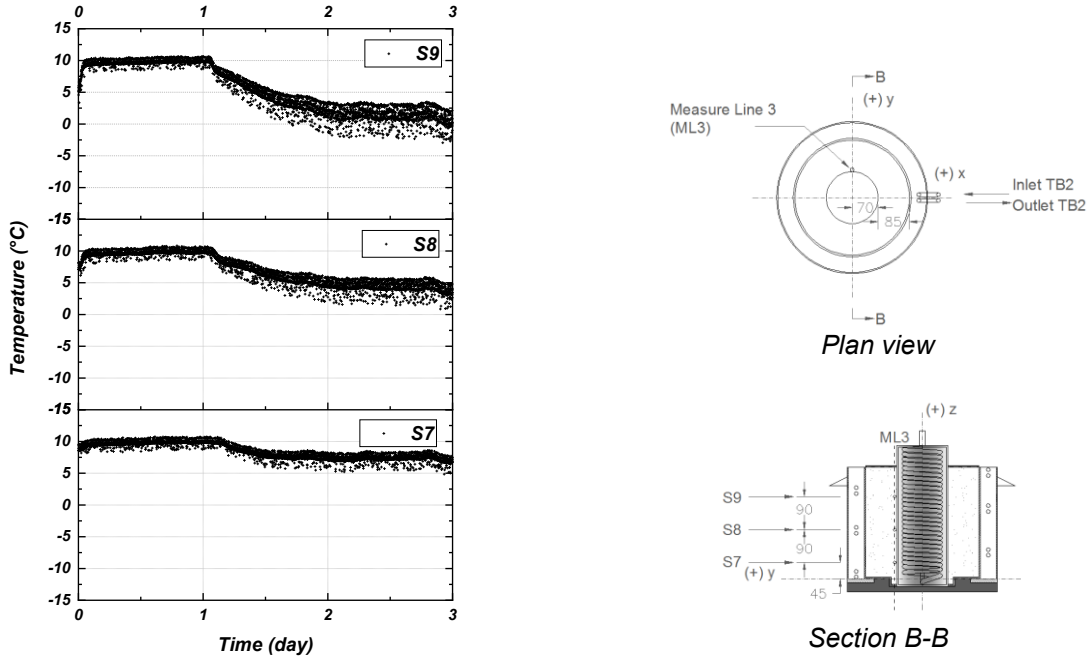

FIGURE 4.11 Temp. vs. time Batch (2), w (35%), Trial 2, Starting (0 °C), TB1on (-20 °C) - TB2on (0 °C) for ML3. Unit: mm.

In general, the charts show consistent and similar behavior in comparison with the same charts for the previous batch of data; they demonstrate that even though there is some disturbance during the installation process it is still possible to obtain reasonable results.

Thermocouples on the Copper Coil

Fig. 4.12 shows the sensors located at the inlet (beginning) and outlet (end) of the actual copper coil inside of the pile where the ethylene glycol is circulating.

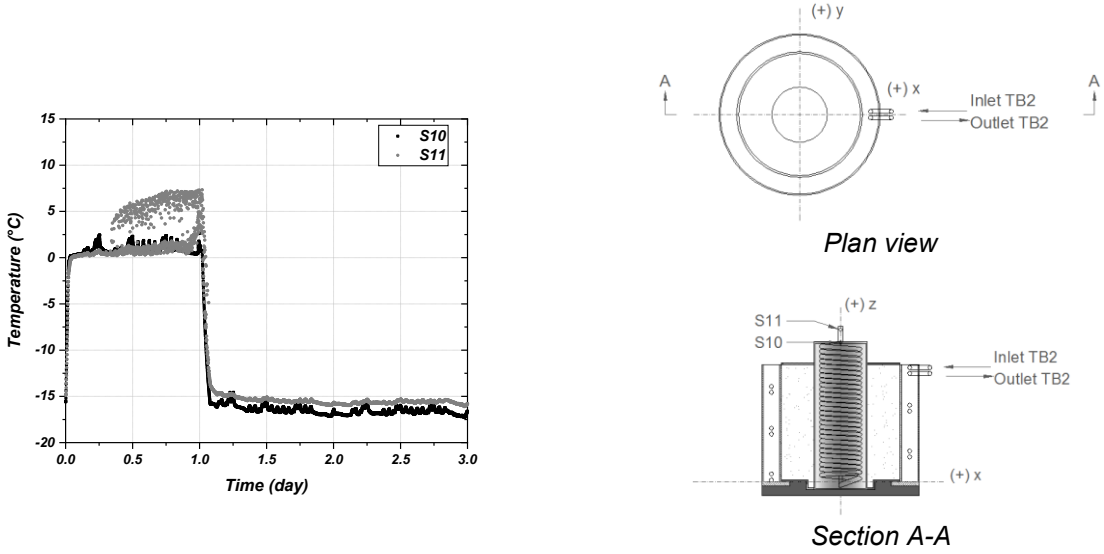

FIGURE 4.12 Temp. vs. time Batch (2), w (35%), Trial (2), starting (0 °C), TB1on (-20 °C) -TB2on (0 °C) for on copper coil.

This chart is consistent with the graph previously shown on Batch (1) (Fig. 4.8), proving that the temperature bath (TB1) pumps the ethylene glycol at a constant temperature of -20 °C and a constant flow velocity during all the batches and trials.

Thermocouple in the Cold Room

This chart (Fig. 4.13) shows the records for a thermocouple that was installed inside of the cold room. The graph indicates four cycles per day and this is because the room is a cooler and not a freezer. The thermocouple was located at the entry of the room at an approximate height of 1.5 meters from the floor. The intention here was to avoid the direct air coming from the fans which are located at the far end of the room close to the roof.

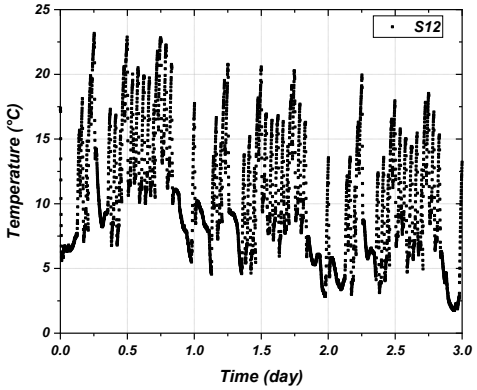

FIGURE 4.13 Temp. vs. time Batch (2), w (35%), Trial (2), starting (0 °C), TB1on (-20 °C) -TB2on (0 °C) temperature cold room.

On the chart, it is also possible to see that when both temperature baths are working at the same time, the temperature of the cold room goes up.

4.1.3.2.2 Trial TB2_Off2

Thermocouples inside of the Soil Sample

The following figures are presented below: figures for trial (TB2_Off2) showing the temperature vs. time when Temperature Bath (TB1) was set up at -20 °C and when Temperature Bath (TB2) was turned off after a homogenization at 0 °C, for thermocouples (sensors) located at different Measurement Lines (ML1), (ML2), and (ML3).

It should be noted that for this trial, after the homogenization stage at 0 °C (day one), the temp bath TB2 was stopped and TB1 was set up at -20 °C.

Fig. 4.14 shows the temperature vs. time registered by the sensors located at ML1. Sensors 1 and 2 reached the desired temperature of 0 °C during the homogenization stage (day one). In the trial, these two sensors show a similar smooth curve with a significant range of temperatures going from 0 °C to about -12.5 °C during the second day of the test; this temperature of about -12.5 °C was kept constant during the third day. Sensor 3 shows a trend during the homogenization stage that is far from the desired temperature, the final temperature recorded being 10 °C. This trend could be because this sensor was located in the upper part of the test cell, and it was not better insulated. It should be noted that at the end of the trial the three sensors reached a temperature of -12.5 °C by the end of day three; this indicates that the whole sample was at that temperature when the trial was finished.

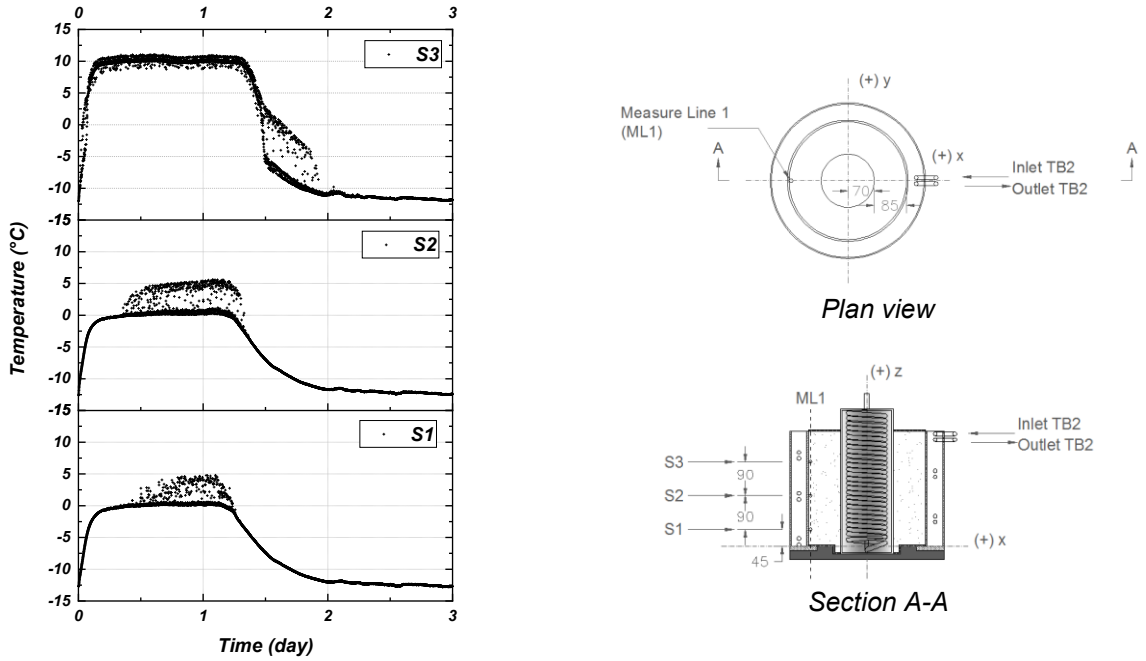

FIGURE 4.14 Temp. vs. time Batch (2), w (35%), Trial (TB2_Off2), starting (0 °C), TB1on (-20 °C) -TB2_off, for ML1. Unit: mm.

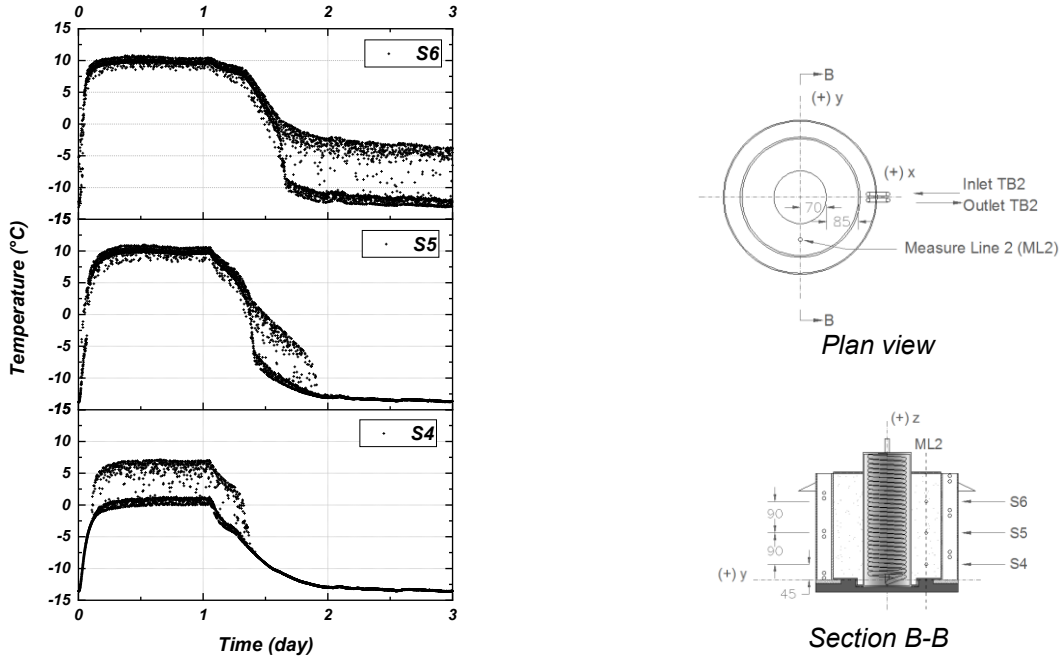

FIGURE 4.15 Temp. vs. time Batch (2), w (35%), Trial (TB2_Off2), starting (0 °C), TB1on (-20 °C) -TB2_off, for ML2. Unit: mm.

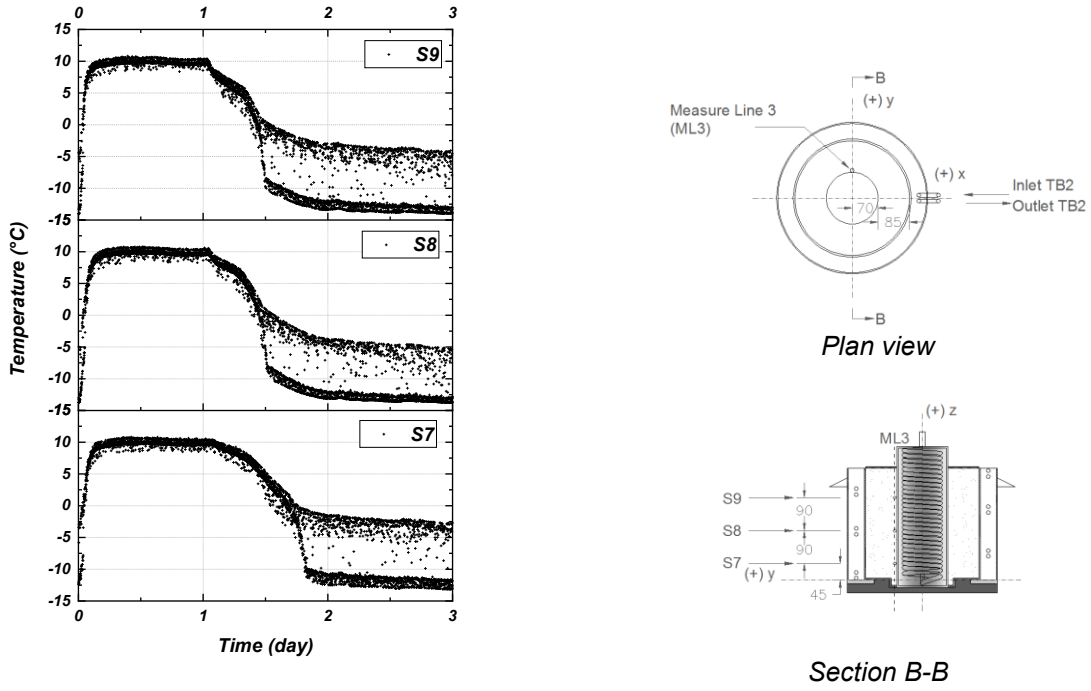

FIGURE 4.16 Temp. vs. time Batch (2), w (35%), Trial (TB2_Off2), starting (0 °C), TB1on (-20 °C) -TB2_off, for ML3. Unit: mm.

Fig. 4.15 shows the temperature vs. time registered by the sensors located at ML2. Sensor 4 shows the trend where the desired temperature of 0 °C was reached during the homogenization stage (day one). Sensor 4 results produce a similar even curve that sensor 1 and sensor 2 show at ML1, reaching a temperature of approximately -13.5 °C by the end of the trial. On the other hand, sensors 5 and 6 show more variability in the readings, and during day one the temperature is around 10 °C, which is far from the 0 °C desired for this stage of the trial.

It is also notable that the transition from positive to negative temperatures is steeper with these two sensors (S5 & S6), and the change happens near day 1.5; the trend is very similar to that shown by sensor 3 at ML1 and this could be because of the location of the sensors inside of the soil sample.

Fig. 4.16 shows the temperature vs. time registered by the sensors located at ML3. This group of sensors shows a higher variability in the readings when compared with the other measure lines in the trial. This performance means that in order for there to be heat transfer these measurements could not be at the same temperature as the glycol inside of the pile; if the soil sample and the

glycol inside of the pile have the same temperature it means that heat transfer is no longer happening, as noted by Geoslope (2018a). It is also notable that the sensor at the top (S9) is warmer than the sensor at the bottom (S7). These readings are due to the copper coil configuration inside of the pile. Also, these three sensors never reached the desired homogenization temperature of 0 °C during day one; their readings were about 10 ° C.

In general, after observing the behavior of the nine sensors at the three measure lines, it can be noted that at the end of the experiment all sensors reached a temperature around -12.5 °C to -13.5 °C. This indicates that the 3 layers evaluated inside of the soil sample were at this temperature at the end of the trial.

Thermocouples on the Copper Coil

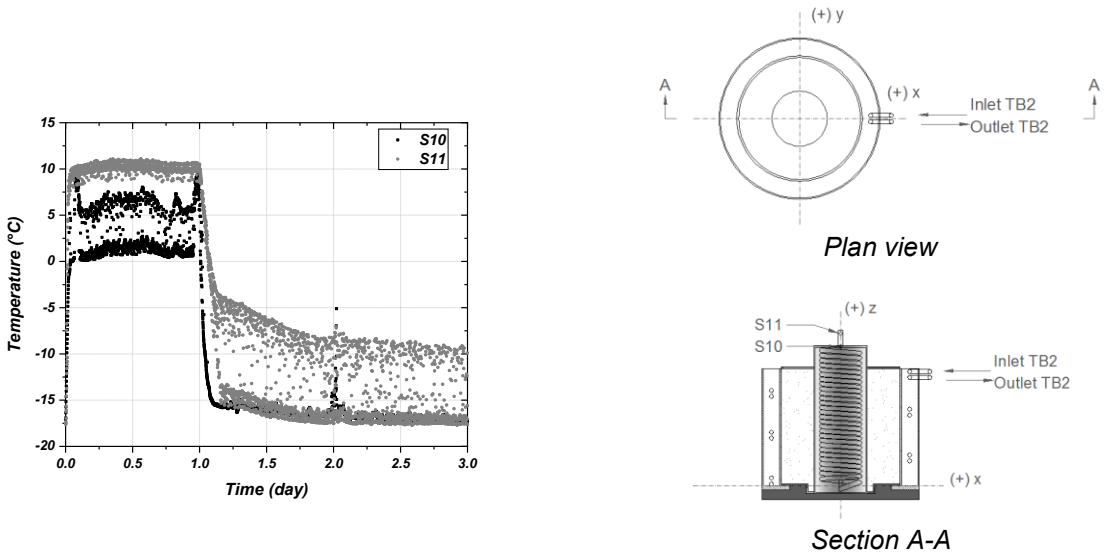

FIGURE 4.17 Temp. vs. time Batch (2), w (35%), Trial (TB2_Off2), starting (0 °C), TB1on (-20 °C) -TB2_off, for on copper coil.

Fig. 4.17 shows the sensors located at the inlet (beginning) and outlet (end) of the actual copper coil inside of the pile where the ethylene glycol is circulating.

Sensor 11, in particular, shows an unevenness caused by the loss of insulation and direct contact on the sensor; this is probably due to the growth of ice at the surface of the copper but in general, it is possible to see the tendency on the curve.

Thermocouple in the Cold Room

This chart (Fig. 4.18) shows the records for the thermocouple that is installed inside of the cold room. The chart clearly shows four cycles per day; this is because the room is a cooler and not a freezer. What is also observable is that the two temperature baths working at the same time inside of the cold room increases the room temperature (day 1), which on average does not climb higher than 20 °C; it is found to be acceptable for a cold room to preserve the moisture of the soil sample according to Clayton (1995).

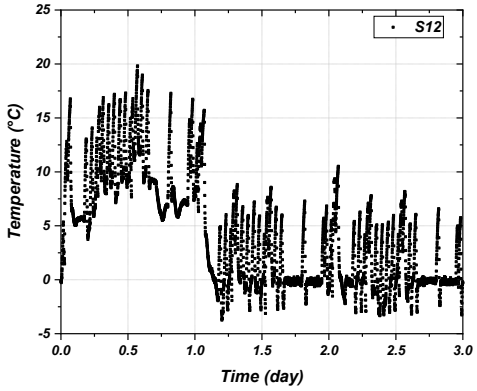

FIGURE 4.18 Temp. vs. time Batch (2), w (35%), Trial (TB2_Off2), starting (0 °C), TB1on (-20 °C) -TB2_off, for cold room.

Density and Water Content

Table 4.2 shows the values of density and water content measured after Batch (2). It can be seen that the values of water content at the bottom of the test cell remain constant until the end of the test, and measure approximately 34.6% vs. the initial 35%. In the upper and middle layers, there is a reduction in values, with about 28.6% at the top and 33% in the middle.

TABLE 4.2 Batch (2) Density and Water Content by Layer

Layer	Sample	Tray empty (gr)	Tray+soil+ ring (gr)	Soil+tray (gr)	Soil $_{Dry}$ +tray (gr)	Soil mass (gr)	Soil mass (kg)	Density (kg/m^3)	Average density (kg/m^3)	Unit weight (kN/m^3)	Average unit weight (kN/m^3)	w (%)	Average w (%)
1	L1-1	4.21	389.47	223.34	174.42	220.86	0.2209	1718.63	1705.34	16.86	16.73	28.74	28.62
	L1-2	4.22	386.02	221.63	173.16	217.40	0.2174	1691.71		16.60		28.69	
	L1-3	4.20	386.99	219.35	171.67	218.39	0.2184	1699.41		16.67		28.47	
	L1-4	4.25	388.61	239.04	186.85	219.96	0.2200	1711.63		16.79		28.58	
2	L2-1	4.22	386.32	217.56	164.24	217.70	0.2177	1694.04	1694.20	16.62	16.62	33.32	32.90
	L2-2	4.21	387.50	215.97	164.44	218.89	0.2189	1703.30		16.71		32.16	
	L2-3	4.22	378.93	207.63	156.67	210.31	0.2103	1636.53		16.05		33.43	
	L2-4	4.22	392.60	223.36	169.38	223.98	0.2240	1742.91		17.10		32.68	
3	L3-1	4.22	392.80	226.56	169.93	224.18	0.2242	1744.46	1736.59	17.11	17.04	34.17	34.59
	L3-2	4.22	391.64	227.16	170.93	223.02	0.2230	1735.44		17.02		33.73	
	L3-3	4.22	391.63	222.80	166.08	223.01	0.2230	1735.36		17.02		35.04	
	L3-4	4.24	391.10	220.61	164.03	222.46	0.2225	1731.08		16.98		35.41	
Total average									1712.04		16.80		32.04

Note 1: Ring dimensions: external diameter = 6.9 cm; internal diameter = 6.65 cm; height = 3.7 cm and weight = 164.40 gr.

Note 2: Column (Soil mass) = column (Tray + soil + ring) – tray – ring.

4.1.3.3 Batch 3

4.1.3.3.1 Trial 2

This batch of data represents the soil with a water content of 20%. It should be noted that for this batch of data the pile segment with the straight part was used.

These charts show the records when both temperature baths are working at the same time at a low water content (20%) after homogenization stage. The response, in general, is similar to the previous batches of data and the previous trials conducted. A notable difference is that in this batch of data there is significant variance in the readings given that the sample is drier, which prevents thermal conductivity. Water has high conductivity in comparison with air. (see Figs. 4.19, 4.20 and 4.21)

Thermocouples inside of the Soil Sample

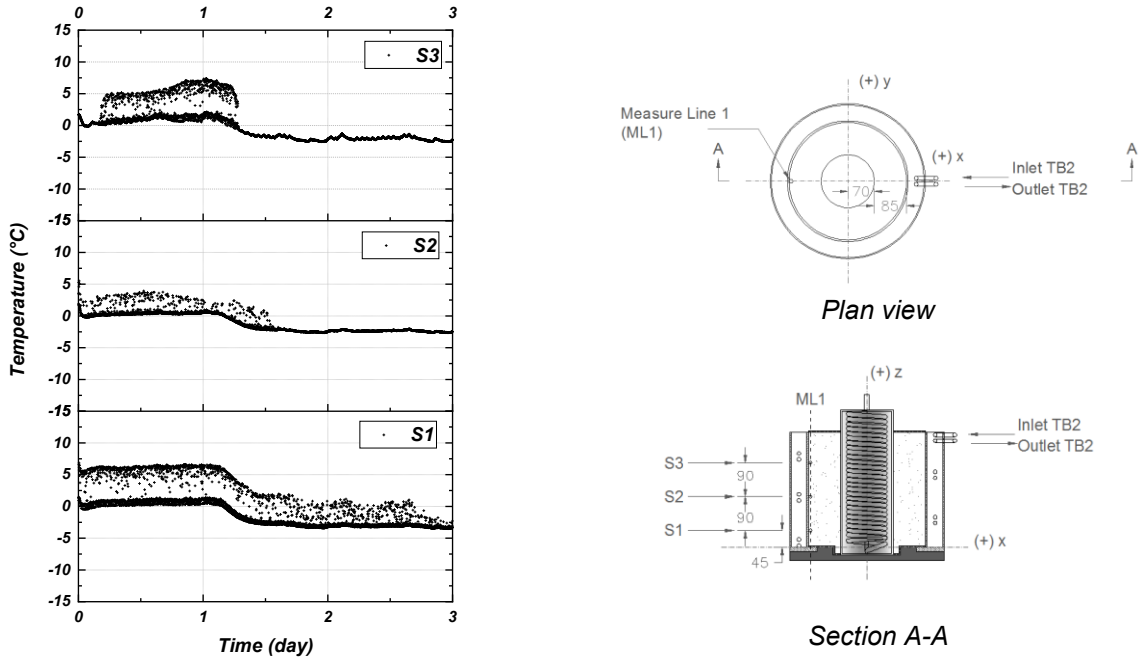

FIGURE 4.19 Temp. vs. time Batch (3), w (20%), Trial (2), starting (0 °C), TB1on (-20 °C) -TB2on (0 °C) for ML1. Unit: mm.

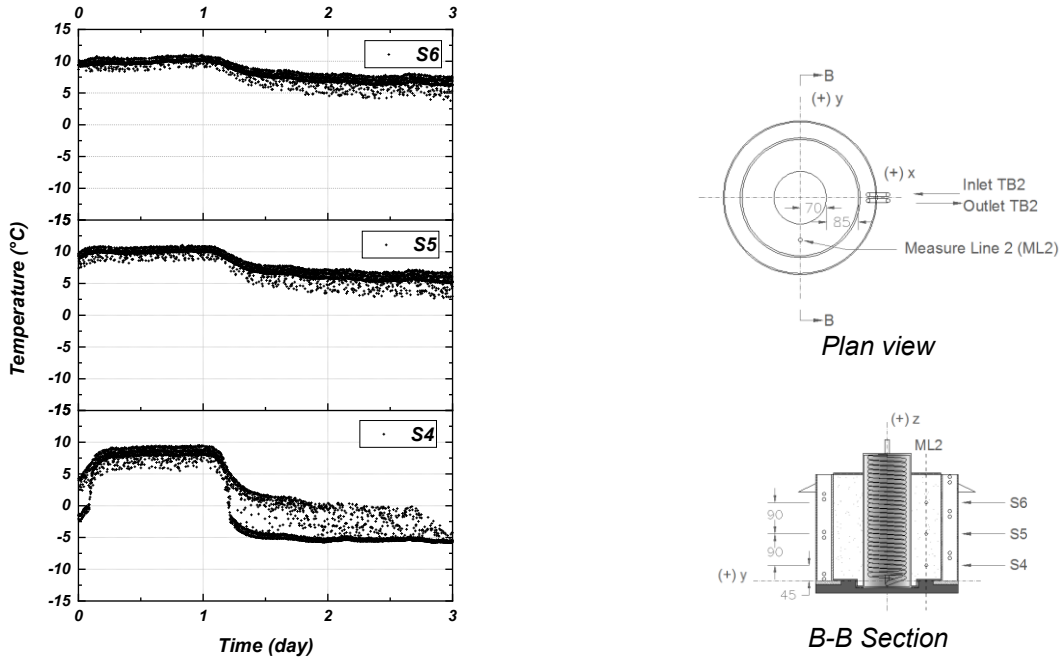

FIGURE 4.20 Temp. vs. time Batch (3), w (20%), Trial (2), starting (0 °C), TB1on (-20 °C) -TB2on (0 °C) for ML2. Unit: mm.

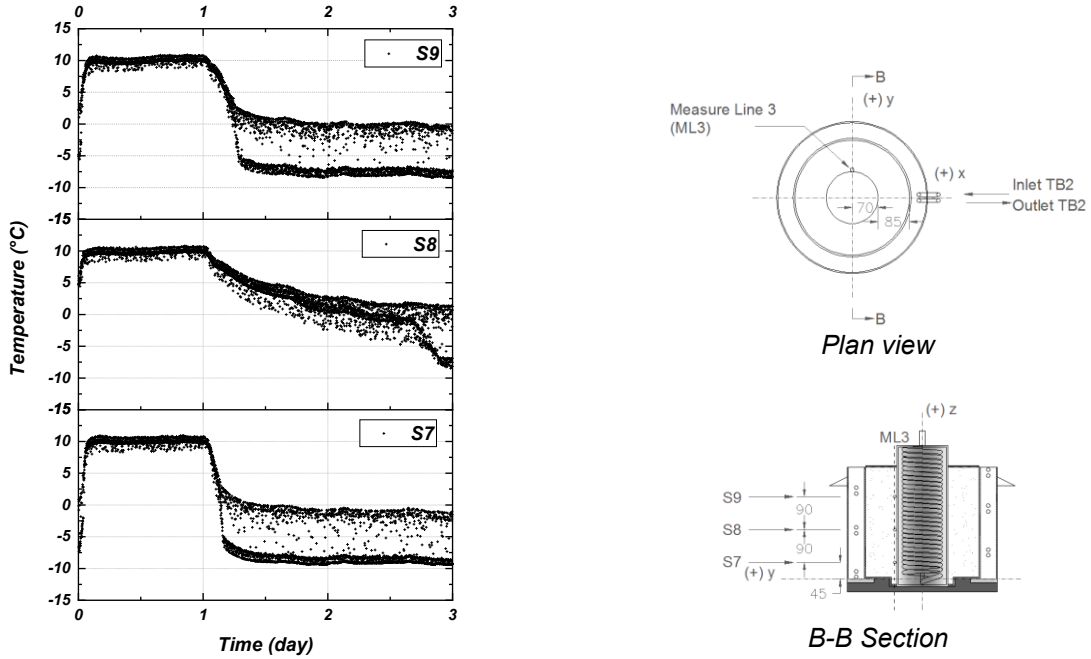

FIGURE 4.21 Temp. vs. time Batch (3), w (20%), Trial (2), starting (0 °C), TB1on (-20 °C) -TB2on (0 °C) for ML3. Unit: mm.

Thermocouples immersed in the Glycol inside of the Pile

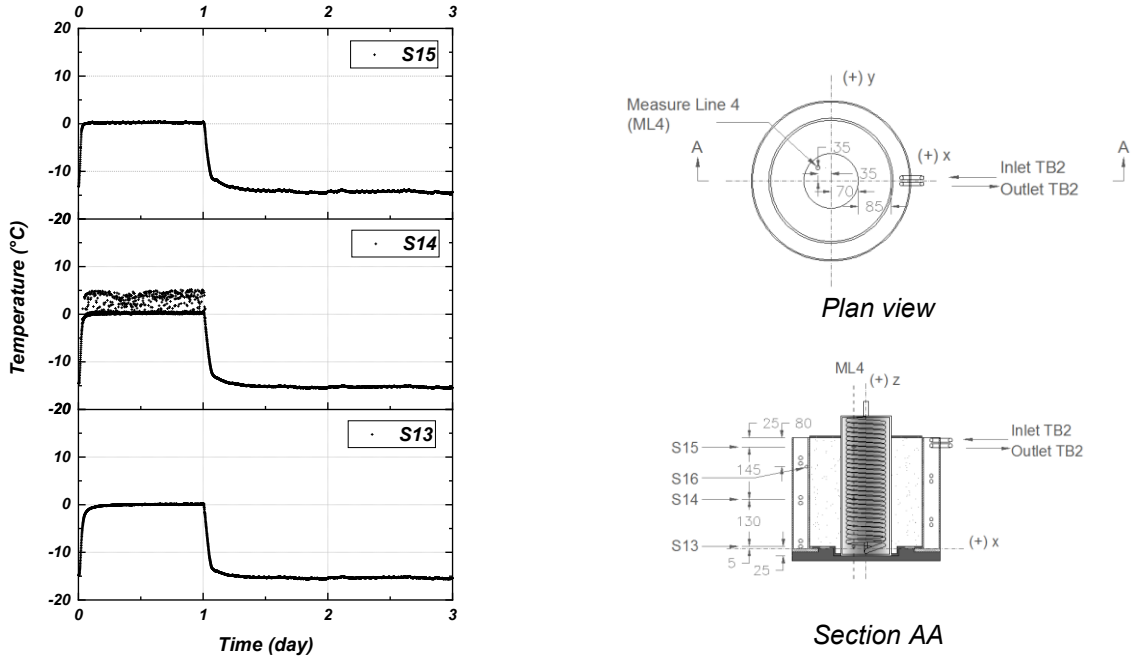

FIGURE 4.22 Temp. vs. time Batch (3), w (20%), Trial (2), starting (0 °C), TB1on (-20 °C) -TB2on (0 °C) for inside glycol in pile. Unit: mm.

Fig. 4.22 shows the temperature vs. time of the thermocouples immersed in the glycol inside of the pile at three different locations: upper (sensor 15), middle (sensor 14), and bottom (sensor 13) at ML4. It is also noteworthy that all three sensors give very similar values and show a very smooth response; sensor 14 shows more variation in the readings during the homogenization stage and this could be due to its location in the middle of the pile.

This figure shows how consistent the temperature bath (TB 1) is during the whole trial. It was delivering a temperature of 0 °C (day 1) during the homogenization stage and -20 °C during the second stage (days 2 and 3), reaching a pretty constant temperature of about -15 °C inside of the pile. This gives a good indication of the actual temperatures delivered by the system that could be used for future calibrations and design.

This graph also proves that the copper coil configuration delivers a constant temperature throughout the length of the entire pile. It is noteworthy that it takes approximately 2 hours for the TB1 to reach -20 °C from 0 °C.

Thermocouple inside of the Test Cell Wall

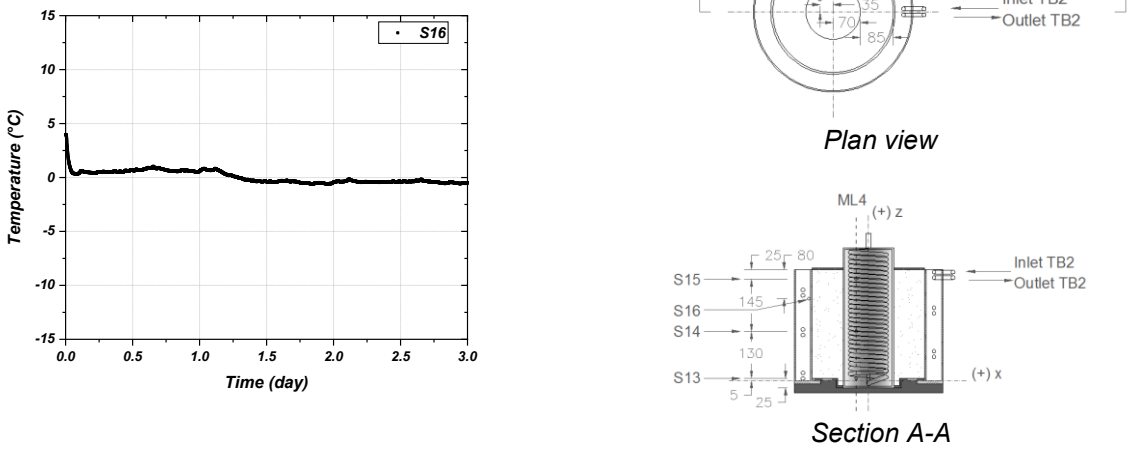

FIGURE 4.23 Temp. vs. time Batch (3), w (20%), Trial (2), starting (0 °C), TB1on (-20 °C) -TB2on (0 °C) for inside glycol test cell. Unit: mm.

This figure (Fig. 4.23) shows the readings of one thermocouple located inside the double wall of the test cell, more precisely, at the middle of the upper section (S16). In this scenario, these readings reflect the temperature that was delivered by the TB2.

4.1.3.3.2 Trial TB2_Off1

Thermocouples inside of the Soil Sample

The following figures are presented below: figures for trial (TB2_Off1) showing the temperature vs. time when Temperature Bath (TB1) was set up at -20 °C and when Temperature Bath (TB2) was turned off after a homogenization at -2.5 °C, for thermocouples (sensors) located at different Measurement Lines (ML1), (ML2), and (ML3).

It should be remarked that for this trial, after the stage of homogenization at -2.5 °C (day one), the temperature bath TB2 was stopped and TB1 was set up at -20 °C.

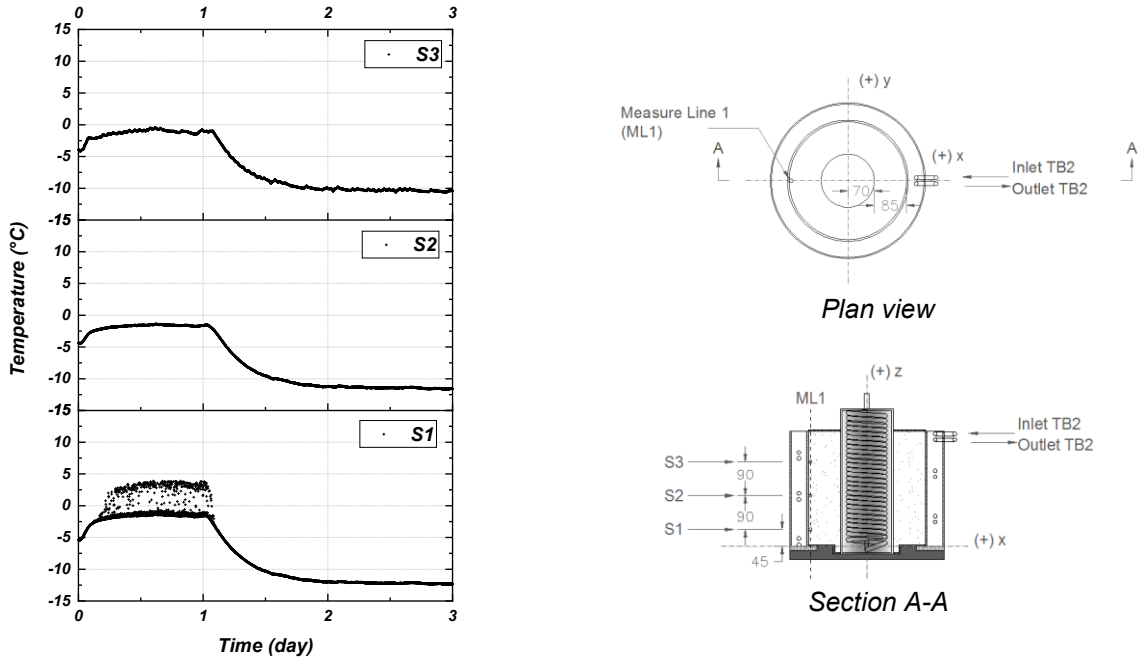

FIGURE 4.24 Temp. vs. time Batch (3), w (20%), Trial (TB2_Off1), starting (-2.5 °C), TB1on (-20 °C) -TB2_off for ML1. Unit: mm.

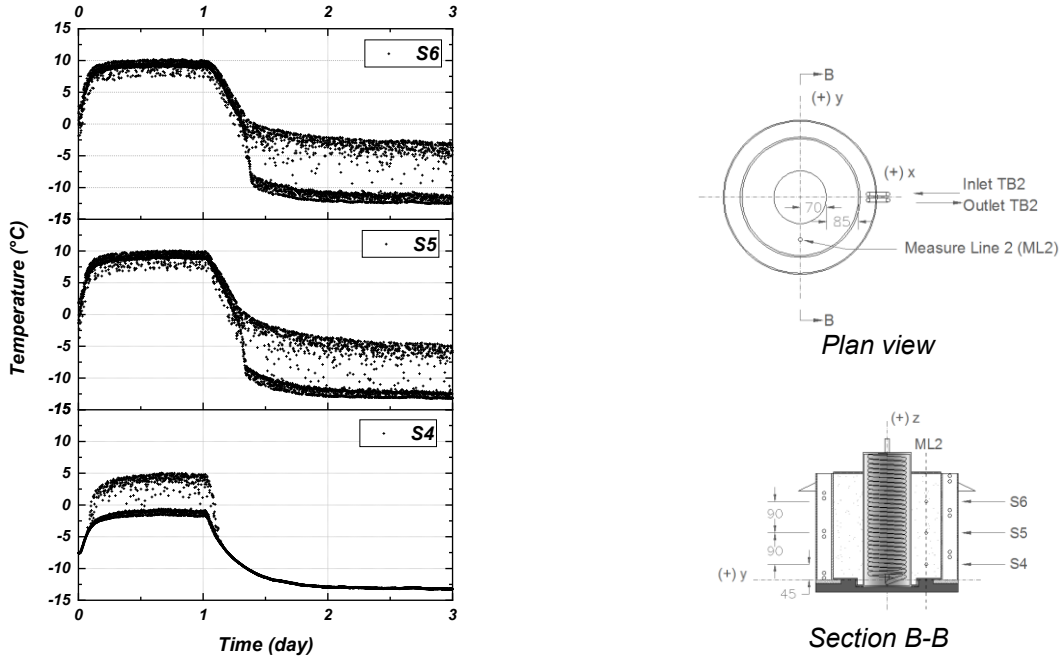

FIGURE 4.25 Temp. vs. time Batch (3), w (20%), Trial (TB2_Off1), starting (-2.5 °C), TB1on (-20 °C) -TB2_off for ML2. Unit: mm.

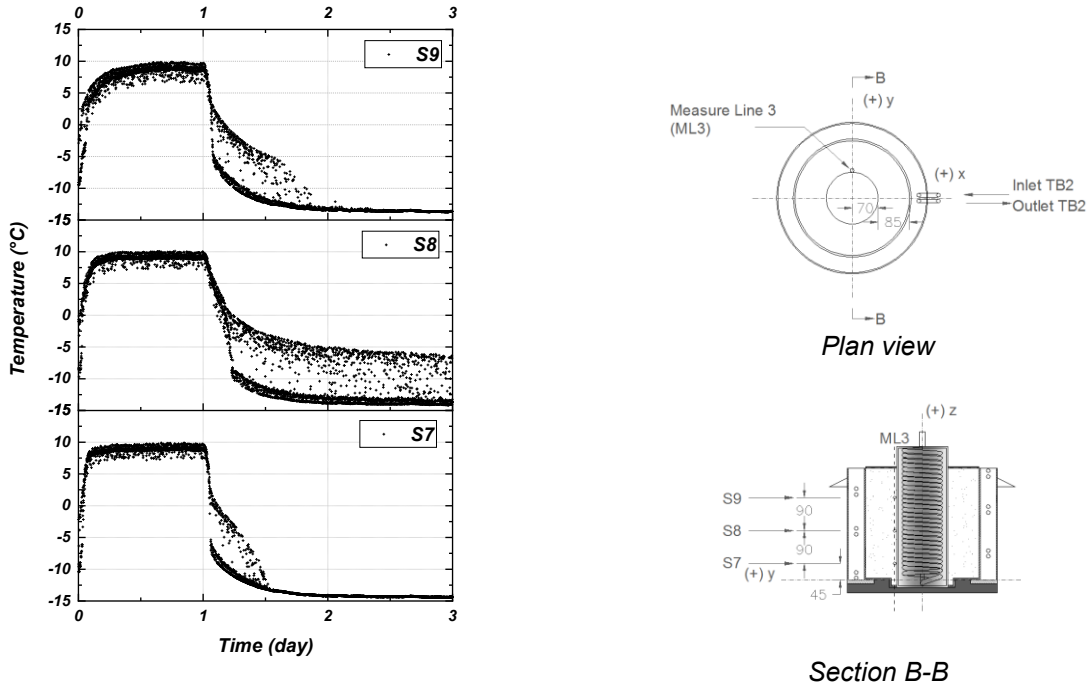

FIGURE 4.26 Temp. vs. time Batch (3), w (20%), Trial (TB2_Off 1), starting (-2.5 °C), TB1on (-20 °C) -TB2_off for ML3. Unit: mm.

Fig. 4.24 shows the temperature vs. time registered by the sensors located at ML1. Sensor 1 and sensor 2 reached the approximate temperature of -2 °C which is close to the desired temperature of -2.5 °C during the homogenization stage (day one); it appears as though decimal values in the temperatures are tough to reach with precision for the temperature bath 2 (TB2). In the trial, these two sensors reflect a similar even curve with a significant range of temperature going from -2 °C to about -12.5 °C (second day of the test) and maintaining this low temperature constant during the third day. Sensor 3, on the other hand, shows a trend during the homogenization stage that is a bit further away from the desired temperature; the temperature recorded was between 0 °C and -2 °C. This trend could be because this sensor was located in the upper part of the test cell and was not insulated well. It should be noted that at the end of the trial sensors 1 and 2 reached a temperature of about -12.5 °C and sensor 3 reached a temperature of about -10 °C by the end of day 3.

Fig. 4.25 shows the temperature vs. time registered by the sensors located at ML2. Sensor 4 shows a trend that reached the desired temperature of -2.5 °C during the homogenization stage

(day one). Sensor 4 presents a similar even curve that sensor 1 and sensor 2 showed at ML1, reaching an approximate temperature of -13 °C by the end of the trial. On the other hand, sensors 5 and 6 show more variability on the readings, and during day one the temperature is around 10 °C, far from the desired -2.5 °C for this stage of the trial.

It is also noteworthy that the transition from positive to negative temperatures is steeper with sensors 5 and 6, and the change occurs close to day 1.5; this could be because of the location of the sensors inside of the soil sample.

Fig. 4.26 shows the temperature vs. time registered by the sensors located at ML3. This group of sensors shows variability in the readings, especially sensor 8. It is also notable that the sensor at the top (S9) is a little warmer than the sensor at the bottom (S7). These readings are such possibly due to the copper coil configuration inside of the pile. Also, these three sensors never reached the desired homogenization temperature of -2.5 °C during day one. Their readings were about 10 ° C.

In general, after seeing the behavior of the 9 sensors at the 3 measure lines, it can be remarked that all the sensors reached a temperature of about -10 °C to -14 °C at the end of the experiment. This indicates that the 3 layers evaluated inside of the soil sample were at this temperature at the end of the trial.

Thermocouples immersed in the Glycol inside of the Pile

Fig. 4.27 shows the temperature vs. time of the thermocouples immersed in the glycol inside of the pile at 3 different locations: upper (sensor 15), middle (sensor 14), and bottom (sensor 13), all at ML4. It is also important to note that all three sensors are very similar in the trend values and very smooth in their responses after day one. Sensors 14 and 15 show some more variation in the readings during the homogenization stage and this could be due to their location in the pile.

This figure shows how consistent the temperature bath (TB 1) is during the whole trial, delivering the approximate temperature of -2.5 °C during the homogenization stage (day 1) and a temperature of -20 °C during the second stage (days 2 and 3); all the sensors are reaching a pretty constant temperature of about -17.5 °C inside of the pile, giving a good indication of the

actual temperatures delivered by the system that could be used for future calibrations and designs.

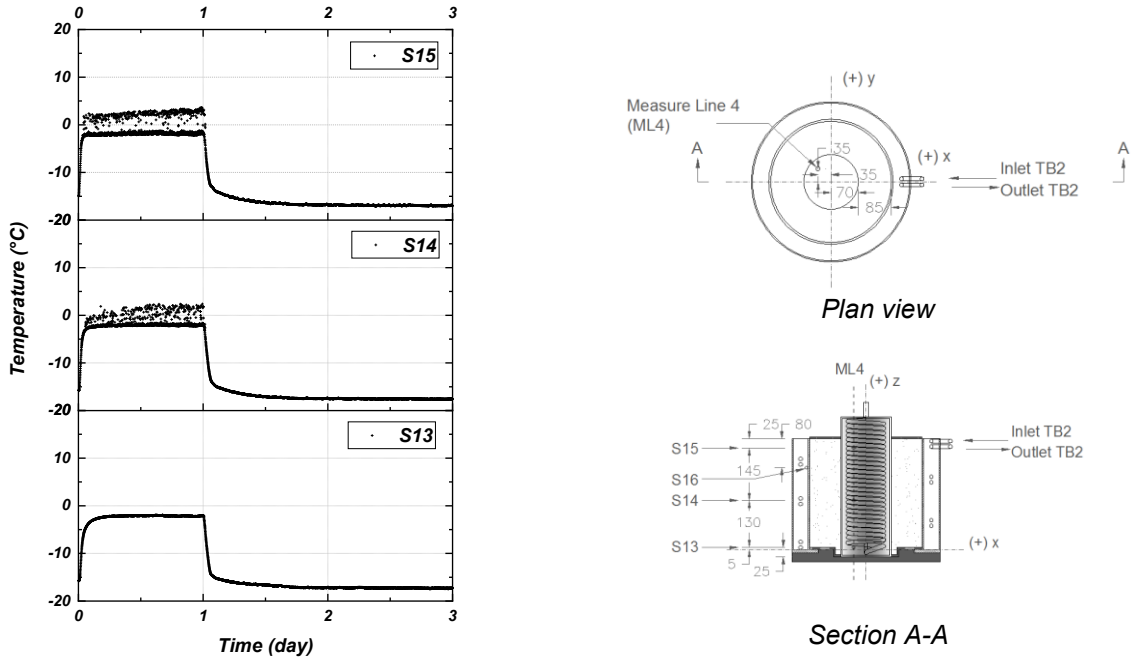

FIGURE 4.27 Temp. vs. time Batch (3), w (20%), Trial (TB2_Off1), starting (-2.5 °C), TB1on (-20 °C) -TB2_off for inside glycol in pile. Unit: mm.

This graph also proves that the copper coil configuration delivers a constant temperature throughout the length of the entire pile. It is important to note that it takes approximately 2 hours for the TB1 to reach -20 °C from an initial temperature of -2.5 °C. Consequently, for TB1 and the copper coil arrangement it is possible to reach temperatures with decimal values, like -2.5 °C, during the homogenization stage.

Thermocouple inside of the Test Cell Wall

This figure (Fig. 4.28) shows the readings of one thermocouple located inside the double wall of the test cell, more precisely, at the middle of the upper section (layer) (S16). These readings demonstrate another way to measure the temperatures inside of the soil sample in this scenario (trial); this has several advantages and can improve the test procedure.

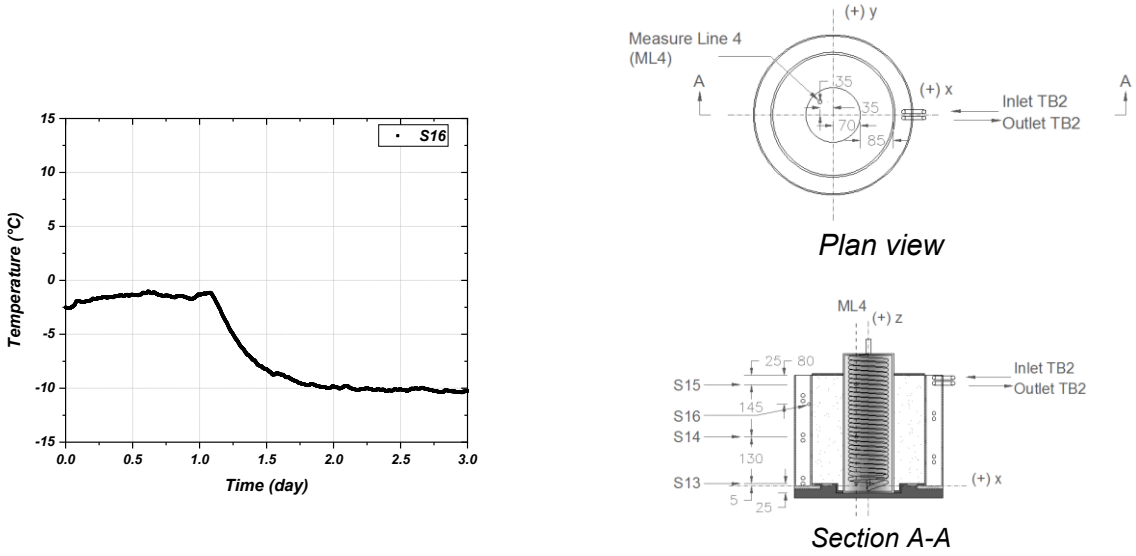

FIGURE 4.28 Temp. vs. time Batch (3), w (20%), Trial (TB2_Off1), starting (-2.5 °C), TB1on (-20 °C) -TB2_off inside glycol test cell. Unit: mm.

Let us now examine these advantages in greater detail.

Firstly, it is easier to install and remove the thermocouple at any moment, even if the soil is frozen. Second, it reflects, in a pretty smooth curve, what is happening near the soil sample which is one of the primary purposes of the experiment. Third, it avoids creating a disturbance of the sample during the installation or removal of the sensors. Next, it allows to locate the sensor precisely at the high level inside of the sample that is meant to be evaluated. Fifth, it avoids damaging the sensors during the removal and recycling of the soil at the end of the experiment. Lastly, it helps to create a real image of the radial temperature of the experiment.

This figure is similar to the trend observed in Fig. 4.24 with sensor 3 and its readings.

Density and Water Content

Table 4.3 shows the values of density and water content measured after Batch (3). It can be seen that the values of water content at the bottom of the test cell remain constant until the end of the test, at approximately 18.66% vs. 20% initially. In the upper and middle layers, there is a decline in water content values, 18.21% at the top and 18.52% in the middle.

TABLE 4.3 Batch (3) Density and Water Content by Layer

Layer	Sample	Tray empty (gr)	Tray+soil+ ring (gr)	Soil+tray (gr)	Soil $_{Dry}$ +tray (gr)	Soil mass (gr)	Soil mass (kg)	Density (kg/m^3)	Average density (kg/m^3)	Unit weight (kN/m^3)	Average Unit weight (kN/m^3)	w (%)	Average w (%)
1	L1-1	4.25	395.95	231.43	196.15	227.30	0.2273	1768.74	1848.02	17.35	18.13	18.38	18.21
	L1-2	4.25	408.75	244.15	207.52	240.10	0.2401	1868.35		18.33		18.02	
	L1-3	4.24	405.08	240.53	204.56	236.44	0.2364	1839.87		18.05		17.96	
	L1-4	4.31	414.82	250.23	211.84	246.11	0.2461	1915.11		18.79		18.50	
2	L2-1	4.27	412.73	248.07	209.72	244.06	0.2441	1899.16	1912.18	18.63	18.76	18.67	18.52
	L2-2	4.24	418.74	254.09	215.28	250.10	0.2501	1946.16		19.09		18.39	
	L2-3	4.28	411.95	247.40	209.63	243.27	0.2433	1893.01		18.57		18.39	
	L2-4	4.26	414.16	249.58	211.05	245.50	0.2455	1910.37		18.74		18.63	
3	L3-1	4.26	408.87	244.12	206.65	240.21	0.2402	1869.20	1868.70	18.34	18.33	18.51	18.66
	L3-2	4.28	405.45	240.75	203.81	236.77	0.2368	1842.43		18.07		18.51	
	L3-3	4.24	407.04	242.24	204.62	238.40	0.2384	1855.12		18.20		18.77	
	L3-4	4.29	413.89	249.23	210.39	245.20	0.2452	1908.03		18.72		18.85	
Total average									1876.30		18.41		18.47

Note 1: Ring dimensions: external diameter = 6.9 cm; internal diameter = 6.65 cm; height = 3.7 cm and weight = 164.40 gr.

Note 2: Column (Soil mass) = column (Tray + soil + ring) – tray – ring.

4.2 Conclusions

- The best test results were observed in the trials where just the pile temperature bath (TB1) was working after the homogenization stage. The soil reached temperatures below 0 °C until approximately -13 °C ± 1 °C at the end of the third day.
- The results of the lab testing proved that freezing the warming soil is feasible in the laboratory.
- The experiment showed that in a short period of time, the temperature of the soil near the pile decreased.
- The temperature of the ethylene glycol traveling through the copper coil can be concentrated near the wall of the pile, making for a better heat transfer.
- It is possible to locate thermocouples (sensors) inside of the test cell wall. The temperature of the soil sample inside of the test cell is transmitted to the ethylene

glycol and then to the sensor which helps to clearly reflect the results of the experiment near the pile.

5. Modeling of Freezing Tests: Analytical Solution and Finite Element Analysis

This chapter presents and discusses the analysis of the test results. The objective of modeling a closed-form solution and a finite element analysis was to compare the energy to be removed, the time for freezing, and the refrigeration plan capacity versus laboratory results. In this way, the laboratory procedure can be validated. The chapter presents the soil sample's physical properties and the thermal parameters and properties necessary to carry out the analysis, examines a closed form solution and a finite element solution for a single pile scenario, and explains the power and energy demand analysis for the test. Moreover, the chapter compares the analytical results to the experimental data.

In this chapter the soil sample at 35% water content with a surrounding soil temperature of 0 °C (homogenization stage) was considered, so as to be consistent with the laboratory results presented in chapter 4, more specifically trial TB2_Off2 when just TB1 was working after the homogenization stage (all analyses are in Appendix A). In the temperature vs. time (Test vs. Finite Element) comparison section, we can observe the results of both 35 and 20% water contents with surrounding soil temperature at 0 °C.

5.1 Physical Soil Sample Properties (w = 35%)

Table 5.1 present the initial properties that have to be measured in the laboratory for the soil sample with a water content of 35%. The water content was calculated during the soil sample preparation and after the consolidation test (insignificant water drainage). The specific gravity of solids was measured in the laboratory through the ASTM D 854-00 – Standard Test for Specific Gravity of Soil Solids by Water Pycnometer. The unit weight of water is a constant value for a temperature of 4 °C and the total unit weight of the soil was estimated at the end of the consolidation stage by the height of the soil sample inside the test cell.

TABLE 5.1 Initial Soil Sample Properties (w = 35%)

Property	Symbol	Value	Unit
Moisture content	w	35	%
Specific gravity of solids	G_s	2.67	
Unit weight of water (4 °C)	γ_w	9.807	kN/m^3
Total unit weight	γ	18.56	kN/m^3

Table 5.1 values represent the initial inputs for the closed-form solution analysis and the finite element analysis. With these properties of the soil sample and using phase relationships it is possible to calculate the other properties of importance for both thermal analyses. The properties calculated with the phase relationships equations are presented in Table 5.2.

TABLE 5.2 Phase Relationships (Physical Properties of the Soil Sample) (w = 35%)

Property	Symbol	Value	Unit
Void ratio	e	0.90	
Porosity	n	0.47	
Degree of saturation	S_r	1.0	
Density of water	ρ_w	1000	kg/m^3
Density of soil	ρ	1892	kg/m^3
Dry density	ρ_d	1402	kg/m^3

5.2 Thermal Parameters of the Soil Sample (w = 35%)

In Table 5.3 some of these values represent thermal constants for the water in different states of matter, i.e. in liquid and solid (ice) stages. The Kersten number, a function of the degree of saturation, is also included. These values are used in the next set of calculations of the thermal properties.

TABLE 5.3 Thermal Parameters of the soil sample (w = 35%)

Thermal parameters	Symbol	Value	Unit	Source
Thermal conductivity of the soil particles	k_s	2.5	W/m · °C	Table 2.1
Thermal conductivity of the pore water	k_w	0.57	W/m · °C	(Andersland & Ladanyi, 2004)
Unfrozen water content	w_u	0.25	%	Eq. 2.6
Thermal conductivity of ice	ki	2.2	W/m · °C	(Andersland & Ladanyi, 2004)
Kersten number for unfrozen coarse grained soil	K_e	1.01		Eq. 2.7
Kersten number for unfrozen fine grained soil	K_e	1.01		Eq. 2.8
Kersten number for frozen soil	K_e	1.0		$K_e=S_r$, Eq. 2.9
Volumetric heat capacity of water	c_{vw}	4.187	MJ/m^3 · °C	(Andersland & Ladanyi, 2004)

In the tests, by the end of day two, w_u was calculated using average temperatures reached T = -12.9 °C for w = 35% (Batch 2) and T = -11.4 °C for w = 20% (Batch 3). This applies to the tests for the sensors analyzed (see section 5.7 and Appendix A Verification of laboratory results).

5.3 Thermal Properties of the Soil Sample (w = 35%)

5.3.1 Thermal Conductivity

The thermal conductivity represents "the quantity of heat that flows through a unit area in a unit time under a unit temperature gradient".

Smoltczyk (2003) reported that frozen soils have a higher thermal conductivity than unfrozen soils in general because ice is a better thermal conductor than water. This concept supports one primary objective, i.e. to artificially freeze the ground while the soil is near the melting point.

There exist numerous methods of estimation for thermal properties, but the method established by Johansen (1975) is considered to be sound because it is applicable to unfrozen and frozen soils showing acceptable results as reported by Andersland & Ladanyi (2004).

Table 5.4 presents the values calculated for thermal conductivity of the soil sample with a water content of 35% using the method developed by Johansen (1975). In this table, it is observable that the values of saturated unfrozen soil and saturated frozen soil are close to the ranges reported by Smoltczyk (2003) for sand and silt (Table 5.5).

Even though the values are reported in degrees Kelvin (K), it is possible to make the comparison with degrees Celsius (C), because ultimately what is important is the difference in temperature; this difference is the same in both degrees Celsius and Kelvin, so basically the units are exactly the same.

TABLE 5.4 Calculated Thermal Conductivity of the Soil Sample (w = 35%)

Thermal conductivity	Value	Unit
Dry, natural soil	0.18	W/m · °C
Dry, crushed rock materials	0.20	W/m · °C
Saturated unfrozen soil	1.24	W/m · °C
Saturated frozen soil	2.34	W/m · °C
Unfrozen	1.25	W/m · °C
Frozen	2.42	W/m · °C
Frozen soil with w_u	2.41	W/m · °C

Typical thermal conductivities for water-saturated soils are given in Table 5.5

TABLE 5.5 Thermal Conductivity of Water-Saturated Soils (Smoltczyk, 2003)

Soil type	Thermal conductivity	
	k_u (unfrozen) W/mK	k_f (frozen) W/mK
Gravel	2.0-3.3	2.9-4.2
Sand	1.5-2.5	2.7-3.9
Silt	1.4-2.0	2.5-3.3
Clay	0.9-1.8	1.5-2.5
Claystone	2.6-3.1	2.7-3.2
Sandstone	3.1-4.3	3.2-4.4

5.3.2 Heat Capacity

The specific heat capacity (c_m) is "the quantity of heat required to raise the temperature of a unit mass of a substance by a unit change of temperature" (Smoltczyk, 2003). The volumetric heat capacity (c_v) is obtained by multiplying the specific heat capacity by the soil density (ρ) (Smoltczyk, 2003). The heat capacity of a multi-phase soil system is the weighted arithmetic mean of each of the individual soil components. Once the unfrozen water content (w_u) was estimated, the volumetric heat capacity of the frozen soil was determined.

Table 5.6 presents the volumetric heat capacities for mineral unfrozen and frozen soil (w = 35%); these values were calculated with equations 2.13 and 2.14 respectively.

TABLE 5.6 Volumetric Heat Capacities of Soil Sample (w = 35%)

Volumetric heat capacities				
Unfrozen	3.05	$MJ/m^3 \cdot °C$	3051.56	$kJ/m^3 \cdot °C$
Frozen	2.03	$MJ/m^3 \cdot °C$	2031.96	$kJ/m^3 \cdot °C$

Comparing the Table 5.6 values with the values reported by Smoltczyk (2003) for volumetric heat capacity of water saturated soil, it can be noted that these values are within the range reported for sand and silt (Table 5.7).

Typical volumetric heat capacities for water-saturated soils are presented in Table 5.7.

TABLE 5.7 Volumetric Heat Capacity of Water-Saturated Soils (Smoltczyk, 2003)

Soil type	Volumetric heat capacity	
	c_{vu} (unfrozen) kJ/m^{3}K	c_{vf} (frozen) kJ/m^{3}K
Gravel	2200-2700	1500-2100
Sand	2500-3000	1800-2200
Silt	2500-3100	1800-2300
Clay	2200-3200	1700-2300
Claystone	2340-2350	2250-2260
Sandstone	2190-2200	2070-2080

Even though the values are reported in the Table 5.7 in degrees Kelvin (K), it is possible to make the comparison with degrees Celsius (C), because ultimately what is important is the difference in temperature.

5.3.3 Latent Heat of Fusion

The quantity of heat energy consumed when a unit mass of ice is transformed into a liquid at the melting point is established as its latent heat of fusion. 162.52 MJ/m^3 was the value obtained (Eq. 2.25) for a soil sample (w = 35%) with a surrounding soil at 0 °C.

5.4 Closed-Form Solution of Soil Sample Batch (2) (w = 35%) (surrounding Soil at 0 °C) (TB2_Off2)

The closed-form solution was implemented to compare the energy to be removed, the time needed for freezing and the refrigeration plant capacity versus laboratory results.

Sanger & Sayles (1979) presented a closed-form solution for steady-state radial heat flow thermal analysis of a single freeze pipe and wall formation, with the absence of seepage flow. The analysis below represents the soil sample with water content at 35% and the surrounding soil at 0 °C. Appendix A shows the analyses for the soil sample with water content at 35% and the surrounding soil at -2.5 °C, and also for the soil sample at 20% with the surrounding soil at 0 °C and -2.5 °C.

Table 5.8 presents the pile dimensions, soil physical properties, and previous soil thermal constants and properties. Table 5.8 values were calculated using the Sanger & Sayles (1979) closed-form solution method.

TABLE 5.8 Input Parameters to the Closed-form Solution

Freeze pipe dimensions		
Spacing (S)	1	m
Radius (r_0)	0.07	m
Soil physical properties		
Soil type	Silt sand	
Density of soil (ρ)	1892.12	kg/m^3
Water content (w)	35	%
Soil dry density (ρ_d)	1401.57	kg/m^3

Soil thermal properties	Value	Unit	Source
Difference between the temperature at the surface of the freeze-pipe and the freezing point of water (v_s)	-20	°C	TB1
Difference between the ambient temperature of the ground and the freezing point of water (v_0)	0	°C	Homogenization stage
Volumetric heat capacity of water (c_{vw})	4.187	$MJ/m^3 \cdot °C$	(Andersland & Ladanyi, 2004)
Frozen thermal conductivity (k_f)	2.42	$W/m \cdot °C$	Eq. 2.17
Amount of heat when water is converted into ice with no change in temperature (L')	333700	J/kg	(Andersland & Ladanyi, 2004)
Volumetric heat capacity for mineral (frozen) soils (c_{vf})	2.03	$MJ/m^3 \cdot °C$	Eq. 2.14
Volumetric heat capacity for mineral (unfrozen) soils (c_{vu})	3.05	$MJ/m^3 \cdot °C$	Eq. 2.13
Volumetric latent heat of the soil (L)	162.52	MJ/m^3	Eq. 2.25
Equivalent latent heat for stage I (L_1)	162.52	MJ/m^3	Eq. 2.32

Table 5.9 shows the results obtained for stage I (ice-soil column growing around the pile), where R represents the radius of the ice-soil column growing, Q the energy extracted, t the time in days, and P the rate of energy extracted (Andersland & Ladanyi, 2004).

TABLE 5.9 Results of Closed Form Solution

Stage I			
R (m)	**Q_I (MJ/m)**	**t_1 (days)**	**P_1 (W/m)**
0.10	6.90	0.05	851.42
0.15	13.37	0.17	398.46
0.20	22.86	0.53	289.27
0.25	35.05	1.09	238.56
0.30	49.90	1.89	208.67
0.35	67.40	2.94	188.69
0.40	87.55	4.26	174.23
0.45	110.34	5.85	163.20
0.50	135.76	7.74	154.46

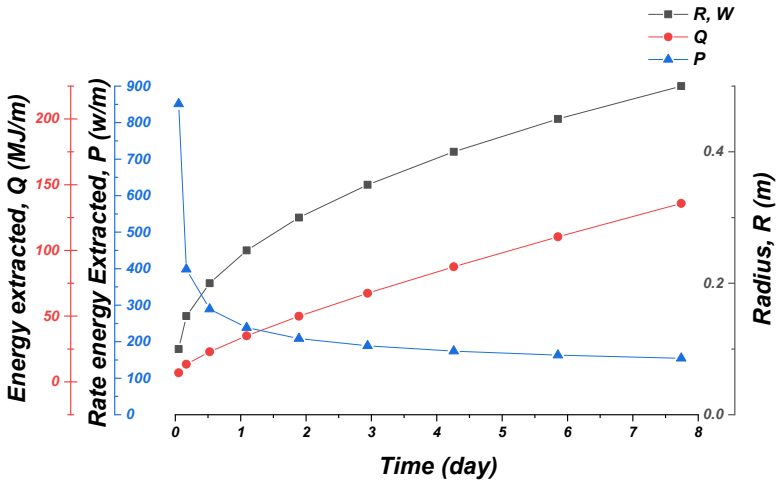

FIGURE 5.1 Results for stage I, Time vs radius R, energy extracted Q, and rate energy extracted P.

Fig. 5.1 shows the results for stage I. To validate the laboratory freezing test of the present research, the values of the rate of energy extracted P from Fig. 5.1 were compared at the end of this chapter against laboratory power results.

5.5 Finite Element Analysis of Artificial Ground Freezing

The finite element analysis of artificial ground freezing was executed to compare the energy to be removed, the time needed for freezing and the refrigeration plant capacity versus laboratory results.

A finite element model was developed on the platform of Temp/W software for the freezing test Batch (2) Trial (TB2_Off2) that had a water content of 35% and the initial soil temperature of 0 °C (homogenization or surrounding temperature). This test was done when the temperature bath 2 was turned off after the homogenization stage. The temperature vs. time curves for this test fit with the finite element model outcomes curves (transient analysis). Tests results and results of finite element analysis of all batches are presented in appendix A.

5.5.1 Model Configuration

To create an opening in the finite element mesh to mimic the freezing pipe pile can be a challenge. To avoid this complexity, a small point is placed at the location of the pile and the pile diameter is defined within the convective surface boundary conditions (Geoslope, 2018a). Fig. 5.2 shows the mesh configuration (global element size 0.5 m, element thickness 1 m).

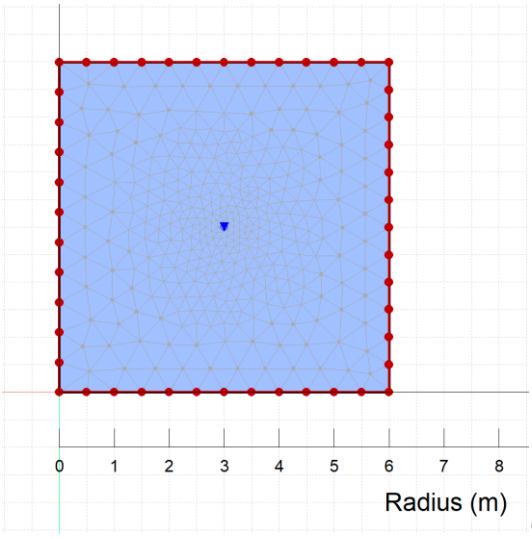

(Red line boundary 0 °C)

FIGURE 5.2 Mesh configuration.

5.5.2 Thermal Material Setting

In order to describe the soil in the thermal material model setting, a steady-state analysis was used; in this examination most of the thermal properties during the transient analysis stay constant, which is basically the purpose of the test i.e. to evaluate the steady conditions of the soil sample. The values of all these parameters were calculated in the previous sections 5.1, 5.2 and 5.3 and are shown in Table 5.10.

TABLE 5.10 Thermal Material Model Setting for Batch (2) Trial (TB2_Off2) (w = 35%) Homogenization Temperature at 0 °C

Parameter	Value	Unit		Value	Unit
Frozen thermal conductivity	2.42	W/m · °C		208.79	kJ/d/m/°C
Unfrozen thermal conductivity	1.25	W/m · °C		107.94	kJ/d/m/°C
Unfrozen water content (w_u)	0.25	%	(for Silty sand)		
Unfrozen volumetric heat capacity	3.05	$MJ/m^3 \cdot °C$		3051.56	$kJ/m^3 \cdot °C$
Frozen volumetric heat capacity	2.03	$MJ/m^3 \cdot °C$		2031.96	$kJ/m^3 \cdot °C$
Insitu water content	0.35				
Activation temperature	0	°C			

The activation temperature represents the temperature of the surrounding ground around the pile (surrounding mesh), which is the homogenization temperature in the test.

5.5.3 Boundary Condition

The boundary condition was defined as a convective surface that according to Geoslope (2018c) is a good approach for a conventional configuration inside of the freeze pipe. The convective heat transfer constants and coefficients are shown in Table 5.11 and are the input to the Temp/W software (latent heat of water 334 kJ/kg).

TABLE 5.11 Convective Heat Transfer Constants and Coefficients at the pile

Parameter	Value	Unit	Source
Glycol thermal conductivity	0.258	(w/m · °C)	(Engineering Toolbox, 2008)
Nusselt number	3.66		(Bergman et al.,2011)
Convective heat transfer coefficient (h)	6.74	$J/sec/m^2/°C$	Eq. 5.1
Fluid temperature	-20	°C	TB1
Surface perimeter	0.44	m	Pile's perimeter

Note: Nusselt number is the ratio of convective to conductive heat transfer at a boundary in a fluid; The constant h is convective heat transfer coefficient of the flow.

The value for the Glycol Thermal Conductivity was taken from Engineering Toolbox (2008) and the corresponding Nusselt number was taken from Bergman (2011).

The size of the pile was specified in the surface perimeter value (0.44 m), which corresponds to the pile's perimeter. The Fluid temperature input corresponds to the temperature setup at the temperature bath 1 (TB1) during the test.

The dimensionless Nusselt number is a function of the pile geometry, the flow regime, and the boundary condition at the pile surface. For this particular case, a circular pile was considered with fully developed laminar flow and a constant pile temperature; the Nusselt number (3.66) was selected from (Bergman et al., 2011).

The freeze pile (pipe) is 140 mm in diameter and filled with ethylene glycol (100% Glycol), with a thermal conductivity of 0.258 w/m°C. The heat transfer coefficient (h) is determined from Equation 5.1:

$$h = \frac{k_b N_u}{D_h} \tag{5.1}$$

where k_b is the thermal conductivity of the glycol, N_u is the dimensionless Nusselt number, D_h=4A/P is the hydraulic diameter, A is the cross-sectional area equal to 0.015 m^2, and P is the wetted perimeter equal to 0.44 m. The value of h is equal to 6.74 J/sec/m^2/°C.

Phase change can be the source of numerical variability in a heat transfer analysis; as a result, it is advisable to have a finer mesh in the phase change zone where the quantity of heat delivered or received is considerable. In this analysis, the mesh is refined near the points representing the freeze pile.

5.5.4 Results and Discussion

Fig. 5.3 (a) shows the temperature contour plot as the time approaches 0.5 days with a data range from -7.236 °C to 0 °C. Fig. 5.3 (b) shows the temperature contour plot as the time approaches 1 day with a data range from -7.815 °C to 0 °C. Fig. 5.3 (c) shows the temperature contour plot as the time approaches 2 days with a data range from -8.335 °C to 0 °C.

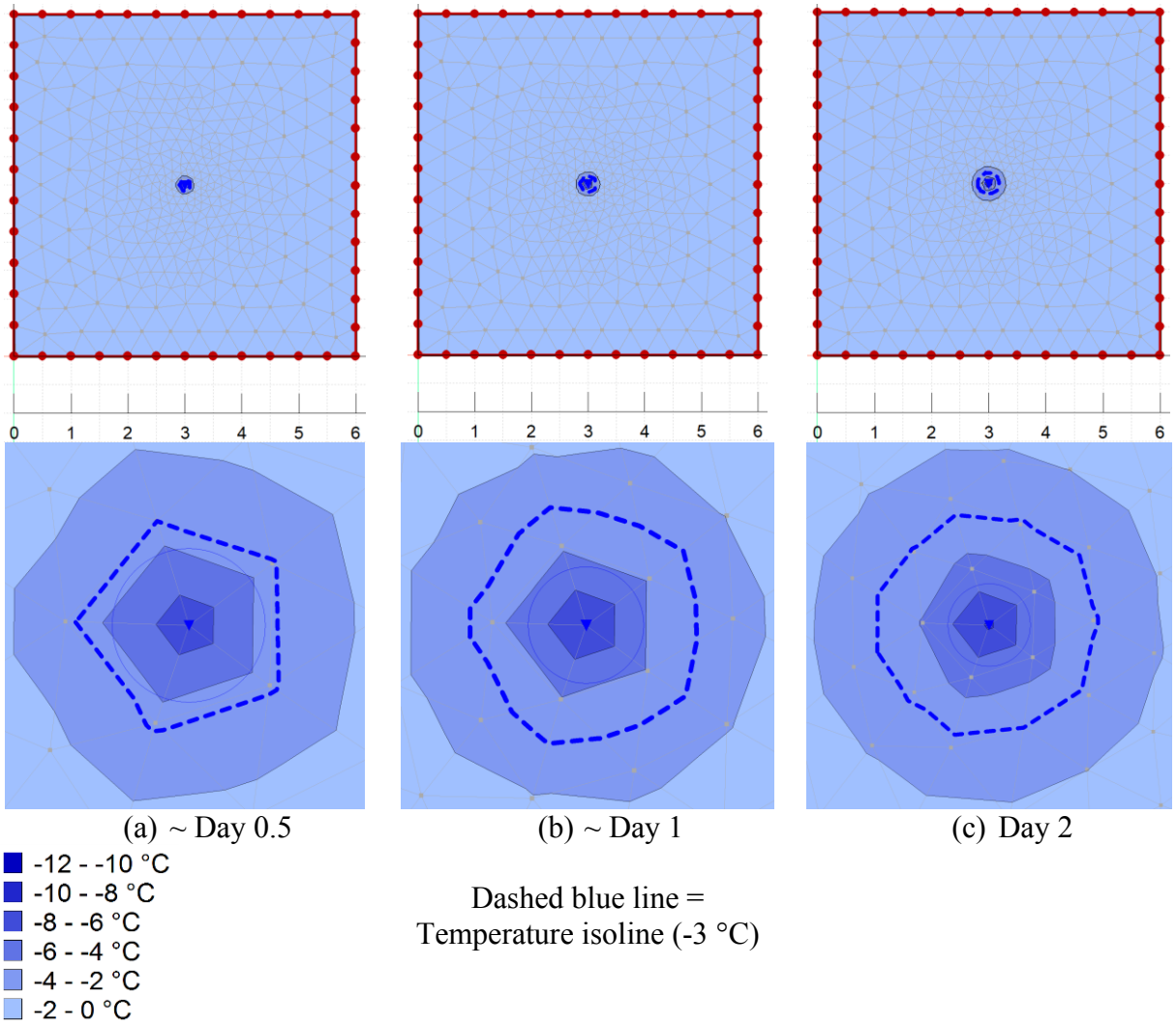

FIGURE 5.3 Radial extent of frozen soil in meters. (a) t = 0.5 day. (b) t = 1 day. (c) t = 2 day.

Fig. 5.4 presents the soil temperature versus time near the pile. Harris (1995) reported that the presence of salt(s), usually melted in the pore water, hinders the freezing process by reducing the freezing point temperature and thereby prolonging the time needed to reach the latent heat step.

It should be remarked that the point in the finite element model simulates the area near the pile.

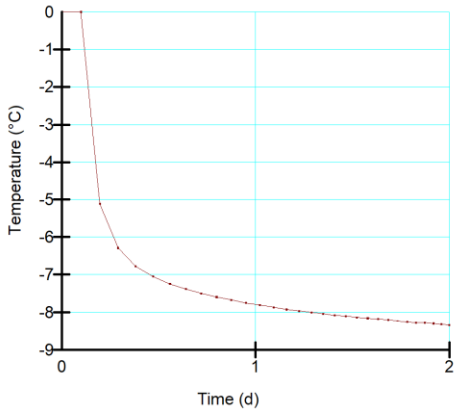

FIGURE 5.4 Temperature vs time (at the point on the mesh).

Fig. 5.5 shows a cut line graph from border to border of the analysis domain passing by the center of the point that simulates the region that is close to the pile.

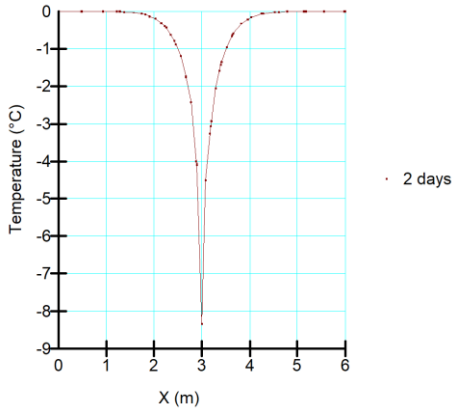

FIGURE 5.5 Temperature profile at day 2.

It should be noted that after two days the soil temperature is higher about -8.5 °C than that of the circulating glycol -20 °C; this is due to the thermal gradient over the pile wall. If the wall temperature reached the temperature of the glycol, there would be no temperature difference and no heat transfer (Geoslope, 2018a).

Fig. 5.6 shows the heat extraction rate per unit length of pile. In the beginning, the curve rises, until the ethylene glycol temperature reaches -20 °C. Next, the rate gently levels off as the soil temperature decreases. This shows the proportionality of the extraction rate and the temperature difference within the ethylene glycol and the soil (Geoslope, 2018a).

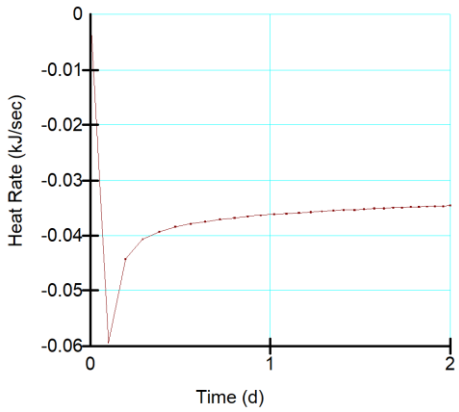

FIGURE 5.6 Heat extraction rate per unit length of pile.

One of the main objectives of artificial ground freezing projects is to estimate how much heat will have to be removed. The long-term heat extraction rate is approximately -0.03462 kJ/sec/m. With this amount it is feasible to calculate the required tons of refrigeration. One ton of refrigeration is equal to:

$$\frac{334\,\frac{\text{kJ}}{\text{kg}}\text{x}\,907.18\,\text{kg}}{24\,\text{h x}\,60\,\frac{\text{min}}{\text{h}}\text{x}60\,\frac{\text{sec}}{\text{min}}} = 3.5\,\frac{\text{kJ}}{\text{sec}} \tag{5.2}$$

where tons of refrigeration is the rate of heat transfer that results in melting one ton (2000 lb or 907.18 kg) of pure ice in 24 hr, and 334 kJ/kg is the latent heat of fusion/solidification of water.

It is important to recognize that expanding the plant capacity would not improve the freezing rate. The heat load is based on what the soil will yield to the ethylene glycol, not what the glycol obtains from the soil. The only way to reduce the cooling time is to add more piles (pipes) or decrease the temperature of the glycol (Geoslope, 2018a).

5.6 Power and Energy Demand for the Test

The cooling power P for the pile was calculated as

$$\text{P} = Q_{glycol}(T_{out} - T_{in})c_{glycol} - P_{loss} \tag{5.3}$$

where Q_{glycol}, T_{in}, T_{out}, c_{glycol} and P_{loss} denote the flux of glycol, temperature of the glycol entering and leaving the system, the volumetric heat capacity of the glycol, and the systematic power loss in the system, respectively (Pimentel et al., 2012).

The glycol flux was taken from the temperature bath manufacturer manual and the temperatures from the thermocouples located at the inlet and outlet of the copper coil during the experiments. The power supplied by the temperature bath 1 was constant throughout the whole experiment and the machine provided a steady temperature of -20 °C at a continuous flow velocity, 15 l/min. The specific heat (2.925 kJ/kg · °C) and the density (1120 kg/m^3) of the water ethylene glycol (approx. 65%) mixture at about -20 °C was taken from Engineering Toolbox (2003).

The following elements can lead to power loss during the experiments: inadequate insulation of the hoses coming from the temperature bath, long distance and considerable difference of head pressure between the refrigeration unit and the soil sample, and the drastic variations in temperature in the cold room.

The power loss P_{loss} was estimated by insulating and isolating the copper coil from the soil model and operating the temperature bath with the identical conditions as those implemented throughout the trials; this was done for the particular case where no cooling power leaves the system (P=0) (Pimentel et al., 2012).

Fig. 4.12 shows the temperature of the ethylene glycol entering and leaving the copper coil, registered by sensors 10 and 11, respectively. To calculate the power P of the system using equation 5.3, one must estimate the power loss P_{loss}. Fig. 5.7 shows the scenario where no cooling power leaves the system (P=0); it shows the temperatures of sensor 10 and sensor 11 on the copper coil outside of the soil model and entirely insulated including the temperature of the cold room. It should be noted that the cold room is a cooler that is subject to freezing cycles. The best observations were recorded during the time the cold room temperature was around 0 °C, as indicated by the circles on the figure. With these conditions, a constant power loss P_{loss} of 659.85 W was determined during the execution of the experiments, following this formula:

$$0 = Q_{glycol}(T_{out} - T_{in})c_{glycol} - P_{loss} \tag{5.4}$$

Fig. 5.8 shows the cooling power in W and the fit curve. By taking the fit curve of Fig. 5.8 and dividing it by the length of the freezing pile segment (0.385 m) it is possible to obtain the cooling power in W/m for the experiment show in Fig. 5.9.

Fig. 5.9 presents the cooling power P and the energy E in W/m. E was calculated by integrating the power over time (Sanger & Sayles, 1979).

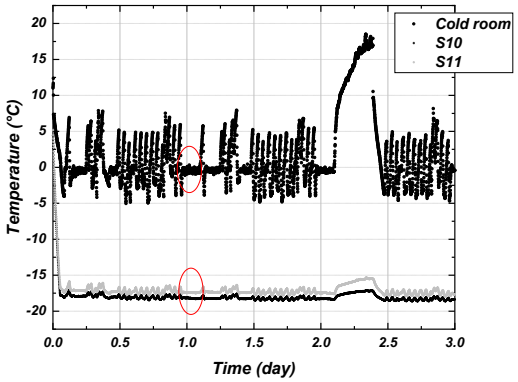

FIGURE 5.7 Inlet (S10) and outlet (S11) temperatures on the copper coil measured at power loss test (P=0).

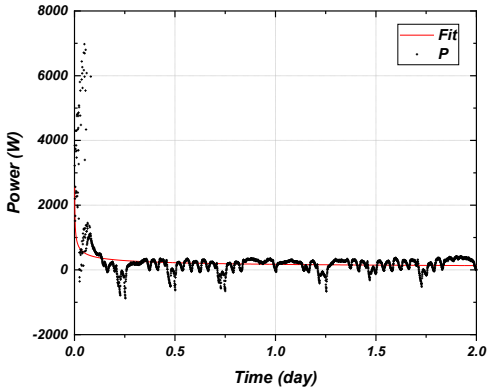

Fit: $y = 172.37 \times^{-0.37}$

FIGURE 5.8 Cooling power P in W (Batch (2) Trial (2)).

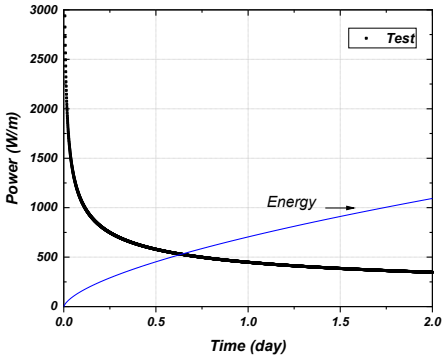

FIGURE 5.9 Cooling power P and energy extracted Q in W/m (Batch (2) Trial (2)).

To validate the laboratory freezing test of the present research, the values of the cooling power P from Fig. 5.9 was compared at the end of this chapter vs. laboratory power results.

5.7 Verification of Laboratory Results

5.7.1 Temperature vs time (Test vs Finite Element)

The trials that demonstrate a better fit with the finite element solution are the ones where the temperature bath (TB2) of the test cell was turned off (after homogenization stage). In Appendix A, it is possible to see all these trials with their comparison charts. These charts compare the temperature versus time of the test result versus finite element solution.

The analysis below is for Batch (2) trial (TB2_Off2) TB1on (-20 °C) -TB2_Off, starting from 0 °C for soil with 35% water content.

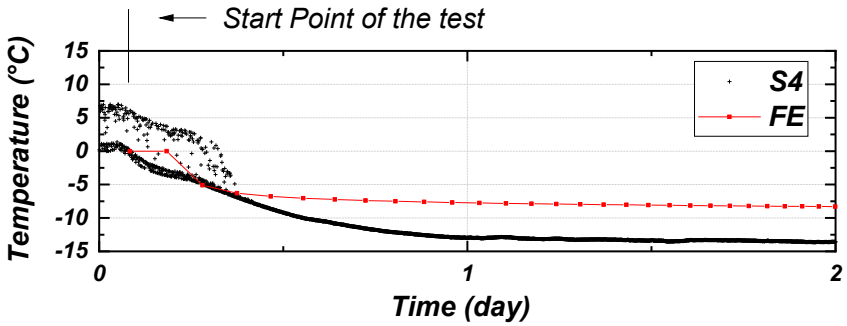

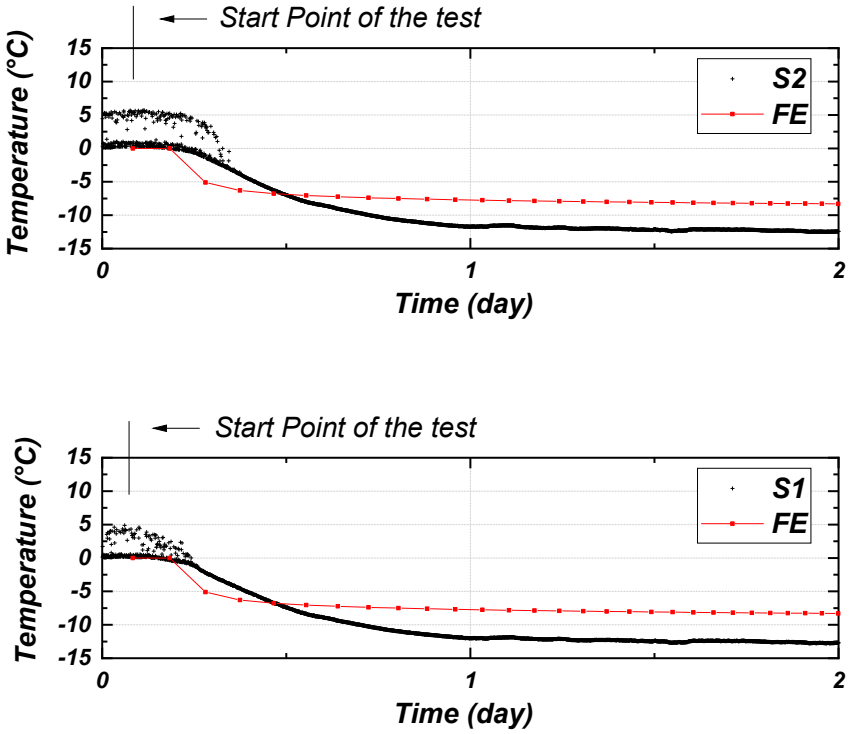

FIGURE 5.10 Temperature vs time of the test result vs finite element solution S1, S2 and S4 w (35%) starting from 0 °C (Batch (2) trial (TB2_Off2)).

Fig. 5.10 compares temperature vs. time of the test results vs. finite element solution for sensors 1, 2, and 4. These particular sensors show a even response after the homogenization stage, allowing for the comparison of the finite element solution with the test outcomes.

The start point of the test is the moment when the temperature in the copper coil inside of the pile achieves the desired temperature of -20 °C. Consequently, at day 0, the Temperature Bath 1 was set up at -20 °C but the temperature started to decrease gradually from 0 °C at the homogenization stage. From this moment on, the test and the simulation could be comparable. It is noteworthy that the sensors show tendencies better to what is outlined by the finite element analysis, i.e. start at 0 °C and finish with a temperature close to -12.5 °C. Comparing these three sensors, the sensor with the most suitable fit is sensor 1. It is notable that before the end of day one sensor 4 reaches the lowest temperature.

The analysis below is for Batch (3) trial (TB2_Off2) TB1on (-20 °C) -TB2_Off, starting from 0 °C for soil with 20% water content.

Fig. 5.11 shows the comparison of the temperature vs. time of the test results vs. finite element solution for sensors 1, 2, 3 and 16. These particular sensors show a pretty even response after the homogenization stage, allowing for the comparison of the finite element solution with the test outcomes.

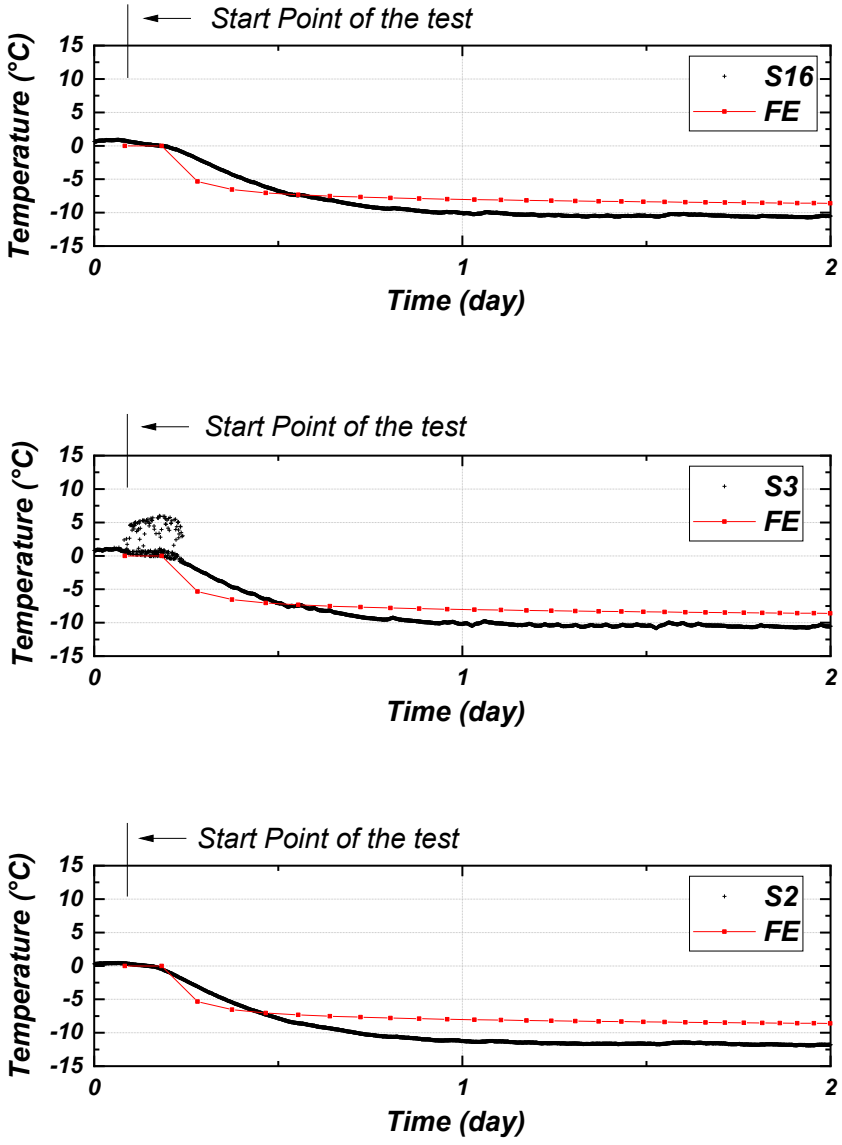

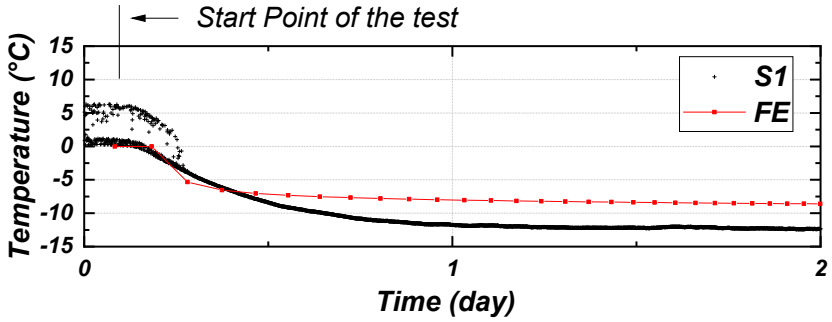

FIGURE 5.11 Temperature vs time of the test result vs finite element solution S1, S2, S3 and S16 w (20%) starting from 0 °C (Batch (3) trial (TB2_Off2)).

The start point of the test is the moment when the temperature in the copper coil inside of the pile achieves the desired temperature of -20 °C. Consequently, at day 0, the temperature bath 1 is set up at -20 °C but the temperature starts to decrease gradually from 0 °C at the homogenization stage. From this moment on, the test and the simulation could be comparable. It is noteworthy that the sensors show tendencies closer to what is outlined by finite element analysis, i.e. both start at 0 °C and finish with a temperature close to -11 °C. Comparing these sensors, the sensors with the best fit are sensors 2, 3, and 16. It is noteworthy that before the end of day one the lowest temperature was reached. Sensors 3 and 16 are equivalent; sensor 16 was taking readings on the inside of the test cell double wall with the glycol and was at the same height as sensor 3. Sensor 16 however, in comparison with Sensor 3, generates a more even curve of temperature vs. time records.

5.7.2 Power (Test vs Closed-Form Solution vs Finite Element)

The analysis below is for Batch (2) trial (TB2_Off2) TB1on (-20 °C) -TB2_Off, starting from 0 °C for soil with 35% water content.

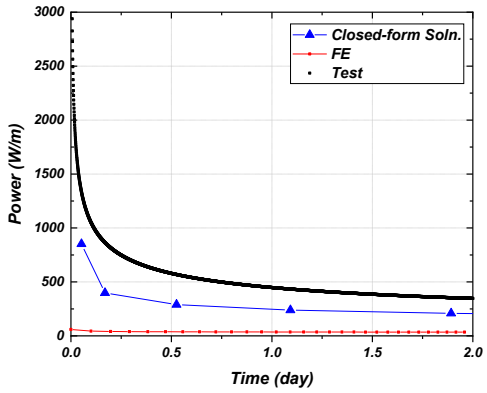

FIGURE 5.12 Cooling power in W/m obtained from for the closed-form solution, finite element solution, and the test (Batch (2) Trial (2)).

Fig. 5.12 shows the cooling power curves in W/m obtained from the closed-form solution, finite element solution, and the test. It is notable that the cooling power of the test and the cooling power calculated by the closed form solution are very close at the end of day two. This confirmed what was mentioned by Braun (1979), namely, that the Sanger & Sayles (1979) closed-form solution is reasonable and has enough accuracy with field observations.

A possible reason why there is a gap between the cooling power reported by the finite element analysis and the test results could be because of the refining of the mesh (i.e., how the dimensions of the small "q" heat flux boundary is computed); and/or to the complex multi-phase system of the soils. It is noteworthy that with more time the curves tend to be closer to the FE curve. The results reported are in agreement with the procedures (templates) and results reported by the manufacturer of the software.

5.7.3 Minimum Freeze Plant Capacity (Tones Refrigeration) (Test vs Closed-Form Solution, FE)

The analysis below is for Batch (2) trial (TB2_Off2) TB1on (-20 °C) -TB2_Off, starting from 0 °C for soil with 35% water content.

Table 5.12 shows the calculations for the minimum freeze plant capacity needed to obtain the tons of refrigeration; the values of the power in W/m at the end of day two were used for this task. An example of the calculations is presented below. With Eq. 5.5 is possible to calculate the minimum freeze plant capacity in tones of refrigeration. In Eq. 5.5 the number (1) represents the

number of freeze pipes or piles in this case, 0.34626 is the test´s cooling power at the end of day 2 in KJ/sec/m, 0.385 is the length of the pile in meters, and 3.5 kJ/sec is the unit conversion factor for one ton of refrigeration (Geoslope, 2018a).

TABLE 5.12 Minimum Freeze Plant Capacity

Method	W/m	KJ/sec/m	Tones of refrigeration
Test	346.26	0.34626	0.03809
Closed-form solution	208.67	0.20867	0.02295
Finite element	34.62075	0.0346208	0.00381

$$\frac{1 \text{ x } 0.34626 \text{ kJ/sec/m x } 0.385 \text{ m}}{3.5 \text{ kJ/sec}} = 0.03809 \text{ Tones of refrigeration} \quad (5.5)$$

5.8 Conclusions

- During the evaluation of the temperature in the soil next to the pile, in an endless one pile scenario the finite element model helps to predict the fittest temperature vs. time curves (transient analysis) and the closed form solution predicts the fittest energy extracted Q and rate energy extracted P curves.
- Using a copper coil inside of the pile filled with ethylene glycol instead of the conventional freeze tube assemblies, and by developing a convective analysis, it is found that this convective analysis continues to be valid for this copper coil configuration.
- TB1on and TB2on scenario was not representative; TB1on and TB2off scenario is more congruent with the theory after the homogenization stage.
- The experiment shows that it is possible to observe reasonable temperature vs. time curves that will be a fair match for the finite element analysis near the pile, for a distance (from the pile border) between r_0 to $2r_0$, r_0 being the radius of the pile.

6. Conclusions and Recommendations

6.1 Conclusions

Examining the actual foundation types used against frost heave and the problem of the melting permafrost (active layer) in the northern territories, it is evident that they are passive solutions with low reliability. What is required is an active and effective method that helps to overcome the changes in temperatures in the active layer that are caused by natural or unnatural circumstances. Exploring alternative energy sources (e.g., Solar, Geothermal) could ultimately make the artificial freezing system sustainable.

- The experiment showed that in a short period of time, the temperature of the soil near the pile decreased, reaching temperatures below 0 °C up to approximately -13 °C ± 1 °C, from the starting temperature. This may reduce the freeze-back time and increase the ad-freeze bond.

- The test procedure elaborated for this thesis is suitable for a complete analysis layer by layer for real size piles where the set-up can be done with an initial ground temperature, water content, and consolidation conditions; initiating a 2D analysis in a layer and subsequently completing the rest of the soil profile it would be possible to complete a 3D analysis of the ice-soil column around the entire pile. Moreover, this test can also be used for conventional configurations of freezing pipes in active artificial ground freezing.

- During the evaluation of the temperature in the soil next to the pile, in an endless one pile scenario the finite element model helps to predict the fittest temperature vs. time curves (transient analysis) and the closed form solution by Sanger & Sayles (1979) predicts the fittest energy extracted Q and rate energy extracted P curves.

- The research proved that using a copper coil inside of the pile filled with ethylene glycol instead of the conventional freeze tube assemblies (see Chapter 2), and by developing a convective analysis, it is found that this convective analysis continues to be valid. Other advantages are that the temperature of the ethylene glycol traveling through the copper coil can be concentrated near the wall of the pile, making for a better heat transfer; consequently less energy is required to power the system because the diameter of the

copper is rather small (3/8 inches) so it needs a small pump and glycol reservoir. Hence, the use of the copper coil can improve the maintenance and monitoring during the artificial ground freezing process.

- Part of the research was to study which scenario performs better for a single pile installation in the endless surrounding in the laboratory. TB1on and TB2on scenario was not representative; TB1on and TB2off scenario is more congruent with the theory. TB1on and TB2on scenario can be used to represent the pile-ground interaction at the surface where the climate can interfere, or there is another source of heat.

- The experiment shows that it is possible to observe reasonable temperature vs. time curves that will be a fair match for the finite element analysis near the pile, for a distance (from the pile border) between r_0 to $2r_0$, r_0 being the radius of the pile. According to Geoslope (2018a), just besides the pile wall the temperature of the ground will be different from the temperature of the glycol inside due to the heat transfer; if the temperatures are equal it means that there is no longer a transfer happening, as can be observed in the readings of the sensors located at ML3.

- It was observed that the power supplied by TB1 under -20 °C and 15 l/min flow conditions was constant during all the trials.

- If the difference of temperature measured from the sensors located at the inlet and outlet of the copper coil inside of the pile is less than 0.5 °C, this could be considered as not a power loss, and this factor can be removed altogether from the cooling power P equation.

- The variability of some of the readings during the test was due to the normal multi-phase condition of the ground.

- Even a narrow layer of frozen soil surrounding the pile can improve the bearing capacity of the foundation system; it proved to be challenging to remove the pile under this condition.

- The test procedure elaborated in this research can be used to select the most appropriate material that can be used as a backfill for the pile foundations and the artificial ground

freezing system. Also, the test procedure can be used to predict the freezing of a segment of the pile in a specific location.

6.2 Recommendations

The best way to represent a scenario when one pile (freeze pipe) is surrounded by a considerable quantity of soil in finite element analysis, is to create a single node in a big 2D mesh (in plan view) and to then carry out a convective analysis to obtain temperature vs. time curves (Geoslope, 2018a).

Better conditions are present at the bottom of the soil sample (test cell). The water content measurements and the variability of the readings with the sensors located at the surface support this.

For practicality during the experiments, sensors (S10 and S11) were located at the inlet and outlet of the copper coil right at its surface; they were attached with aluminum tape and plastic ties and were well insulated. This method of measurement is valid because the idea was to capture the difference in temperature, the delta. It is recommended to locate the sensors directly in the flow of the ethylene glycol at the inlet and outlet locations of the coil.

It is also recommended to use a freezer as a cold room instead of a cooler because it does not have fan cycles, and the temperature of 0 °C can be kept more constant.

It is highly advisable to insulate the hoses coming from the temperature bath during the experiments and to locate the temperature baths as close as possible to the test cell (soil sample) to reduce power loss due to imperfections, fittings, and head pressure.

When carrying out these artificial ground freezing tests it is recommended to take data in a short interval of time (e.g. in minutes, seconds) so it is possible to see the tendency better on the charts. Moreover, it is advisable to use sticks to precisely locate the sensors when the water content of the sample is about 35%. When the water content is less than 20% the sensors have to be buried during the sample preparation step.

It was not possible to obtain accurate temperatures with decimal values (e.g., -2.5 °C) in the temperature bath 2 (TB2), however, it was possible to get integer values (e.g., -2.0 °C) according to the readings; the reason for this is that the copper coil helix inside of the test cell

wall was more spacious in its design and more separated from the test cell wall. Comparing the two coils, the coil right inside of the pile was more efficient in terms of heat transfer due to the tight configuration and the proximity to the pile wall.

It is possible to locate thermocouples (sensors) inside of the test cell wall. The temperature of the soil sample inside of the test cell is transmitted to the ethylene glycol and then to the sensor which helps to clearly reflect the results of the experiment near the pile, this being one of the primary advantages, amongst others. The sensors can be easy to install and remove at any time and there is no disturbance in the sample. It is possible to locate the sensor precisely which helps create a useful tendency of the temperature vs. time curve of the test without too much variability in the readings that would be usually found at the same level inside of the soil sample.

It is equally important to continue the research in the laboratory and in the field. Furthermore, it would be useful to continue the research under seepage condition using different soil types (e.g. clay material) and the same screw micropile foundations system. Additionally, it is also suggested to compare the results obtained with different sustainable technologies and other types of coolants which are more environmentally friendly.

A possible future research objective could be the correlation of results under seepage condition with this test procedure. By doing this, could be possible to simulate an equivalent seepage condition that can be measured with this procedure without a more complex set-up.

The test method developed for this thesis is proper for an entire analysis layer by layer for a complete size pile, to decide the most suitable material as backfill and also to freeze a specific location inside the pile (Fig. 6.1 to Fig. 6.3).

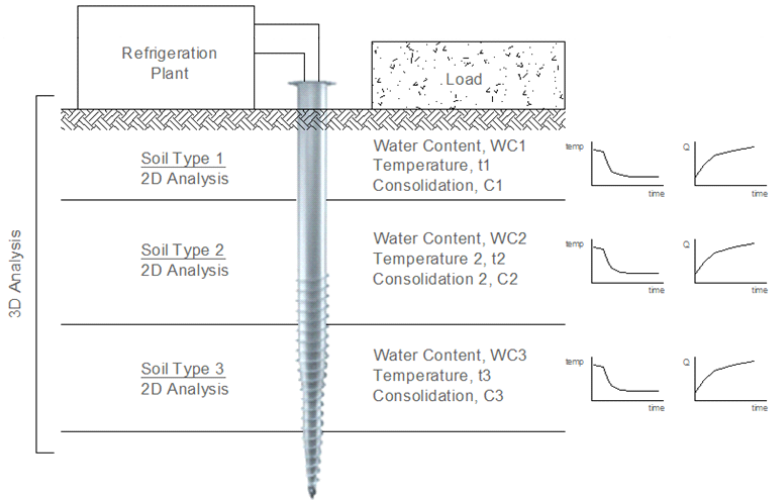

FIGURE 6.1 Complete analysis layer by layer.

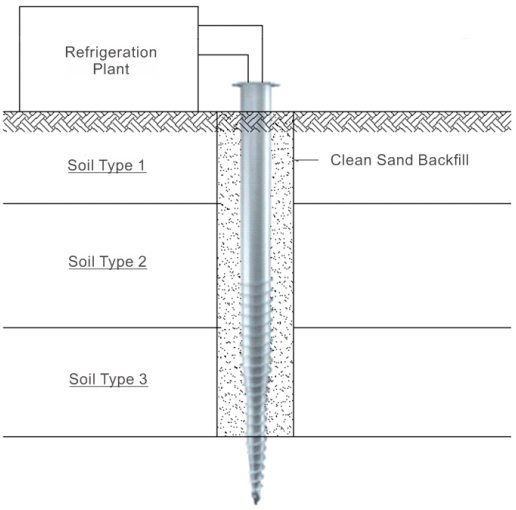

FIGURE 6.2 Backfill with better thermal conductivity conditions.

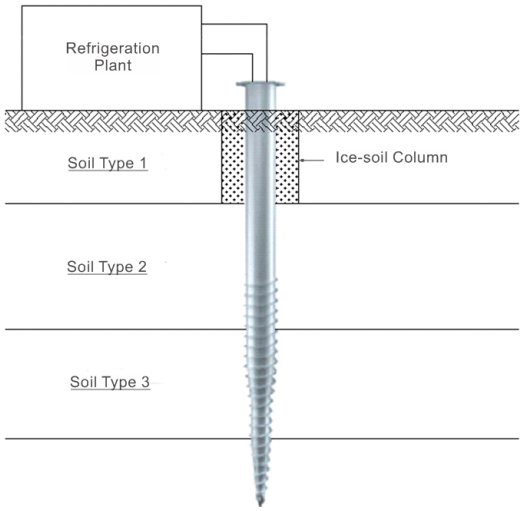

FIGURE 6.3 AGF in a specific segment of the pile.

Bibliography

Andersland, O. B., & Ladanyi, B. (2004). *Frozen ground engineering.* John Wiley & Sons.

Arctic Foundations of Canada. (2019). *Passive ground feezing technology: Thermopiles*. Retrieved from http://arcticfoundations.ca/service/thermopiles/

Aurora Research Institute. (2016). *Poster: Piling infrastructure monitoring at the western arctic research centre.* Retrieved from https://nwtresearch.com/resources/publications-and-reports

Bergman, T. L., Incropera, F. P., DeWitt, D. P., & Lavine, A. S. (2011). *Fundamentals of heat and mass transfer.* John Wiley & Sons.

Biggar, K. W. (1993). *Adfreeze and grouted piles in saline permafrost. Ph.D. Thesis.* Edmonton: University of Alberta.

Braun, B., Shuster, J., & Burnham, E. (1979). Ground freezing for support of open excavations. *Engineering Geology, 13*(1-4), 429-453.

Campbell Scientific Inc. (2015). *CR 3000 Micrologger.* Retrieved from https://s.campbellsci.com/documents/af/manuals/cr3000.pdf

Clayton, C. R., Matthews, M. C., & Simons, N. E. (1995). *Site investigation (2nd Edition).* Wiley Blackwell.

Concrete Network. (2019). *Why is cold weather a problem?* Retrieved from https://www.concretenetwork.com/cold-weather-concrete/weather.html

Engineering Toolbox. (2003). *Ethylene Glycol Heat-Transfer Fluid*. Retrieved from https://www.engineeringtoolbox.com/ethylene-glycol-d_146.html

Engineering Toolbox. (2008). *Thermal Conductivities for some common liquids*. Retrieved from https://www.engineeringtoolbox.com/thermal-conductivity-liquids-d_1260.html

Fisher Scientific. (2005). *Isotemp Bath circulators.* Retrieved from https://fscimage.fishersci.com/webimages_FSC/downloads/IsotempCatv.5RM5-18.pdf

Geoslope. (2018). *Mine shaft freezing.* Retrieved from https://www.geoslope.com/support/support-resources/example-files/example?id=examples:tempw:mineshaftfreezing&resourceVersion=10.1.0.00000

Geoslope. (2018). *Thermosyphons in pipeline piles.* Retrieved from http://downloads.geoslope.com/geostudioresources/examples/9/0/TempW/Thermosyphons%20in%20Pipeline%20Piles.pdf

Geo-slope International Ltd. (2014). *Thermal modeling with temp/w.* Retrieved from http://downloads.geo-slope.com/geostudioresources/books/8/15/temp%20modeling.pdf

Government of Canada. (2019). *Natural Resources Canada: Permafrost*. Retrieved from https://www.nrcan.gc.ca/earth-sciences/sciences/earth-sciences-permafrost-ice-and-snow/permafrost/10990

Government of the NorthwestTerritories. (2015). *NWT State of the Environment Report*. Retrieved from https://www.enr.gov.nt.ca/en/state-environment/13-permafrost

Halubec, I. (2008). *Flat loop thermosyphon foundations in warm permafrost.* Retrieved from https://pievc.ca/sites/default/files/gnwt_foundations_northwest_territories_and_yukon_report.pdf

Halubec, I. (2008). *Thermosyphon foundations in warm permafrost.* Retrieved from https://pievc.ca/sites/default/files/gnwt_thermosyphons_and_buildings_assessment_presentation.pdf

Harris, J. S. (1995). *Ground freezing in practice.* Thomas Telford.

Hivon, E. (1993). *Behaviour of saline frozen soils. Ph.D. Thesis.* Edmonton: University of Alberta.

Hutchinson, D. (1989). *Model pile load tests in frozen saline silty sand. MSc Thesis.* Edmonton: University of Alberta.

Jaeger, J. C., & Carslaw, H. S. (1959). *Conduction of heat in solids.* Clarendon P.

Jessberger, H. L. (1980). Theory and application of ground freezing in civil engineering. *Cold Regions Science and Technology, 3(1)*, 3-27.

Johansen, O. (1975). *Thermal conductivity of soils. Ph.D. diss.* Throndheim: Norwegian Technical Univ.

Johansen, O., & Frivik, P. E. (1980, June). Thermal properties of soils and rock materials. *In Proceedings of the 2nd International Symposium on Ground Freezing, NTH, Trondheim, Norwegen*, 427-452.

Kersten, M. S. (1949). *Laboratory Research for the Determination of the Thermal Properties of Soils.* Minneapolis, MN: University of Minnesota Engineering Experiment Station.

Khakimov, K. R. (1957). *The Theory and Practice of Artificial Soil Freezing.* AN SSSR.

Krinner the ground screw. (2018). *Product Catalogue Professional Ground Screws.* Retrieved from https://www.schraubfundamente.de/en/downloads/

Makowski, E. (1986). *Modellierung der künstlichen Bodenvereisung imgrundwasserdurchströmten Untergrund mit der Methode der finitenElemente.* German: Schriftenreihe des Instituts für Grundbau, Wasserwesen und Verkehrswesen, Serie Grundbau Heft 10.

McFadden, T. T. (2000). *Design manual for new foundations on permafrost.* Fairbanks, AK: Pemafrost Technology Foundation.

Moretrench. (2018). *Ground freezing.* Retrieved from https://www.moretrench.com/brochures/

National Snow and Ice Data Center. (2019). *All About Frozen Ground*. Retrieved from https://nsidc.org/cryosphere/frozenground/people.html

Optimum Instruments Inc. (2019). *Data Dolphin Tech Note: Connecting a thermocouple to the model 400.* Retrieved from http://www.datadolphin.com/uploads/tech_note/10/D40103__Connecting_a_Type_T_Thermocouple.pdf

Park, R., & Hoersch, H. (1993). *Manual on the use of thermocouples in temperature measurement.* (M. M. ASTM, Ed.)

Penny Giles . (2012). *SLS130 Linear displacement sensor.* Retrieved from https://www.dimed.eu/downloads/dl/file/id/38/product/28/penny_giles_sls130_data_jan12_en.pdf

Penny Giles. (2012). *SLS190 Linear displacement sensor.* Retrieved from https://www.dimed.eu/downloads/dl/file/id/9/product/11/penny_giles_sls190_data_jan12_en.pdf

Pimentel, E., Sres, A., & Anagnostou, G. (2012). Large-scale laboratory tests on artificial ground freezing under seepage-flow conditions. *Geotechnique, 62*(3), 227.

Sanger, F. J., & Sayles, F. H. (1979). Thermal and rheological computations for artificially frozen ground construction. *Engineering geology, 13(1-4)*, 311-337.

Schmidt, R. (2004, June). Deep foundations: Helical foundations…what an engineer needs to know. *Structure magazine*, 30. Retrieved from https://www.structuremag.org/wp-content/uploads/2014/10/F-Deep-Foundations1.pdf

Sego, D. C., Shultz, T., & Banasch, R. (1982). Strength and deformation behavior of frozen saline sand. p 11-17(SEE N 83-15691 06-42).

Smoltczyk, U. (Ed.). (2003). *Geotechnical Engineering Handbook* (Vol. 2 Procedures). John Wiley & Sons.

Williams, P. J. (1973, October). Determination of heat capacities of freezing soils. *In Symposium on Frost Action on Roads, Paris (1973), Vol. 1, No. Conf Paper*.

A. Appendix A

Test Results

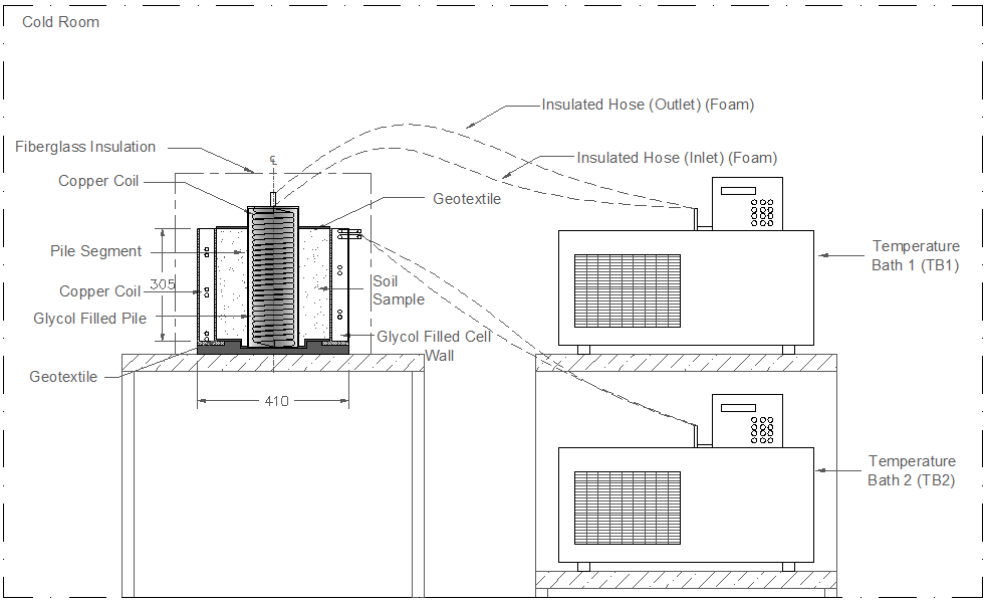

FIGURE A.1 Complete schematic of the apparatus setup used in the freezing stage. Unit: mm.

TABLE A.1 Test Matrix

Batch (#)	w (%)	Trial (Name)	Homogenization temp (°C)	TB1 (Status and temp)	TB2 (Status and temp)	Thermocouples (Sensors)					Density and water content	Pile segment (Name)	Duration (day)
						Inside soil sample (ML1, ML2 and ML3) (S1 to S9)	On the copper coil (S10 and S11)	In the cold room (S12)	Inside glycol in pile (ML4) (S13 to S15)	Inside test cell wall (S16)			
Consolidation													3
1	35	1	5	on (-20 °C)	on (5 °C)	✓	✓	×	×	×		Threaded	3
		2	0	on (-20 °C)	on (0 °C)	✓	✓	×	×	×			3
		3	-2.5	on (-20 °C)	on (-2.5 °C)	✓	✓	×	×	×			3
Consolidation													3
2	35	1	5	on (-20 °C)	on (5 °C)	✓	✓	✓	×	×	✓	Straight	3
		2	0	on (-20 °C)	on (0 °C)	✓	✓	✓	×	×			3
		3	-2.5	on (-20 °C)	on (-2.5 °C)	✓	✓	✓	×	×			3
		TB2_Off1	-2.5	on (-20 °C)	off	✓	✓	✓	×	×			3
		TB2_Off2	0	on (-20 °C)	off	✓	✓	✓	×	×			3
Consolidation													3
3	20	1	5	on (-20 °C)	on (5 °C)	✓	✓	✓	✓	✓	✓	Straight	3
		2	0	on (-20 °C)	on (0 °C)	✓	✓	✓	✓	✓			3
		3	-2.5	on (-20 °C)	on (-2.5 °C)	✓	✓	✓	✓	✓			3
		TB2_Off1	-2.5	on (-20 °C)	off	✓	✓	✓	✓	✓			3
		TB2_Off2	0	on (-20 °C)	off	✓	✓	✓	✓	✓			3
Power loss													3

Grain Size Distribution

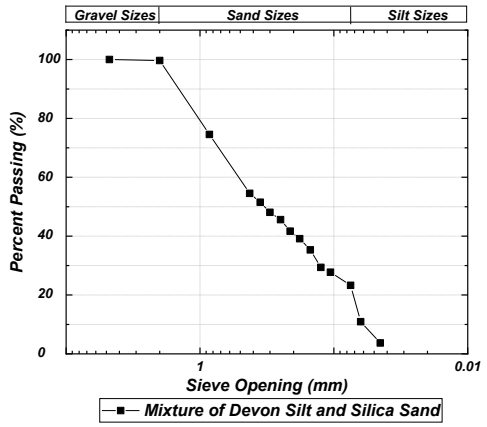

FIGURE A.2 Grain size distribution of mixture of Devon Silt and Silica Sand.

Batch 1

Consolidation

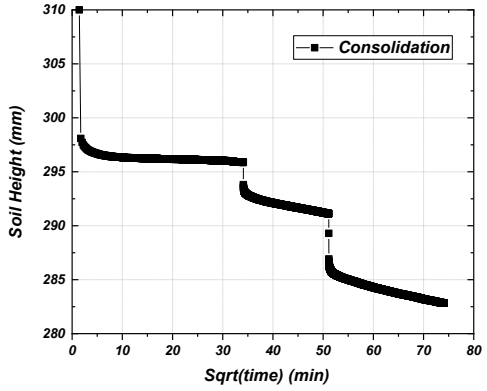

FIGURE A.3 Soil height vs Sqrt(time) Batch (1) consolidation.

Freezing

Trial 1

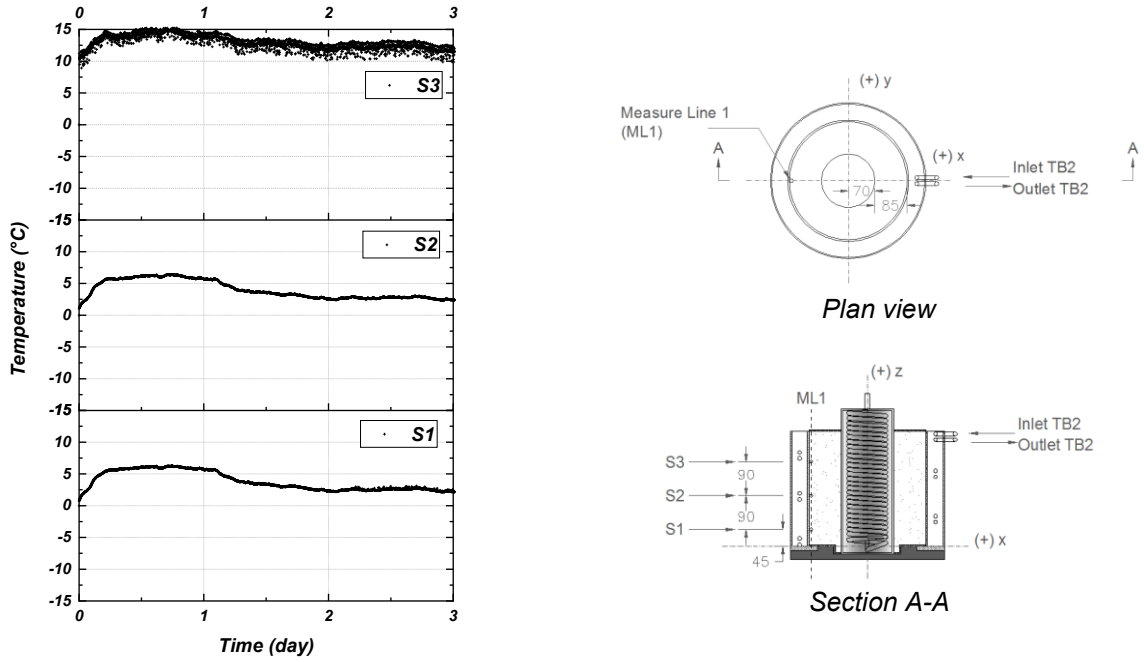

FIGURE A.4 Temp. vs. time Batch (1) w (35%) Trial (1) starting from 5 °C TB1on(-20 °C)_TB2on(5 °C) for ML1 (S1 to S3). Unit: mm.

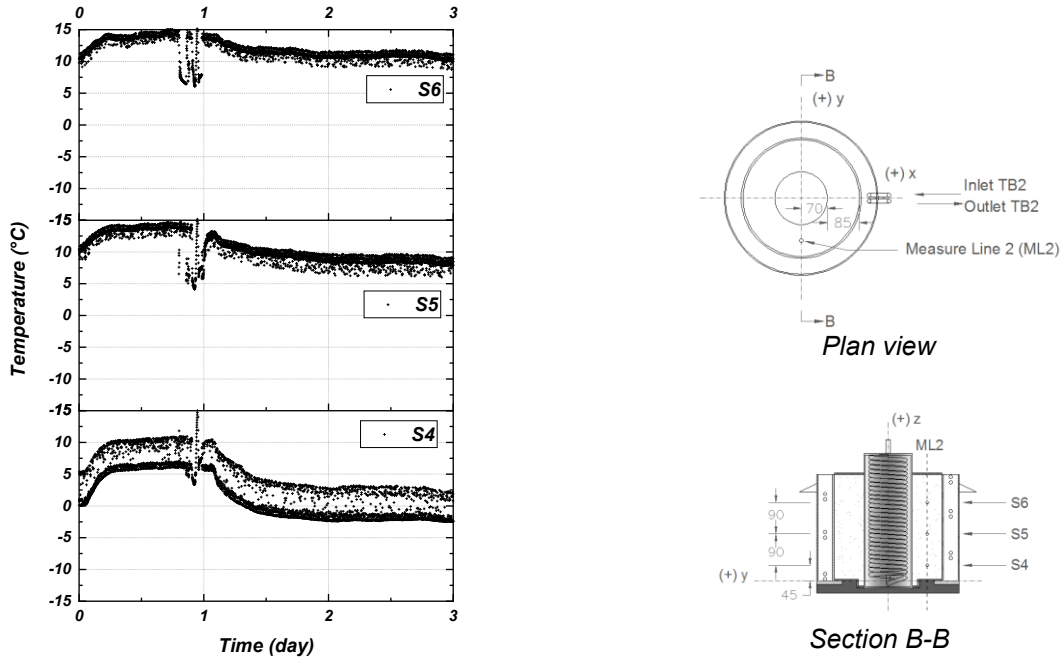

FIGURE A.5 Temp. vs. time Batch (1) w (35%) Trial (1) starting from 5 °C TB1on(-20 °C)_TB2on(5 °C) for ML2 (S4 to S6). Unit: mm.

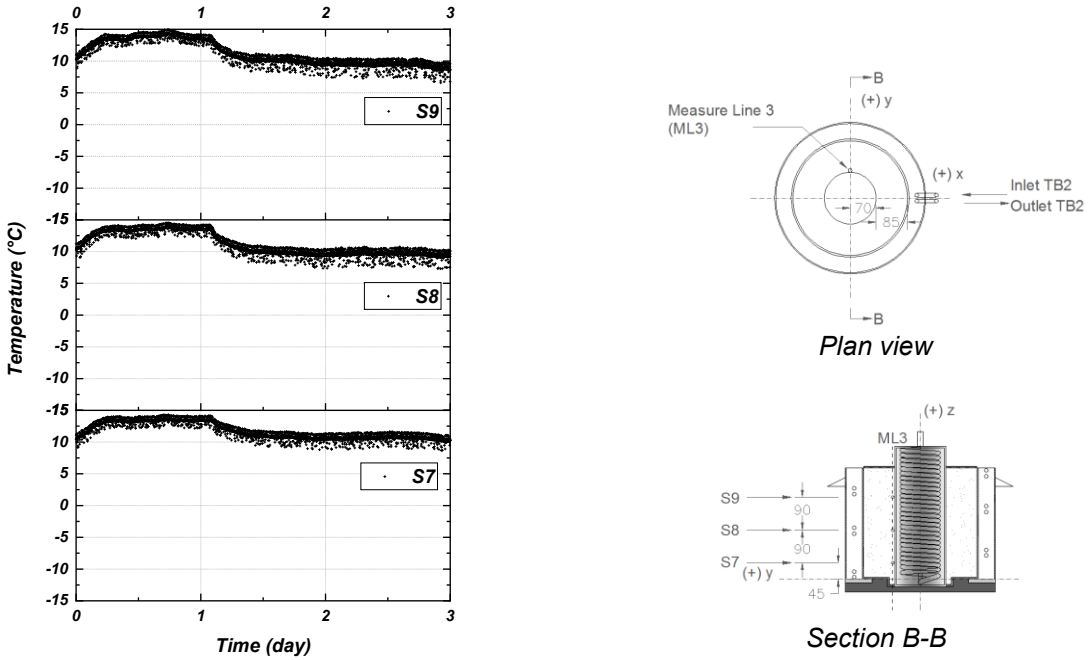

FIGURE A.6 Temp. vs. time Batch (1) w (35%) Trial (1) starting from 5 °C TB1on(-20 °C)_TB2on(5 °C) for ML3 (S7 to S9). Unit: mm.

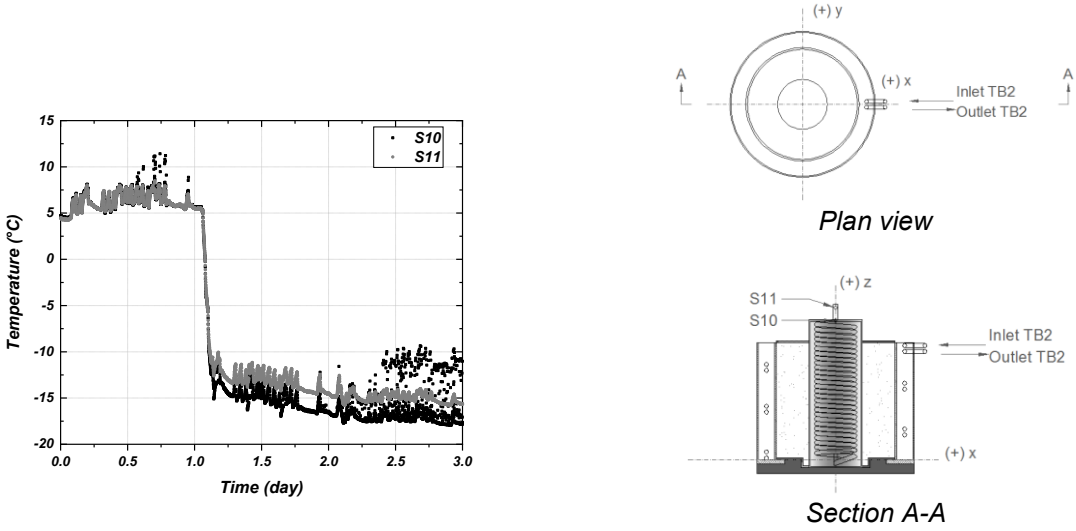

FIGURE A.7 Temp. vs. time Batch (1) w (35%) Trial (1) starting from 5 °C TB1on(-20 °C)_TB2on(5 °C) for on the copper coil (S10 and S11).

Trial 2

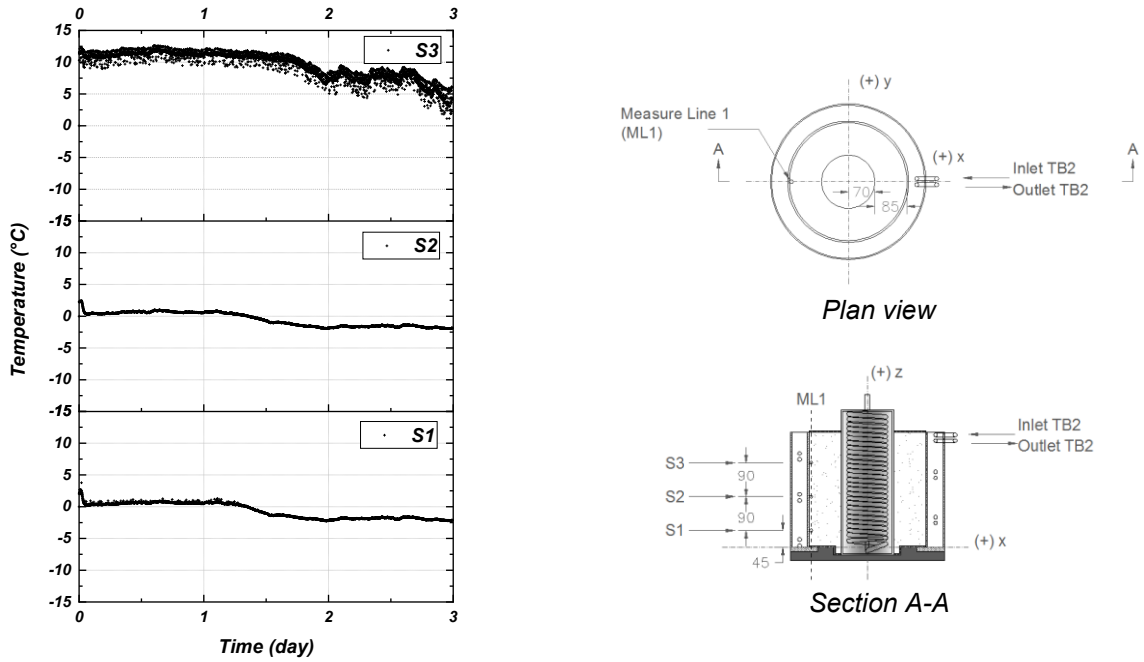

FIGURE A.8 Temp. vs. time Batch (1) w (35%) Trial (2) starting from 0 °C TB1on(-20 °C)_TB2on(0 °C) for ML1 (S1 to S3). Unit: mm.

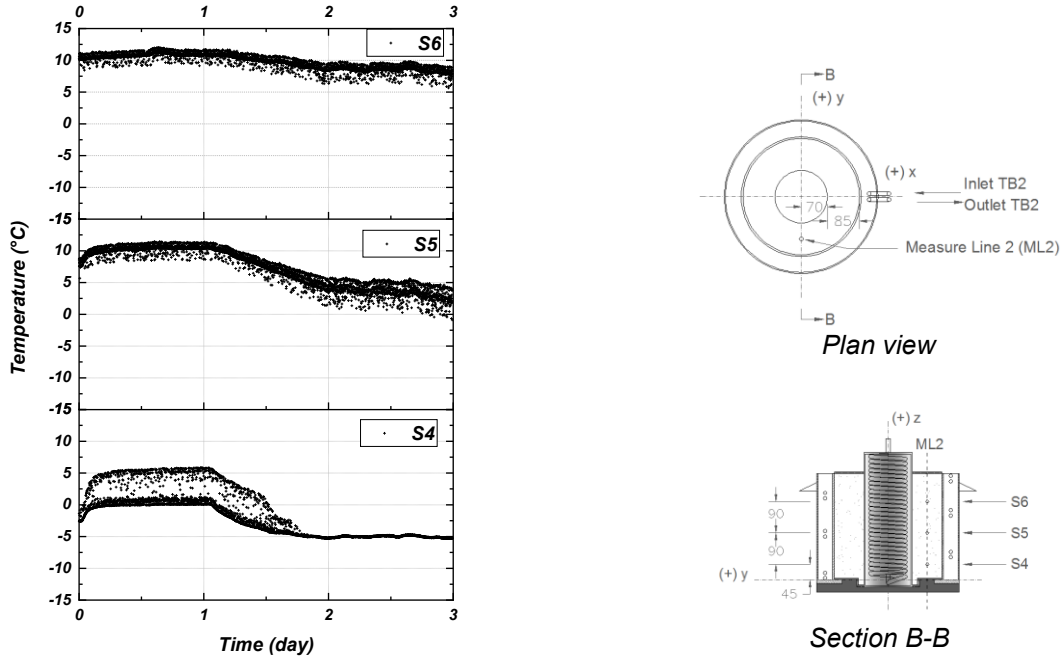

FIGURE A.9 Temp. vs. time Batch (1) w (35%) Trial (2) starting from 0 °C TB1on(-20 °C)_TB2on(0 °C) for ML2 (S4 to S6). Unit: mm.

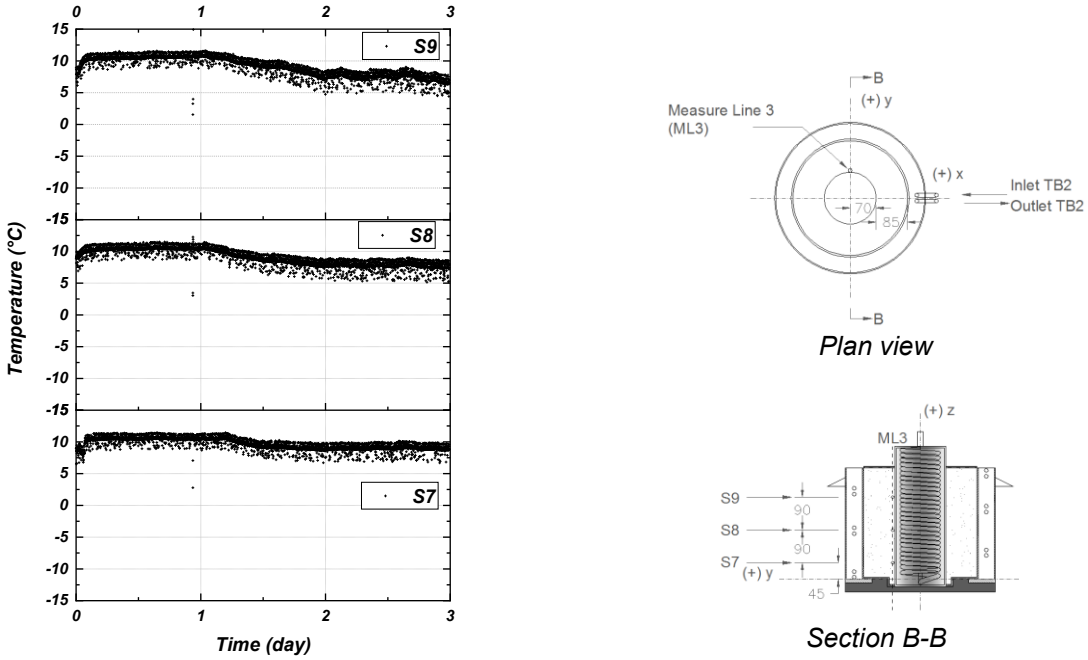

FIGURE A.10 Temp. vs. time Batch (1) w (35%) Trial (2) starting from 0 °C TB1on(-20 °C)_TB2on(0 °C) for ML3 (S7 to S9). Unit: mm.

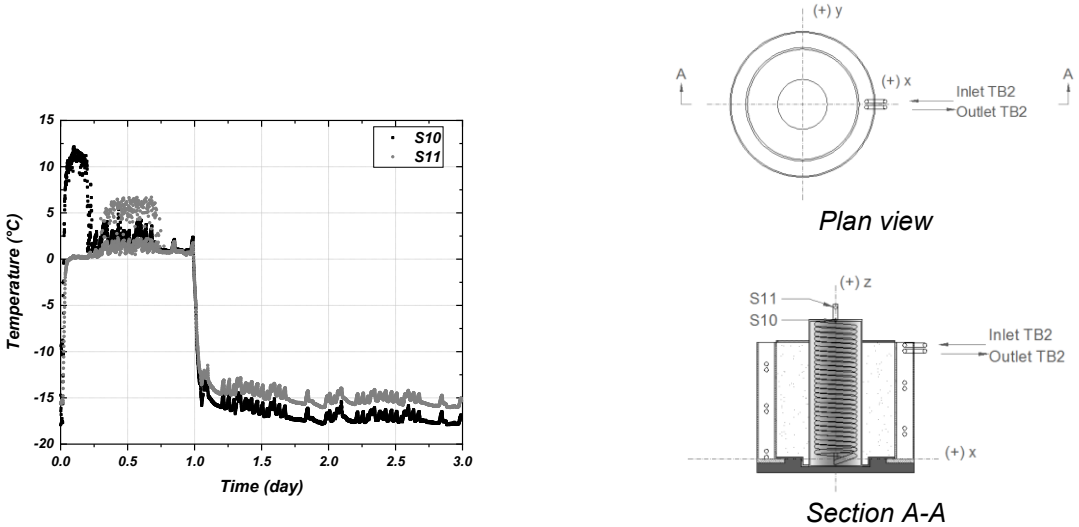

FIGURE A.11 Temp. vs. time Batch (1) w (35%) Trial (2) starting from 0 °C TB1on(-20 °C)_TB2on(0 °C) for on the copper coil (S10 and S11).

Trial 3

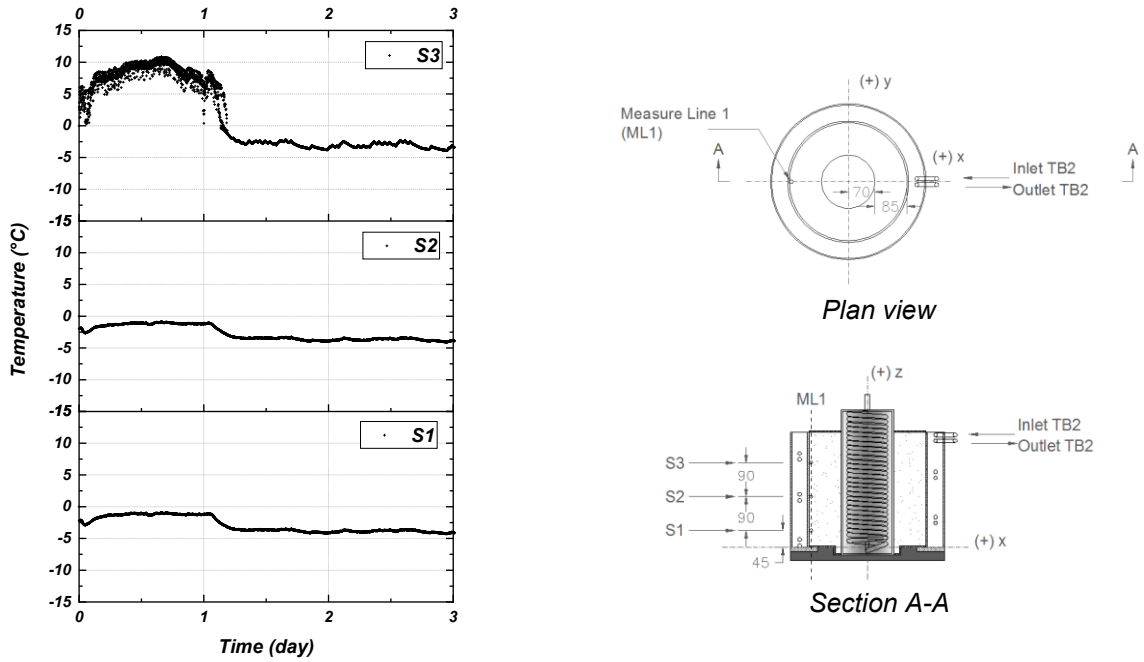

FIGURE A.12 Temp. vs. time Batch (1) w (35%) Trial (3) starting from -2.5 °C TB1on(-20 °C)_TB2on(-2.5 °C) for ML1 (S1 to S3). Unit: mm.

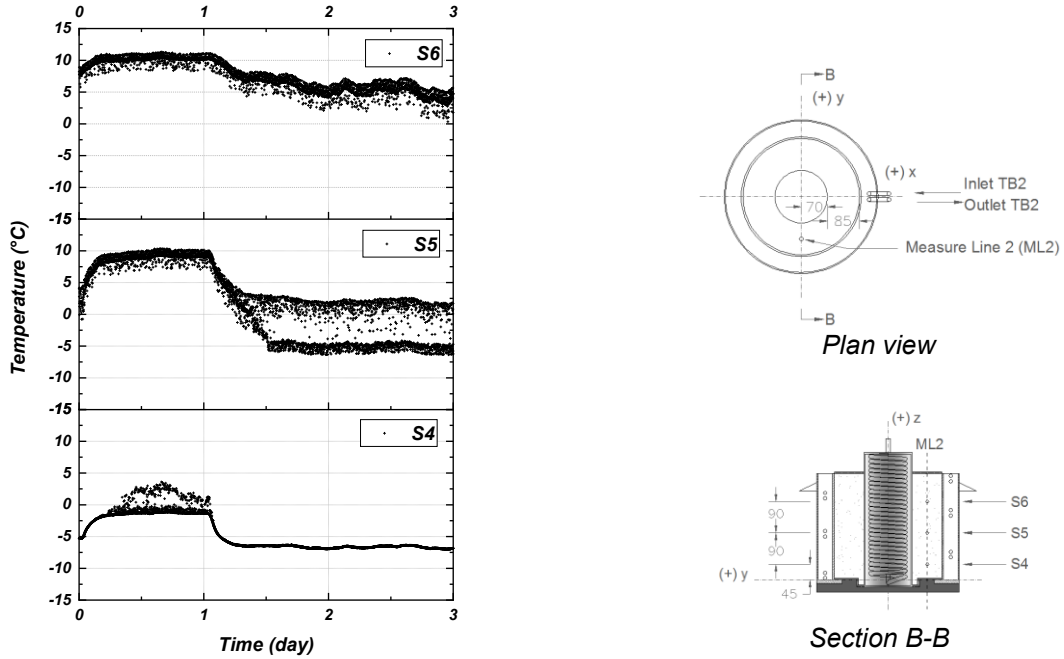

FIGURE A.13 Temp. vs. time Batch (1) w (35%) Trial (3) starting from -2.5 °C TB1on(-20 °C)_TB2on(-2.5 °C) for ML2 (S4 to S6). Unit: mm.

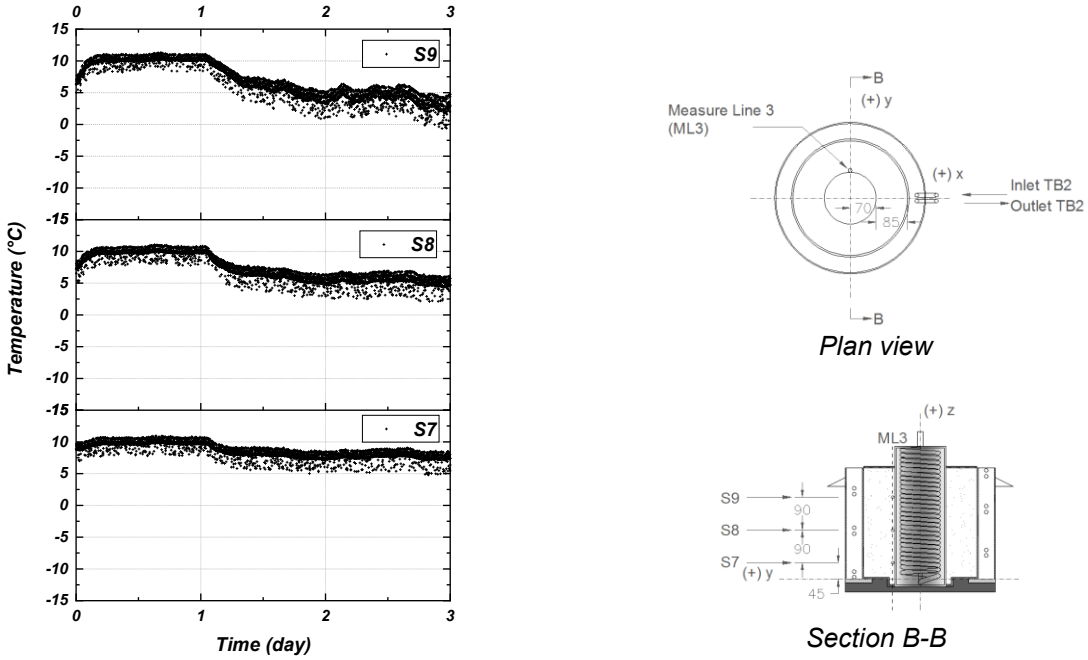

FIGURE A.14 Temp. vs. time Batch (1) w (35%) Trial (3) starting from -2.5 °C TB1on(-20 °C)_TB2on(-2.5 °C) for ML3 (S7 to S9). Unit: mm.

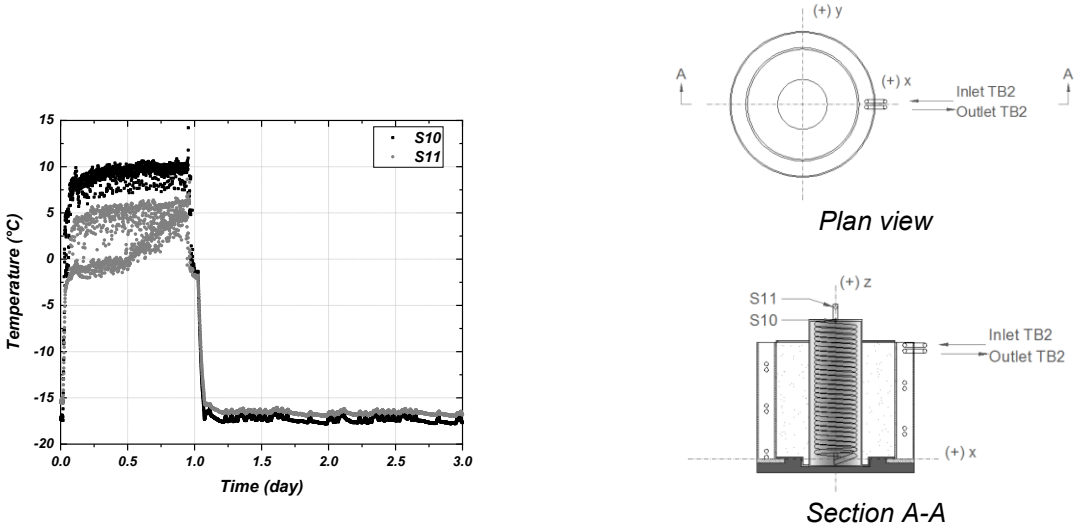

FIGURE A.15 Temp. vs. time Batch (1) w (35%) Trial (3) starting from -2.5 °C TB1on(-20 °C)_TB2on(-2.5 °C) for on the copper coil (S10 and S11).

Batch 2

Consolidation

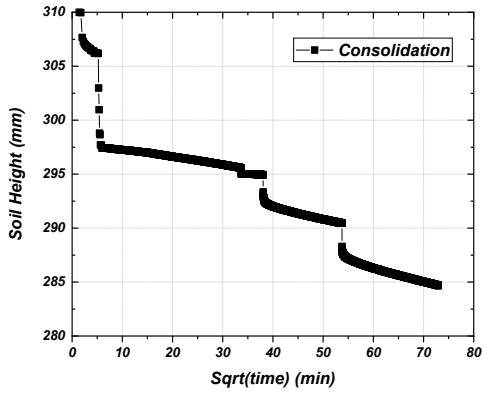

FIGURE A.16 Soil height vs Sqrt(time) Batch (2) consolidation.

Freezing

Trial 1

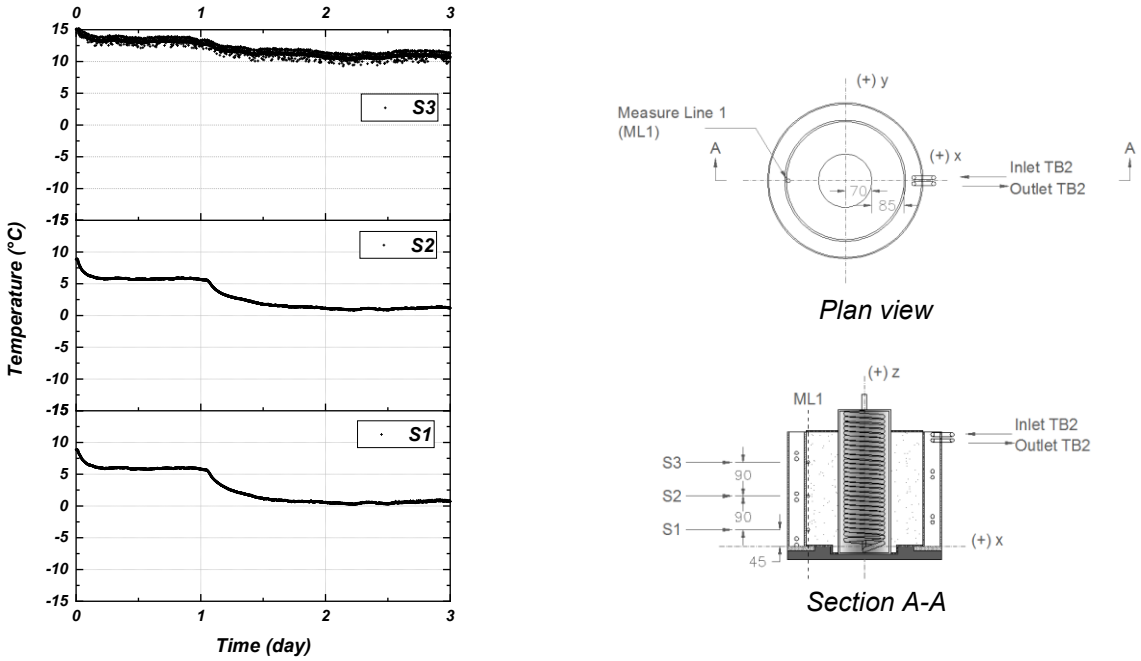

FIGURE A.17 Temp. vs. time Batch (2) w (35%) Trial (1) starting from 5 °C TB1on(-20 °C)_TB2on(5 °C) for ML1 (S1 to S3). Unit: mm.

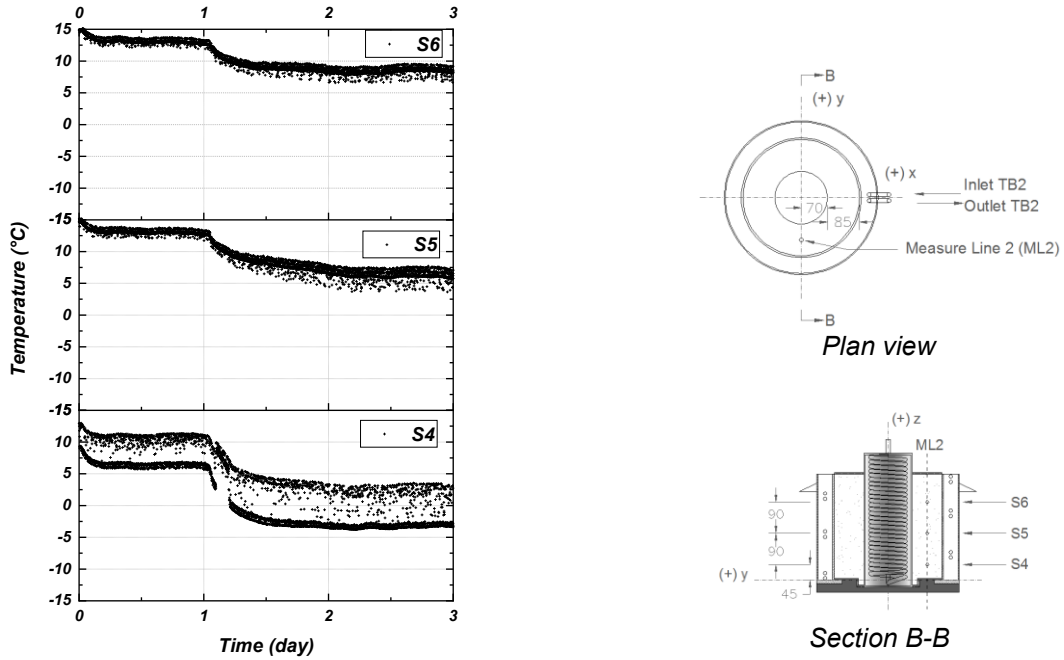

FIGURE A.18 Temp. vs. time Batch (2) w (35%) Trial (1) starting from 5 °C TB1on(-20 °C)_TB2on(5 °C) for ML2 (S4 to S6). Unit: mm.

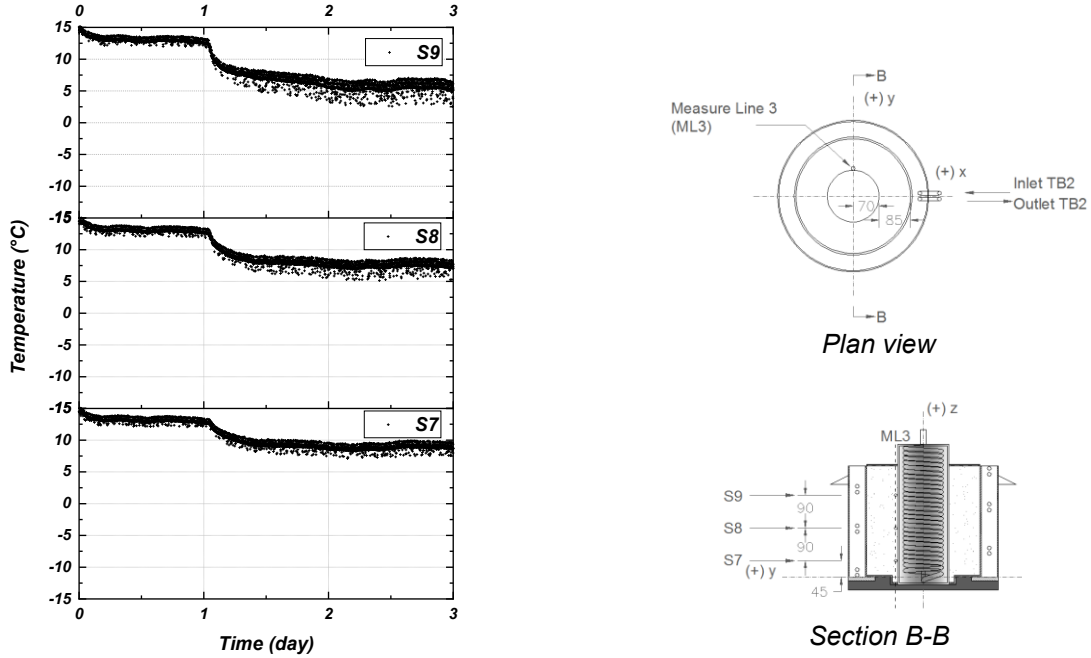

FIGURE A.19 Temp. vs. time Batch (2) w (35%) Trial (1) starting from 5 °C TB1on(-20 °C)_TB2on(5 °C) for ML3 (S7 to S9). Unit: mm.

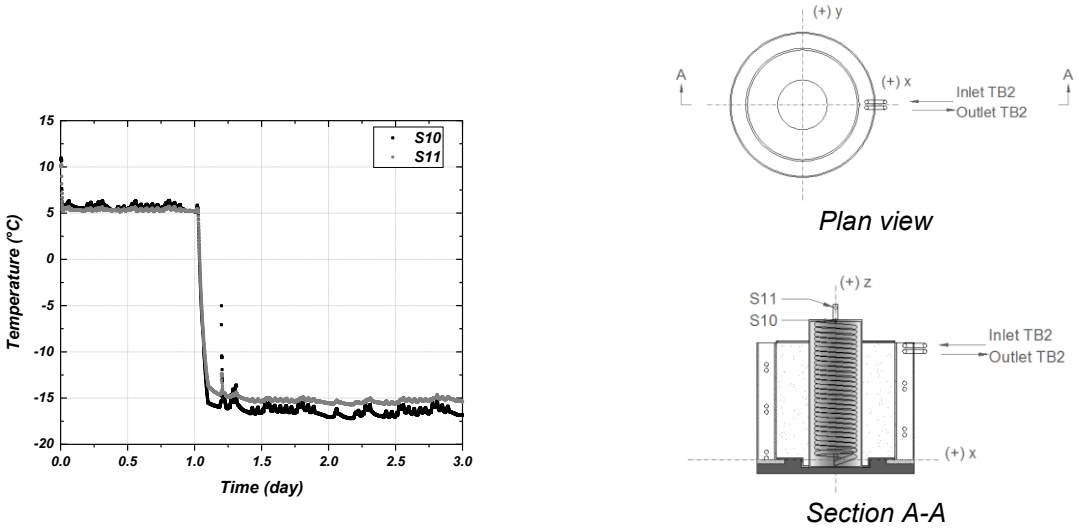

FIGURE A.20 Temp. vs. time Batch (2) w (35%) Trial (1) starting from 5 °C TB1on(-20 °C)_TB2on(5 °C) for on the copper coil (S10 and S11).

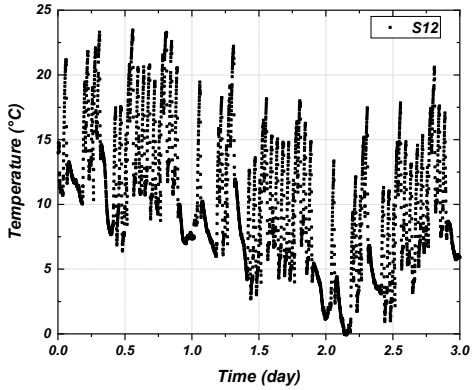

FIGURE A.21 Temp. vs. time Batch (2) w (35%) Trial (1) starting from 5 °C TB1on(-20 °C)_TB2on(5 °C) for in the cold room (S12).

Trial 2

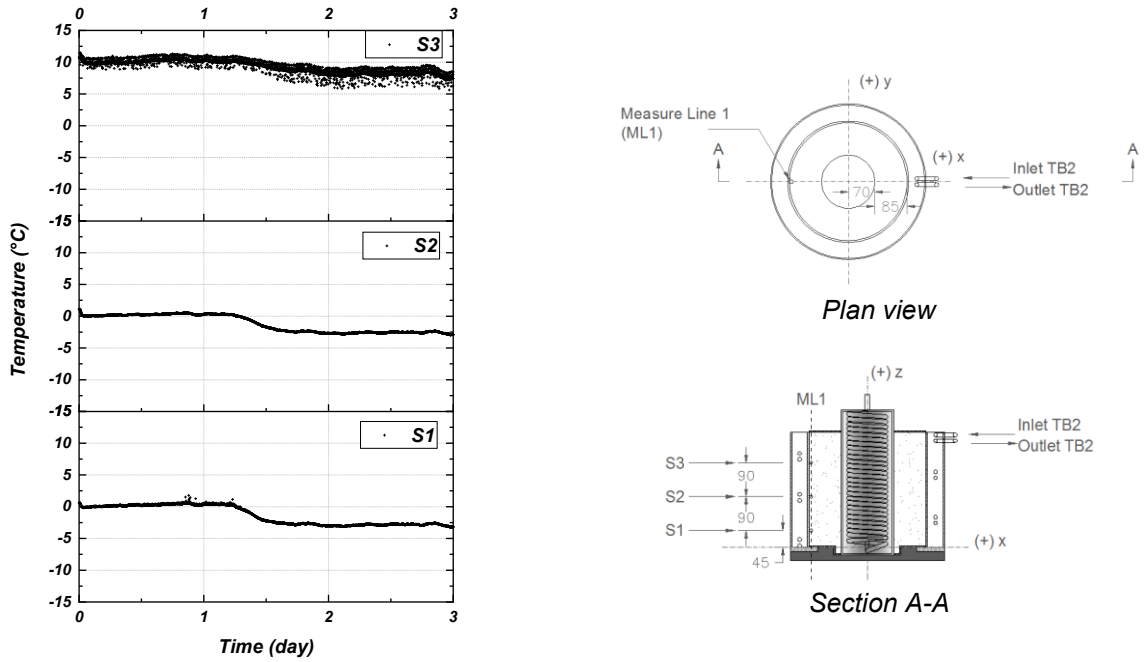

FIGURE A.22 Temp. vs. time Batch (2) w (35%) Trial (2) starting from 0 °C TB1on(-20 °C)_TB2on(0 °C) for ML1 (S1 to S3). Unit: mm.

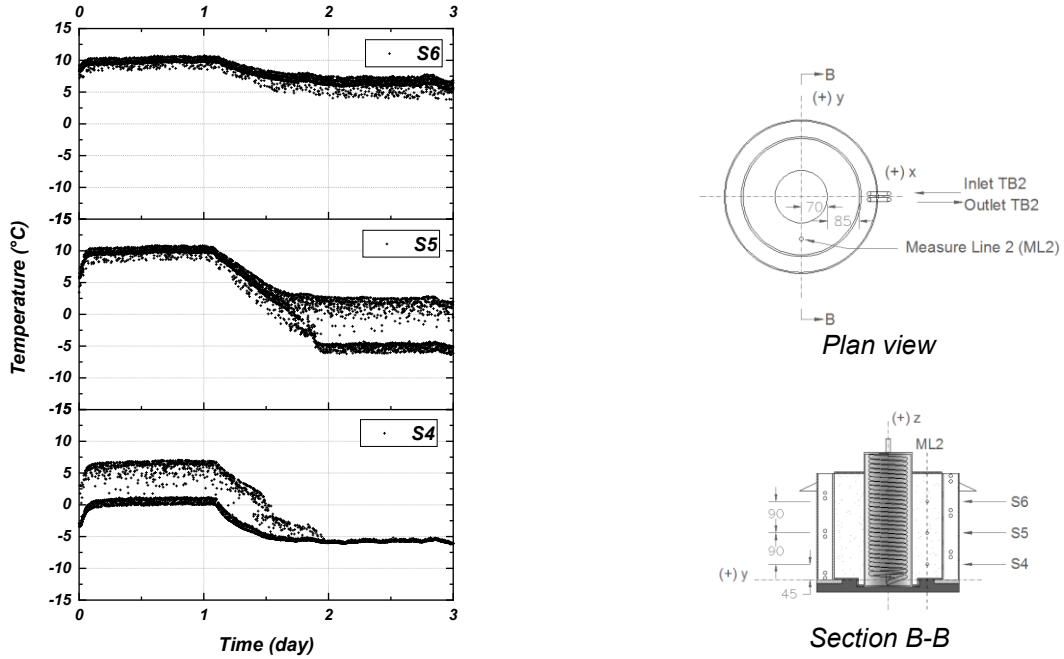

FIGURE A.23 Temp. vs. time Batch (2) w (35%) Trial (2) starting from 0 °C TB1on(-20 °C)_TB2on(0 °C) for ML2 (S4 to S6). Unit: mm.

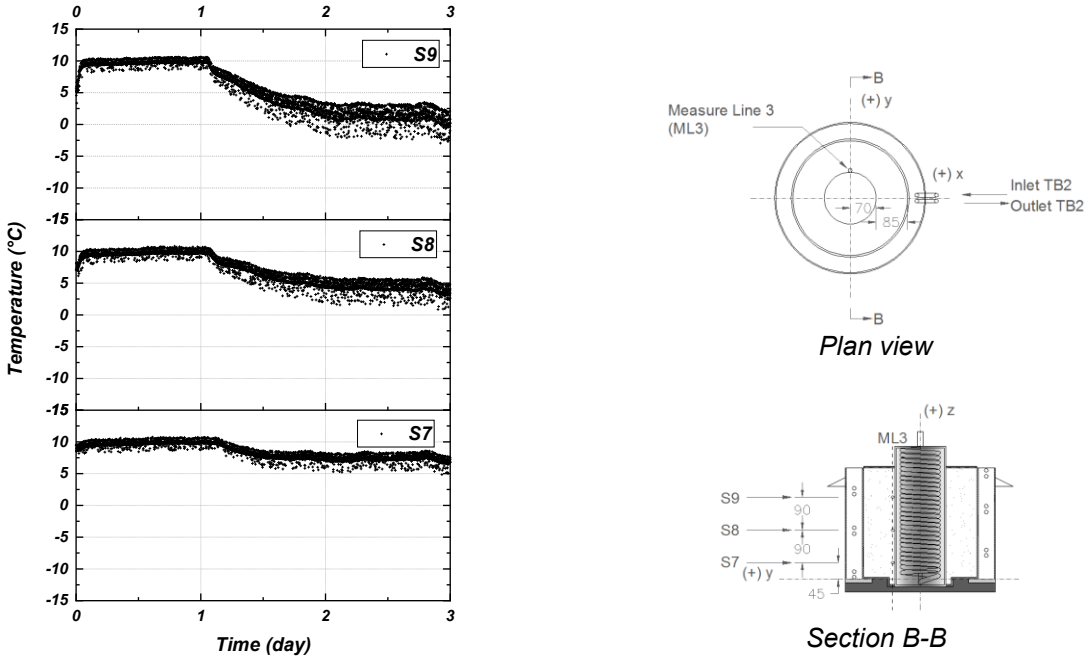

FIGURE A.24 Temp. vs. time Batch (2) w (35%) Trial (2) starting from 0 °C TB1on(-20 °C)_TB2on(0 °C) for ML3 (S7 to S9). Unit: mm.

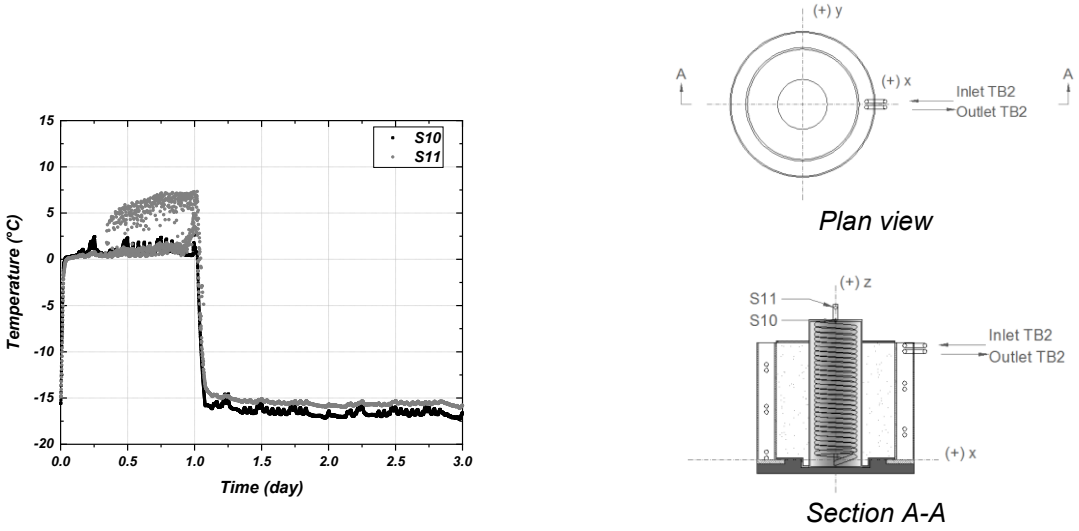

FIGURE A.25 Temp. vs. time Batch (2) w (35%) Trial (2) starting from 0 °C TB1on(-20 °C)_TB2on(0 °C) for on the copper coil (S10 and S11).

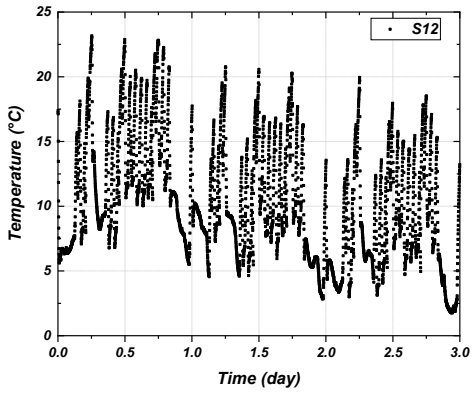

FIGURE A.26 Temp. vs. time Batch (2) w (35%) Trial (2) starting from 0 °C TB1on(-20 °C)_TB2on(0 °C) for in the cold room (S12).

Trial 3

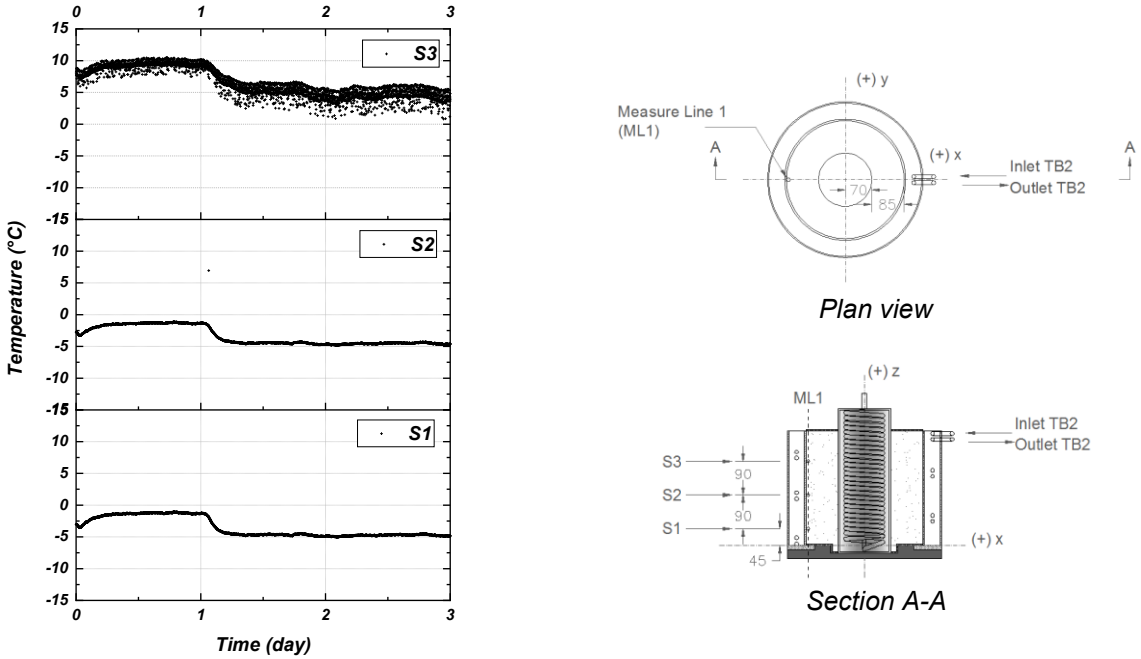

FIGURE A.27 Temp. vs. time Batch (2) w (35%) Trial (3) starting from -2.5 °C TB1on(-20 °C)_TB2on(-2.5 °C) for ML1 (S1 to S3). Unit: mm.

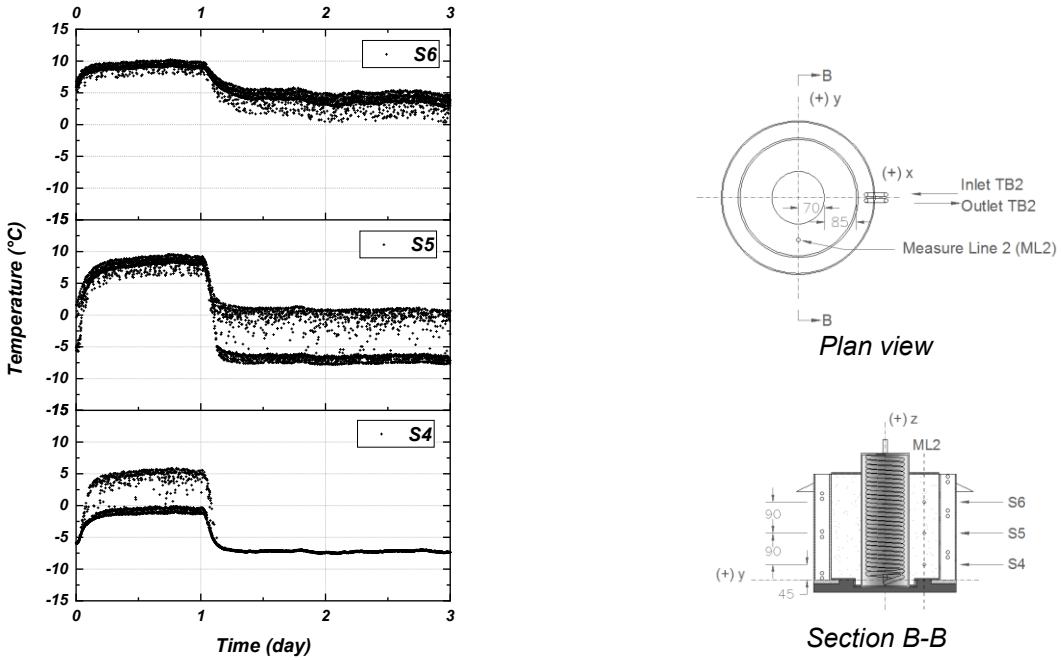

FIGURE A.28 Temp. vs. time Batch (2) w (35%) Trial (3) starting from -2.5 °C TB1on(-20 °C)_TB2on(-2.5 °C) for ML2 (S4 to S6). Unit: mm.

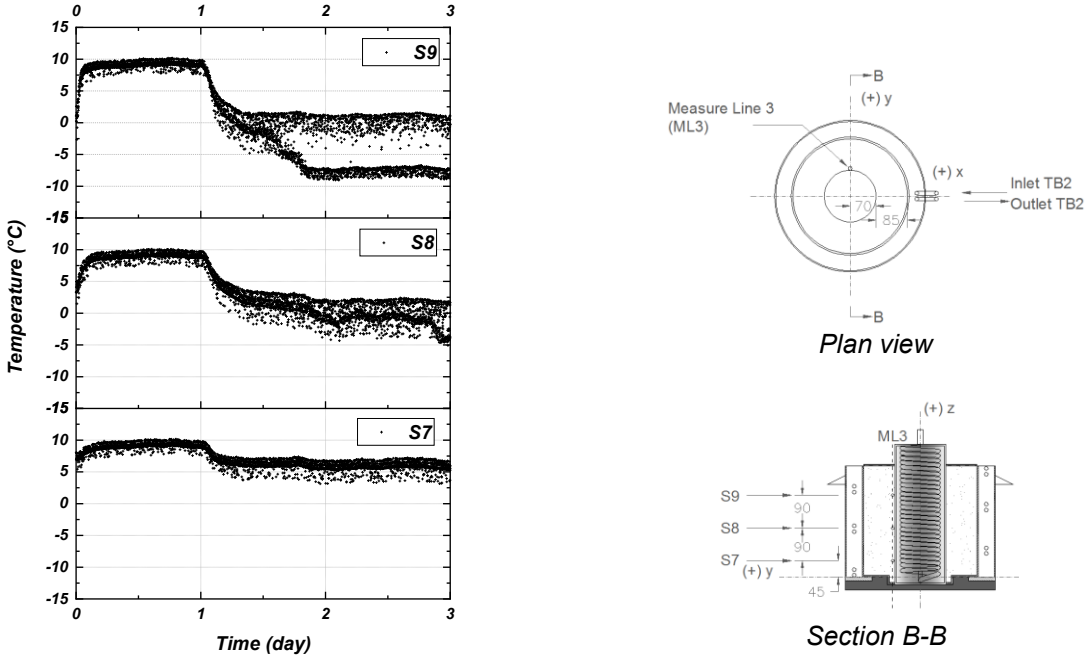

FIGURE A.29 Temp. vs. time Batch (2) w (35%) Trial (3) starting from -2.5 °C TB1on(-20 °C)_TB2on(-2.5 °C) for ML3 (S7 to S9). Unit: mm.

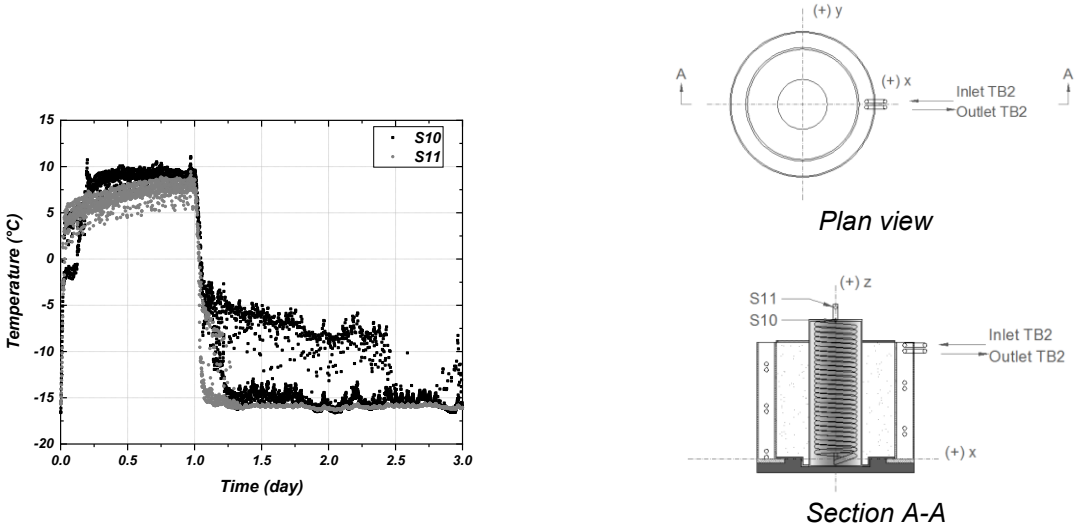

FIGURE A.30 Temp. vs. time Batch (2) w (35%) Trial (3) starting from -2.5 °C TB1on(-20 °C)_TB2on(-2.5 °C) for on the copper coil (S10 and S11).

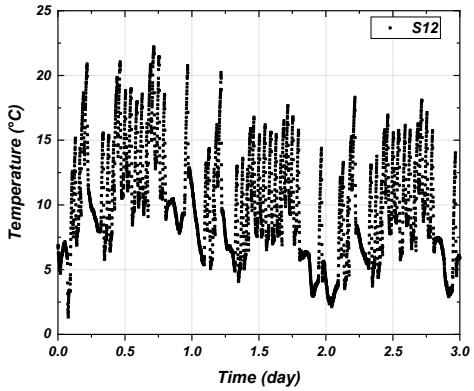

FIGURE A.31 Temp. vs. time Batch (2) w (35%) Trial (3) starting from -2.5 °C TB1on(-20 °C)_TB2on(-2.5 °C) for in the cold room (S12).

Trial (TB2_Off1)

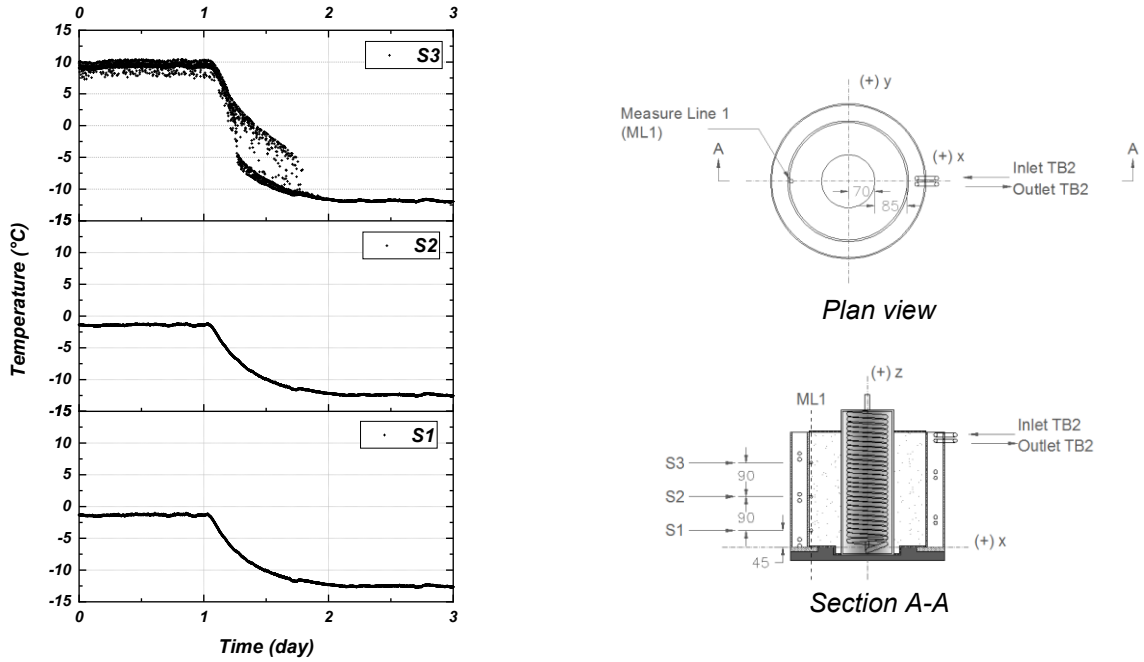

FIGURE A.32 Temp. vs. time Batch (2) w (35%) Trial (TB2_Off1) starting from -2.5 °C TB1on(-20 °C)_ TB2off for ML1 (S1 to S3). Unit: mm.

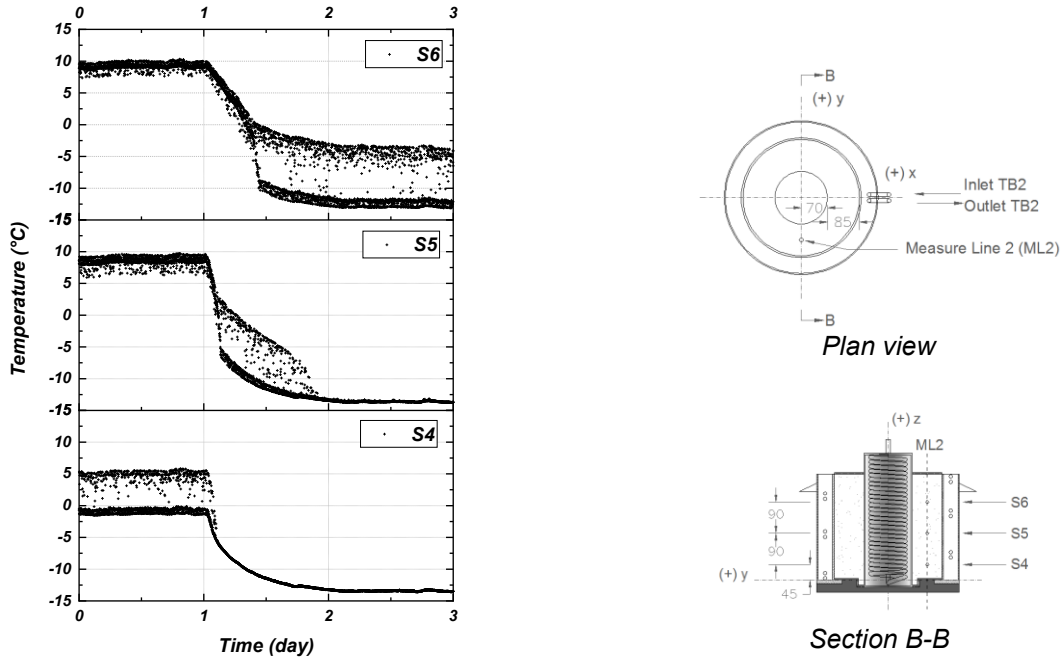

FIGURE A.33 Temp. vs. time Batch (2) w (35%) Trial (TB2_Off1) starting from -2.5 °C TB1on(-20 °C)_ TB2off for ML2 (S4 to S6). Unit: mm.

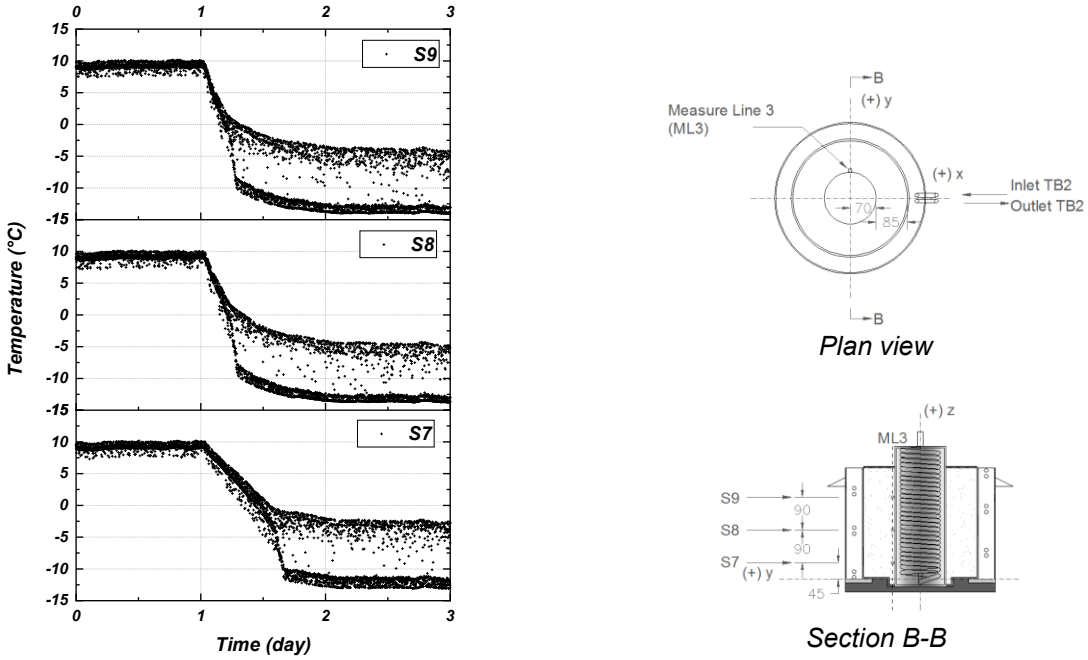

FIGURE A.34 Temp. vs. time Batch (2) w (35%) Trial (TB2_Off1) starting from -2.5 °C TB1on(-20 °C)_ TB2off for ML3 (S7 to S9). Unit: mm.

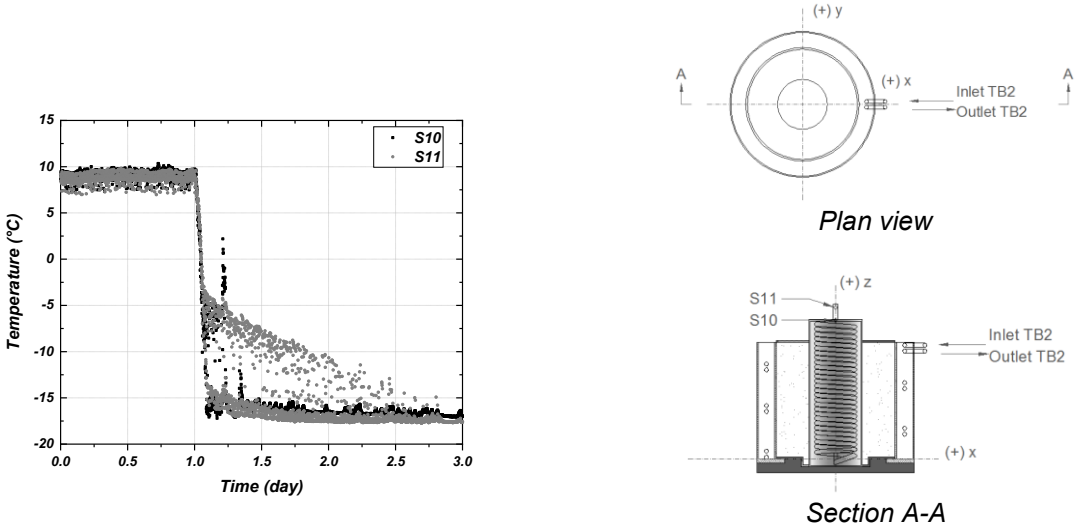

FIGURE A.35 Temp. vs. time Batch (2) w (35%) Trial (TB2_Off1) starting from -2.5 °C TB1on(-20 °C)_ TB2off for on the copper coil (S10 and S11).

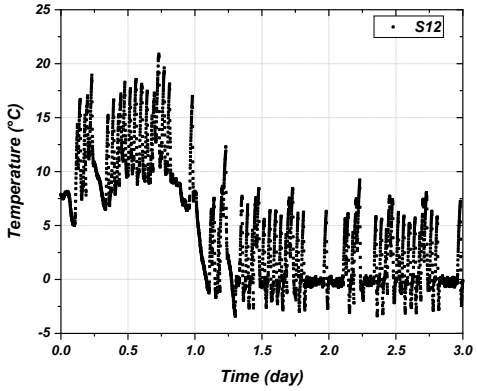

FIGURE A.36 Temp. vs. time Batch (2) w (35%) Trial (TB2_Off1) starting from -2.5 °C TB1on(-20 °C)_ TB2off for in the cold room (S12).

Trial (TB2_Off2)

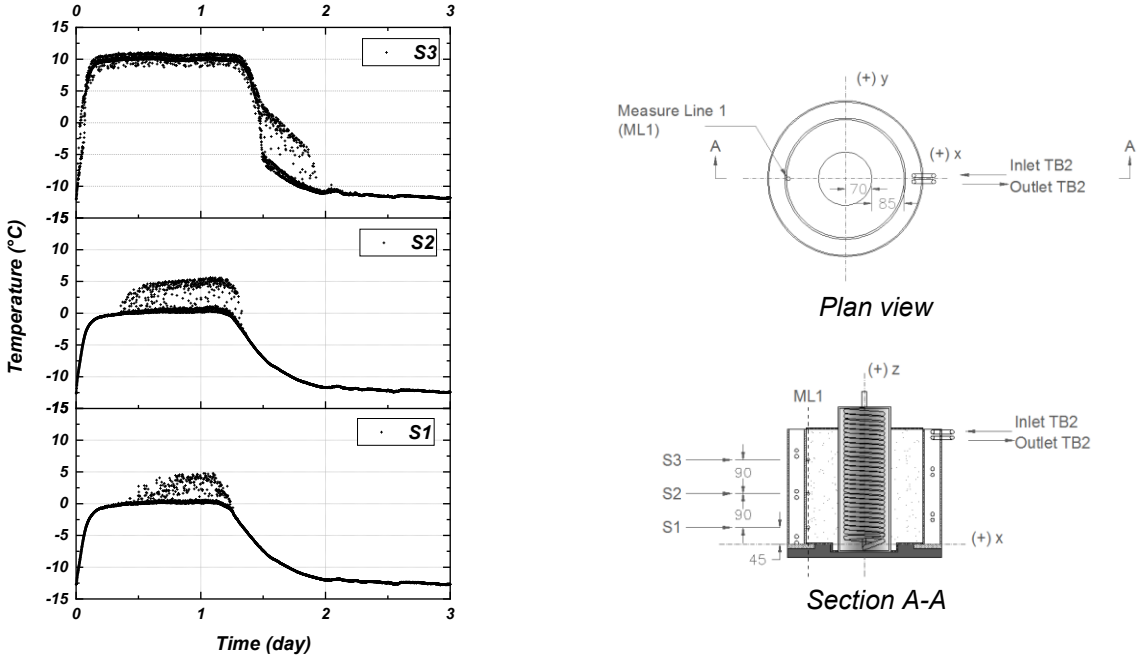

FIGURE A.37 Temp. vs. time Batch (2) w (35%) Trial (TB2_Off2) starting from 0 °C TB1on(-20 °C)_ TB2off for ML1 (S1 to S3). Unit: mm.

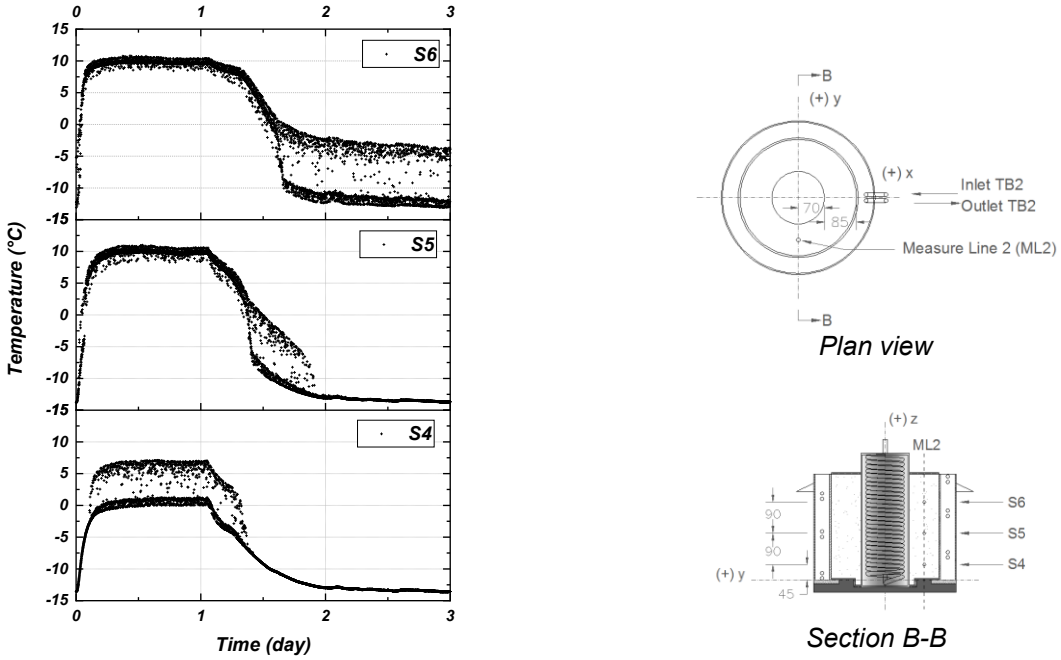

FIGURE A.38 Temp. vs. time Batch (2) w (35%) Trial (TB2_Off2) starting from 0 °C TB1on(-20 °C)_ TB2off for ML2 (S4 to S6). Unit: mm.

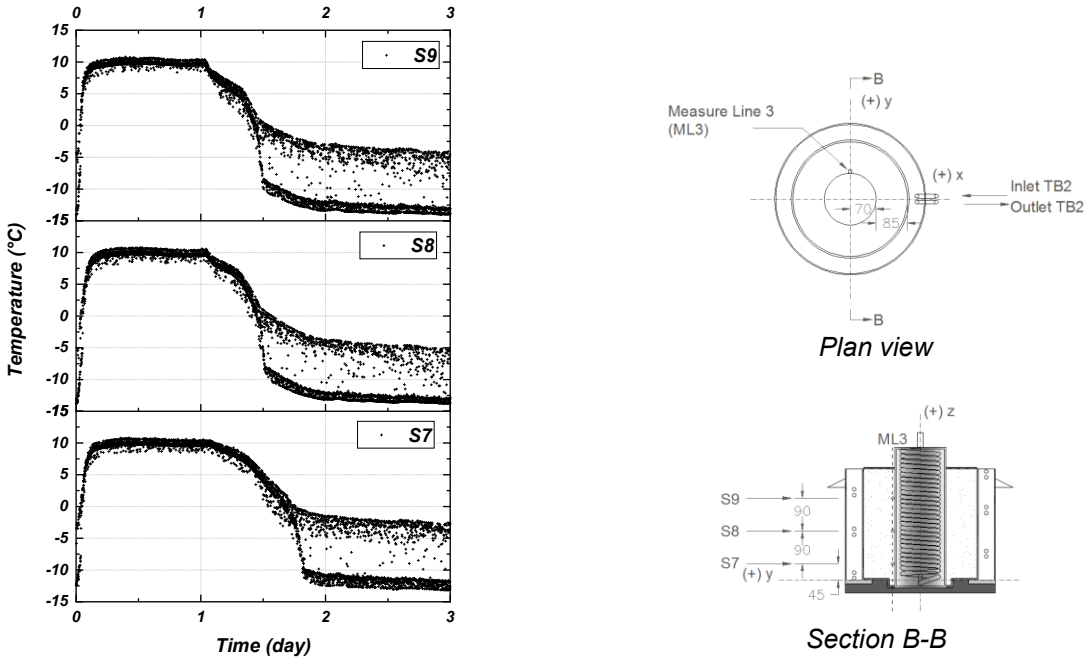

FIGURE A.39 Temp. vs. time Batch (2) w (35%) Trial (TB2_Off2) starting from 0 °C TB1on(-20 °C)_ TB2off for ML3 (S7 to S9). Unit: mm.

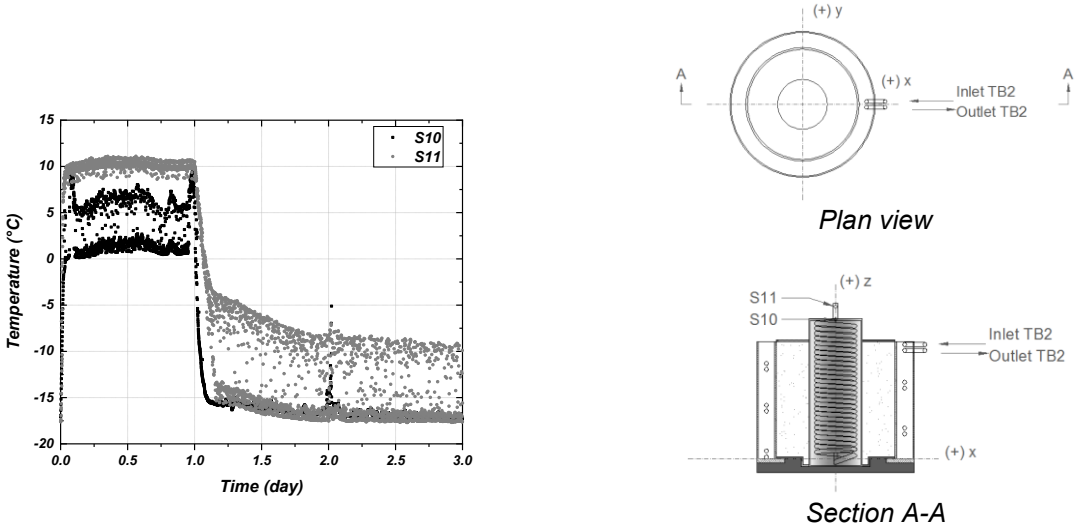

FIGURE A.40 Temp. vs. time Batch (2) w (35%) Trial (TB2_Off2) starting from 0 °C TB1on(-20 °C)_ TB2off for on the copper coil (S10 and S11).

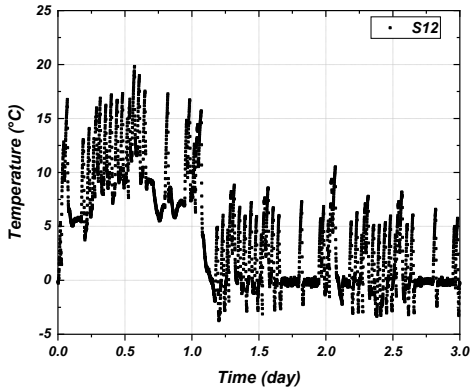

FIGURE A.41 Temp. vs. time Batch (2) w (35%) Trial (TB2_Off2) starting from 0 °C TB1on(-20 °C)_ TB2off for in the cold room (S12).

Density and Water Content

TABLE A.2 Batch (2) Density and Water Content by Layer

Layer	Sample	Tray empty (gr)	Tray+soil+ring (gr)	Soil+tray (gr)	$Soil_{Dry}$ +tray (gr)	Soil mass (gr)	Soil mass (kg)	Density (kg/m^3)	Average density (kg/m^3)	Unit weight (kN/m^3)	Average unit weight (kN/m^3)	w (%)	Average w (%)
1	L1-1	4.21	389.47	223.34	174.42	220.86	0.2209	1718.63	1705.34	16.86	16.73	28.74	28.62
	L1-2	4.22	386.02	221.63	173.16	217.40	0.2174	1691.71		16.60		28.69	
	L1-3	4.20	386.99	219.35	171.67	218.39	0.2184	1699.41		16.67		28.47	
	L1-4	4.25	388.61	239.04	186.85	219.96	0.2200	1711.63		16.79		28.58	
2	L2-1	4.22	386.32	217.56	164.24	217.70	0.2177	1694.04	1694.20	16.62	16.62	33.32	32.90
	L2-2	4.21	387.50	215.97	164.44	218.89	0.2189	1703.30		16.71		32.16	
	L2-3	4.22	378.93	207.63	156.67	210.31	0.2103	1636.53		16.05		33.43	
	L2-4	4.22	392.60	223.36	169.38	223.98	0.2240	1742.91		17.10		32.68	
3	L3-1	4.22	392.80	226.56	169.93	224.18	0.2242	1744.46	1736.59	17.11	17.04	34.17	34.59
	L3-2	4.22	391.64	227.16	170.93	223.02	0.2230	1735.44		17.02		33.73	
	L3-3	4.22	391.63	222.80	166.08	223.01	0.2230	1735.36		17.02		35.04	
	L3-4	4.24	391.10	220.61	164.03	222.46	0.2225	1731.08		16.98		35.41	
Total average									1712.04		16.80		32.04

Batch 3

Consolidation

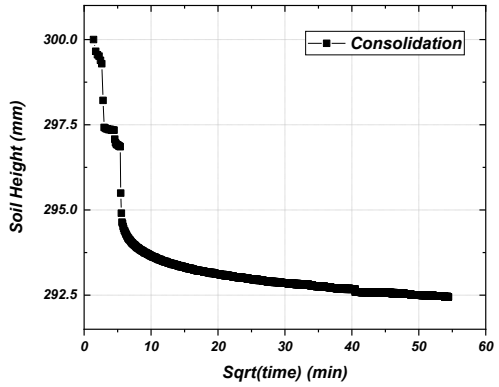

FIGURE A.42 Soil height vs Sqrt(time) Batch (3) consolidation.

Freezing

Trial 1

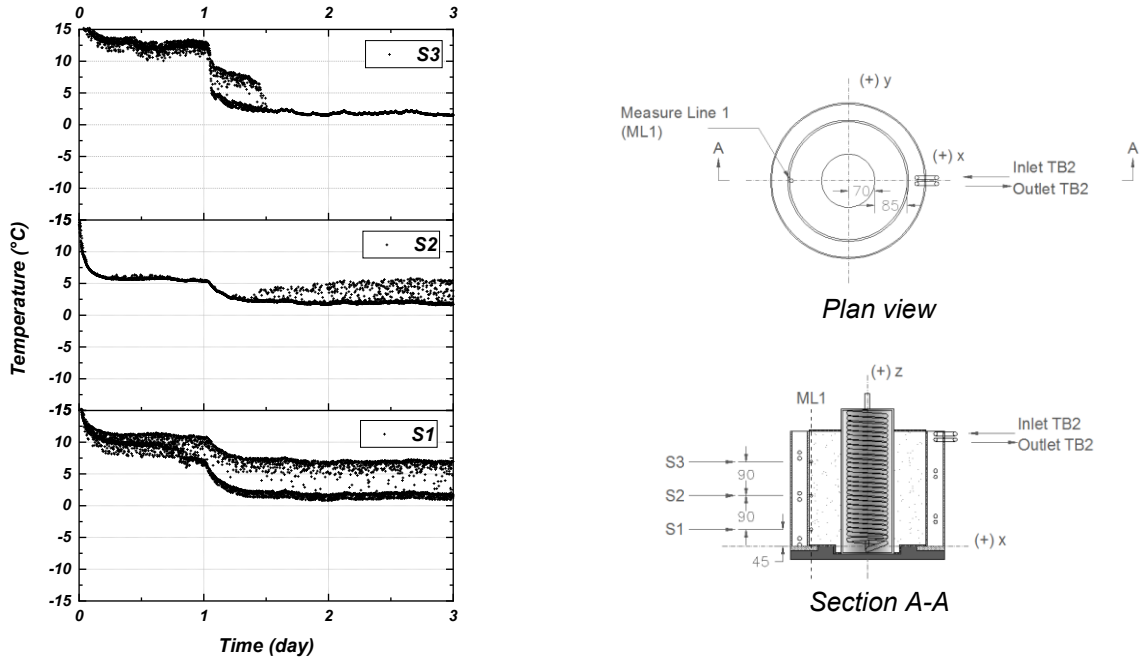

FIGURE A.43 Temp. vs. time Batch (3) w (20%) Trial (1) starting from 5 °C TB1on(-20 °C)_TB2on(5 °C) for ML1 (S1 to S3). Unit: mm.

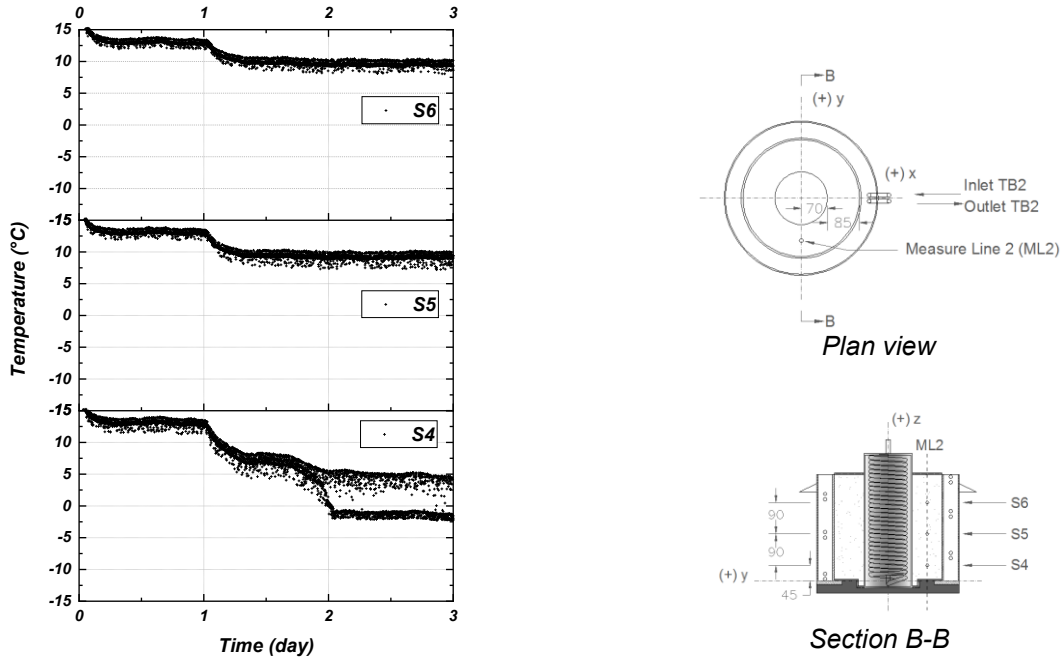

FIGURE A.44 Temp. vs. time Batch (3) w (20%) Trial (1) starting from 5 °C TB1on(-20 °C)_TB2on(5 °C) for ML2 (S4 to S6). Unit: mm.

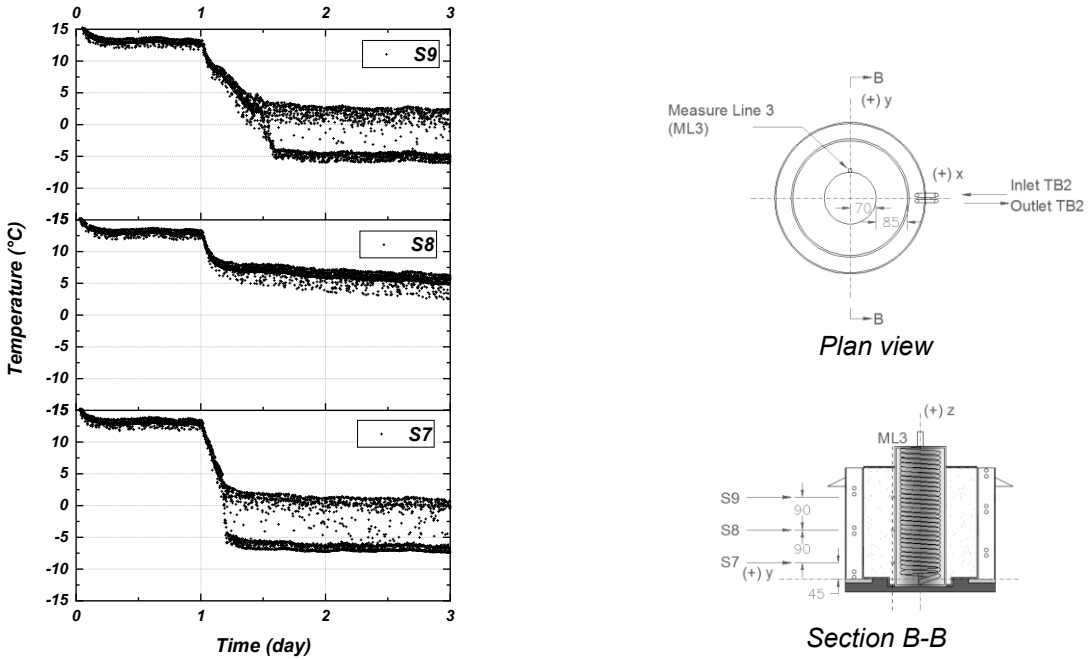

FIGURE A.45 Temp. vs. time Batch (3) w (20%) Trial (1) starting from 5 °C TB1on(-20 °C)_TB2on(5 °C) for ML3 (S7 to S9). Unit: mm.

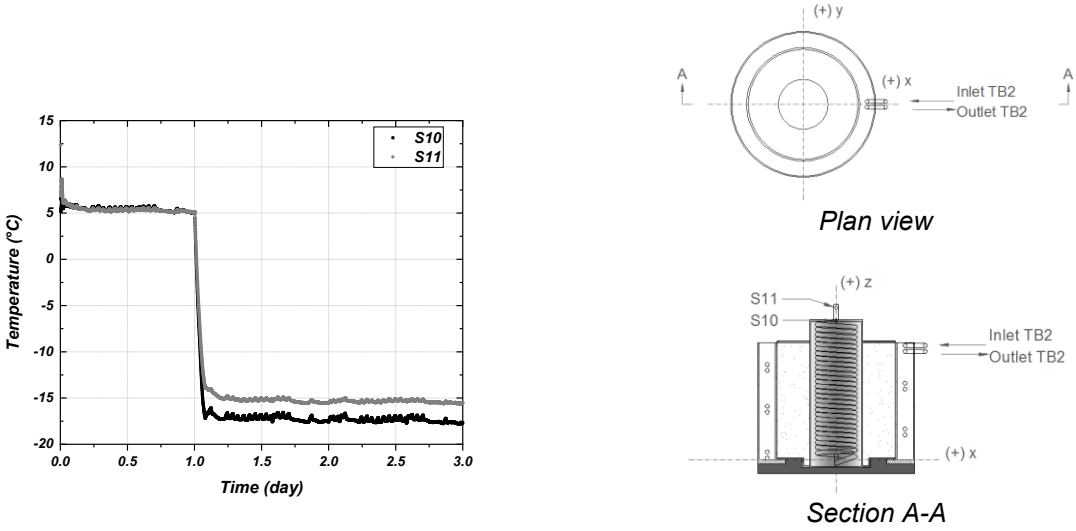

FIGURE A.46 Temp. vs. time Batch (3) w (20%) Trial (1) starting from 5 °C TB1on(-20 °C)_TB2on(5 °C) for on the copper coil (S10 and S11).

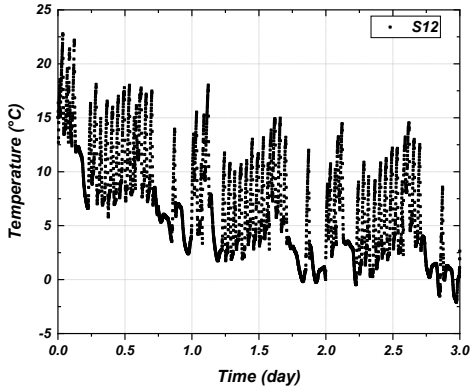

FIGURE A.47 Temp. vs. time Batch (3) w (20%) Trial (1) starting from 5 °C TB1on(-20 °C)_TB2on(5 °C) for in the cold room (S12).

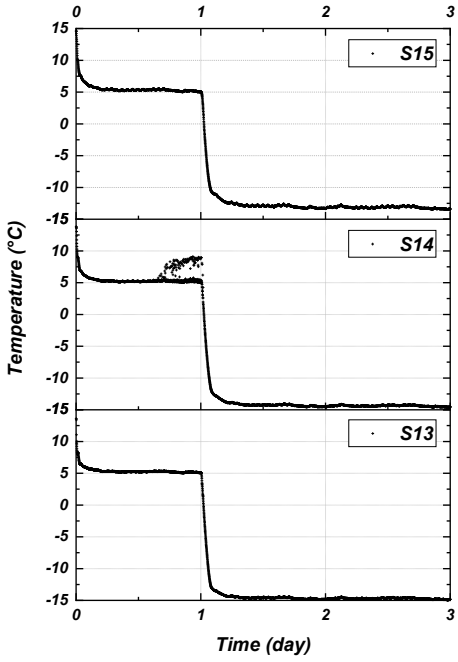

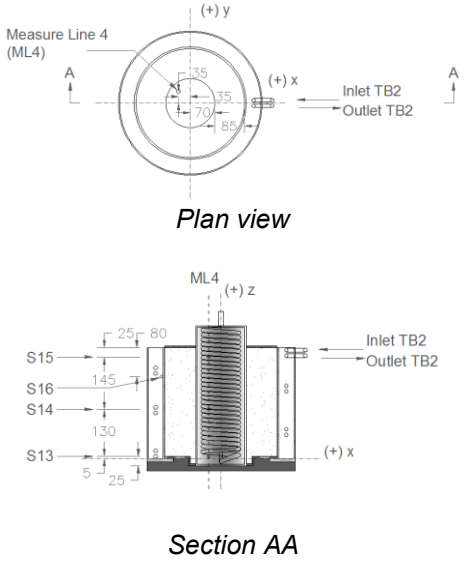

FIGURE A.48 Temp. vs. time Batch (3) w (20%) Trial (1) starting from 5 °C TB1on(-20 °C)_TB2on(5 °C) for inside glycol in pile (ML4) (S13 to S15). Unit: mm.

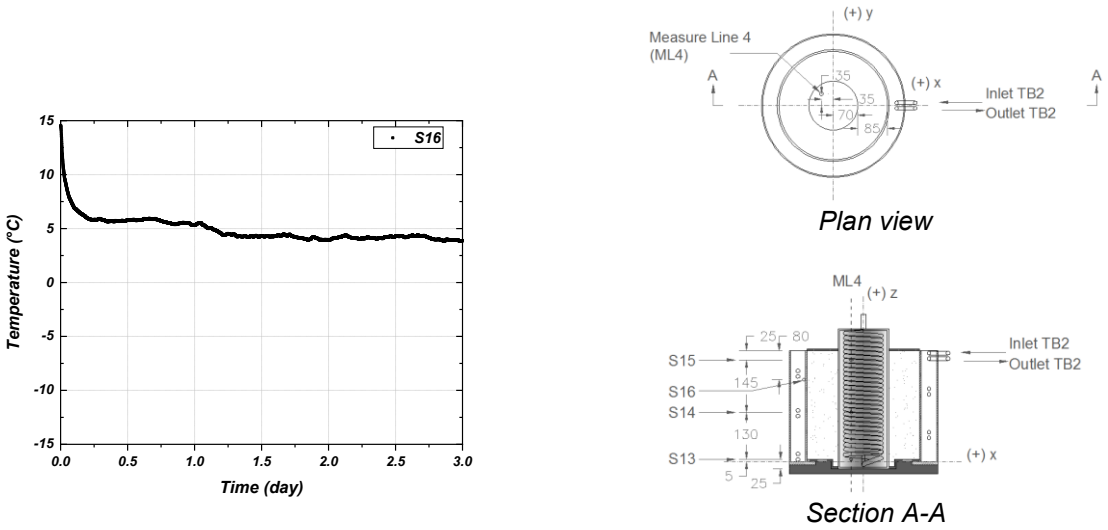

FIGURE A.49 Temp. vs. time Batch (3) w (20%) Trial (1) starting from 5 °C TB1on(-20 °C)_TB2on(5 °C) for inside of test cell wall (S16). Unit: mm.

Trial 2

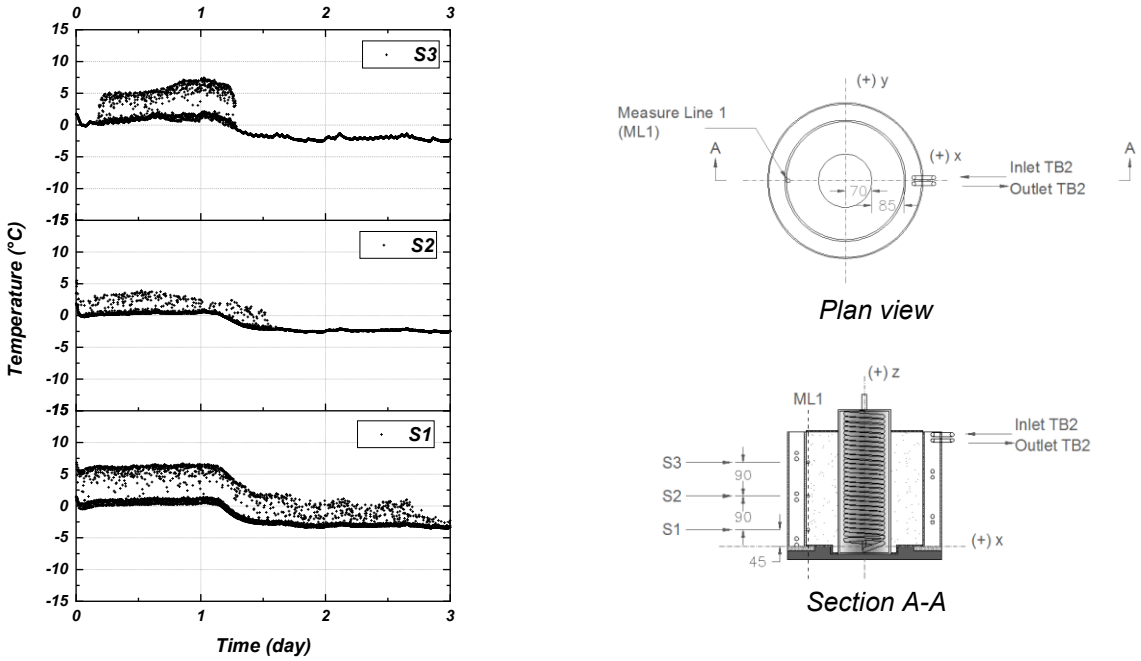

FIGURE A.50 Temp. vs. time Batch (3) w (20%) Trial (2) starting from 0 °C TB1on(-20 °C)_TB2on(0 °C) for ML1 (S1 to S3). Unit: mm.

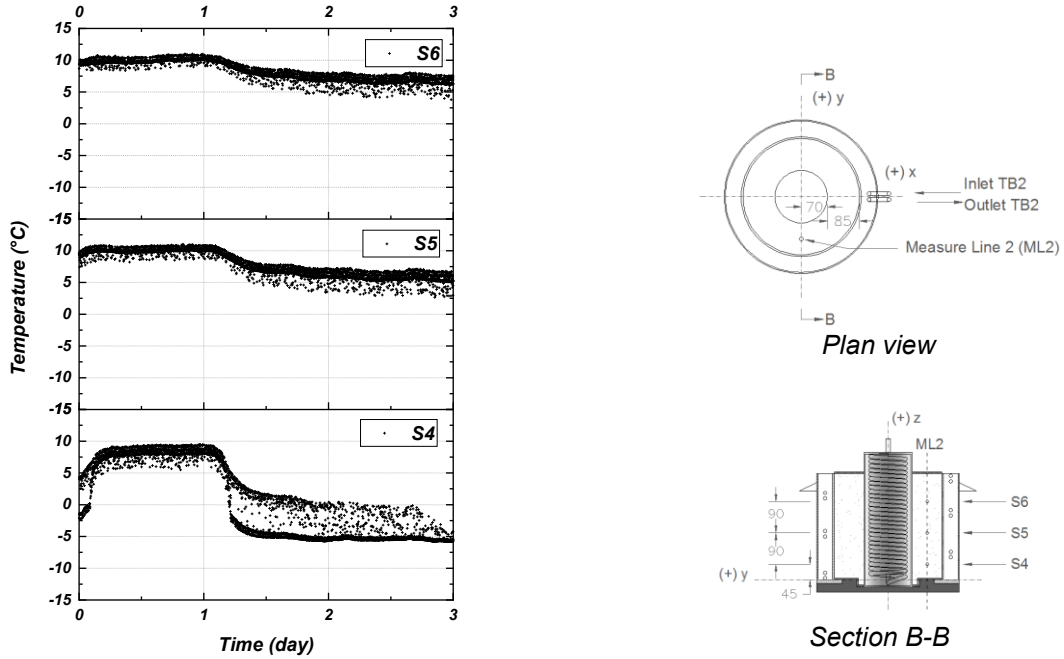

FIGURE A.51 Temp. vs. time Batch (3) w (20%) Trial (2) starting from 0 °C TB1on(-20 °C)_TB2on(0 °C) for ML2 (S4 to S6). Unit: mm.

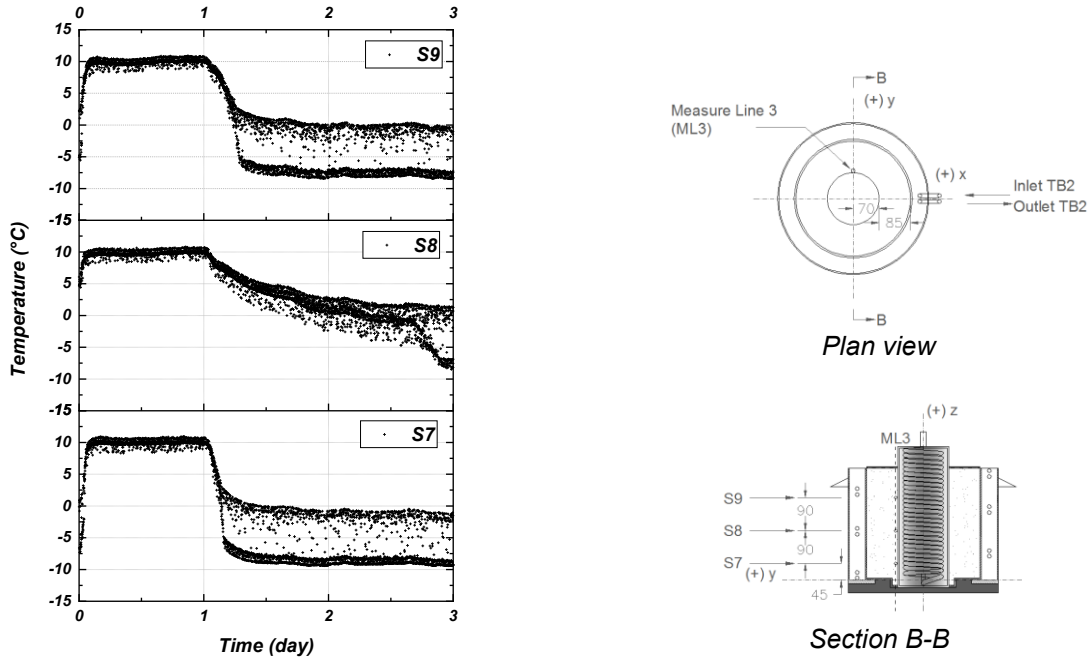

FIGURE A.52 Temp. vs. time Batch (3) w (20%) Trial (2) starting from 0 °C TB1on(-20 °C)_TB2on(0 °C) for ML3 (S7 to S9). Unit: mm.

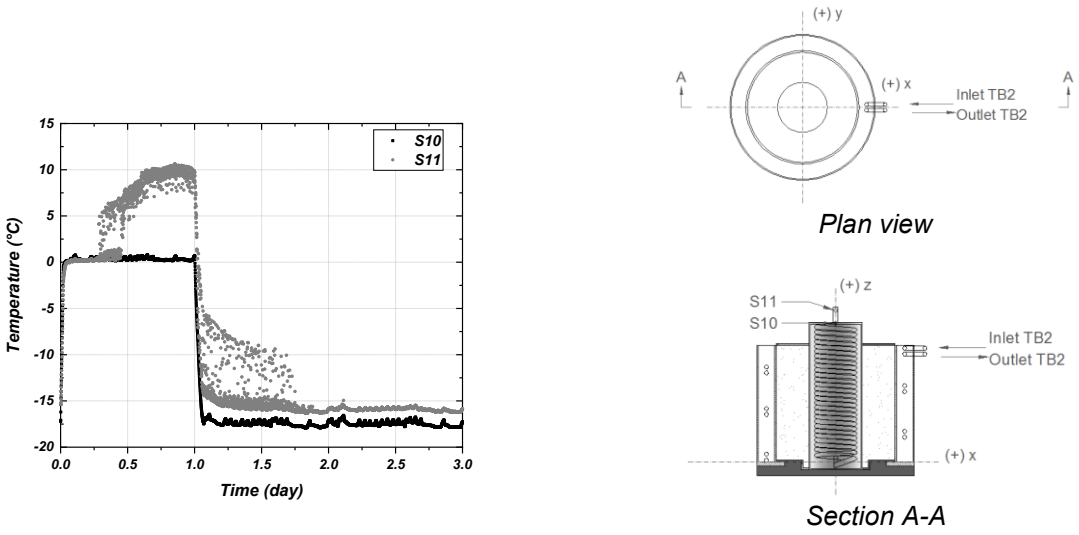

FIGURE A.53 Temp. vs. time Batch (3) w (20%) Trial (2) starting from 0 °C TB1on(-20 °C)_TB2on(0 °C) for on the copper coil (S10 and S11).

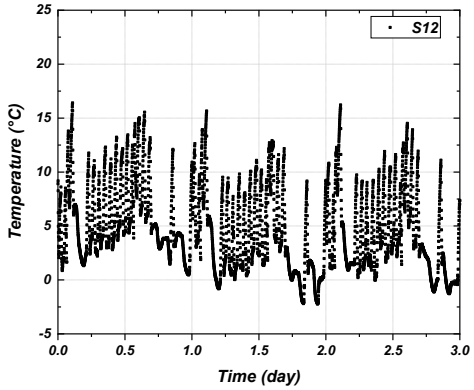

FIGURE A.54 Temp. vs. time Batch (3) w (20%) Trial (2) starting from 0 °C TB1on(-20 °C)_TB2on(0 °C) for in the cold room (S12).

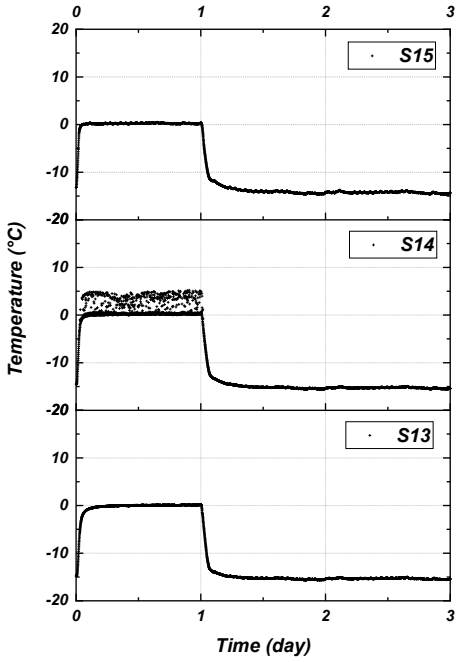

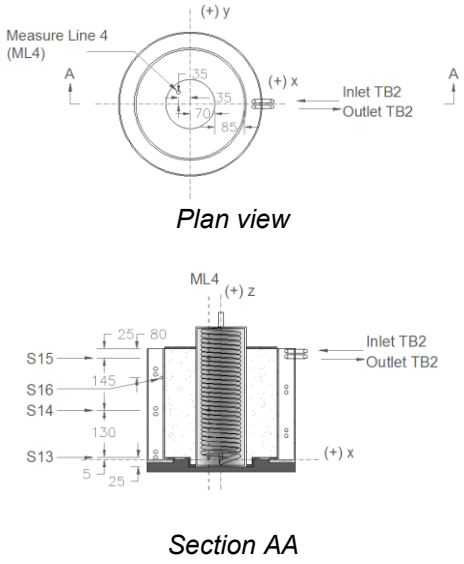

FIGURE A.55 Temp. vs. time Batch (3) w (20%) Trial (2) starting from 0 °C TB1on(-20 °C)_TB2on(0 °C) for inside glycol in pile (ML4) (S13 to S15). Unit: mm.

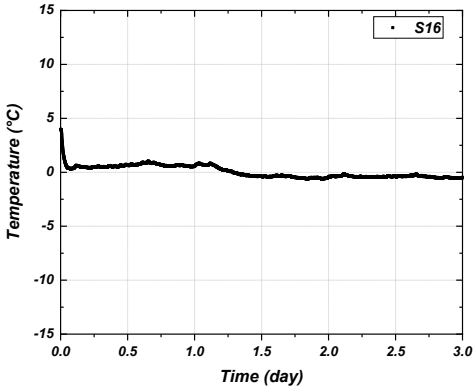

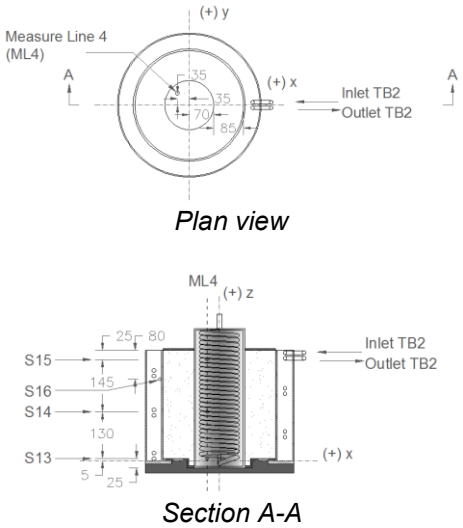

FIGURE A.56 Temp. vs. time Batch (3) w (20%) Trial (2) starting from 0 °C TB1on(-20 °C)_TB2on(0 °C) for inside of test cell wall (S16). Unit: mm.

Trial 3

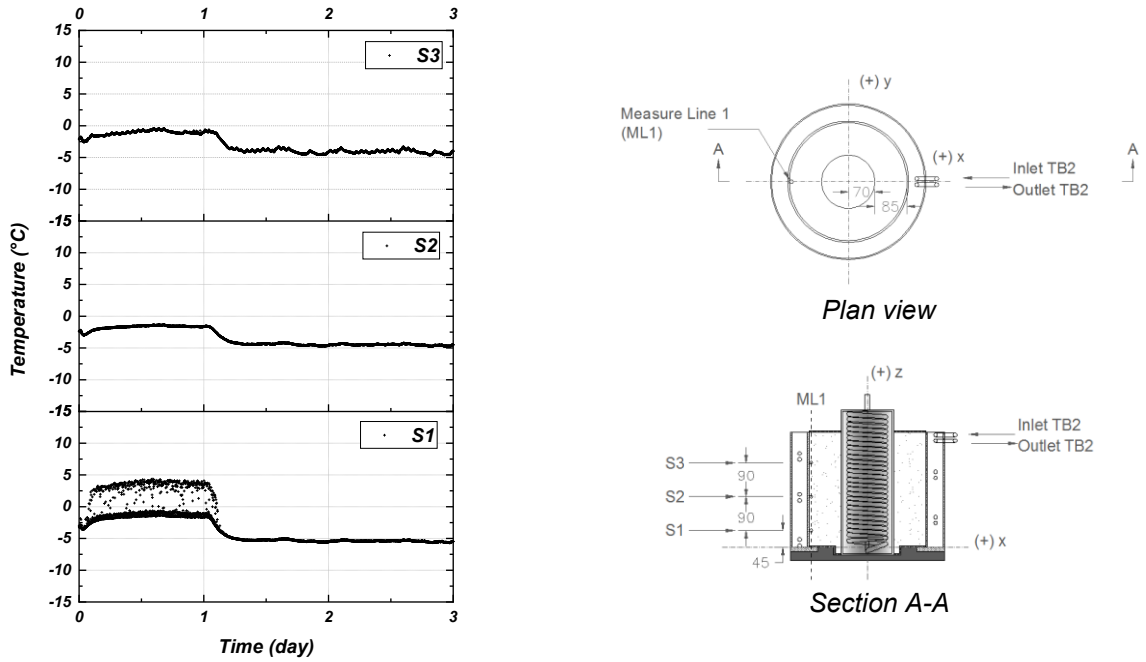

FIGURE A.57 Temp. vs. time Batch (3) w (20%) Trial (3) starting from -2.5 °C TB1on(-20 °C)_TB2on(-2.5 °C) for ML1 (S1 to S3). Unit: mm.

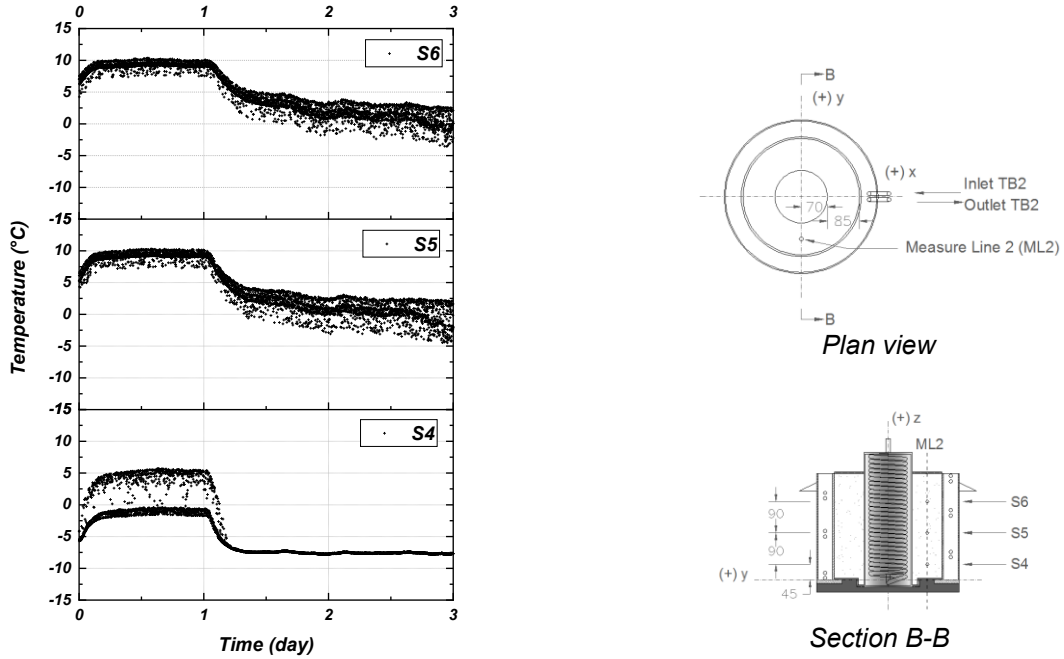

FIGURE A.58 Temp. vs. time Batch (3) w (20%) Trial (3) starting from -2.5 °C TB1on(-20 °C)_TB2on(-2.5 °C) for ML2 (S4 to S6). Unit: mm.

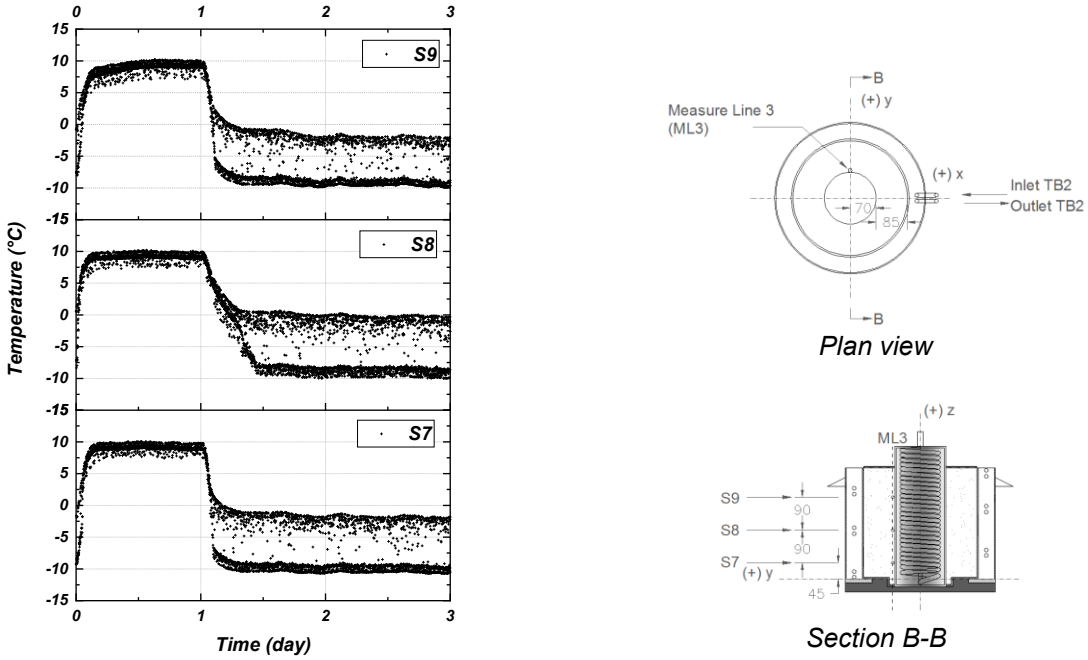

FIGURE A.59 Temp. vs. time Batch (3) w (20%) Trial (3) starting from -2.5 °C TB1on(-20 °C)_TB2on(-2.5 °C) for ML3 (S7 to S9). Unit: mm.

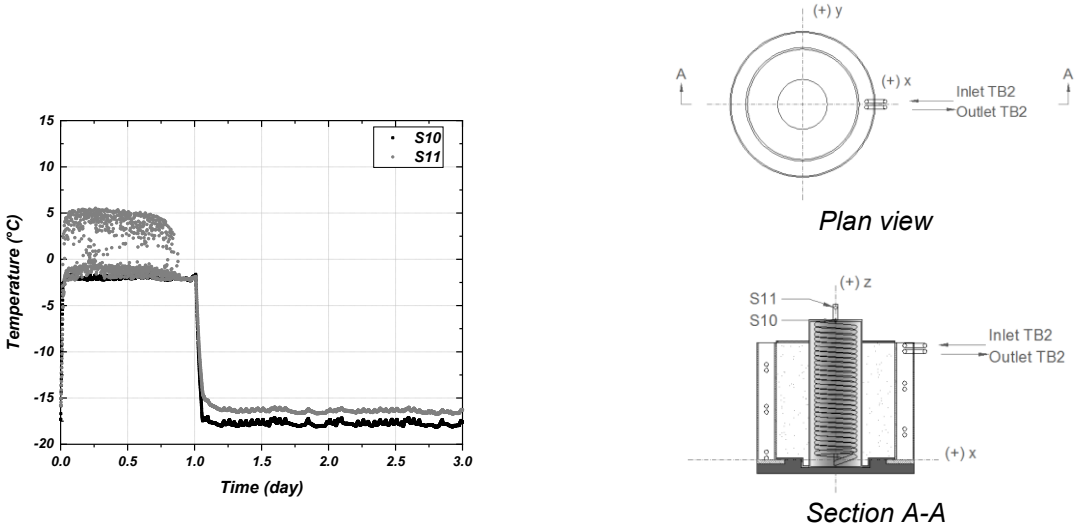

FIGURE A.60 Temp. vs. time Batch (3) w (20%) Trial (3) starting from -2.5 °C TB1on(-20 °C)_TB2on(-2.5 °C) for on the copper coil (S10 and S11).

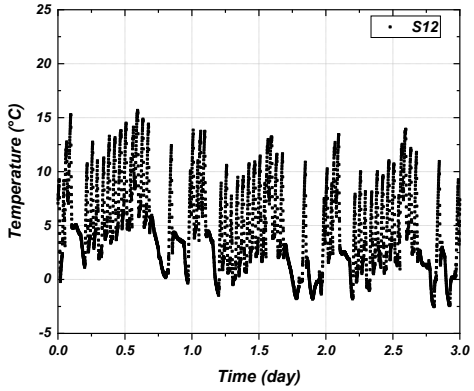

FIGURE A.61 Temp. vs. time Batch (3) w (20%) Trial (3) starting from -2.5 °C TB1on(-20 °C)_TB2on(-2.5 °C) for in the cold room (S12).

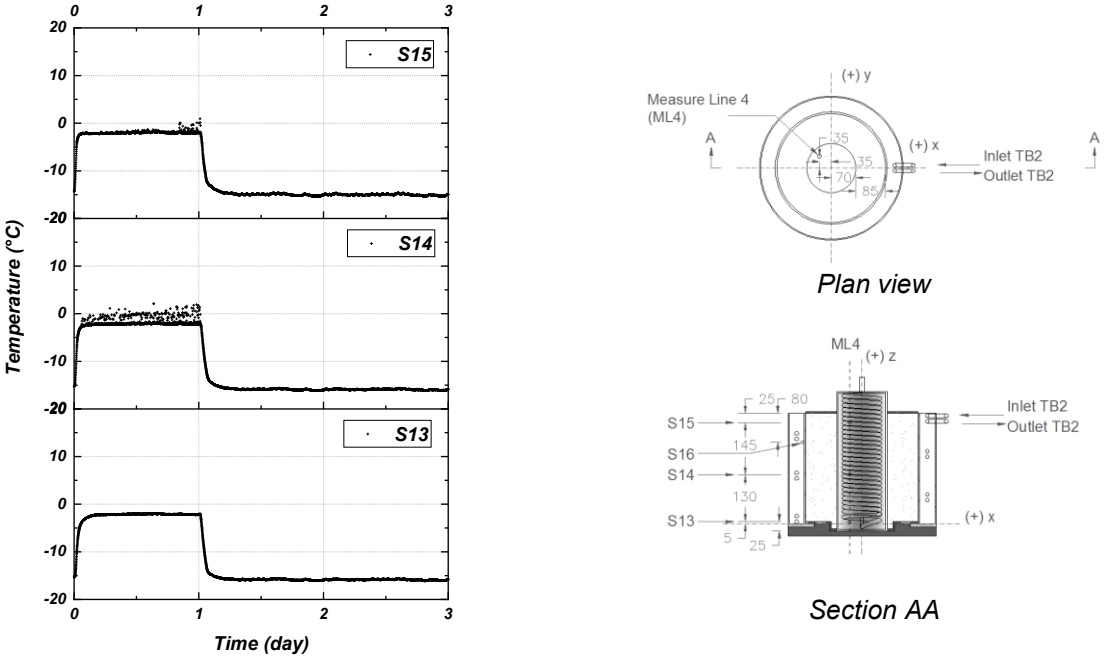

FIGURE A.62 Temp. vs. time Batch (3) w (20%) Trial (3) starting from -2.5 °C TB1on(-20 °C)_TB2on(-2.5 °C) for inside glycol in pile (ML4) (S13 to S15). Unit: mm.

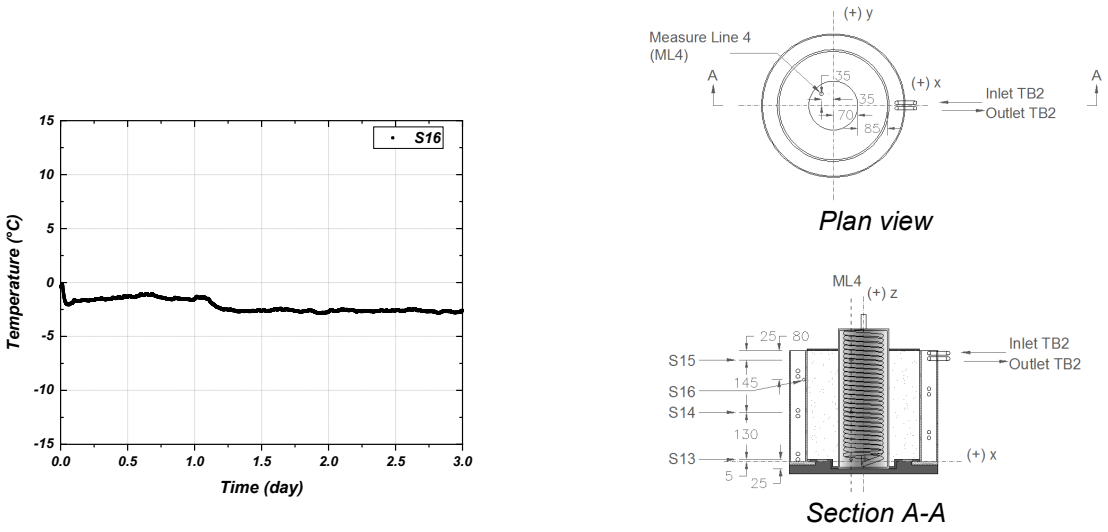

FIGURE A.63 Temp. vs. time Batch (3) w (20%) Trial (3) starting from -2.5 °C TB1on(-20 °C)_TB2on(-2.5 °C) for inside of test cell wall (S16). Unit: mm.

Trial (TB2_Off1)

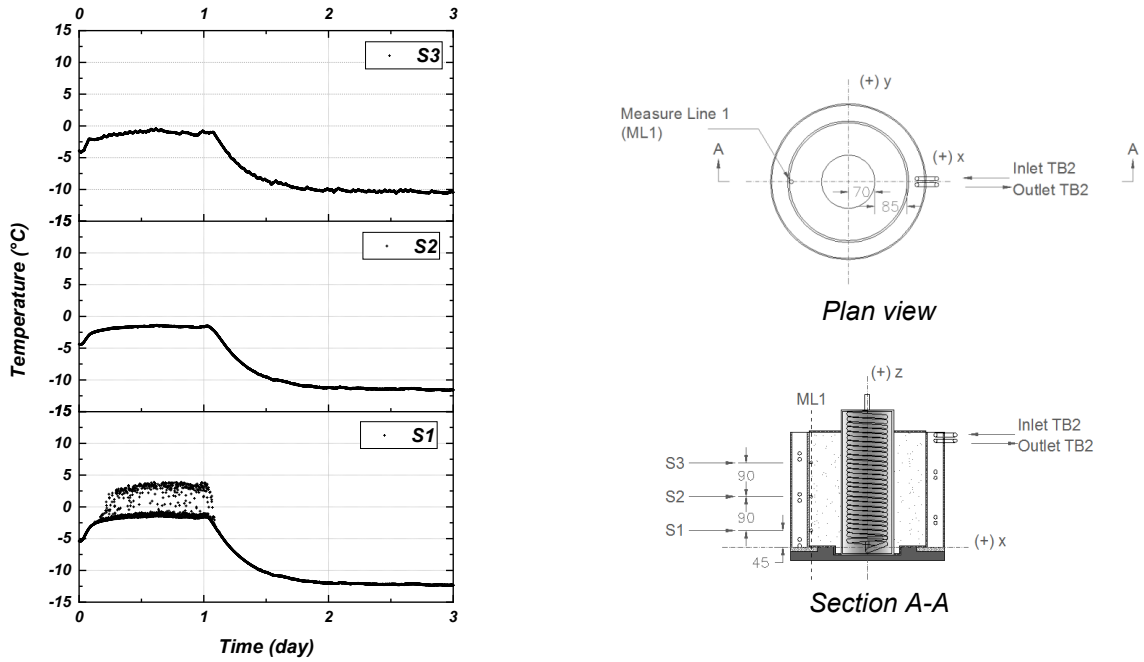

FIGURE A.64 Temp. vs. time Batch (3) w (20%) Trial (TB2_Off1) starting from -2.5 °C TB1on(-20 °C)_ TB2off for ML1 (S1 to S3). Unit: mm.

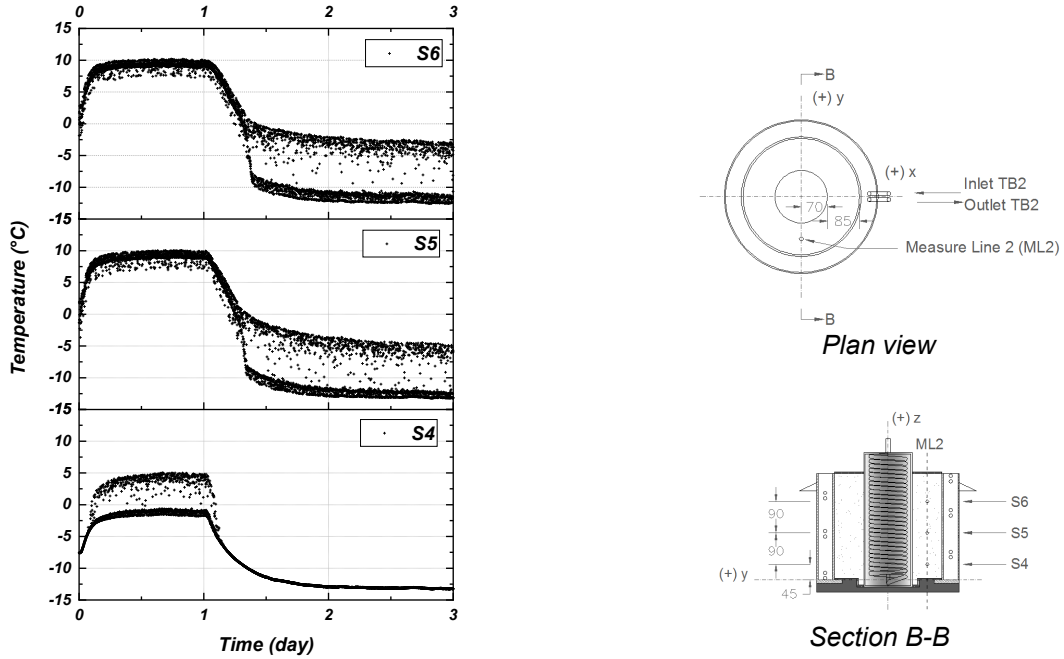

FIGURE A.65 Temp. vs. time Batch (3) w (20%) Trial (TB2_Off1) starting from -2.5 °C TB1on(-20 °C)_ TB2off for ML2 (S4 to S6). Unit: mm.

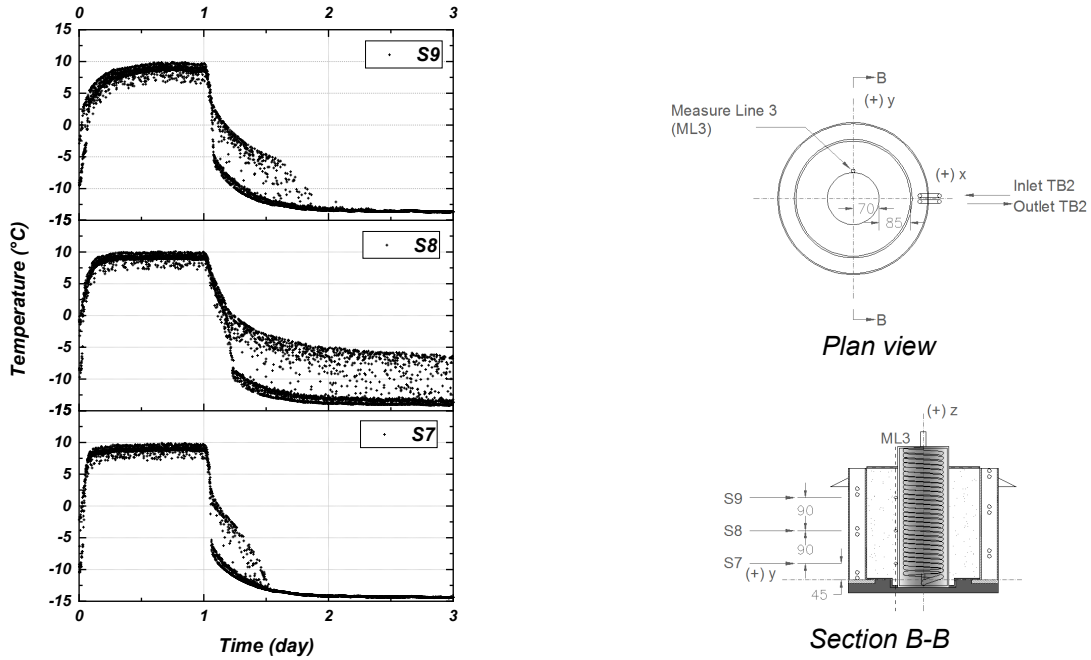

FIGURE A.66 Temp. vs. time Batch (3) w (20%) Trial (TB2_Off1) starting from -2.5 °C TB1on(-20 °C)_ TB2off for ML3 (S7 to S9). Unit: mm.

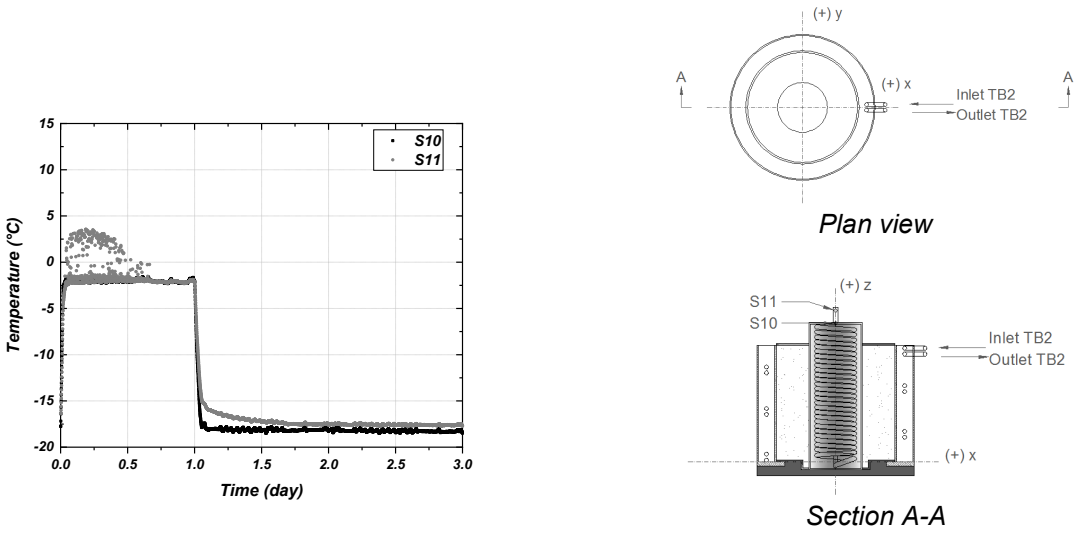

FIGURE A.67 Temp. vs. time Batch (3) w (20%) Trial (TB2_Off1) starting from -2.5 °C TB1on(-20 °C)_ TB2off for on the copper coil (S10 and S11).

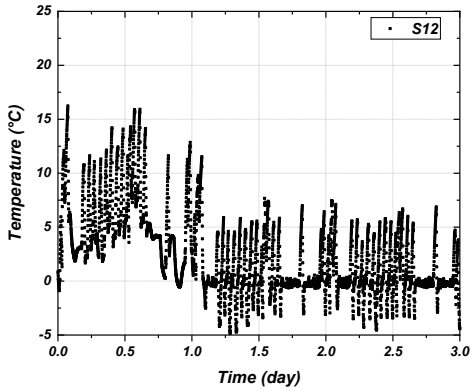

FIGURE A.68 Temp. vs. time Batch (3) w (20%) Trial (TB2_Off1) starting from -2.5 °C TB1on(-20 °C)_ TB2off for in the cold room (S12).

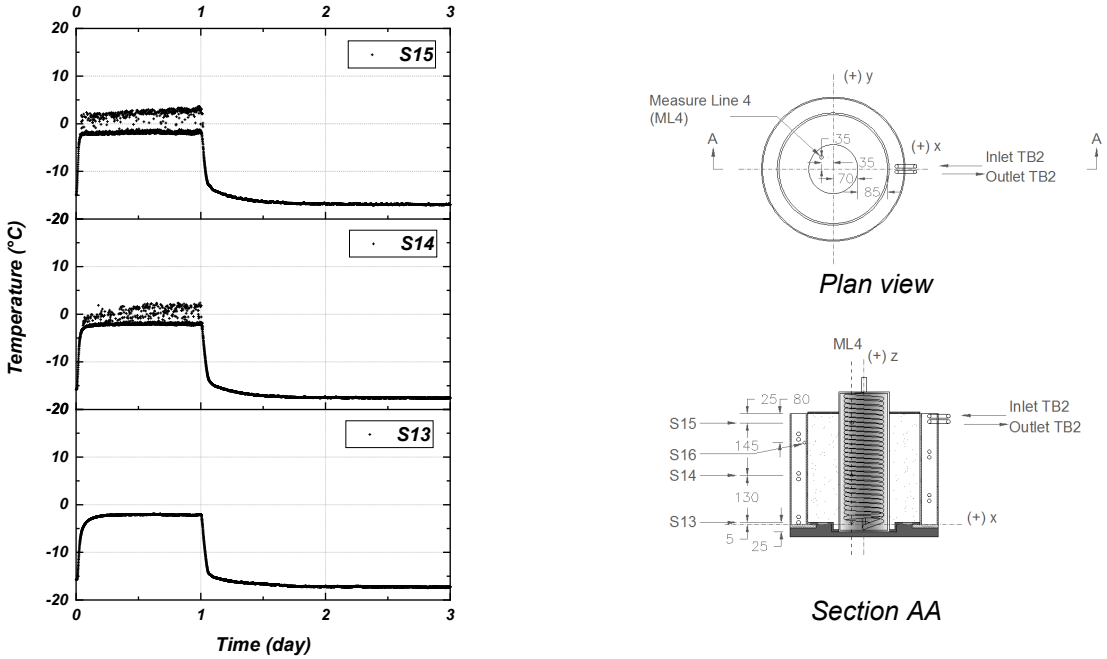

FIGURE A.69 Temp. vs. time Batch (3) w (20%) Trial (TB2_Off1) starting from -2.5 °C TB1on(-20 °C)_ TB2off for inside glycol in pile (ML4) (S13 to S15). Unit: mm.

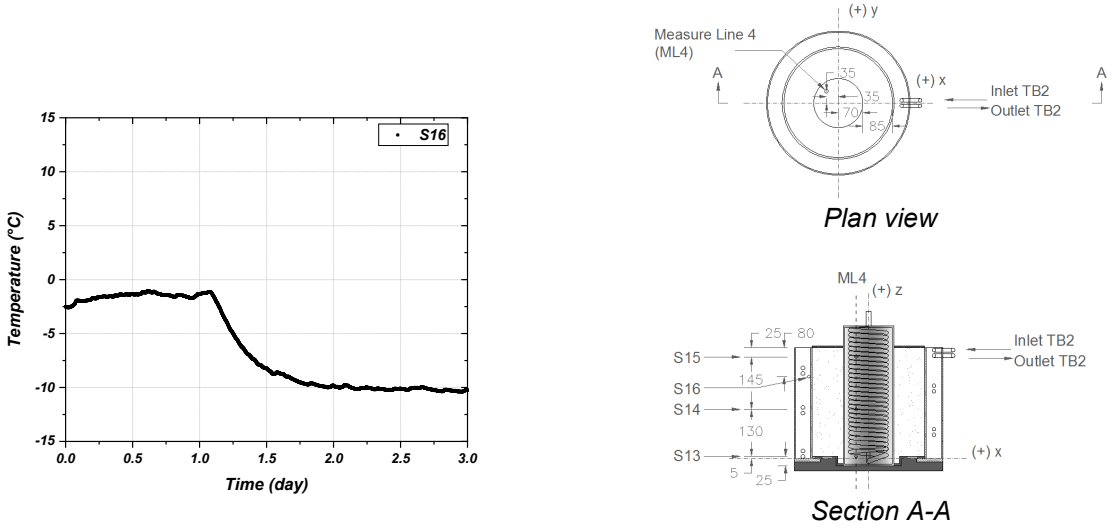

FIGURE A.70 Temp. vs. time Batch (3) w (20%) Trial (TB2_Off1) starting from -2.5 °C TB1on(-20 °C)_ TB2off for inside of test cell wall (S16). Unit: mm.

Trial (TB2_Off2)

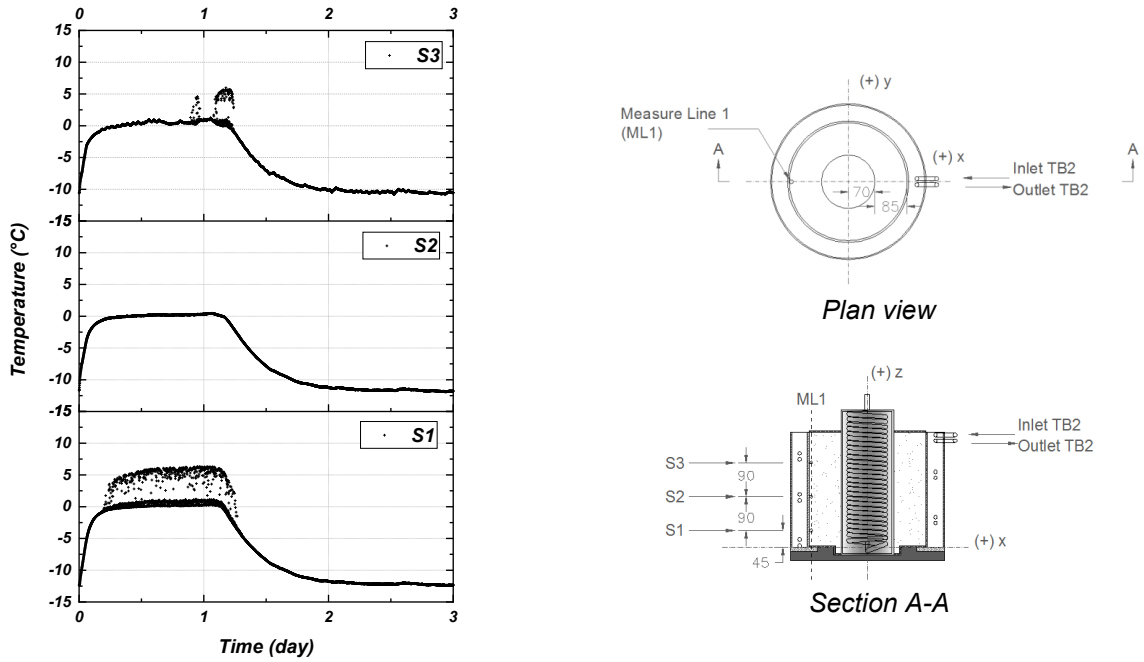

FIGURE A.71 Temp. vs. time Batch (3) w (20%) Trial (TB2_Off2) starting from 0 °C TB1on(-20 °C)_ TB2off for ML1 (S1 to S3). Unit: mm.

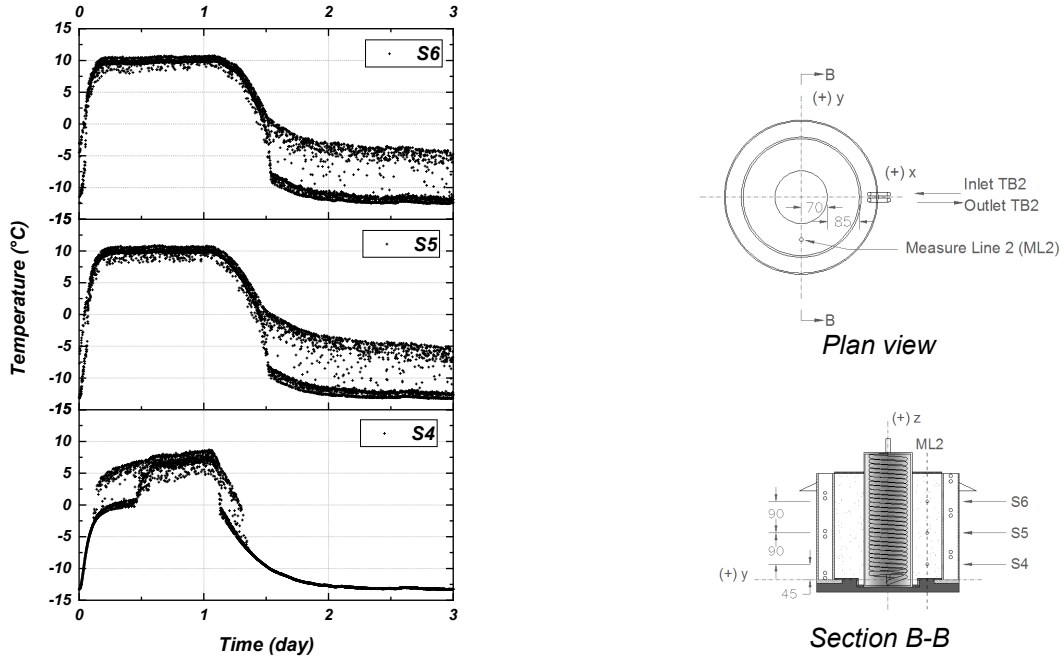

FIGURE A.72 Temp. vs. time Batch (3) w (20%) Trial (TB2_Off2) starting from 0 °C TB1on(-20 °C)_ TB2off for ML2 (S4 to S6). Unit: mm.

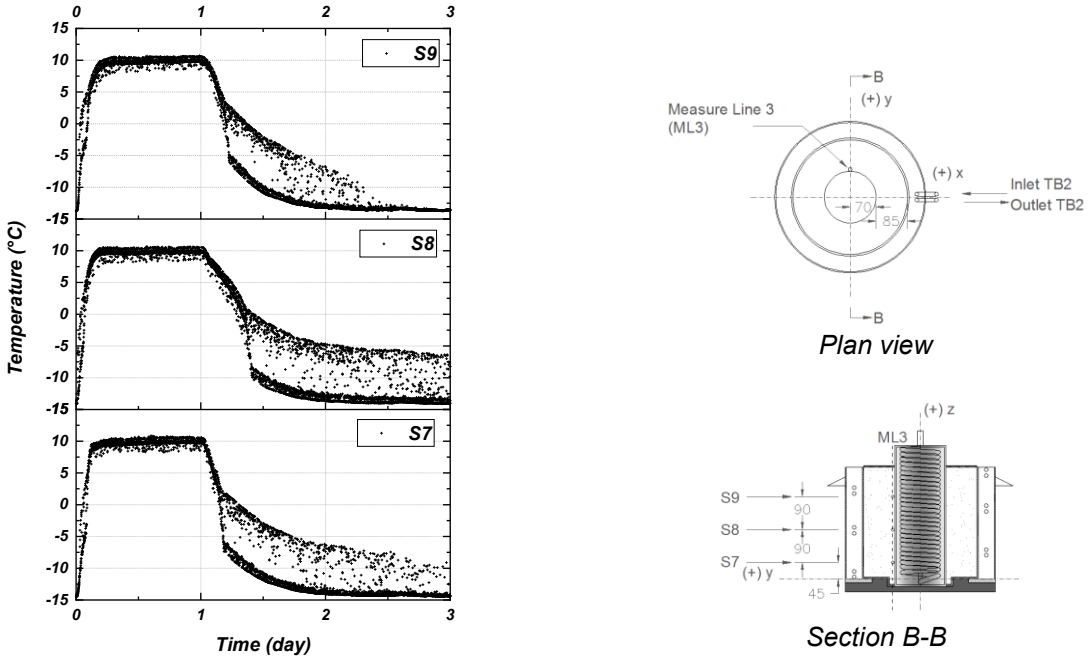

FIGURE A.73 Temp. vs. time Batch (3) w (20%) Trial (TB2_Off2) starting from 0 °C TB1on(-20 °C)_ TB2off for ML3 (S7 to S9). Unit: mm.

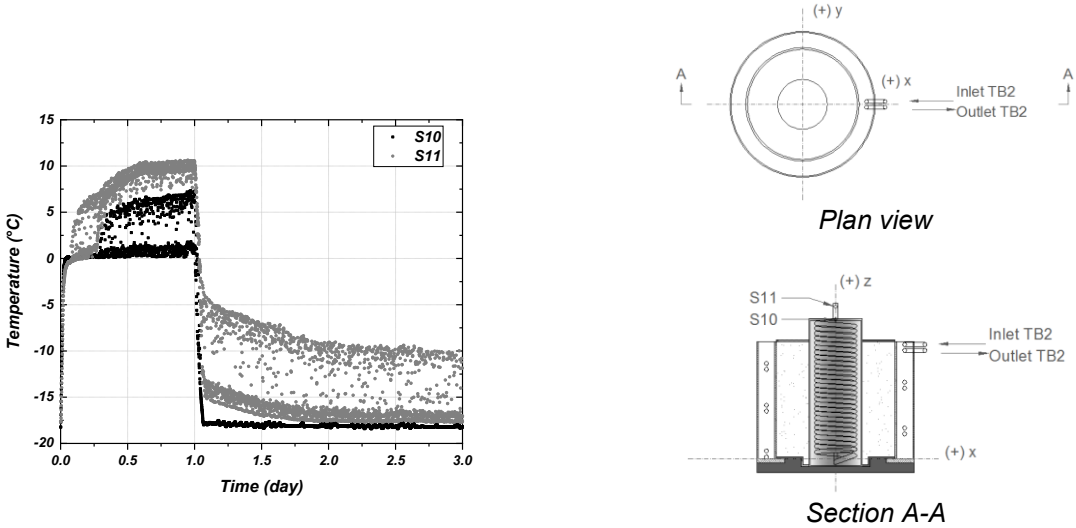

FIGURE A.74 Temp. vs. time Batch (3) w (20%) Trial (TB2_Off2) starting from 0 °C TB1on(-20 °C)_ TB2off for on the copper coil (S10 and S11).

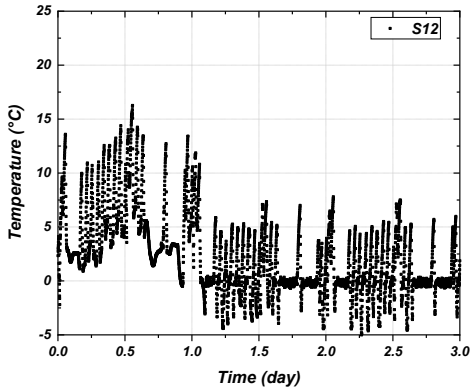

FIGURE A.75 Temp. vs. time Batch (3) w (20%) Trial (TB2_Off2) starting from 0 °C TB1on(-20 °C)_ TB2off for in the cold room (S12).

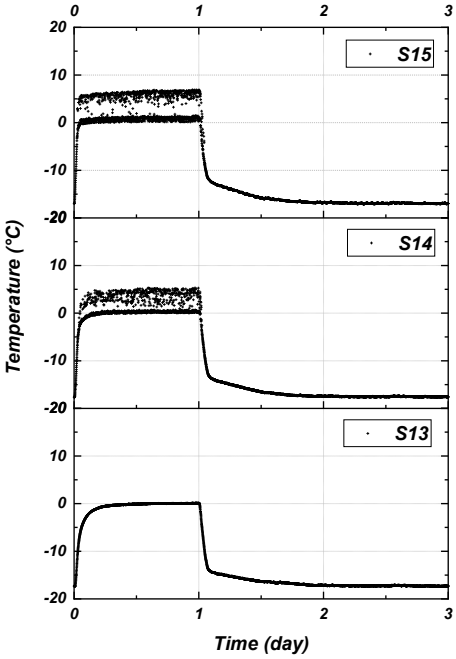

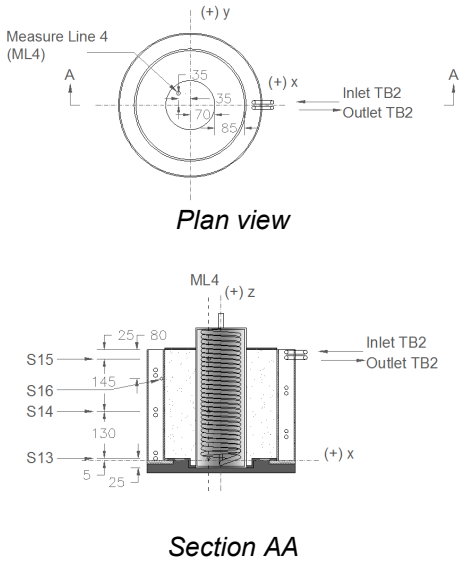

FIGURE A.76 Temp. vs. time Batch (3) w (20%) Trial (TB2_Off2) starting from 0 °C TB1on(-20 °C)_ TB2off for inside glycol in pile (ML4) (S13 to S15). Unit: mm.

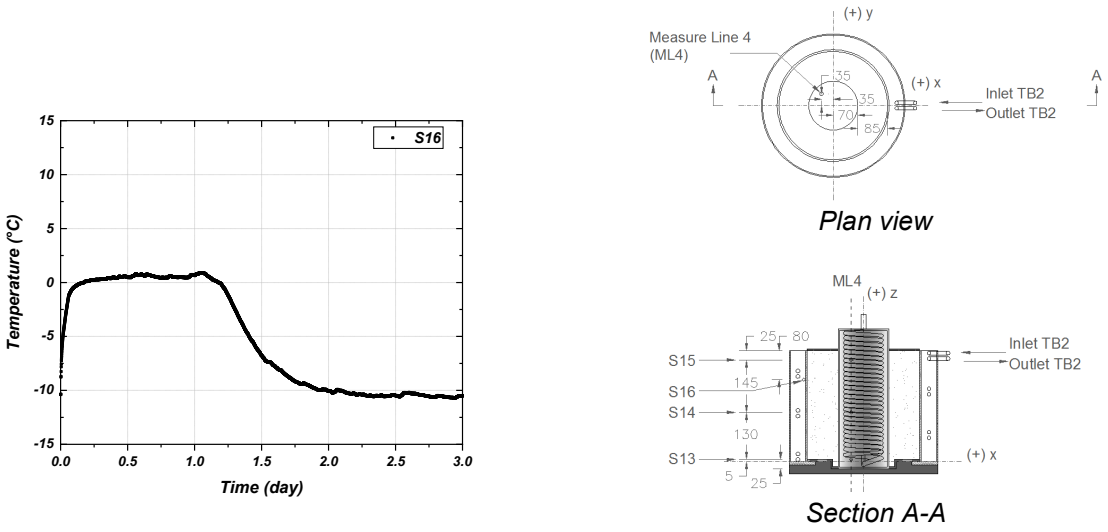

FIGURE A.77 Temp. vs. time Batch (3) w (20%) Trial (TB2_Off2) starting from 0 °C TB1on(-20 °C)_ TB2off for inside of test cell wall (S16). Unit: mm.

Density and Water Content

TABLE A.3 Batch (3) Density and Water Content by Layer

Layer	Sample	Tray empty (gr)	Tray+soil+ ring (gr)	Soil+tray (gr)	Soil $_{Dry}$ +tray (gr)	Soil mass (gr)	Soil mass (kg)	Density (kg/m^3)	Average density (kg/m^3)	Unit weight (kN/m^3)	Average Unit weight (kN/m^3)	w (%)	Average w (%)
1	L1-1	4.25	395.95	231.43	196.15	227.30	0.2273	1768.74	1848.02	17.35	18.13	18.38	18.21
	L1-2	4.25	408.75	244.15	207.52	240.10	0.2401	1868.35		18.33		18.02	
	L1-3	4.24	405.08	240.53	204.56	236.44	0.2364	1839.87		18.05		17.96	
	L1-4	4.31	414.82	250.23	211.84	246.11	0.2461	1915.11		18.79		18.50	
2	L2-1	4.27	412.73	248.07	209.72	244.06	0.2441	1899.16	1912.18	18.63	18.76	18.67	18.52
	L2-2	4.24	418.74	254.09	215.28	250.10	0.2501	1946.16		19.09		18.39	
	L2-3	4.28	411.95	247.40	209.63	243.27	0.2433	1893.01		18.57		18.39	
	L2-4	4.26	414.16	249.58	211.05	245.50	0.2455	1910.37		18.74		18.63	
3	L3-1	4.26	408.87	244.12	206.65	240.21	0.2402	1869.20	1868.70	18.34	18.33	18.51	18.66
	L3-2	4.28	405.45	240.75	203.81	236.77	0.2368	1842.43		18.07		18.51	
	L3-3	4.24	407.04	242.24	204.62	238.40	0.2384	1855.12		18.20		18.77	
	L3-4	4.29	413.89	249.23	210.39	245.20	0.2452	1908.03		18.72		18.85	
Total average									1876.30		18.41		18.47

Results of the Modeling of freezing Tests

Batch (2) w (35%) Trial (TB2_Off1) starting from -2.5 °C TB1on(-20 °C)_TB2off

Physical Soil Sample Properties

TABLE A.4 Initial Soil Sample Properties Batch (2) Trial (TB2_Off1)

Property	Symbol	Value	Unit
Moisture content	w	35	%
Specific gravity of solids	G_s	2.67	
Unit weight of water (4 °C)	γ_w	9.807	kN/m^3
Total unit weight	γ	18.56	kN/m^3

TABLE A.5 Phase Relationships (Physical Properties of the Soil Sample)

Property	Symbol	Value	Unit
Void ratio	e	0.90	
Porosity	n	0.47	
Degree of saturation	S_r	1.0	
Density of water	ρ_w	1000	kg/m^3
Density of soil	ρ	1892	kg/m^3
Dry density	ρ_d	1402	kg/m^3

Thermal Parameters of the Soil Sample

TABLE A.6 Thermal Parameters

Thermal parameters	Symbol	Value	Unit	Source
Thermal conductivity of the soil particles	k_s	2.5	W/m · °C	Table 2.1
Thermal conductivity of the pore water	k_w	0.57	W/m · °C	(Andersland & Ladanyi, 2004)
Unfrozen water content	w_u	0.25	%	Eq. 2.6
Thermal conductivity of ice	ki	2.2	W/m · °C	(Andersland & Ladanyi, 2004)
Kersten number for unfrozen coarse grained soil	K_e	1.01		Eq. 2.7
Kersten number for unfrozen fine grained soil	K_e	1.01		Eq. 2.8
Kersten number for frozen soil	K_e	1.0		$K_e=S_r$, Eq. 2.9
Volumetric heat capacity of water	c_{vw}	4.187	$MJ/m^3 \cdot °C$	(Andersland & Ladanyi, 2004)

Thermal Properties of the Soil Sample

TABLE A.7 Thermal Conductivity Results

Thermal conductivity	Value	Unit
Dry, natural soil	0.18	W/m · °C
Dry, crushed rock materials	0.20	W/m · °C
Saturated unfrozen soil	1.24	W/m · °C
Saturated frozen soil	2.34	W/m · °C
Unfrozen	1.25	W/m · °C
Frozen	2.42	W/m · °C
Frozen soil with w_u	2.41	W/m · °C

TABLE A.8 Volumetric Heat Capacities Results

Volumetric heat capacities				
Unfrozen	3.05	$MJ/m^3 \cdot °C$	3051.56	$kJ/m^3 \cdot °C$
Frozen	2.03	$MJ/m^3 \cdot °C$	2031.96	$kJ/m^3 \cdot °C$

Latent heat of fusion (L) = 162.52 MJ/m^3 Eq. 2.25

Closed-Form Solution

TABLE A.9 Input Parameters Closed-Form Solution

Freeze pipe dimensions		
Spacing (S)	1	m
Radius (r_0)	0.07	m
Soil Physical Properties		
Soil type	Silt sand	
Density of soil (ρ)	1892.12	kg/m^3
Water content (w)	35	%
Soil dry density (ρ_d)	1401.57	kg/m^3

Soil thermal properties	**Value**	**Unit**	**Source**
Difference between the temperature at the surface of the freeze-pipe and the freezing point of water (v_s)	-20	°C	TB1
Difference between the ambient temperature of the ground and the freezing point of water (v_0)	-2.5	°C	Homogenization stage
Volumetric heat capacity of water (c_{vw})	4.187	$MJ/m^3 \cdot °C$	(Andersland & Ladanyi, 2004)
Frozen thermal conductivity (k_f)	2.42	$W/m \cdot °C$	Eq. 2.17
Amount of heat when water is converted into ice with no change in temperature (L')	333700	J/kg	(Andersland & Ladanyi, 2004)
Volumetric heat capacity for mineral (frozen) soils (c_{vf})	2.03	$MJ/m^3 \cdot °C$	Eq. 2.14
Volumetric heat capacity for mineral (unfrozen) soils (c_{vu})	3.05	$MJ/m^3 \cdot °C$	Eq. 2.13
Volumetric latent heat of the soil (L)	162.52	MJ/m^3	Eq. 2.25
Equivalent latent heat for stage I (L_1)	190.30	MJ/m^3	Eq. 2.32
Equivalent latent heat for stage II (L_F)	201.80	MJ/m^3	Eq. 2.36

TABLE A.10 Results Closed-Form Solution

Stage I			
R (m)	Q_I (MJ/m)	t_1 (days)	P_1 (W/m)
0.10	7.77	0.06	851.42
0.15	15.34	0.19	398.46
0.20	26.35	0.60	289.27
0.25	40.50	1.25	238.56
0.30	57.75	2.18	208.67
0.35	78.09	3.39	188.69
0.40	101.51	4.92	174.23
0.45	128.01	6.77	163.20
0.50	157.58	8.96	154.46

Stage II					
W (m)	x = W/S	t_{IIF} (days)	t_{total} (days)	Q_{IIF} (MJ/m^2)	P_{IIF} (W/m^2)
0.80	0.80	0.00	8.96	0.0	0.0
0.85	0.85	0.62	9.58	171.5	227.4
0.90	0.90	1.15	10.11	181.6	214.8
0.95	0.95	1.71	10.67	191.7	203.5
1.00	1.00	2.30	11.26	201.8	193.3
1.05	1.05	2.91	11.87	211.9	184.1

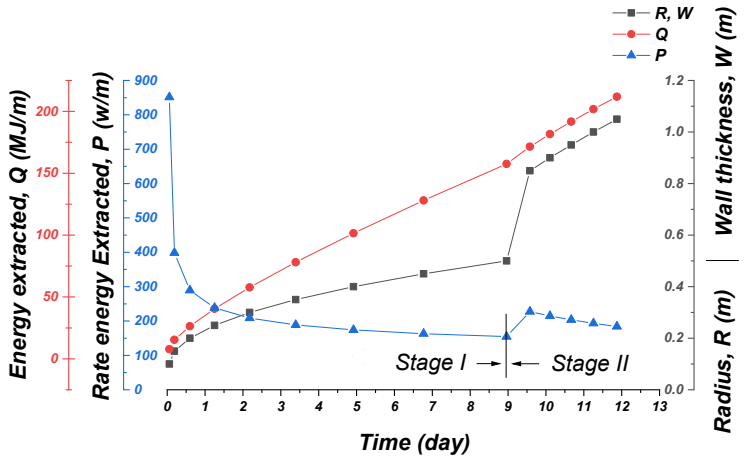

FIGURE A.78 Results for stage I and stage II, time vs radius R, wall thickness W, energy extracted Q, and rate energy extracted P Batch (2) Trial (TB2_Off1).

Finite Element Analysis

Model Configuration

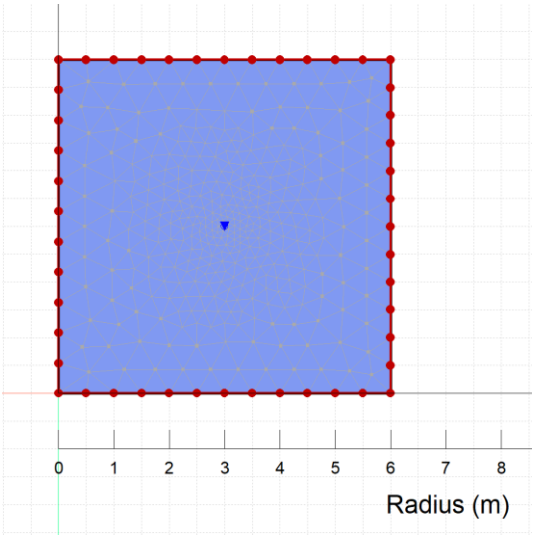

FIGURE A.79 Mesh configuration.

Thermal Material Setting

TABLE A.11 Thermal Material Model Setting

Parameter	Value	Unit		Value	Unit
Frozen thermal conductivity	2.42	W/m · °C		208.79	kJ/d/m/°C
Unfrozen thermal conductivity	1.25	W/m · °C		107.94	kJ/d/m/°C
Unfrozen water content (w_u)	0.25	%	(for Silty sand)		
Unfrozen volumetric heat capacity	3.05	MJ/m^3 · °C		3051.56	kJ/m^3 · °C
Frozen volumetric heat capacity	2.03	MJ/m^3 · °C		2031.96	kJ/m^3 · °C
Insitu water content	0.35				
Activation temperature	-2.5	°C			

Boundary Condition

TABLE A.12 Convective Heat Transfer Constants and Coefficients

Parameter	Value	Unit	Source
Glycol thermal conductivity	0.258	(w/m · °C)	(Engineering Toolbox, 2008)
Nusselt number	3.66		(Bergman et al.,2011)
Convective heat transfer coefficient (h)	6.74	J/sec/m^2/°C	Eq. 5.1
Fluid temperature	-20	°C	TB1
Surface perimeter	0.44	m	Pile's perimeter

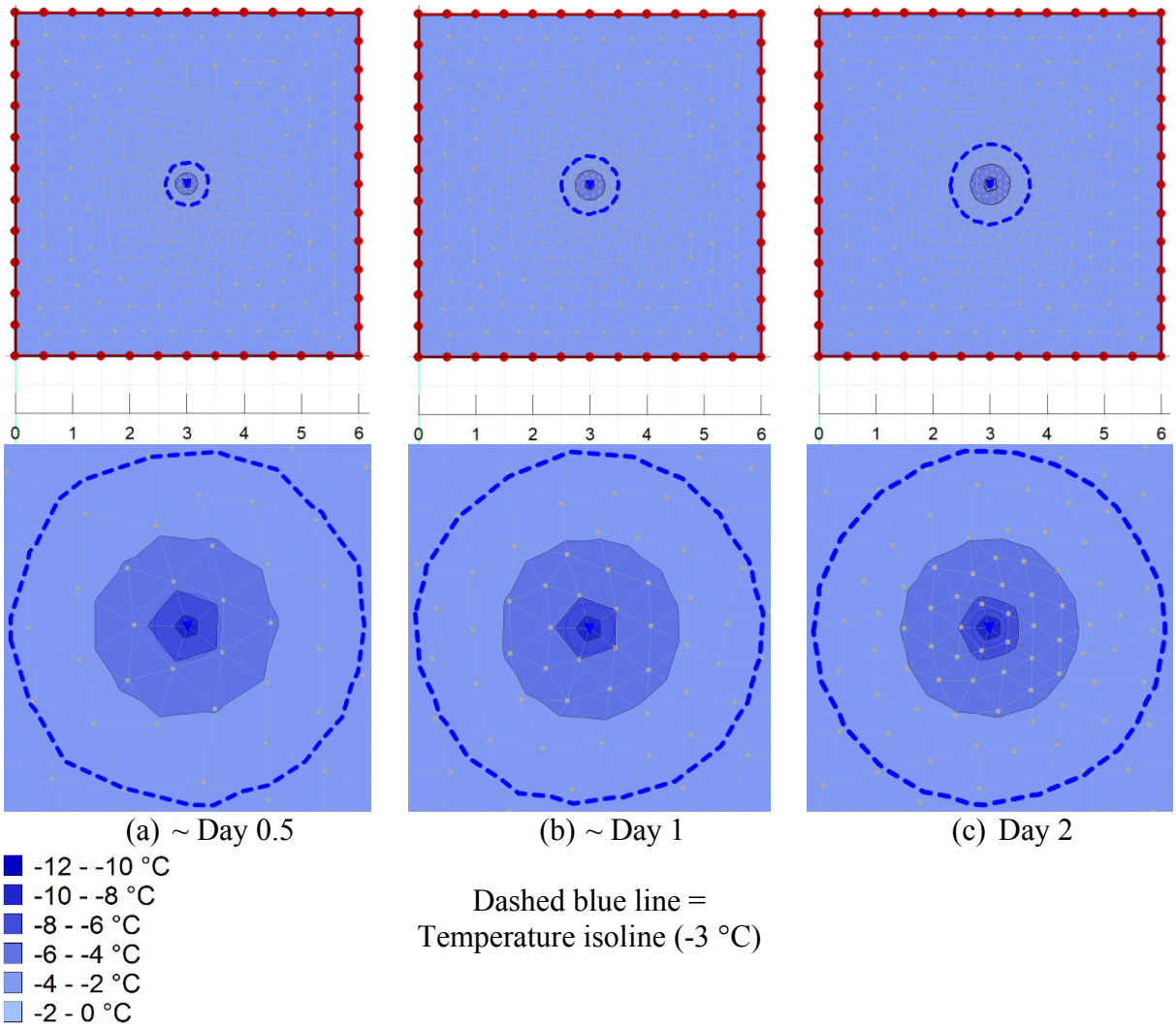

FIGURE A.80 Radial extent of frozen soil in meters. (a) day 0.5. (b) day 1. (c) day 2.

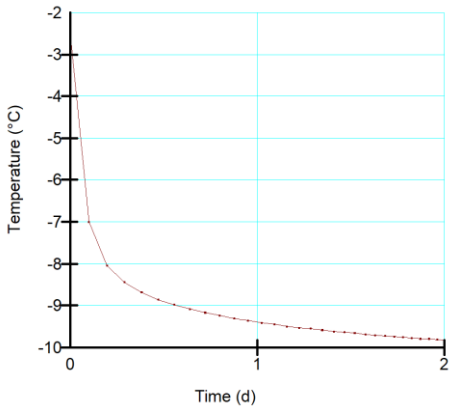

FIGURE A.81 Temperature vs time (at the point on the mesh).

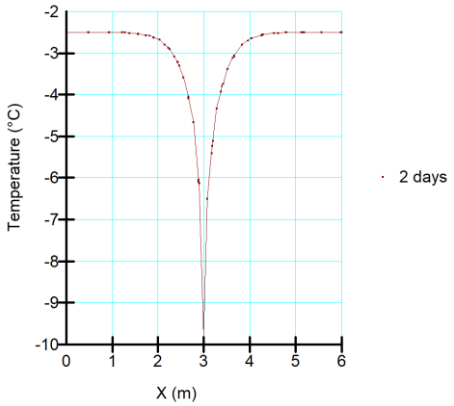

FIGURE A.82 Temperature profile at day 2.

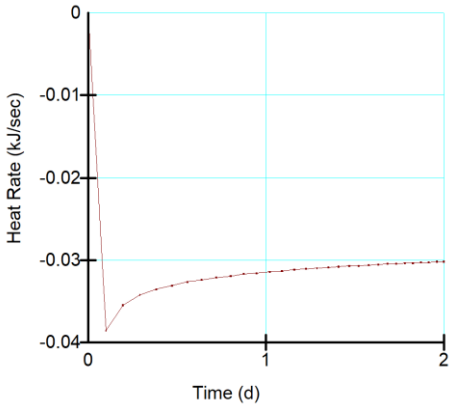

FIGURE A.83 Heat extraction rate per unit length of pile.

Batch (2) w (35%) Trial (TB2_Off2) starting from 0 °C TB1on(-20 °C)_TB2off

Physical Soil Sample Properties

TABLE A.13 Initial Soil Sample Properties Batch (2) Trial (TB2_Off2)

Property	Symbol	Value	Unit
Moisture content	w	35	%
Specific gravity of solids	G_s	2.67	
Unit weight of water (4 °C)	γ_w	9.807	kN/m^3
Total unit weight	γ	18.56	kN/m^3

TABLE A.14 Phase Relationships (Physical Properties of the Soil Sample)

Property	Symbol	Value	Unit
Void ratio	e	0.90	
Porosity	n	0.47	
Degree of saturation	S_r	1.0	
Density of water	ρ_w	1000	kg/m^3
Density of soil	ρ	1892	kg/m^3
Dry density	ρ_d	1402	kg/m^3

Thermal Parameters of the Soil Sample

TABLE A.15 Thermal Parameters

Thermal parameters	Symbol	Value	Unit	Source
Thermal conductivity of the soil particles	k_s	2.5	W/m · °C	Table 2.1
Thermal conductivity of the pore water	k_w	0.57	W/m · °C	(Andersland & Ladanyi, 2004)
Unfrozen water content	w_u	0.25	%	Eq. 2.6
Thermal conductivity of ice	ki	2.2	W/m · °C	(Andersland & Ladanyi, 2004)
Kersten number for unfrozen coarse grained soil	K_e	1.01		Eq. 2.7
Kersten number for unfrozen fine grained soil	K_e	1.01		Eq. 2.8
Kersten number for frozen soil	K_e	1.0		$K_e=S_r$, Eq. 2.9
Volumetric heat capacity of water	c_{vw}	4.187	$MJ/m^3 \cdot °C$	(Andersland & Ladanyi, 2004)

Thermal Properties of the Soil Sample

TABLE A.16 Thermal Conductivity Results

Thermal conductivity	Value	Unit
Dry, natural soil	0.18	W/m · °C
Dry, crushed rock materials	0.20	W/m · °C
Saturated unfrozen soil	1.24	W/m · °C
Saturated frozen soil	2.34	W/m · °C
Unfrozen	1.25	W/m · °C
Frozen	2.42	W/m · °C
Frozen soil with w_u	2.41	W/m · °C

TABLE A.17 Volumetric Heat Capacities Results

Volumetric heat capacities				
Unfrozen	3.05	$MJ/m^3 \cdot °C$	3051.56	$kJ/m^3 \cdot °C$
Frozen	2.03	$MJ/m^3 \cdot °C$	2031.96	$kJ/m^3 \cdot °C$

Latent heat of fusion (L) = 162.52 MJ/m^3 Eq. 2.25

Closed-Form Solution

TABLE A.18 Input Parameters Closed-Form Solution

Freeze pipe dimensions		
Spacing (S)	1	m
Radius (r_0)	0.07	m
Soil physical properties		
Soil type	Silt sand	
Density of soil (ρ)	1892.12	kg/m^3
Water content (w)	35	%
Soil dry density (ρ_d)	1401.57	kg/m^3

Soil thermal properties	**Value**	**Unit**	**Source**
Difference between the temperature at the surface of the freeze-pipe and the freezing point of water (v_s)	-20	°C	TB1
Difference between the ambient temperature of the ground and the freezing point of water (v_0)	0	°C	Homogenization stage
Volumetric heat capacity of water (c_{vw})	4.187	$MJ/m^3 \cdot °C$	(Andersland & Ladanyi, 2004)
Frozen thermal conductivity (k_f)	2.42	$W/m \cdot °C$	Eq. 2.17
Amount of heat when water is converted into ice with no change in temperature (L')	333700	J/kg	(Andersland & Ladanyi, 2004)
Volumetric heat capacity for mineral (frozen) soils (c_{vf})	2.03	$MJ/m^3 \cdot °C$	Eq. 2.14
Volumetric heat capacity for mineral (unfrozen) soils (c_{vu})	3.05	$MJ/m^3 \cdot °C$	Eq. 2.13
Volumetric latent heat of the soil (L)	162.52	MJ/m^3	Eq. 2.25
Equivalent latent heat for stage I (L_1)	162.52	MJ/m^3	Eq. 2.32
Equivalent latent heat for stage II (L_F)	182.84	MJ/m^3	Eq. 2.36

TABLE A.19 Results Closed-Form Solution

Stage I			
R (m)	Q_I (MJ/m)	t_1 (days)	P_1 (W/m)
0.10	6.90	0.05	851.42
0.15	13.37	0.17	398.46
0.20	22.86	0.53	289.27
0.25	35.05	1.09	238.56
0.30	49.90	1.89	208.67
0.35	67.40	2.94	188.69
0.40	87.55	4.26	174.23
0.45	110.34	5.85	163.20
0.50	135.76	7.74	154.46

Stage II					
W (m)	x = W/S	t_{IIF} (days)	t_{total} (days)	Q_{IIF} (MJ/m^2)	P_{IIF} (W/m^2)
0.80	0.80	0.00	7.74	0.0	0.0
0.85	0.85	0.56	8.30	155.4	227.4
0.90	0.90	1.04	8.78	164.6	214.8
0.95	0.95	1.55	9.29	173.7	203.5
1.00	1.00	2.08	9.82	182.8	193.3
1.05	1.05	2.64	10.38	192.0	184.1

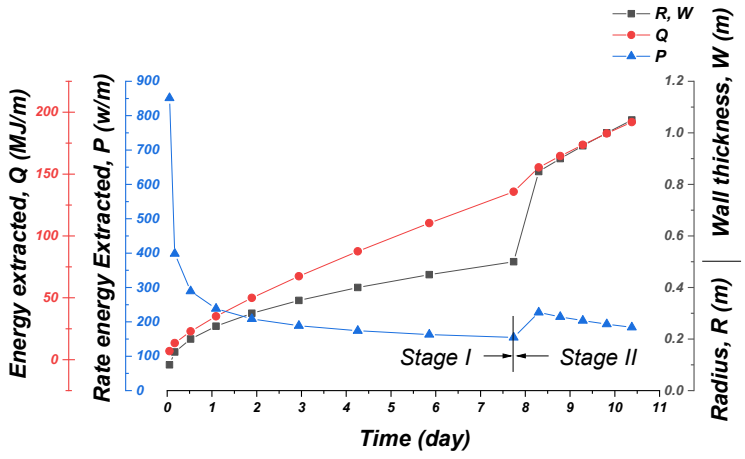

FIGURE A.84 Results for stage I and stage II, time vs radius R, wall thickness W, energy extracted Q, and rate energy extracted P Batch (2) Trial (TB2_Off2).

Finite Element Analysis

Model Configuration

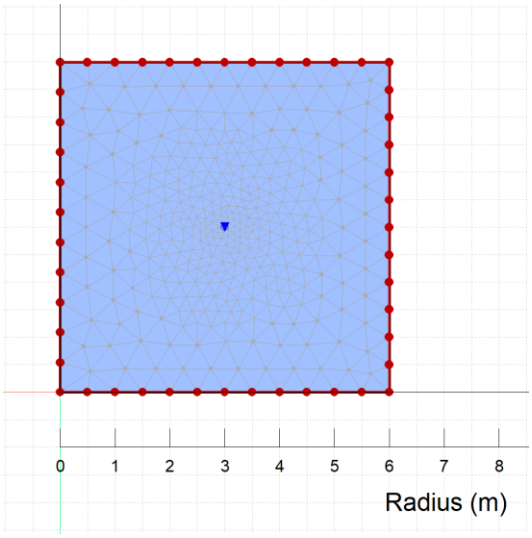

FIGURE A.85 Mesh configuration.

Thermal Material Setting

TABLE A.20 Thermal Material Model Setting

Parameter	Value	Unit		Value	Unit
Frozen thermal conductivity	2.42	W/m · °C		208.79	kJ/d/m/°C
Unfrozen thermal conductivity	1.25	W/m · °C		107.94	kJ/d/m/°C
Unfrozen water content (w_u)	0.25	%	(for Silty sand)		
Unfrozen volumetric heat capacity	3.05	MJ/m^3 · °C		3051.56	kJ/m^3 · °C
Frozen volumetric heat capacity	2.03	MJ/m^3 · °C		2031.96	kJ/m^3 · °C
Insitu water content	0.35				
Activation temperature	0	°C			

Boundary Condition

TABLE A.21 Convective Heat Transfer Constants and Coefficients

Parameter	Value	Unit	Source
Glycol thermal conductivity	0.258	(w/m · °C)	(Engineering Toolbox, 2008)
Nusselt number	3.66		(Bergman et al.,2011)
Convective heat transfer coefficient (h)	6.74	J/sec/m^2/°C	Eq. 5.1
Fluid temperature	-20	°C	TB1
Surface perimeter	0.44	m	Pile's perimeter

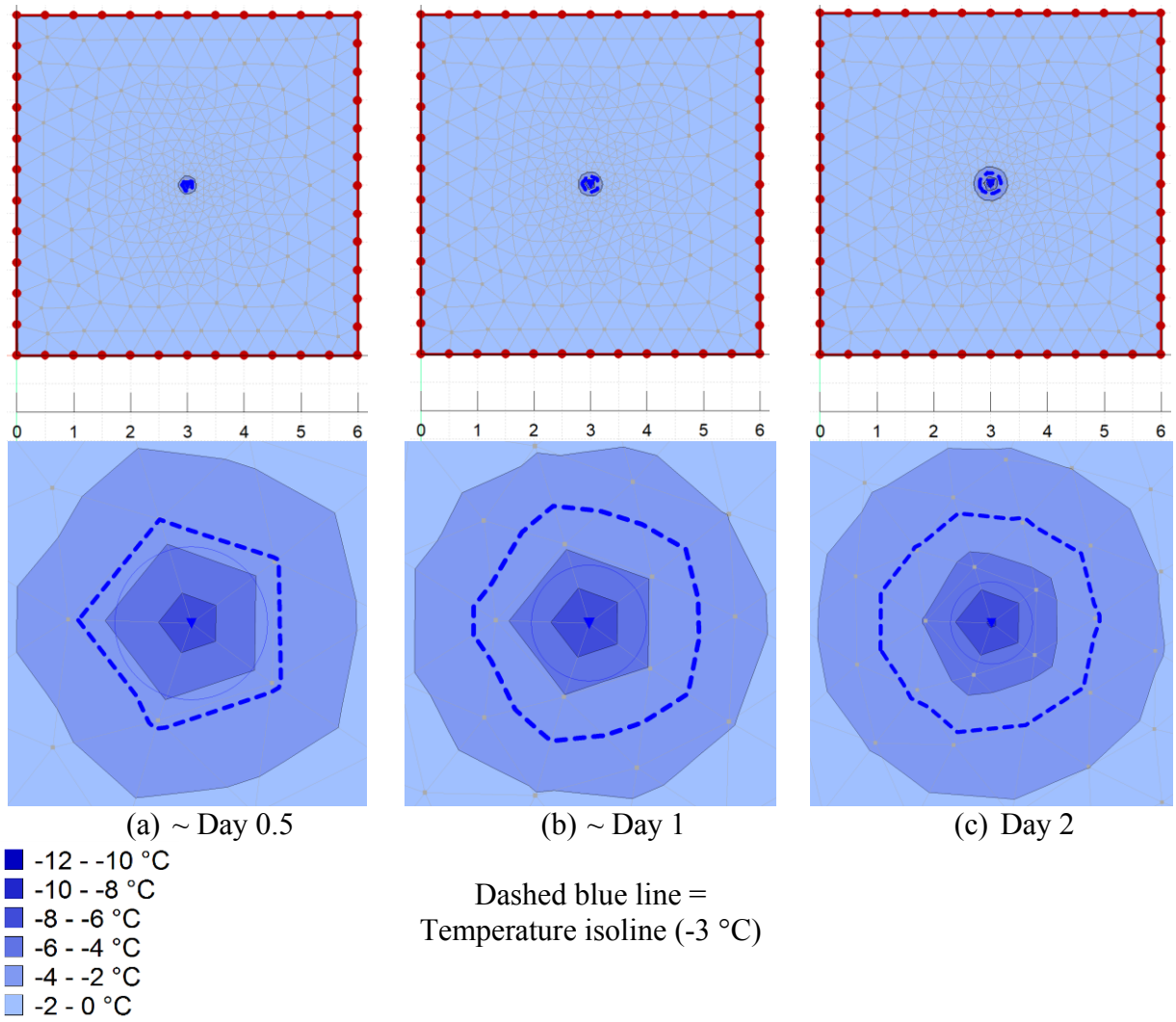

(a) ~ Day 0.5 (b) ~ Day 1 (c) Day 2

FIGURE A.86 Radial extent of frozen soil in meters. (a) day 0.5. (b) day 1. (c) day 2.

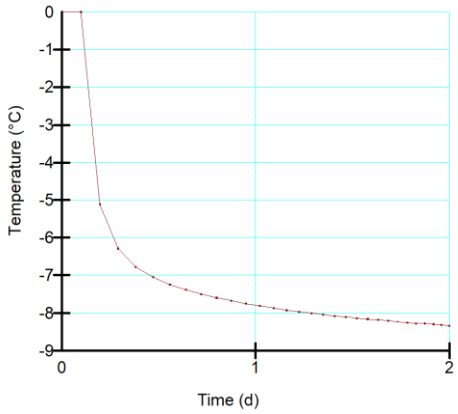

FIGURE A.87 Temperature vs time (at the point on the mesh).

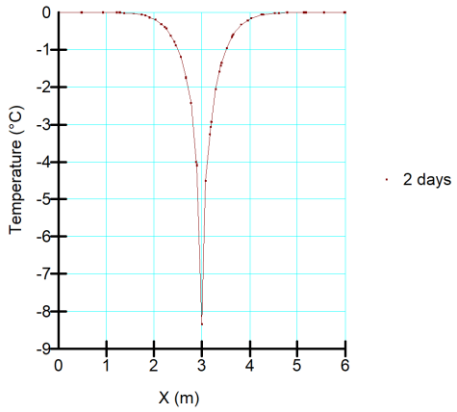

FIGURE A.88 Temperature profile at day 2.

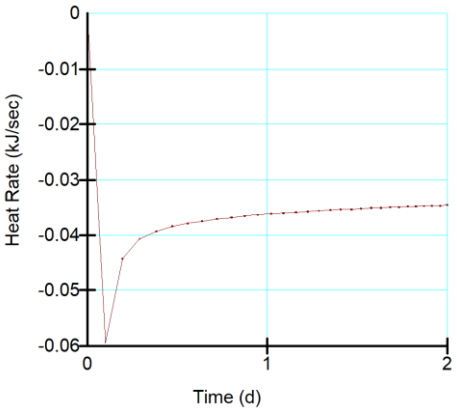

FIGURE A.89 Heat extraction rate per unit length of pile.

Batch (3) w (20%) Trial (TB2_Off1) starting from -2.5 °C TB1on(-20 °C)_TB2off

Physical Soil Sample Properties

TABLE A.22 Initial Soil Sample Properties Batch (3) Trial (TB2_Off1)

Property	Symbol	Value	Unit
Moisture content	w	20	%
Specific gravity of solids	G_s	2.67	
Unit weight of water (4 °C)	γ_w	9.807	kN/m^3
Total unit weight	γ	20.10	kN/m^3

TABLE A.23 Phase Relationships (Physical Properties of the Soil Sample)

Property	Symbol	Value	Unit
Void ratio	e	0.56	
Porosity	n	0.36	
Degree of saturation	S_r	0.95	
Density of water	ρ_w	1000	kg/m^3
Density of soil	ρ	2048	kg/m^3
Dry density	ρ_d	1707	kg/m^3

Thermal Parameters of the Soil Sample

TABLE A.24 Thermal Parameters

Thermal parameters	Symbol	Value	Unit	Source
Thermal conductivity of the soil particles	k_s	2.5	W/m · °C	Table 2.1
Thermal conductivity of the pore water	k_w	0.57	W/m · °C	(Andersland & Ladanyi, 2004)
Unfrozen water content	w_u	0.27	%	Eq. 2.6
Thermal conductivity of ice	ki	2.2	W/m · °C	(Andersland & Ladanyi, 2004)
Kersten number for unfrozen coarse grained soil	K_e	0.98		Eq. 2.7
Kersten number for unfrozen fine grained soil	K_e	0.98		Eq. 2.8
Kersten number for frozen soil	K_e	0.95		$K_e=S_r$, Eq. 2.9
Volumetric heat capacity of water	c_{vw}	4.187	$MJ/m^3 \cdot °C$	(Andersland & Ladanyi, 2004)

Thermal Properties of the Soil Sample

TABLE A.25 Thermal Conductivity Results

Thermal conductivity	Value	Unit
Dry, natural soil	0.27	W/m · °C
Dry, crushed rock materials	0.37	W/m · °C
Saturated unfrozen soil	1.47	W/m · °C
Saturated frozen soil	2.38	W/m · °C
Unfrozen	1.45	W/m · °C
Frozen	2.27	W/m · °C
Frozen soil with w_u	2.26	W/m · °C

TABLE A.26 Volumetric Heat Capacities Results

Volumetric heat capacities				
Unfrozen	2.64	$MJ/m^3 \cdot °C$	2644.53	$kJ/m^3 \cdot °C$
Frozen	1.94	$MJ/m^3 \cdot °C$	1939.58	$kJ/m^3 \cdot °C$

Latent heat of fusion (L) = 112.37 MJ/m^3 Eq. 2.25

Closed-Form Solution

TABLE A.27 Input Parameters Closed-Form Solution

Freeze pipe dimensions		
Spacing (S)	1	m
Radius (r_0)	0.07	m
Soil physical properties		
Soil type	Silt sand	
Density of soil (ρ)	2048.45	kg/m^3
Water content (w)	20	%
Soil dry density (ρ_d)	1707.04	kg/m^3

Soil thermal properties	**Value**	**Unit**	**Source**
Difference between the temperature at the surface of the freeze-pipe and the freezing point of water (v_s)	-20	°C	TB1
Difference between the ambient temperature of the ground and the freezing point of water (v_0)	-2.5	°C	Homogenization stage
Volumetric heat capacity of water (c_{vw})	4.187	$MJ/m^3 \cdot °C$	(Andersland & Ladanyi, 2004)
Frozen thermal conductivity (k_f)	2.27	$W/m \cdot °C$	Eq. 2.17
Amount of heat when water is converted into ice with no change in temperature (L')	333700	J/kg	(Andersland & Ladanyi, 2004)
Volumetric heat capacity for mineral (frozen) soils (c_{vf})	1.94	$MJ/m^3 \cdot °C$	Eq. 2.14
Volumetric heat capacity for mineral (unfrozen) soils (c_{vu})	2.64	$MJ/m^3 \cdot °C$	Eq. 2.13
Volumetric latent heat of the soil (L)	112.37	MJ/m^3	Eq. 2.25
Equivalent latent heat for stage I (L_1)	136.44	MJ/m^3	Eq. 2.32
Equivalent latent heat for stage II (L_F)	148.20	MJ/m^3	Eq. 2.36

TABLE A.28 Results Closed-Form Solution

Stage I			
R (m)	Q_I (MJ/m)	t_1 (days)	P_1 (W/m)
0.10	5.99	0.05	799.02
0.15	11.44	0.16	373.93
0.20	19.47	0.48	271.47
0.25	29.78	1.00	223.88
0.30	42.35	1.72	195.83
0.35	57.15	2.67	177.07
0.40	74.18	3.86	163.51
0.45	93.43	5.30	153.16
0.50	114.91	7.00	144.95

Stage II					
W (m)	x = W/S	t_{IIF} (days)	t_{total} (days)	Q_{IIF} (MJ/m^2)	P_{IIF} (W/m^2)
0.80	0.80	0.00	7.00	0.0	0.0
0.85	0.85	0.48	7.48	126.0	213.4
0.90	0.90	0.90	7.90	133.4	201.6
0.95	0.95	1.34	8.33	140.8	191.0
1.00	1.00	1.80	8.80	148.2	181.4
1.05	1.05	2.28	9.28	155.6	172.8

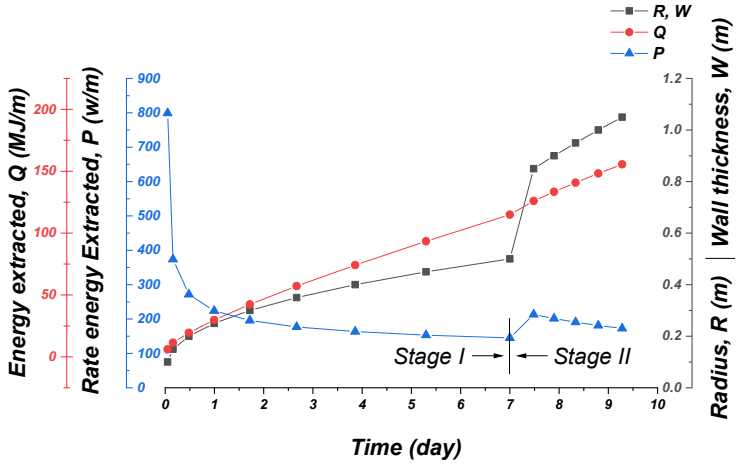

FIGURE A.90 Results for stage I and stage II, time vs radius R, wall thickness W, energy extracted Q, and rate energy extracted P Batch (3) Trial (TB2_Off1).

Finite Element Analysis

Model Configuration

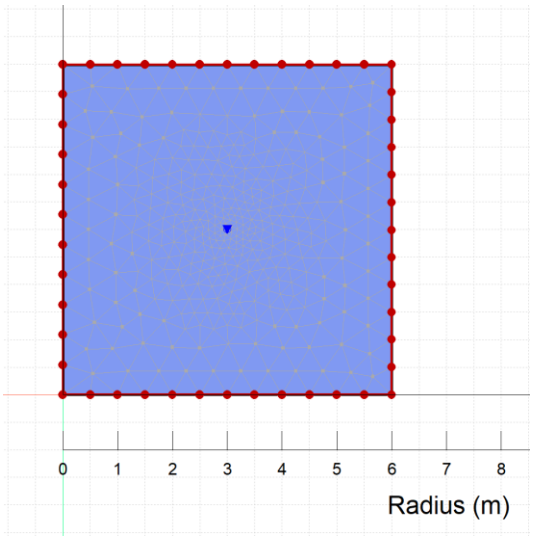

FIGURE A.91 Mesh configuration.

Thermal Material Setting

TABLE A.29 Thermal Material Model Setting

Parameter	Value	Unit		Value	Unit
Frozen thermal conductivity	2.27	W/m · °C		195.94	kJ/d/m/°C
Unfrozen thermal conductivity	1.45	W/m · °C		125.07	kJ/d/m/°C
Unfrozen water content (w_u)	0.27	%	(for Silty sand)		
Unfrozen volumetric heat capacity	2.64	MJ/m^3 · °C		2644.53	kJ/m^3 · °C
Frozen volumetric heat capacity	1.94	MJ/m^3 · °C		1939.58	kJ/m^3 · °C
Insitu water content	0.2				
Activation temperature	-2.5	°C			

Boundary Condition

TABLE A.30 Convective Heat Transfer Constants and Coefficients

Parameter	Value	Unit	Source
Glycol thermal conductivity	0.258	(w/m · °C)	(Engineering Toolbox, 2008)
Nusselt number	3.66		(Bergman et al.,2011)
Convective heat transfer coefficient (h)	6.74	J/sec/m^2/°C	Eq. 5.1
Fluid temperature	-20	°C	TB1
Surface perimeter	0.44	m	Pile's perimeter

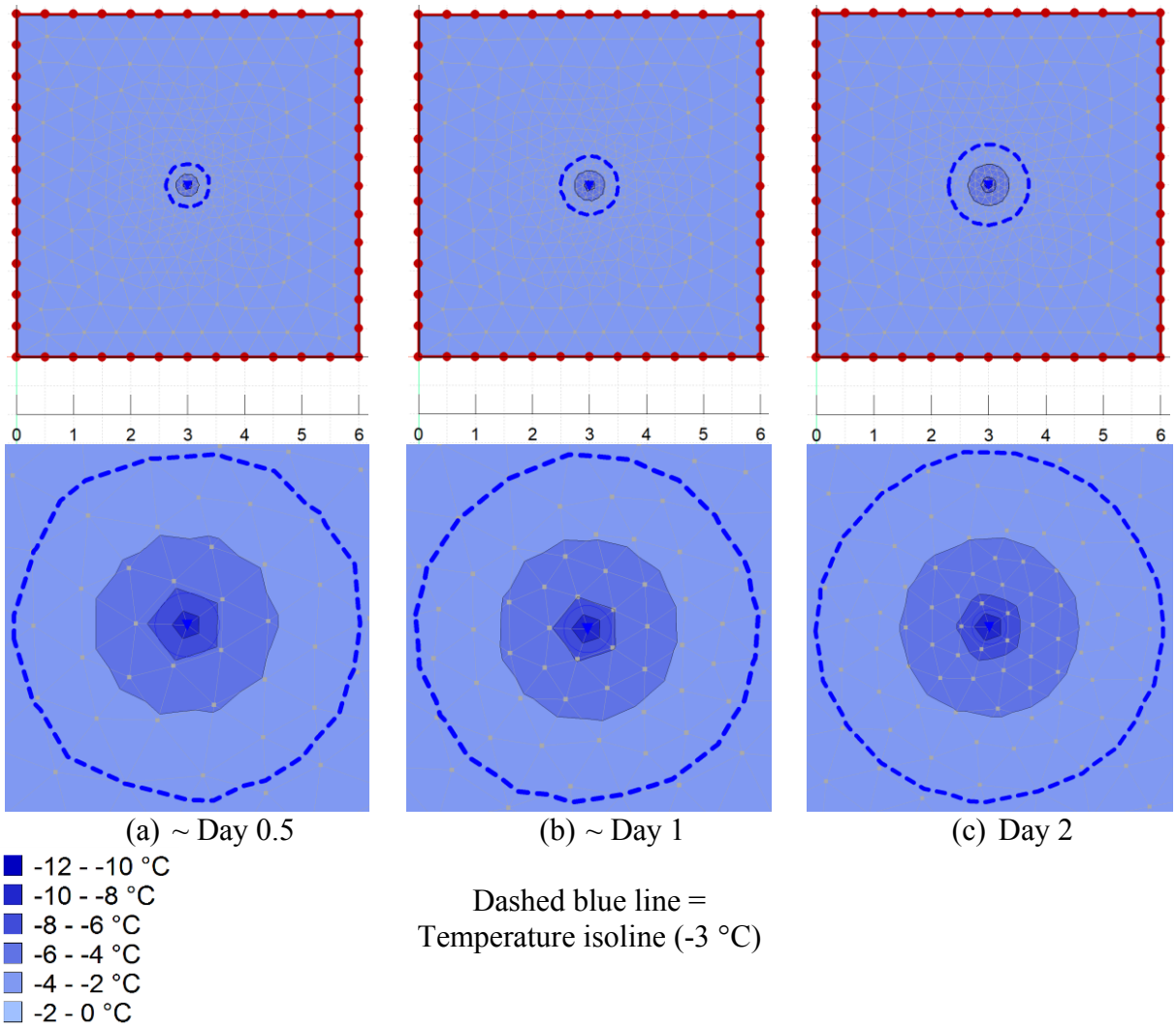

FIGURE A.92 Radial extent of frozen soil in meters. (a) day 0.5. (b) day 1. (c) day 2.

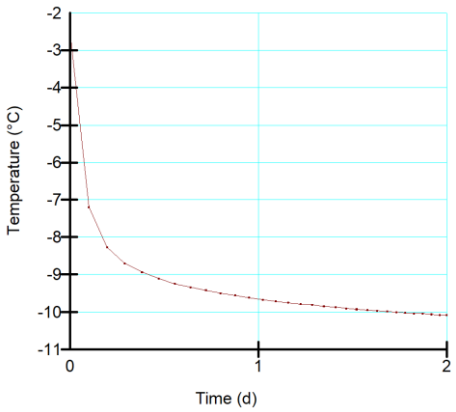

FIGURE A.93 Temperature vs time near by the pile (at the point).

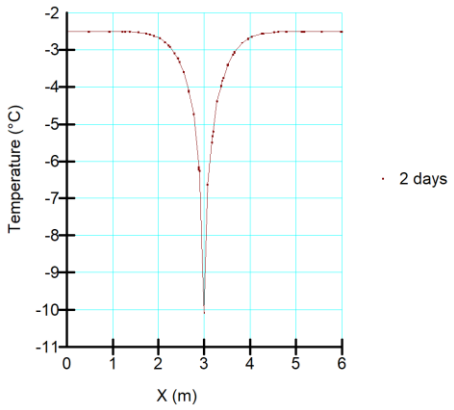

FIGURE A.94 Temperature profile at day 2.

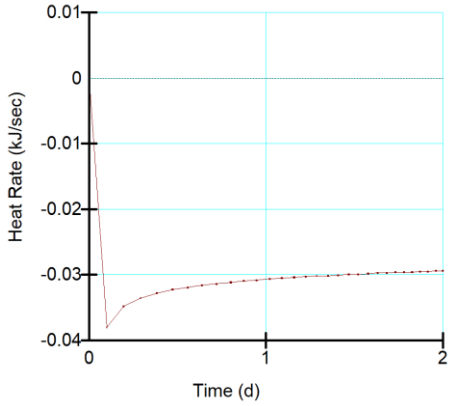

FIGURE A.95 Heat extraction rate per unit length of pile.

Batch (3) w (20%) Trial (TB2_Off2) starting from 0 °C TB1on(-20 °C)_TB2off

Physical Soil Sample Properties

TABLE A.31 Initial Soil Sample Properties Batch (3) Trial (TB2_Off2)

Property	Symbol	Value	Unit
Moisture content	w	20	%
Specific gravity of solids	G_s	2.67	
Unit weight of water (4 °C)	γ_w	9.807	kN/m^3
Total unit weight	γ	20.10	kN/m^3

TABLE A.32 Phase Relationships (Physical Properties of the Soil Sample)

Property	Symbol	Value	Unit
Void ratio	e	0.56	
Porosity	n	0.36	
Degree of saturation	S_r	0.95	
Density of water	ρ_w	1000	kg/m^3
Density of soil	ρ	2048	kg/m^3
Dry density	ρ_d	1707	kg/m^3

Thermal Parameters of the Soil Sample

TABLE A.33 Thermal Parameters

Thermal parameters	Symbol	Value	Unit	Source
Thermal conductivity of the soil particles	k_s	2.5	W/m · °C	Table 2.1
Thermal conductivity of the pore water	k_w	0.57	W/m · °C	(Andersland & Ladanyi, 2004)
Unfrozen water content	w_u	0.27	%	Eq. 2.6
Thermal conductivity of ice	ki	2.2	W/m · °C	(Andersland & Ladanyi, 2004)
Kersten number for unfrozen coarse grained soil	K_e	0.98		Eq. 2.7
Kersten number for unfrozen fine grained soil	K_e	0.98		Eq. 2.8
Kersten number for frozen soil	K_e	0.95		$K_e=S_r$, Eq. 2.9
Volumetric heat capacity of water	c_{vw}	4.187	$MJ/m^3 \cdot °C$	(Andersland & Ladanyi, 2004)

Thermal Properties of the Soil Sample

TABLE A.34 Thermal Conductivity Results

Thermal conductivity	Value	Unit
Dry, natural soil	0.27	W/m · °C
Dry, crushed rock materials	0.37	W/m · °C
Saturated unfrozen soil	1.47	W/m · °C
Saturated frozen soil	2.38	W/m · °C
Unfrozen	1.45	W/m · °C
Frozen	2.27	W/m · °C
Frozen soil with w_u	2.26	W/m · °C

TABLE A.35 Volumetric Heat Capacities Results

Volumetric heat capacities				
Unfrozen	2.64	$MJ/m^3 \cdot °C$	2644.53	$kJ/m^3 \cdot °C$
Frozen	1.94	$MJ/m^3 \cdot °C$	1939.58	$kJ/m^3 \cdot °C$

Latent heat of fusion (L) = 112.37 MJ/m^3 Eq. 2.25

Closed-Form Solution

TABLE A.36 Input Parameters Closed-Form Solution

Freeze pipe dimensions		
Spacing (S)	1	m
Radius (r_0)	0.07	m
Soil physical properties		
Soil type	Silt sand	
Density of soil (ρ)	2048.45	kg/m^3
Water content (w)	20	%
Soil dry density (ρ_d)	1707.04	kg/m^3

Soil thermal properties	**Value**	**Unit**	**Source**
Difference between the temperature at the surface of the freeze-pipe and the freezing point of water (v_s)	-20	°C	TB1
Difference between the ambient temperature of the ground and the freezing point of water (v_0)	0	°C	Homogenization stage
Volumetric heat capacity of water (c_{vw})	4.187	$MJ/m^3 \cdot °C$	(Andersland & Ladanyi, 2004)
Frozen thermal conductivity (k_f)	2.27	$W/m \cdot °C$	Eq. 2.17
Amount of heat when water is converted into ice with no change in temperature (L')	333700	J/kg	(Andersland & Ladanyi, 2004)
Volumetric heat capacity for mineral (frozen) soils (c_{vf})	1.94	$MJ/m^3 \cdot °C$	Eq. 2.14
Volumetric heat capacity for mineral (unfrozen) soils (c_{vu})	2.64	$MJ/m^3 \cdot °C$	Eq. 2.13
Volumetric latent heat of the soil (L)	112.37	MJ/m^3	Eq. 2.25
Equivalent latent heat for stage I (L_1)	112.37	MJ/m^3	Eq. 2.32
Equivalent latent heat for stage II (L_F)	131.76	MJ/m^3	Eq. 2.36

TABLE A.37 Results Closed-Form Solution

Stage I			
R (m)	Q_I (MJ/m)	t_1 (days)	P_1 (W/m)
0.10	5.24	0.05	799.02
0.15	9.74	0.14	373.93
0.20	16.44	0.41	271.47
0.25	25.06	0.85	223.88
0.30	35.54	1.46	195.83
0.35	47.88	2.25	177.07
0.40	62.08	3.25	163.51
0.45	78.12	4.45	153.16
0.50	96.00	5.87	144.95

Stage II					
W (m)	x = W/S	t_{IIF} (days)	t_{total} (days)	Q_{IIF} (MJ/m^2)	P_{IIF} (W/m^2)
0.80	0.80	0.00	5.87	0.0	0.0
0.85	0.85	0.43	6.30	112.0	213.4
0.90	0.90	0.80	6.67	118.6	201.6
0.95	0.95	1.19	7.06	125.2	191.0
1.00	1.00	1.60	7.47	131.8	181.4
1.05	1.05	2.03	7.90	138.4	172.8

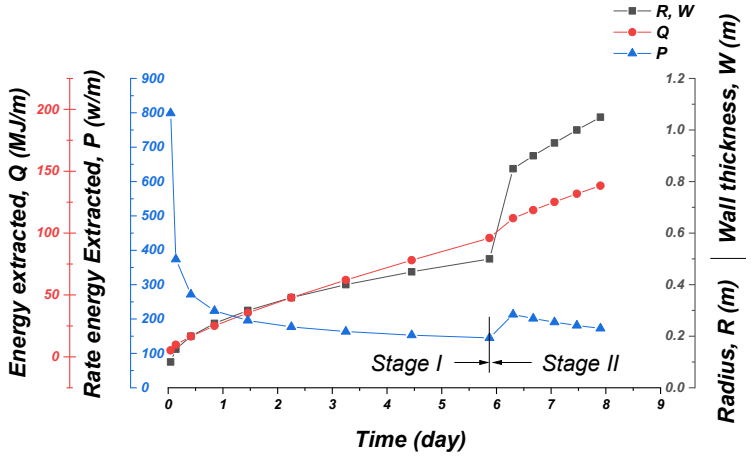

FIGURE A.96 Results for stage I and stage II, time vs radius R, wall thickness W, energy extracted Q, and rate energy extracted P Batch (3) Trial (TB2_Off2).

Finite Element Analysis

Model Configuration

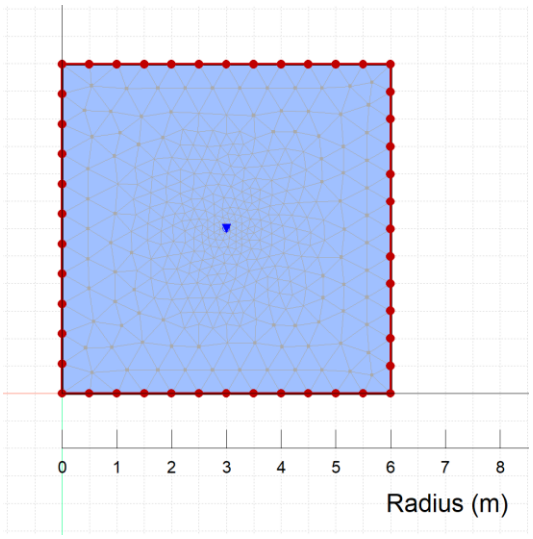

FIGURE A.97 Mesh configuration.

Thermal Material Setting

TABLE A.38 Thermal Material Model Setting

Parameter	Value	Unit		Value	Unit
Frozen thermal conductivity	2.27	W/m · °C		195.94	kJ/d/m/°C
Unfrozen thermal conductivity	1.45	W/m · °C		125.07	kJ/d/m/°C
Unfrozen water content (w_u)	0.27	%	(for Silty sand)		
Unfrozen volumetric heat capacity	2.64	$MJ/m^3 \cdot °C$		2644.53	$kJ/m^3 \cdot °C$
Frozen volumetric heat capacity	1.94	$MJ/m^3 \cdot °C$		1939.58	$kJ/m^3 \cdot °C$
Insitu water content	0.2				
Activation temperature	0	°C			

Boundary Condition

TABLE A.39 Convective Heat Transfer Constants and Coefficients

Parameter	Value	Unit	Source
Glycol thermal conductivity	0.258	(w/m · °C)	(Engineering Toolbox, 2008)
Nusselt number	3.66		(Bergman et al.,2011)
Convective heat transfer coefficient (h)	6.74	$J/sec/m^2/°C$	Eq. 5.1
Fluid temperature	-20	°C	TB1
Surface perimeter	0.44	m	Pile's perimeter

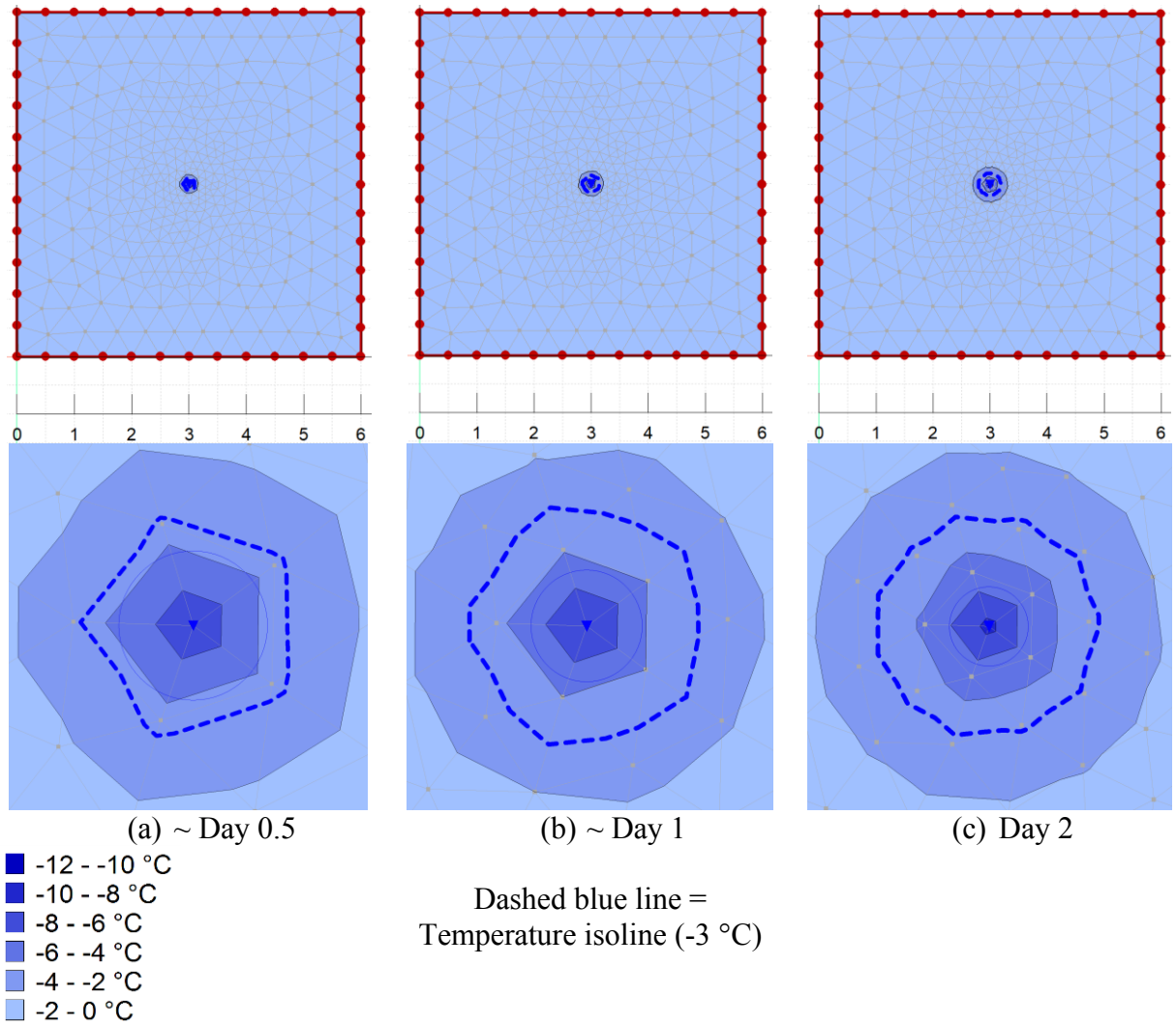

(a) ~ Day 0.5 (b) ~ Day 1 (c) Day 2

FIGURE A.98 Radial extent of frozen soil in meters. (a) day 0.5. (b) day 1. (c) day 2.

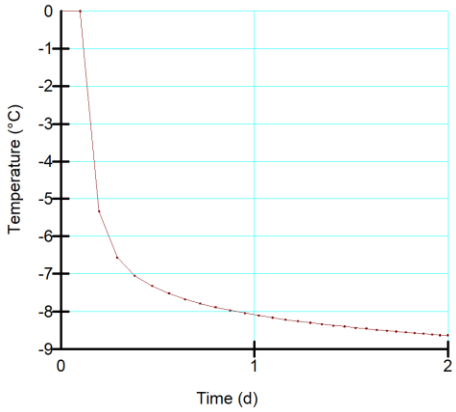

FIGURE A.99 Temperature vs time (at the point on the mesh).

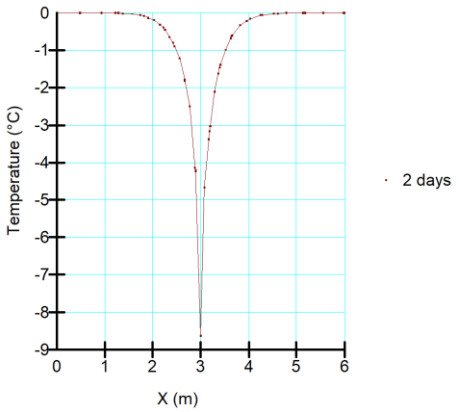

FIGURE A.100 Temperature profile at day 2.

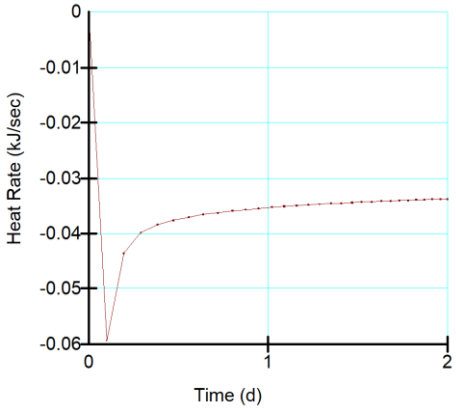

FIGURE A.101 Heat extraction rate per unit length of pile.

Power and Energy Demand for the Test

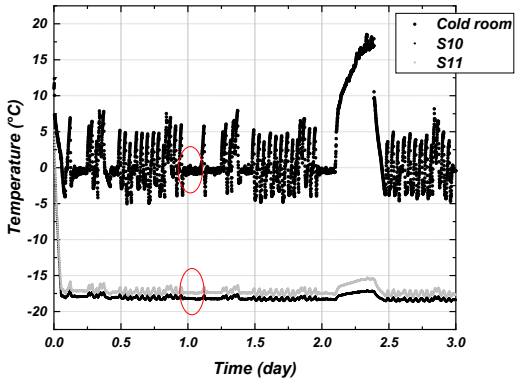

FIGURE A.102 Inlet (S10) and outlet (S11) temperatures on the copper coil measured during the power lost test (P=0).

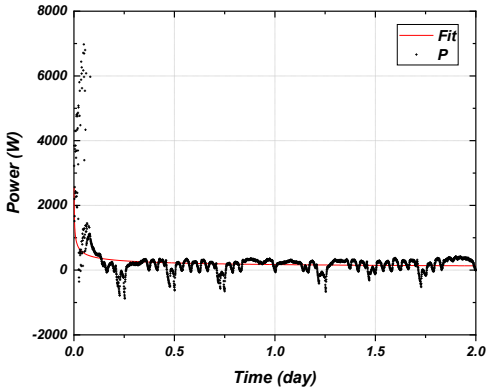

FIGURE A.103 Cooling power in W.

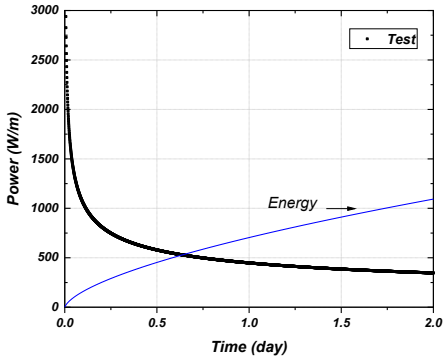

FIGURE A.104 Cooling power and energy extracted W/m.

Verification of Laboratory results (Comparing Solutions)

Temperature vs time (Test vs Finite Element)

Batch (2) w (35%) Trial (TB2_Off1) starting from -2.5 °C TB1on(-20 °C)_TB2off

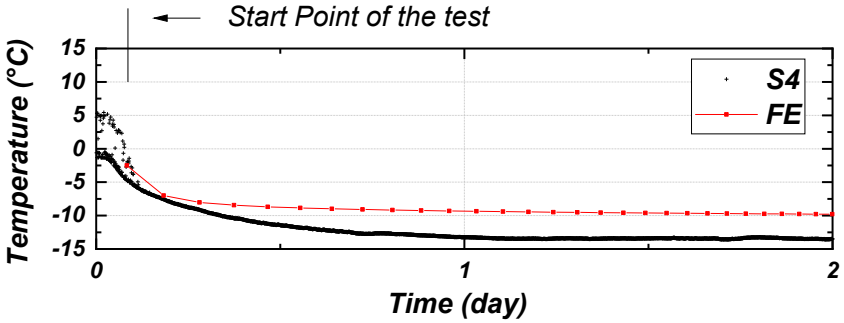

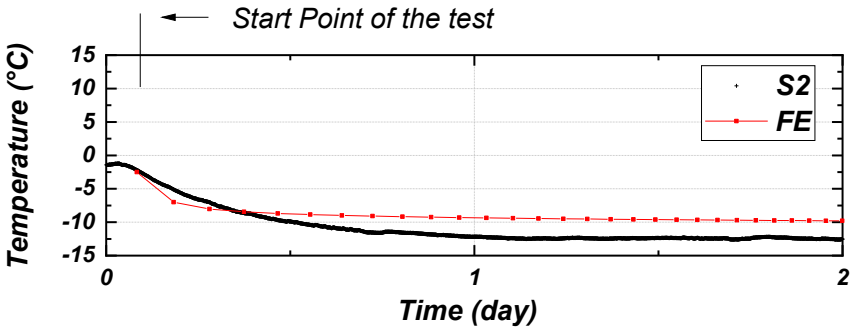

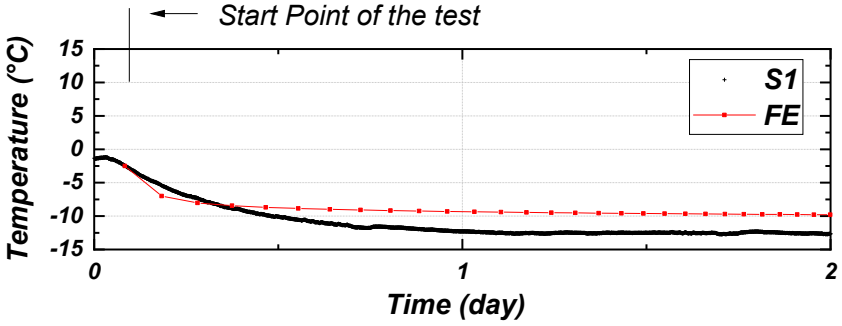

FIGURE A.105 Comparison temperature vs time of the test result vs finite element solution S1, S2 and S4 Batch (2) w (35%) Trial (TB2_Off1).

Batch (2) w (35%) Trial (TB2_Off2) starting from 0 °C TB1on(-20 °C)_TB2off

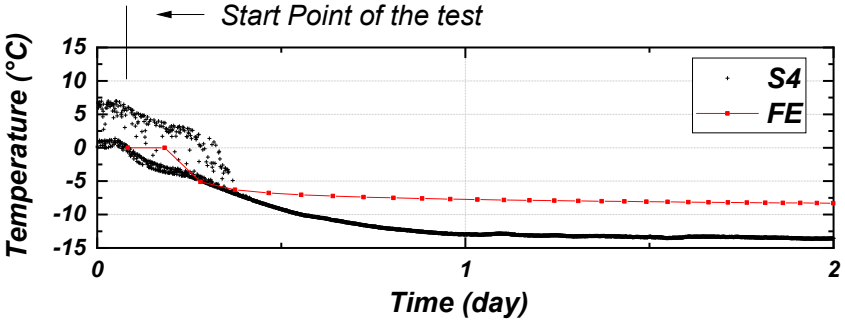

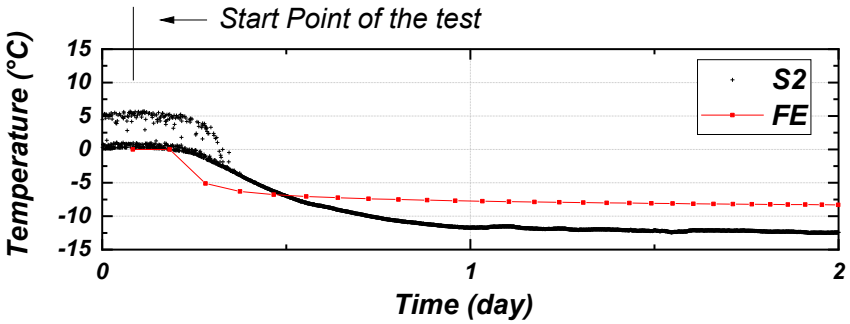

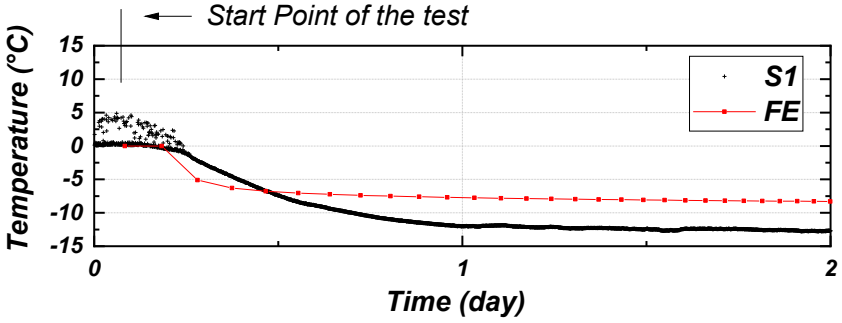

FIGURE A.106 Comparison temperature vs time of the test result vs finite element solution S1, S2 and S4 Batch (2) w (35%) Trial (TB2_Off2).

Batch (3) w (20%) Trial (TB2_Off1) starting from -2.5 °C TB1on(-20 °C)_TB2off

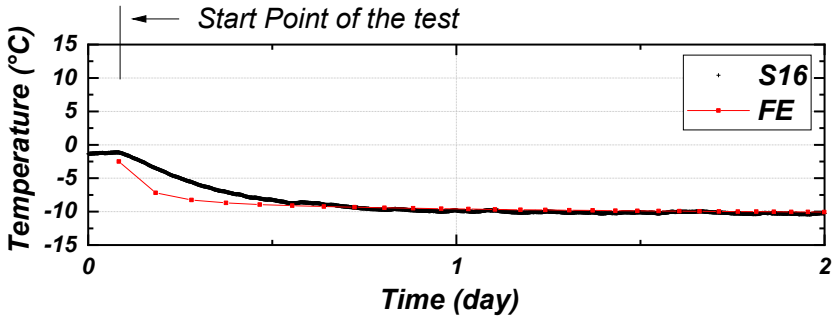

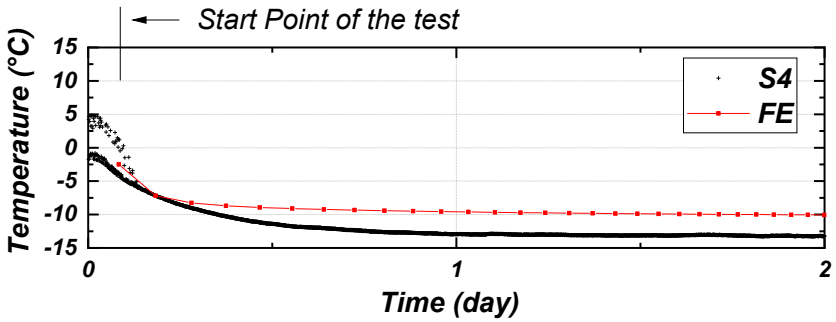

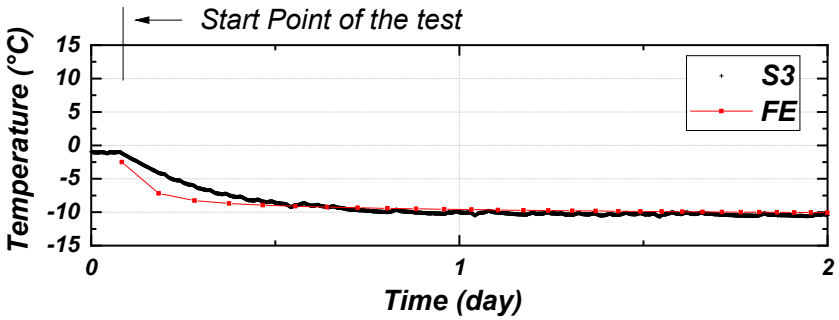

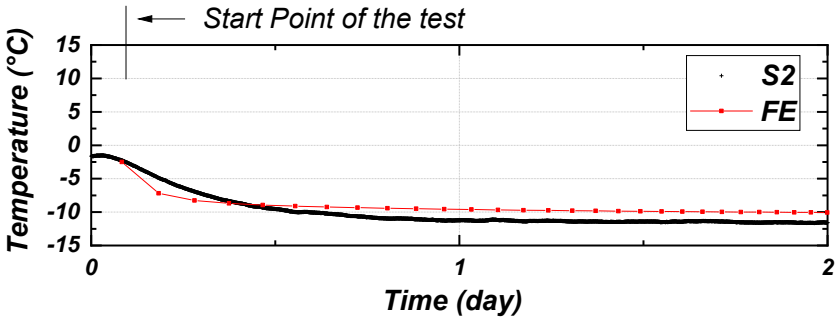

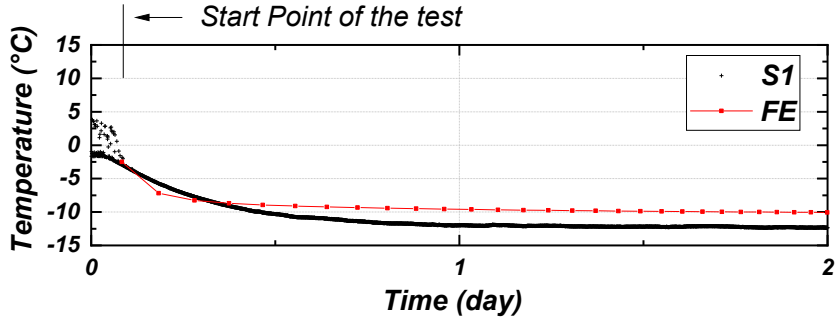

FIGURE A.107 Comparison temperature vs time of the test result vs finite element solution S1, S2, S3 and S16 Batch (3) w (20%) Trial (TB2_Off1).

Batch (3) w (20%) Trial (TB2_Off2) starting from 0 °C TB1on(-20 °C)_TB2off

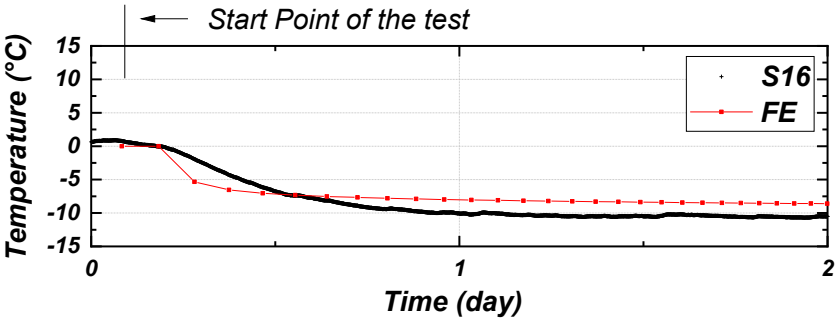

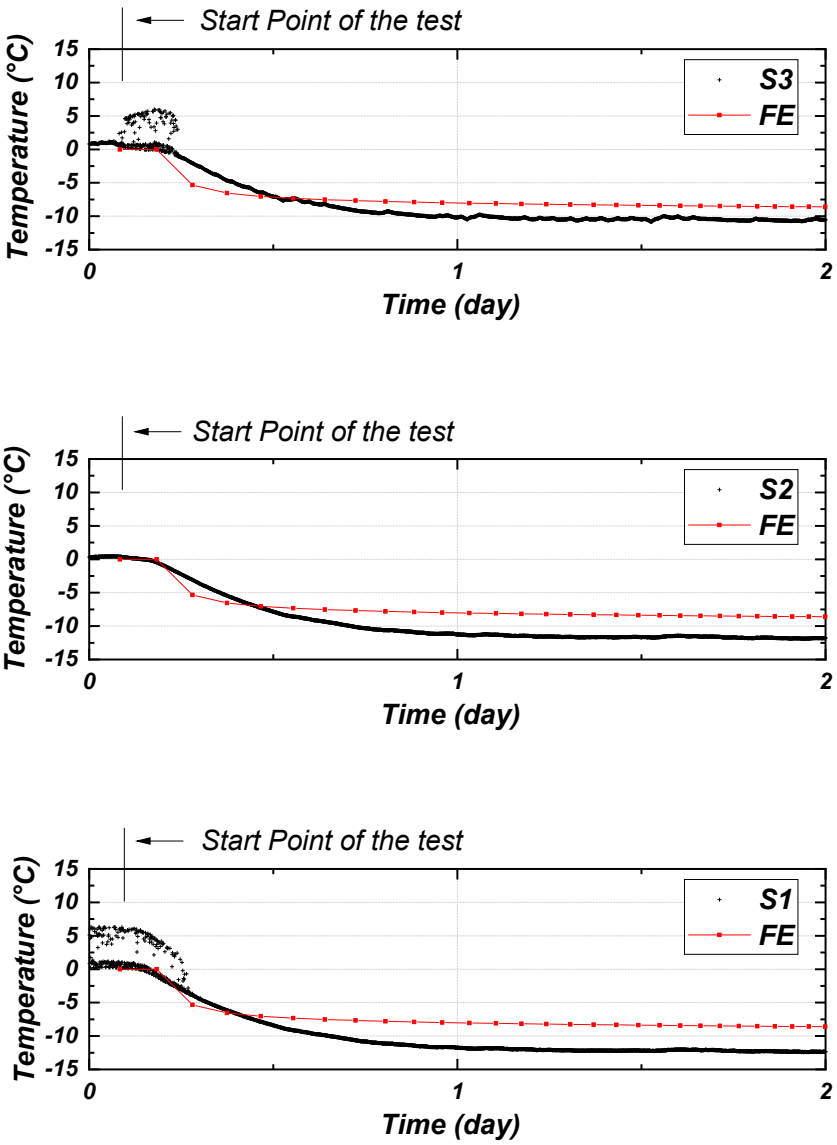

FIGURE A.108 Comparison temperature vs time of the test result vs finite element solution S1, S2, S3 and S16 Batch (3) w (20%) Trial (TB2_Off2).

Power (Test vs Closed-form soln. vs Finite element)

The analysis below is for Batch (2) trial (TB2_Off2) TB1on (-20 °C) -TB2_Off, starting from 0 °C for 35% water content

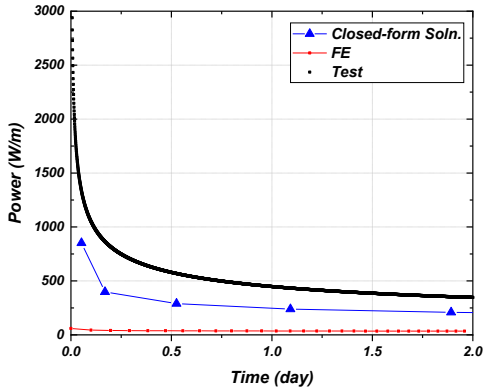

FIGURE A.109 Cooling power comparison in W/m for the Closed-form soln, Finite element soln. and the test.

Minimum Freeze Plant Capacity (Tones Refrigeration) (Test vs Closed-form Soln, FE)

TABLE A.40 Minimum Freeze Plant Capacity

Method	W/m	KJ/sec/m	Tones of refrigeration
Test	346.26	0.34626	0.03809
Closed-form solution	208.67	0.20867	0.02295
Finite element	34.62075	0.0346208	0.00381

B. Appendix B

Photographs

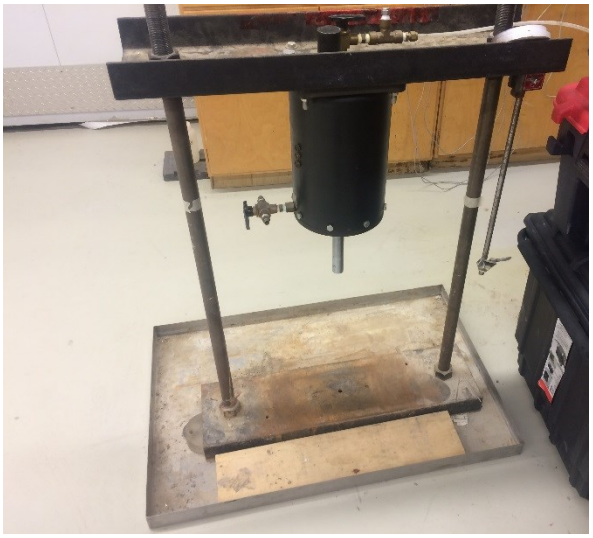

FIGURE B.1 The loading frame.

FIGURE B.2 Load plate 1.

FIGURE B.3 Adapter for load plate 2.

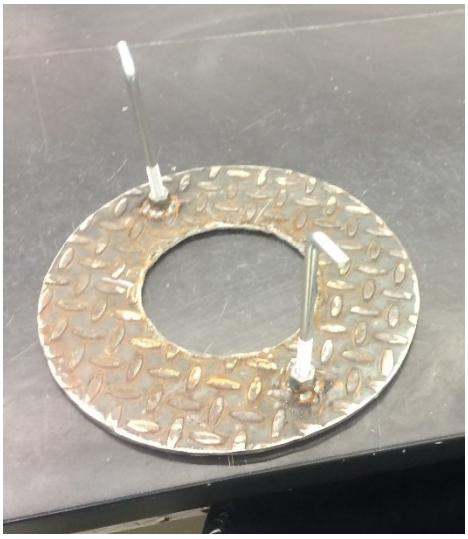

FIGURE B.4 Load plate 2.

FIGURE B.5 Test cell.

FIGURE B.6 The screw micropile.

FIGURE B.7 Pile segment I threaded.

FIGURE B.8 Pile segment I threaded, bottom part.

FIGURE B.9 Pile segment II straight.

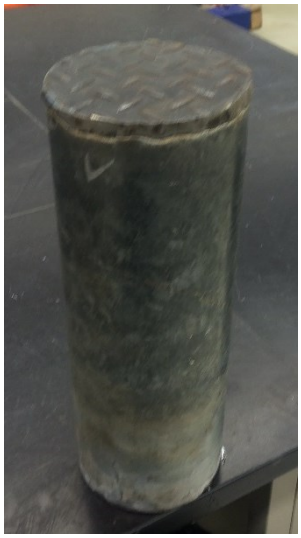

FIGURE B.10 Pile segment II straight, bottom part.

FIGURE B.11 Temperature bath.

FIGURE B.12 Thermocouples.

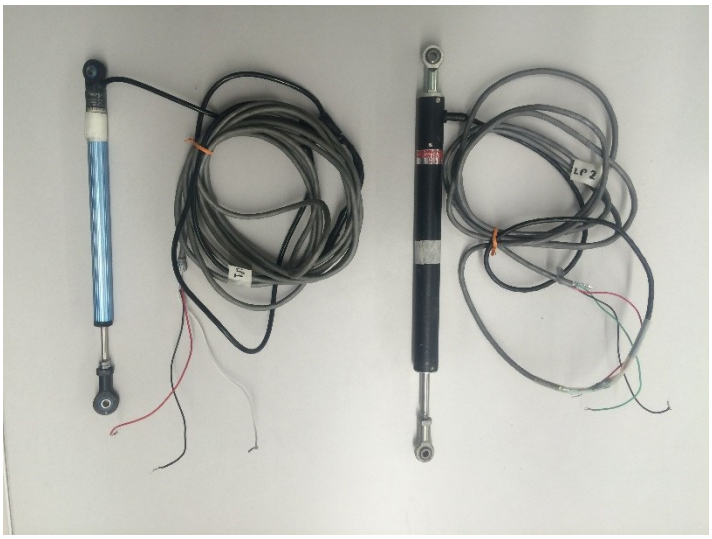

FIGURE B.13 Linear displacement sensors SLS 130 and 190.

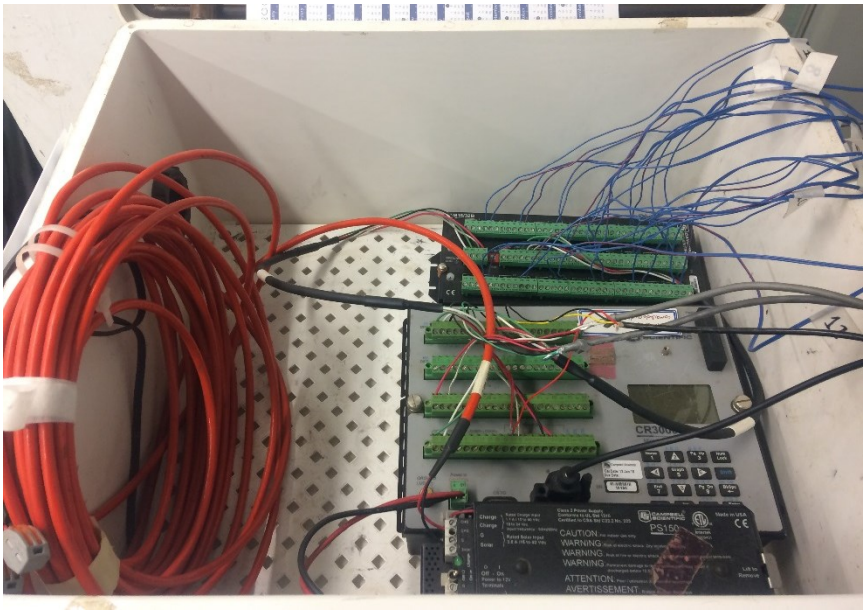

FIGURE B.14 Data logger.

FIGURE B.15 Cold room.

FIGURE B.16 Copper coil.

FIGURE B.17 Copper coil fittings inlet and outlet.

FIGURE B.18 Soil sample preparation w (20%).

FIGURE B.19 Consolidation of the soil sample (pile segment II straight).

FIGURE B.20 Ethylene glycol.

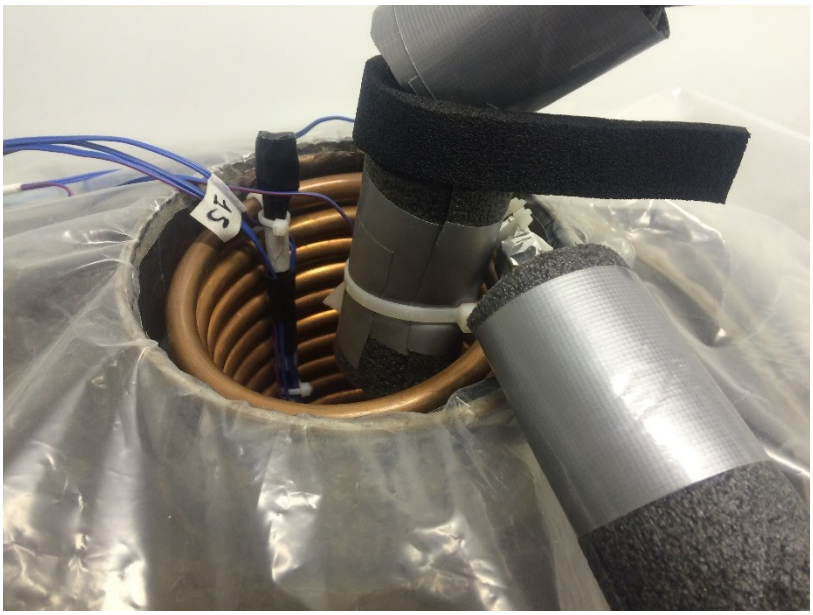

FIGURE B.21 Copper coil inside of the pile, protective plastic for the filling with glycol.

FIGURE B.22 Test cell fiberglass insulation (the test cell was cover complete) and hoses foam insulation.

FIGURE B.23 Complete apparatus setup used in the freezing stage.

FIGURE B.24 Density measuring ring.

FIGURE B.25 Power loss test, fiberglass insulation (the copper coil was cover complete).

C. Appendix C

Test Procedure and Analysis

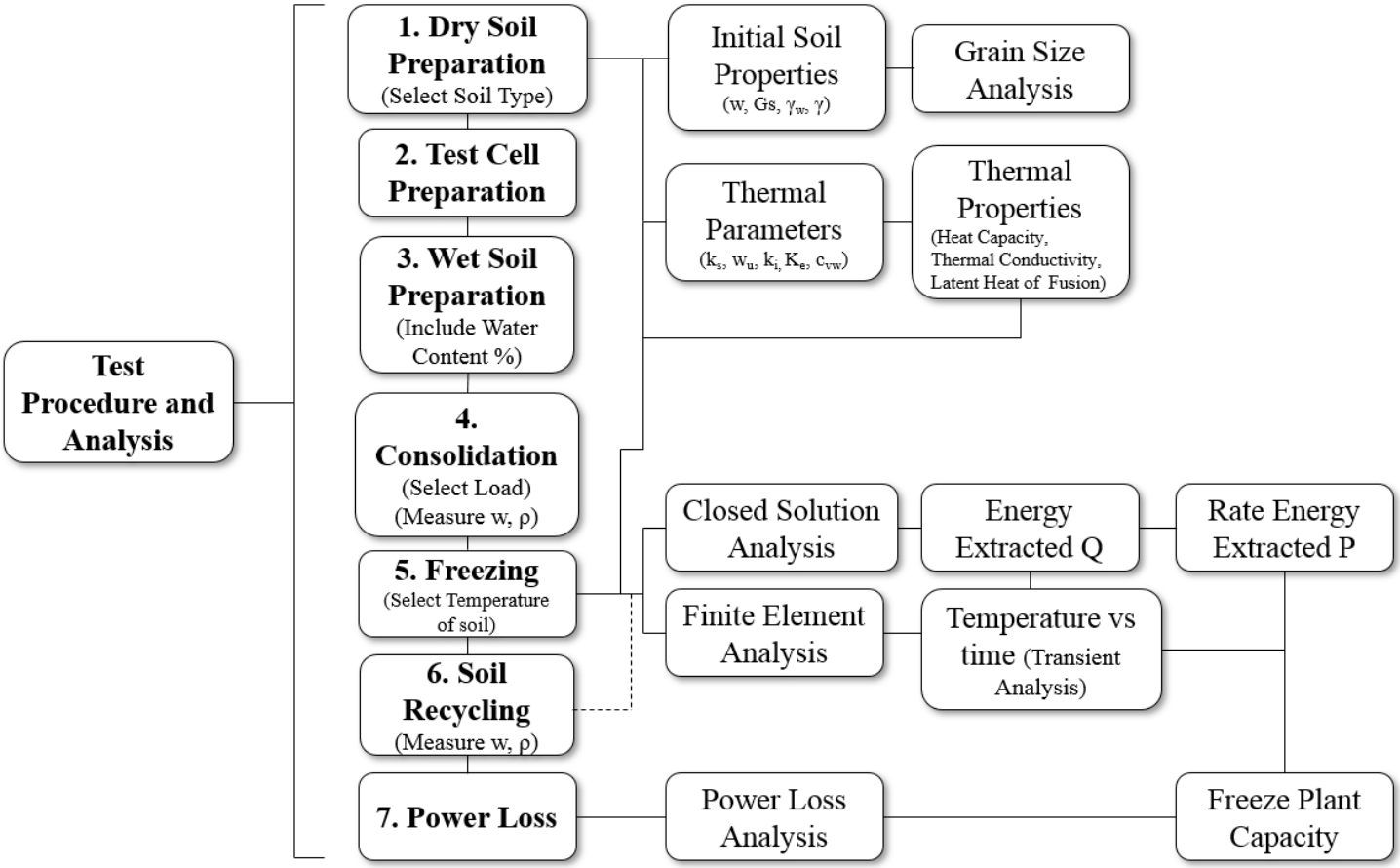

FIGURE C.1 Test Procedure and Analysis